A model of the physical processes in the neutral envelopes of planetary nebulae

Gouldsworthy, Simon Nicholas

A MODEL OF THE PHYSICAL PROCESSES IN THE NEUTRAL ENVELOPES OF PLANETARY NEBULAE

by

Simon Nicholas Gouldsworthy M.A. (Cantab)

A Thesis submitted to the University of Durham in candidature for the Degree of Doctor of Philosophy

September 1994

Abstract

The aim of this thesis is to predict the column densities of various neutral and ionised molecular species that are formed, or are likely to be formed, in the neutral envelope of a planetary nebula (PN). To this end a computer program has been constructed based on existing code (Abgrall *et al.* 1992) that considers a large set of chemical reactions covering the formation and destruction of the chemical species considered in the model.

The rate coefficient of a chemical reaction will either depend on the local gas kinetic temperature if it is a gas phase reaction, or on the local radiation field spectrum if it is a photoreaction. To model the reaction network it is therefore also required to model the heating and cooling processes in the nebula to determine the kinetic temperature and also to solve the radiative transfer equation to determine the energy spectrum of ultraviolet radiation. Formation of the H_2 molecule on the surface of dust grains and cosmic ray interactions are also considered.

The ultraviolet absorption spectrum of the dominant molecules H_2 and CO and the photodissociation rates are both functions of the rotational population. Rate coefficients for collisional cooling also depend on the rotational state. For these reasons, to model the thermal processes and the radiative transfer accurately it is also required to model the processes contributing to rotational excitation and de-excitation of H_2 and CO to determine the distribution amongst their various rotational levels.

Dust grains play a significant rôle in much of the physics occurring in the nebula, not least because they represent the catalyst for the formation of molecular hydrogen. Dust also represents the most important source of opacity for the ultraviolet radiation field and hence a significant part of the thesis is devoted to a consideration of the probable dust composition and optical properties.

The results of the model are shown and a comparison is made between the predictions of the model and recent computations of molecular column densities based on astronomical observations of planetary nebulae. The probable sources of large discrepancies are discussed within the context of assumptions and possible omissions in the physical model.

Acknowledgements

My sincere thanks to the Science and Engineering Research Council for providing financial support for the three year period in which the major part of this work was done. My thanks are extended towards Dr. J. V. Major and Prof. D. R. Flower for accepting me as a Research Student in Durham.

I am grateful to my supervisor Prof. D. R. Flower and to Dr. J. Le Bourlot for providing me with the outline code and giving me a kickstart into the project. I owe a great deal to a small group of people at Durham who were always willing to lend a helping hand without complaint when I was experiencing difficulties and it is my pleasure to thank in particular Drs. E. L. Heck and J. F. McCann. I also thank Drs. R. M. Potvliege and M. Plummer for their occasional help and Pauline for producing a couple of diagrams for the thesis.

I am grateful to Dr. G. Stasińska for providing me with data on emission line and hydrogen continuum intensities from her work on modelling the ionised region of a planetary nebula.

Many thanks to my office mates Emine Meşe, Andrew Fearnside and Henry Day and my girlfriend Helen Hooper for refreshing insights and even more refreshing visits to the pub.

Declaration

I declare that the work contained in this thesis has not been submitted for a degree at this University or any other. All the work presented herein was conducted by the author, unless stated otherwise.

Simon N. Gouldsworthy
Department of Physics, University of Durham

September 1994

Dedicated to my family

The atoms are at war with one another as they
move along in the void owing to their dissimilarity
and their other differences, and as they move
they collide and are interlaced in a manner which
makes them touch and be near to one another.

Democritus (*c.* 470-380 B.C.)

Look at the stars! look, look up at the skies!
O look at all the fire-folk sitting in the air!
The bright boroughs, the circle-citadels there!

Gerard Manley Hopkins (1844-1889)

Contents

Chapter 1

Introduction

A planetary nebula represents the final stages in the life of an intermediate mass star. Unlike massive stars ($M > 8M\odot$) which end their brief life in a supernova explosion, lower mass stars (where $M > 0.8M\odot$) are destined to end their existence in a less spectacular manner. As the thermonuclear fuel in the star is exhausted the star swells enormously in size to form a red giant. The outer bulk of this star is then shed to form a spherical shell of gas and dust which expands rapidly away from the remnant of the central star. The shell of matter contains both light and heavy elements and the constitution of the nebula reflects the mixing and dredge-up processes that occurred in the star to bring heavy elements (carbon, nitrogen, oxygen) from the deep interior to the outer layers. The dense remnant star left at the centre of the nebula now attains a very high temperature, possibly up to about 3.5×10^5 K. As a consequence of this high temperature much of the radiation emitted by the central star is in the energetic ultraviolet portion of the spectrum. This radiation impinges on the expanding shell of gas causing single and multiple ionisations of the atoms and making any molecular species extremely short lived. In this region of the gas shell, close to the central star, hydrogen is practically entirely in ionised form.

The star can only emit a finite number of ionising photons per unit time and at a certain distance from the central star there exists no radiation beyond the Lyman limit ($\lambda = 912\,\text{Å}$) capable of ionising hydrogen. Thus the nebula is surrounded by a Strömgren sphere of ionised hydrogen, helium and other elements with a sharp boundary separating it from a more diffuse, cooler neutral region where hydrogen is practically all in neutral form. The details of the ionisation structure, e.g. the extent of the ionised helium, depend on the form of the radiation spectrum (Osterbrock 1974a).

Within the neutral region the radiation field is sufficiently attenuated to allow the formation of molecular species. The existence of molecules in the planetary nebula (PN) environment is undisputed although only a relatively small number of different species have been observed. CO is the most commonly observed species, mainly through millimetre transitions. Mufson *et al.* (1975) first observed CO in the young PN NGC 7027. Since then there have have been extensive CO ($J = 2 \rightarrow 1$) surveys of PNe (Huggins and Healy 1989) and mapping (Bachiller *et al.* 1989; Forveille and Huggins 1991; Cox *et al.* 1991). A number of other molecules have been observed in NGC 7027: HCN (Olofsson *et al.* 1982), CN

(Thronson and Bally 1986), HCO^+ (Deguchi *et al.* 1990). Cox *et al.* (1987) made the first detection of a hydrocarbon molecule in a planetary nebula by observing the ortho and para transitions of cyclopropenylidene (C_3H_2) in NGC 7027. The detection of this ring molecule possibly provides further evidence for the theory that Polycyclic Aromatic Hydrocarbon (PAH) molecules are present in the PN environment. The evidence for such large hydrocarbon ring molecules exists in the form of bright infrared emission bands now commonly attributed to vibrational transitions in PAH molecules (Allamandola *et al.* 1987). If a chemical pathway exists for the creation of PAH molecules from smaller hydrocarbon ring molecules then the observations of Cox *et al.* add weight to the PAH hypothesis especially since the location of the observed emission lines coincides with the primary source of the infrared bands. The presence of C_3H_2 almost certainly implies the presence of acetylene (C_2H_2) in the nebula since this molecule is crucial to the synthesis of the ring molecule (see below). Allamandola *et al.* (1989) consider the possible chemical routes to form PAH molecules from C_2H_2.

Aside from these observations of NGC 7027 other workers have made molecular observations of PNe. For example Bachiller *et al.* (1989) detected weak emission from HCN, HNC and HCO^+ from the bipolar PN NGC 2346. In a study of the two evolved PNe NGC 6072 and IC 4406 Cox *et al.* (1992) detected millimetre transitions of CN, HCO^+, HCN and HNC. These two PNe are also strong sources of H_2 and CO emission.

The model presented in this thesis simplifies the molecular chemistry in the nebula by ignoring any possible molecule formation in the phases of stellar evolution prior to the planetary nebula stage. In fact it is assumed for the purposes of the model that all molecule formation originates and proceeds in the neutral region through gas-phase reactions alone (with the one exception of H_2 formation on the surface of dust grains). The omission in the model of grain surface chemistry is almost certainly an oversimplification but with the uncertainties that still exist concerning the exact composition of the nebular dust and associated chemical parameters, the role of such reactions in the nebular chemistry is still not fully understood.

The alternative hypothesis for the source of molecules in planetary nebulae is that they are remnants from chemistry which occurred at an earlier stage in the evolution of the star. A complex chemistry is thought to occur in the superwind of a red giant star, the precursor phase to a planetary nebula. The chemistry in the superwind is most likely dominated by photoprocesses, ion-molecule reactions and shock wave heating. Models of the chemistry in the outflow of red giant stars predict significant abundances of small molecules such as CH^+, CH_2^+, CH and NH (Howe *et al.* 1992). If the outflowing gas tends to form into clumps this may

allow the formation and survival of a small amount of larger molecules, e.g. HCN, C_2H_2, HC_3N. Being protected by the clumped nature of the gas these may survive the transition to a planetary nebula and by this process fully developed planetary nebulae may show observable amounts of polyatomic species.

There have certainly been molecular observations of precursor stars. Many species have been observed in the AGB carbon star IRC+10°216 including the organo-sulphur species C_2S and C_3S (Yamamoto *et al.* 1987), the hydrocarbons C_nH, n=2-6 (Bieging and Rieu 1988) and the cyanopolyynes $HC_{2n+1}N$, n=1-5. The infrared source CRL 618 is thought to be at the transition phase between AGB star and planetary nebula. It has a carbon-rich envelope and has been the source of a large number of molecular observations such as CO, CS, HCN, HCO^+, HC_3N and H_2CO (e.g. Shibata *et al.* 1993; Cernicharo *et al.* 1989; Gammie *et al.* 1989).

The origin of the molecules observed in fully developed PNe is more probably a combination of these two processes. Molecules formed in the precursor phase of the PN and protected from photodissociation by clumping of the gas will presumably end up in the neutral shell of the planetary nebula, if they survive the transition period. Here they will take part in the chemistry and molecular association that must proceed in the shielded environment of the neutral shell of gas. Whether this hypothesis of molecular survival to the PN phase is correct and to what extent it may occur is at present unknown.

In the context of the model presented here the underlying assumption is of molecule formation being initiated in the neutral shell of the fully developed planetary nebula. The further assumptions are made that the hydrogen nuclei abundance is constant throughout the neutral shell and that the gas is in chemical equilibrium. The assumption of constant density is clearly a gross oversimplification of reality. However, the supposition that because the gas is expanding spherically outwards from the central star the density would fall off as $1/r^2$ is also an approximation that ignores observational evidence. Practically all observations of PNe show clumping of the gas and/or asymmetry in the outflow to a greater or lesser extent. Essentially all the PNe which have been well resolved in CO show clumping on the smallest size scales observed, from the extended envelope of the young PN NGC 7027 to the thin shells of the much more evolved Helix nebula. In these two cases the clump scale size is $\leq$0.02-0.01 pc (Huggins 1993).

The symmetry of the nebula is dominated to a large extent by the degree to which the gas is concentrated in a preferred (equatorial) plane. Observations suggest that young PNe which have recently made the rapid transition from the mass-losing AGB phase show greater spherical symmetry than more highly developed PNe. In NGC 7027 and CRL 618 for example, the CO envelope is fairly complete.

Observations of more evolved PNe tend to show a more toroidal structure to the gas or that the gas is concentrated in isolated condensations. A case in hand is the bipolar nebula NGC 2346 where the gas forms a bow-tie like structure around the central star.

Thus the assumption of a constant density model is an idealisation which has some justification in that clumping of the nebular gas will create large irregularities in a density function deduced from the assumed symmetry. There is no doubt that the further out from the central star the model progresses the worse this assumption gets as of course the nebula is ultimately expanding into, and mixing with, the diffuse interstellar gas. This creates the non-trivial problem of deciding when to stop the model and declare that the column densities computed are the final values. The response to this problem was to run the model until the computed column density of CO was equal to the observed column density of CO in a typical PN with a history of molecular observation. NGC 2346, albeit a young PN, was chosen for this purpose due to the fact Bachiller *et al.* (1989) have calculated column densities in this object based on mapping the $J = 2 \rightarrow 1$ and $1 \rightarrow 0$ emission lines of CO.

The other basic, underlying assumption of the model is that the gas is in chemical equilibrium. This assumption enables the complications of a time-dependent model to be avoided but the validity of the assumption must be questioned. Apart from the fact that high-speed shock waves may propagate through the gas cloud (a scenario not considered in this model) which would plainly invalidate the assumption of steady-state chemistry, it is also possible that the chemical reactions themselves do not proceed rapidly enough compared to the lifetime of the object in question.

If a molecule in the nebula is destroyed primarily by photons at a rate γ (s^{-1}) then the timescale for the number density of the molecule to approach the equilibrium value will be of the order of $1/\gamma$. At the ionised/neutral interface of the nebula photodestruction rates are predicted to be typically of the order of 10^{-6} s^{-1} and hence equilibrium should be attained within a few multiples of 10^6 seconds, i.e. of the order of a month. Much deeper into the neutral cloud where the radiation field is heavily attenuated by dust and (primarily) H_2, photodestruction rates will drop to much lower values, of the order of 10^{-10} s^{-1}. Under these conditions equilibrium would be achieved on a timescale of several thousand years, probably a lot longer for species whose chemistry is dominated by slow chemical reactions rather than photoprocesses.

A planetary nebula is a relatively short phase in the life cycle of a star. The age of a PN can be inferred from measurements of the size of the nebula and the rate

at which the expansion is slowing. Typical upper limits on the ages of observed nebulae range from about thirty thousand to a hundred thousand years. Clearly the assumption of chemical equilibrium, although reasonable close to the central star, is very questionable at large distances from the star where equilibrium time is comparable to the lifetime of the nebula. A steady-state chemical model renders the problem very amenable to solution but remains a very debatable, perhaps invalid, assumption. The view taken is that steady-state and time-dependent are two complementary approaches to nebular modelling. Although not taking into account the variation with time a steady-state model can more easily take into account abundance variations within the nebula and subsequently make predictions about molecular column densities.

Although this model rests on the assumptions discussed above which are justifiable to varying degrees, the physical and chemical modelling within the framework of the assumptions is as detailed and accurate as possible. Radiative transfer in the nebula is solved 'exactly' in the various absorption lines of H_2 and CO and continuum absorption by dust grains so that molecular self-shielding and mutual shielding are automatically taken into account when calculating the dissociation probabilities. Recent ionisation cross-section measurements have been taken from the literature and utilised in the model to provide the most accurate possible determination of ionisation rates for a large fraction of the species considered in the chemistry. The distribution amongst the various rotational levels of the molecules H_2 and CO is determined at each point in the nebula by considering the dominant physical processes that are capable of causing rotational transitions (including optical pumping of the H_2 molecule). Extensive thermal calculations are carried out at each point in the nebula to determine the heating and cooling rates and thus the kinetic temperature of the gas (under the assumption of thermal equilibrium). Heating processes considered include photoejection of electrons from dust grains and PAH molecules and heat input from the chemical reactions (including cosmic ray and gas-dust interactions). The cooling of the gas is achieved through collisional excitation of atomic species (C, C^+, O) to fine structure levels followed by radiative decay and through rotational excitation of H_2 and CO. The temperature of the dust grains is required in the overall calculation of the gas temperature and is computed by considering the balance between UV absorption and isotropic infrared reemission.

To model the physical and optical properties of the dust in the nebula it is necessary to know or to assume what the grains are composed of. Previous nebular models commonly make the tacit assumption that the dust in a planetary nebula will exhibit the same composition and range of sizes as observed for interstellar

dust (Mezger *et al.* 1982) and functional forms for the grain size distribution are often used which have been successful in explaining the observed continuum IR emission from interstellar grains (Mathis *et al.* 1977). Events in the interstellar medium (e.g. shock waves from supernovae) are liable to alter the characteristics of the dust ejected from PNe and at the present state of knowledge it is unknown whether interstellar dust exhibits the same structure and absorption properties as dust in planetary nebulae.

Recent observations suggest that a large fraction of the dust in carbon-rich PNe is in the form of amorphous or polycrystalline carbon (Cohen *et al.* 1984; Hoare 1990; Hoare *et al.* 1992) and the optical properties of amorphous carbon have been taken from the literature (Williams and Arakawa 1972; Duley 1984) and adopted in the model. Using Mie theory the optical properties of amorphous carbon deduced from the data on refractive index in the literature seem to predict a level of absorption in the ultraviolet comparable to (or even slightly less than) the amount of absorption in the visible (§7.2). It has long been known that graphite particles exhibit far greater extinction in the UV than the visible spectrum (Spitzer 1978) and it was surprising to find the data predicting actually slightly less extinction in the UV than the visible region for amorphous carbon. If the data on refractive index is assumed to be reliable then the general outcome of using the modelled opacity in the ultraviolet is that there will be very little absorption in the UV spectrum by grains leading to photoionisation and photodissociation rates that are very high even at large optical depths (see Chapter 8). For example, using amorphous carbon dust characteristics, the C^+/C ratio in a molecular shell with $n_H = 1000$ cm^{-3} is predicted to remain above unity throughout almost the entire cloud (§8.1) and this is primarily due to the very small τ_λ/τ_V ratio in the ultraviolet. It is obviously of interest to see the results obtained from the model if the absorption properties of graphite are used instead which would predict a far greater selective extinction in the UV region and this is done in §8.2 using 'standard' interstellar graphite optical properties (Mathis *et al.* 1983).

Thus detailed calculations are performed to determine the gas temperature and the UV radiation spectrum at each point in the nebula. From this data it is then possible to determine the rate coefficients of all the chemical reactions considered in the model and solve the set of steady-state equations to determine the abundances of all the species. The chemical reaction set (Appendix B) comprises over one thousand reactions covering ninety chemical species composed from seven elements (H, He, C, O, N, S, Fe). The reaction network includes the reactions involving the important and abundant smaller molecules as well as the reactions that involve larger molecules which have been observed in PNe (HCN, HNC, HCO^+ for example). It

is inevitable that a large majority of the chemical species in the model are only hypothesised to exist in planetary nebulae. To date only a handful of molecules have been positively detected in PNe including H_2, CO, CN, HCN, HNC, HCO^+ and C_3H_2. It is wrong to assume that absence of evidence is evidence of absence of other molecular species. Given the elemental composition of a nebula it is reasonable to suppose that simple diatomic and triatomic molecules composed of the elemental species are likely to be present, provided adequately rapid exothermic reactions exist to create the molecules in question.

The conspicuous lack of observation of certain simple molecules is more likely to imply excitation conditions in the nebula that make line emission infrequent rather than imply the absence of the molecule. NGC 7027 exhibits significant abundances of carbon and sulphur (e.g. Shields *et al.* 1978). After the initiation of the hydrocarbon chemistry and the formation of CH_2 the formation of CS is likely to proceed by the ion-molecule reaction

$$S^+ + CH_2 \rightarrow HCS^+ + H$$

followed by rapid dissociative recombination of the HCS^+ ion.

The known abundances of carbon and sulphur in NGC 7027 would justify the expectation of observation of the carbon monosulphide molecule. In their molecular survey of NGC 7027 Thronson and Bally (1986) made a search for, among others, the CS molecule. It was surprising that a positive detection was not made and Thronson and Bally attribute the result to the excitation conditions in the nebula although it is not possible to rule out CS being underabundant for some (unknown) reason. The argument is that the maximum volume density in NGC 7027 is so low that it is difficult to excite the higher rotational levels of large dipole moment molecules. This is also the reason these workers give for the lack of positive detection of the ammonia molecule (NH_3).

The observations that have been made of some molecules lend great weight to the hypothesis of the presence of certain unobserved molecules. The detection by Cox *et al.* (1987) of the hydrocarbon ring molecule C_3H_2 in NGC 7027 gives credence to believing that acetylene (C_2H_2) is also present in the nebula since this molecule is involved in the most likely synthesis of C_3H_2 (Herbst *et al.* 1984). Similarly one can then hypothesise that the ethynyl radical C_2H is also present since production of this molecule in objects like NGC 7027 is suggested to occur via photodissociation of acetylene (Huggins *et al.* 1984):

$$C_2H_2 + h\nu \rightarrow C_2H + H$$

Thronson and Bally (1986) estimate an extremely low abundance of C_2H from their observations of NGC 7027 which implies a correspondingly small abundance of C_2H_2. However, the upper limit these workers place on the abundance of C_2H is not inconsistent with the abundance of C_3H_2 in NGC 7027 derived by Cox *et al.*

The model of the chemistry in a planetary nebula presented here does not include the effects of a shock wave passing through the gas cloud. This is possibly an omission since theories of stellar evolution predict that, at some point after the Asymptotic Giant Branch (AGB) phase the central star will undergo a period of mass loss which, although occurring at a very low rate (10^{-7} to 10^{-10} M$\odot$ year^{-1}), travels at a very high velocity (one to four thousand kilometres per second). This fast wind forms a shock wave which impinges on the surrounding nebula which, through the transport of large amounts of energy and momentum, is bound to affect the nebular gas dynamically and chemically.

This is, however, theory and there is evidence to suggest that some PNe have not been affected by shock waves. Taylor *et al.* (1990) deduced from observations of the planetary nebula IC 418 that the expansion velocity of the ionised gas is very similar to that of the surrounding neutral envelope indicating that the ionised and neutral components are not undergoing violent collision. The neutral shell also exhibits an approximately inverse-square density gradient which would not occur in a shocked shell of gas strongly indicating that the neutral component of IC 418 does not represent post-shock gas.

The general effect of the passage of a shock wave is to alter the density and temperature of the gas it passes through. This would then enable certain chemical reactions which are suppressed at low temperatures to proceed efficiently and is possibly the explanation behind observed abundances of certain molecules (e.g. CH^+, HCO^+) in diffuse interstellar clouds (Draine and Katz 1986). For example, the celebrated endothermic reaction:

$$C^+ + H_2 \rightarrow CH^+ + H - 4640K$$

can proceed rapidly if $T \geq 1000$ K (Flower 1989) and in the aftermath of a shock wave is capable of producing large amounts of CH^+, the abundance of which is generally predicted (using unshocked models) to be orders of magnitude lower than observations of interstellar clouds. However, the invocation of shock waves in explaining observations often creates further questions as well as providing solutions in, for example, producing predicted column densities of rotationally excited H_2 which are in conflict with observation.

A more palpable omission in the model is that the effect of the interstellar background radiation field is neglected in the treatment of the chemistry. Many workers have made estimates of the mean interstellar radiation field in the vicinity of the Sun due to the ensemble of stars in the Galaxy (Habing 1968; Draine 1978; Gondhalekar *et al.* 1980; Mathis *et al.* 1983). Close to the central star of the planetary nebula the ISRF will have a negligible effect on the photochemistry; the proximity of the central star provides a photon flux several orders of magnitude more intense than the ISRF (§3.2.1.1) and the interstellar flux will itself have been attenuated in travelling from the exterior edge of the nebula to the interior. However, near the exterior of the molecular cloud the picture is very different. The central star flux will now have been greatly attenuated and diluted through the spherical geometry and the ISRF impinging on the nebula will have a comparable, if not greater, effect on photoionisation and photodissociation of the molecular species. This would have the effect of limiting the abundances of molecules in this region just as the central star flux keeps the gas primarily atomic near the ionised/neutral interface. In reality there is thus probably a shell of primarily molecular material in the neutral zone of a PN surrounded on the interior by atomic gas maintained in that state by the central star radiation field and on the exterior by atomic gas maintained in that state by the interstellar radiation field. To include the effect of the ISRF on the chemistry in the nebula is an extremely difficult problem as it involves solution of the radiative transfer equation in two opposite directions simultaneously; this affords an extremely attractive project for future theoreticians.

The structure of this thesis is as follows:
Chapter 2 derives the form of the radiation field incident on the neutral region from the contributing factors (Planck spectrum from the central star and continuum and line emission from the ionised region). An outline of the general theory behind radiative transfer in the presence of gas and dust particles is then given and how the theory has been applied to this model of a planetary nebula, paying particular attention to spectral line absorption by H, H_2 and CO. The way in which line absorption by these species affects the outgoing photon flux is described as well as the mechanism by which H_2 and CO photodissociate and how the rates are accurately calculated.

Chapter 3 contains a discussion of the gas phase and photo-chemistry that would occur in the nebula. It describes the likely chemical composition of the gas and how the rate coefficients for the various reactions are computed. The different sorts of reactions and their likely importance in the nebular chemistry is discussed.

Chapter 4 describes the various processes that contribute to rotational excitation of the H_2 and CO molecules. Recent laboratory and theoretical rates for collisionally-induced rotational transitions and dissociation probabilities and cascade coefficients for optical pumping are utilised to fully model the likely distribution of these molecules amongst the different levels.

Chapter 5 discusses the different processes by which the nebular gas is heated. This includes photoionisation (of atoms/molecules, larger polycyclic molecules and dust grains), heat production through exothermic reactions, heat transfer between gas and dust and heat input through cosmic ray events. The way in which the dust grain temperature is evaluated is also explained.

Chapter 6 describes the corresponding processes which tend to cool the gas. The bulk of this chapter is centred around fine structure excitation of C, C^+ and O. Rate coefficients for collisions between these important coolants with other abundant species are reported based on experimental or quantum mechanical calculations of the corresponding cross-sections. Suitable approximation formulae for the rates are derived in the likely temperature range of the neutral region. Cooling by collisionally induced rotational excitation of H_2 and CO is also discussed.

Chapter 7 describes the dust grain attributes (size, composition, dust/gas mass ratio) assumed for the model. Amorphous carbon particles are the basis of the grain model and, using standard Mie theory, the optical properties of such a material is derived using appropriate data in the literature. The attenuation of the outgoing radiation field due to the presence of dust is described.

Chapter 8 displays the results of the model and contains an analysis of the chemistry that produces the predicted molecular abundances. Predicted molecular column densities are compared with recent observations of planetary nebulae and possible explanations for large discrepancies between prediction and observation are discussed.

Chapter 2

Radiative transfer in the nebula

Within the nebula both matter and electromagnetic radiation will be present. The matter is in the form of atoms, molecules and much larger dust grains. The source of the radiation field is the central star of the planetary nebula but after being emitted from the star it will interact with the matter and energy may be subtracted or added to the field by absorption and emission. The interaction processes will cause attenuation of the outgoing ultraviolet radiation field since re-emission of electromagnetic energy from the molecular species will generally occur isotropically and will be emitted at lower frequencies through the process of fluorescence.

The ultraviolet (UV) radiation field is by far the dominant controlling mechanism of the physics in the nebula. Through absorption of UV radiation and subsequent re-emission at much lower energy infrared (IR) radiation the dust grains will be heated to a characteristic temperature T_d. The UV radiation field will also cause photoionisation of atoms, molecules and dust grains which will subsequently cause heating of the gas through elastic collisions with the ejected photoelectrons. The UV field will also cause photodissociation and excitation of the various molecular species.

2.1 Radiation field incident on the nebula

The ultraviolet radiation field plays a crucial rôle in the chemical equilibrium in the nebula and hence it is important to be able to represent the spectrum of radiation energy as accurately as possible. To accomplish this two problems need to be addressed - the form of the spectrum of radiation incident on the nebula and how the radiation field is affected as it penetrates the nebula. The latter problem, that of radiative transfer, is discussed later on in this chapter (§2.2). In this section the form of the initial radiation spectrum is derived.

Within the model the incident radiation field is assumed to have three components: the diluted stellar field emitted by the central star, a two-photon continuum of radiation emitted by atomic hydrogen in the ionised region and an array of spectral lines emitted by various neutral atoms and ions in the ionised region.

The emission line intensities and the hydrogen two-photon continuum have been determined from models of the ionised region of a planetary nebula (Stasińska, private communication). However, such models have not taken into account attenuation of the radiation field by dust in the ionised region and hence the spectrum

of incident radiation energy employed in this model actually represents an upper limit. This problem is further discussed in Chapter 8 where the attenuation by dust in the ionised region is taken into account, albeit very crudely, to examine the effects on the resulting molecular abundances.

2.1.1 Background stellar field

The star at the centre of the planetary nebula is assumed to emit black-body radiation at a temperature of $T_* = 10^5$ K. This is a considerable approximation since theoretical work on stellar atmospheres show that there are important deviations between the emergent fluxes from stars and Planck functions, particularly at the points in the spectrum where there are large changes in opacity with wavelength, such as at the Lyman limit of atomic hydrogen ($\lambda_H = 912$ Å). However, models of stellar atmospheres also conclude that a Planck function is a reasonable approximation to the stellar field at high enough wavelengths - generally speaking, $\lambda > \lambda_H$ (Osterbrock 1974a). It is assumed in the model that no L_c radiation (radiation with $\lambda < \lambda_H$) reaches the neutral region as photons beyond this energy limit have all been absorbed in the process of ionisation of atomic hydrogen in the ionised region. Subsequent recombination of hydrogen ions and electrons will generally occur to all possible energy levels followed by radiative cascade to the ground state so that L_c radiation is degraded to lower energy photons effectively removing it from the energy spectrum. All H^+-e^- recombinations will ultimately lead to the emission of either Lyα spectral radiation or a contribution to the hydrogen two-photon continuum (§2.1.2).
Under this assumption of black-body emission the radiation emerging from the star surface has an energy density of the form (see e.g. Lang 1986):

$$\Phi^{\text{surface}}(\lambda) = \frac{8\pi hc}{\lambda^5} \frac{1}{e^{hc/\lambda kT_*} - 1} \tag{2.1}$$

$\Phi^{\text{surface}}(\lambda)$ is the radiation field energy density at the star surface (erg cm^{-3} Å^{-1})
λ is the wavelength of the radiation (Å)
T_* is the effective temperature of the star (K)

As the radiation propagates away from the star the energy density will go down due to geometrical dilution. At a distance r from the star the energy density of the radiation field will be reduced to

$$\Phi(\lambda, r) = W\Phi^{\text{surface}}(\lambda) \tag{2.2}$$

where W, the dilution factor, is given by the expression:

$$W = \frac{1}{2}\left[1 - \left(1 - \frac{R_*^2}{r^2}\right)^{\frac{1}{2}}\right] \tag{2.3}$$

R_* is the radius of the central star

This expression derives from considering the solid angle subtended by the star at a point a distance r from it divided by the total solid angle 4π.
If $r \gg R_*$ (as is the case when the radiation is incident on the neutral region) then using the Binomial Theorem equation (2.3) reduces to:

$$W = \left(\frac{R_*}{2r}\right)^2 \qquad \text{for } r \gg R_* \tag{2.4}$$

The radius of the central star is taken to be $R_* = 2 \times 10^{10}$ cm.

The interface between the ionised and the neutral region is taken to exist at a distance of $r_0 = 1.835 \times 10^{17}$ cm from the central star. A model of the ionised region of a planetary nebula constructed with the same star parameters and elemental abundances predicts that at this distance from the star the ratio $n(\mathrm{H}^+)/n_{\mathrm{H}} = 3 \times 10^{-3}$ (Stasińska, private communication) which, for the purposes of this model, is taken as the start of the neutral region.
Hence the background stellar spectrum incident on the neutral region of the nebula is taken to be:

$$\Phi_0^{\text{black-body}}(\lambda) = \left(\frac{R_*}{2r_0}\right)^2 \frac{8\pi hc}{\lambda^5} \frac{1}{e^{hc/\lambda kT_*} - 1} \qquad \text{for } \lambda > 912\,\text{Å}$$

$$\Phi_0^{\text{black-body}}(\lambda) = 0 \qquad \text{for } \lambda < 912\,\text{Å} \tag{2.5}$$

2.1.2 Hydrogen two-photon continuum

Recombination of hydrogen nuclei and electrons in the ionised region of the planetary nebula gives rise to line radiation as the electron cascades to the ground state of the atom. However if there is a recombination or cascade to the 2^2S level of the atom then there is no single electric dipole transition connecting this level to the ground 1^2S state. The excited atom may decay by the emission of quadrupole

radiation but it is far more likely that de-excitation will proceed through the emission of two dipole photons which constitute a continuum of radiation according to the equation:

$$H^+ + e^- \rightarrow H^0(2^2S) \rightarrow H^0(1^2S) + 2 \text{ photons}$$

The two photons emitted satisfy the energy conservation equation $h\nu' + h\nu'' = 10.2$ eV with a smooth emission probability profile between $h\nu = 0$ and $h\nu = 10.2$ eV. Let ν_{12} be the frequency of a Lyα photon from atomic hydrogen ($\nu_{12} = 2.47 \times 10^{15}$ Hz). Hence the frequencies of the two emitted photons will be $y\nu_{12}$ and $(1-y)\nu_{12}$ where $0 \leq y \leq 1$.
Let $A(y)dy$ be the probability per unit time that a photon is emitted in the two-photon process with a frequency in the range $y\nu_{12}$ to $(y+dy)\nu_{12}$.
The function $A(y)$ is given by the expression:

$$A(y)\,(\mathrm{s}^{-1}) = \frac{9\alpha^6\nu_{\mathrm{H}}}{2^{10}}\psi(y) \tag{2.6}$$

ν_{H} is the frequency of the Lyman limit of atomic hydrogen ($\nu_{\mathrm{H}} = 3.29 \times 10^{15}$ Hz)
α is the fine structure constant; $\alpha = 2\pi e^2/hc$ ($\alpha = 1/137.037 = 7.297 \times 10^{-3}$)

The function $\psi(y)$ is given by (Spitzer and Greenstein 1951):

$$\psi(y) = y^3(1-y)^3 \left| \sum_{m=2}^{\infty} R_{mp}^{1s} R_{mp}^{2s} \left(\frac{3}{1+3y-4/m^2} + \frac{3}{4-3y-4/m^2} \right) + \int_0^{\infty} C_{1s} C_{2s} \left(\frac{3}{1+3y+4x^2} + \frac{3}{4-3y+4x^2} \right) dx \right|^2 \tag{2.7}$$

The quantities R_{mp}^{ns} and C_{ns} are radial quantum integrals defined in the literature (Breit and Teller 1940).

Values of the function $\psi(y)$ are given in Table 2.1. Since $\psi(y) = \psi(1-y)$ only values up to $y = 0.5$ are tabulated.

The Einstein A coefficient for the spontaneous transition between levels 2^2S and 1^2S is then given by:

$$\mathrm{A}_{2^2\mathrm{S},1^2\mathrm{S}} = \frac{1}{2}\int_0^1 A(y)\,dy = \frac{9\alpha^6\nu_{\mathrm{H}}}{2^{11}}\int_0^1 \psi(y)\,dy \tag{2.8}$$

Table 2.1

Values of the function $\psi(y)$ for the emission probability in the hydrogen two-photon process

y	λ (Å)	$\psi(y)$
0.00	∞	0.000
0.05	24310	1.725
0.10	12160	2.783
0.15	8105	3.481
0.20	6078	3.961
0.25	4862	4.306
0.30	4052	4.546
0.35	3473	4.711
0.40	3039	4.824
0.45	2702	4.889
0.50	2431	4.907

The factor of 1/2 in equation (2.8) arises from the fact that two photons are emitted in the process.

Numerical integration yields the result $\int_0^1 \psi(y)\,dy = 3.770$ and hence

$$A_{2^2S,1^2S} = \frac{9\alpha^6\nu_H}{2^{11}} \times 3.770 = 8.23\ s^{-1}$$

Hence the lifetime of the metastable 2^2S level is

$$\Gamma_{2^2S} = \frac{1}{A_{2^2S,1^2S}} = 0.12\ s$$

Substituting values for the constants in equation (2.6) we have

$$A(y)\,(s^{-1}) = 4.366\psi(y) \tag{2.9}$$

If the total energy flux from the two-photon continuum incident on the neutral cloud is expressed as a multiple x of the incident energy flux due to the Hβ transition in the ionised region then

$$\int_0^{\nu_{12}} E(\nu)\,d\nu = xE_{H\beta} \tag{2.10}$$

$E(\nu)$ is the incident energy flux due to the hydrogen two-photon process (erg cm^{-2} s^{-1} Hz^{-1})
$E_{\mathrm{H}\beta}$ is the incident energy flux due to the Hβ transition (erg cm^{-2} s^{-1})

Now let $\nu = y\nu_{12}$ where $0 \leq y \leq 1$. The profile of $E(\nu)$ is the profile of $\psi(y)$ scaled by a constant energy factor E_0 so that

$$\int_0^{\nu_{12}} E(\nu)\, d\nu = \nu_{12} E_0 \int_0^1 \psi(y)\, dy \tag{2.11}$$

Hence from equations (2.10) and (2.11) we have

$$E_0 \text{ (erg cm}^{-2} \text{ s}^{-1} \text{ Hz}^{-1}) = \frac{x E_{\mathrm{H}\beta}}{\nu_{12} \int_0^1 \psi(y)\, dy} \tag{2.12}$$

The model of the ionised region of a PN constructed by Stasińska *et al.* and adopting the same star parameters and elemental abundances predicts that (Stasińska, private communication):

$$E_{\mathrm{H}\beta} = 0.5880 \quad \text{erg cm}^{-2} \text{ s}^{-1}$$

$$x = 7.554$$

Hence

$$E_0 = \frac{7.554 \times 0.5880}{2.47 \times 10^{15} \times 3.770} = 4.77 \times 10^{-16} \text{ erg cm}^{-2} \text{ s}^{-1} \text{ Hz}^{-1} \tag{2.13}$$

Converting from an energy flux to an energy density we have for the energy density from the hydrogen two-photon process at the interface between the ionised and neutral regions:

$$\Phi_0^{\text{H continuum}}(\lambda) = \frac{10^8}{\lambda^2} E_0 \psi\left(\frac{\lambda_{12}}{\lambda}\right) \qquad \text{for } \lambda \geq \lambda_{12} \tag{2.14}$$

λ_{12} is the wavelength of the Lyα transition ($\lambda_{12} = 1215.7$ Å)
λ is the wavelength under consideration (Å)
$\Phi_0^{\text{H continuum}}(\lambda)$ is the energy density produced from the hydrogen two-photon process (erg cm^{-3} Å^{-1})
E_0 is a constant ($E_0 = 4.77 \times 10^{-16}$ erg cm^{-2} s^{-1} Hz^{-1})

Linear interpolation is used to determine the values of $\psi(\lambda_{12}/\lambda)$ intermediate to the data points of Table 2.1.

2.1.3 Spectral line emission

As well as continuum emission in the form of the stellar background field and the hydrogen two-photon continuum the other contribution to the modelled incident radiation field arises from spectral line radiation emitted by the various chemical species in the ionised region.
Assuming that in the high temperature regime of the ionised region Doppler broadening of the spectral lines dominates over natural broadening (see also §2.3.4) then the spectral line profile will be of the form (see §2.3.4.1):

$$\phi_\nu^{\text{Doppler}}(\nu) = \frac{1}{\sqrt{2\pi}\sigma} \exp\left(-\frac{(\nu-\nu_0)^2}{2\sigma^2}\right) \tag{2.15}$$

where

$$2\sigma^2 = \frac{\nu_0^2}{c^2}\left(\bar{V}^2 + \frac{2kT}{M}\right) \tag{2.16}$$

T is the temperature of the gas in the ionised region (K)
M is the mass of the gas particle (g)
$\bar{V}$ is the mean turbulent velocity of material in the ionised region (cm s^{-1})

The profile has a full width to half maximum (FWHM) given by

$$\Delta\nu_D = 2(\log_e 2)^{\frac{1}{2}} \frac{\nu_0}{c} V_D \tag{2.17}$$

where

$$V_D = \left(\bar{V}^2 + \frac{2kT}{M}\right)^{\frac{1}{2}} \tag{2.18}$$

is the effective Doppler velocity of the chemical species combining thermal and turbulent motion.

Hence the energy flux from a particular spectral line incident on the neutral region is given by:

$$E(\nu)\,(\text{erg cm}^{-2}\ \text{s}^{-1}\ \text{Hz}^{-1}) = \frac{A}{\sqrt{2\pi}\sigma} \exp\left(-\frac{(\nu-\nu_0)^2}{2\sigma^2}\right) \tag{2.19}$$

A is a constant for a particular spectral line (erg cm^{-2} s^{-1})

Now let I be the total energy flux incident on the nebula due to a particular spectral line:

$$I = \int_{\text{line}} E(\nu)\,d\nu = \frac{A}{\sqrt{2\pi}} \int_0^\infty \exp\left(-\frac{(\nu-\nu_0)^2}{2\sigma^2}\right) d\nu \tag{2.20}$$

Making the substitution $\Lambda^2 = (\nu - \nu_0)^2/2\sigma^2$ we arrive at

$$I = \frac{A}{\sqrt{\pi}} \int_{\alpha}^{\infty} e^{-\Lambda^2} \, d\Lambda \tag{2.21}$$

where $\alpha = -\nu_0/\sqrt{2}\sigma = -c/V_D$

Hence

$$I = \frac{1}{2} A \left[1 + \mathrm{erf}\left(\frac{c}{V_D} \right) \right] \tag{2.22}$$

where $\mathrm{erf}(x)$ is the error function (see §6.2.2).

Now $V_D \ll c$ and it is an extremely good approximation to set $\mathrm{erf}(c/V_D) = 1$ so that we have simply

$$I = A \tag{2.23}$$

Now expressing the energy flux integrated over the spectral line as a multiple x of the incident energy flux from the Hβ line; $I = xE_{\mathrm{H}\beta}$, we have from equation (2.19):

$$E(\nu) = \frac{xE_{\mathrm{H}\beta}}{\sqrt{2\pi}\sigma} \exp\left(-\frac{(\nu - \nu_0)^2}{2\sigma^2} \right) \tag{2.24}$$

Converting the energy flux to an energy density and working in terms of wavelength we have as the profile of a particular spectral line:

$$\Phi_0^{\mathrm{line}}(\lambda) = \frac{xE_{\mathrm{H}\beta}\lambda_0}{\sqrt{\pi}V_D\lambda^2} \exp\left(-\frac{c^2(\lambda - \lambda_0)^2}{V_D^2\lambda^2} \right) \tag{2.25}$$

The model of the ionised region of a planetary nebula constructed by Stasińska *et al.* provides the required data on λ_0 and x for a large number of spectral lines (Stasińska, private communication). The model also predicts $E_{\mathrm{H}\beta}$ (§2.1.2).
The kinetic temperature assumed for Doppler velocity calculations was 10^4 K and a mean turbulent velocity of $\bar{V} = 8$ km s^{-1} was used to calculate V_D for each species in the ionised region.

The FWHM of each line is given by the expression

$$\Delta\lambda_D = 2(\log_e 2)^{\frac{1}{2}} \lambda_0 \frac{V_D}{c} \tag{2.26}$$

Appendix D contains data on each spectral line included in the initial radiation field.

2.2 General theory behind radiative transfer

The photons travelling by a point $\mathbf{r}$ at a time t will each have a different direction, denoted by the unit vector $\hat{\kappa}$ and a different frequency ν. The specific intensity $I_\nu(\hat{\kappa}, \mathbf{r}, t)$ of the radiation field is defined so that $I_\nu d\nu d\Omega dA dt$ is the energy of the photons which, in a time interval dt, pass through the area dA, whose frequency lie within the element $d\nu$ about ν and whose direction is within the solid angle $d\Omega$ about $\hat{\kappa}$. The vector area $d\mathbf{A}$ is located at the position $\mathbf{r}$ and is parallel to the photon direction $\hat{\kappa}$.
I_ν will be changed through interaction with matter and the amount of change is governed by the equation of transfer. Consider a small cylinder of length ds and cross-sectional area dA. The emission coefficient or emissivity $j_\nu(\hat{\kappa}, \mathbf{r}, t)$ is defined so that $j_\nu dV d\nu d\Omega dt$ is the energy emitted by the volume element dV ($dV = ds dA$) in the intervals $d\nu$, $d\Omega$ and dt. The absorption coefficient κ_ν is such that $\kappa_\nu I_\nu dV d\nu d\Omega dt$ is the corresponding energy absorbed from a beam of specific intensity I_ν. The change of I_ν along a distance ds is then

$$\frac{dI_\nu}{ds} = -\kappa_\nu I_\nu + j_\nu \tag{2.27}$$

This is known as the equation of transfer.

The optical depth at the frequency ν, τ_ν, is defined by the expression:

$$d\tau_\nu = \kappa_\nu ds \tag{2.28}$$

All processes which, in some way or another, remove energy from the flux of radiation will contribute to the optical depth through the cloud. For the purposes of the model this includes UV continuum absorption by dust grains, UV line absorption by H_2 and CO and line absorption in the Lyman lines of H.
If we consider the radiation received from a region or cloud of total optical depth τ'_ν at a frequency ν then equation (2.27) may be integrated to yield:

$$I_\nu = I_\nu(0)e^{-\tau'_\nu} + \int_0^{\tau'_\nu} \frac{j_\nu}{\kappa_\nu} e^{-\tau_\nu} d\tau_\nu \tag{2.29}$$

$I_\nu(0)$ represents the specific intensity of radiation incident on the cloud where the optical depth is defined as zero

What is being studied in this model is a planetary nebula - an expanding cloud of gas and dust at the centre of which is an extremely hot star. The radiation field

relevant to the model is the outgoing flux of ultraviolet radiation from the central star and a primary function of the model is to record how the UV radiation field is diluted and attenuated as it passes through, and eventually out of, the nebula. An accurate representation of the UV field is required in order to model the interaction between matter and the photon flux as accurately as possible. Within this context, since the atoms and molecules that absorb UV radiation will tend to decay back to the ground state via radiative cascade through one or more intermediate levels emitting radiation of much lower frequency (generally in the optical or infrared region of the spectrum), the amount of UV light re-emitted will be very small. It is thus a reasonable approximation to ignore the contribution isotropic re-emission makes to the outgoing ultraviolet radiation spectrum and this is done in the model. Hence, under this assumption of ignoring the re-emitted, diffuse radiation field it follows that at every point in the nebula the situation may be regarded as a problem with plane-parallel geometry; radiation travelling in one single direction is incident on one side of a slab of gas and dust.

As well as being attenuated through absorption the radiation field is also diluted through the simple fact of spreading spherically outwards from the central source. Thus, under the assumption of ignoring the re-emitted UV field, the energy density of the radiation field will be modified as it passes through the nebula according to the formula:

$$\Phi(r, \lambda, \tau_\lambda) = \Phi_0(r_0, \lambda, \tau_\lambda = 0) e^{-\tau_\lambda} \left(\frac{r_0}{r}\right)^2 \tag{2.30}$$

$\Phi(r, \lambda, \tau_\lambda)$ is the radiation field energy density at a radial distance r from the central star (erg cm^{-3} Å^{-1})

$\Phi_0(r, \lambda, \tau_\lambda = 0)$ is the radiation field energy density incident on the nebula at some distance r_0 from the star where the optical depth τ_λ is taken to be zero

τ_λ is the optical depth through the nebula at a distance r from the central star as a function of wavelength λ

All the physics concerning the attenuation of the radiation field - line absorption by atoms and molecules and continuum absorption by photoionisation and dust grains is reflected in the value of τ_λ, the optical depth, and the difficulty in the radiative transfer problem arises through attempting to accurately model all the important absorption processes.

2.3 Ultraviolet line absorption

Because of the large abundance of the elements hydrogen, carbon and oxygen (§3.1.1) atomic hydrogen and the molecules H_2 and CO will exhibit large number densities in the nebula and will make the most important contribution to the attenuation of the radiation field, absorption by these species dominating over other much less abundant chemical species. Hence the model explicitly takes into account the various different UV transitions for these three species as an approximation to the effect of atomic and molecular line absorption on the spectrum of the radiation field.

The absorption of UV photons by these species will create absorption lines in the ultraviolet spectrum with a characteristic shape and width depending on the gas temperature (§2.3.4.1). It is important to model accurately how the radiation is absorbed over the entire line because as the photons penetrate further into the nebula the central core of the line tends to become saturated (i.e. is totally extinguished due to absorption). As the centre of the absorption line becomes more and more extinguished the line wings play an increasingly important rôle in the process of photodissociation of the molecules H_2 and CO. Hence the model computes the absorption effect of each UV transition of H, H_2 and CO over the entire (broadened) line.

2.3.1 H Lyman transitions

For the neutral hydrogen atom the Einstein spontaneous transition probability $A_{nL,n'L'}$ from a level with principal quantum number n and angular momentum quantum number L to a level with corresponding quantum numbers n', L' $(n' < n)$ are all of the order of 10^4 to 10^8 s^{-1} and hence the corresponding mean lifetime of the level nL, defined by:

$$t_{nL} = \frac{1}{\sum_{n'<n} A_{nL,n'L'}} \tag{2.31}$$

is of the order 10^{-4} to 10^{-8} s. For the hydrogen atom, a one-electron system, a permitted transition must obey the selection rule $\Delta L = \pm 1$ and hence the 2^2S level represents a metastable level in that the only level lower in energy is the ground 1^2S state which also exhibits L=0. A transition may occur with the emission of two photons with a probability of $A_{2^2S,1^2S} = 8.23$ s^{-1} (see also §2.1.2) and a corresponding mean lifetime of 0.12 s. In the nebular environment, even this lifetime is short compared with the mean lifetime of an H atom against photoionisation or radiative excitation to a higher lying energy level and hence the assumption is made that all the hydrogen atoms in the nebula are in the ground 1^2S state.

Under this (very accurate) approximation, the only transitions that need to be taken into account to model the effect of atomic H on the radiation spectrum are Lyman transitions; a transition from the level 1^2S to a state $n'L'$ where $n' > 1$. The situation being modelled is the molecular region of a planetary nebula and hence by implication the radiation field now contains no L_c radiation. Photoionisation of H thus plays no part in the model; UV line absorption is the only contribution atomic hydrogen makes to the radiative transfer.

To model this transfer effect the first 49 transitions in the Lyman series of H are considered (i.e. $n = 1 \rightarrow 2$, $n = 1 \rightarrow 3$ up to $n = 1 \rightarrow 50$). Appendix E contains a list of all the necessary data regarding these transitions.

For the Lyman series in H the absorption oscillator strength is given by the following formula (Menzel and Pekeris 1935):

$$f_{n=1,n'} = \frac{2^8 n'^5 (n'-1)^{2n'-4}}{3(n'+1)^{2n'+4}}$$

Values for the lifetimes of the upper electronic states of H were taken from Wiese *et al.* (1966).

2.3.2 H_2 ultraviolet line absorption

The model considers UV transitions in the H_2 molecule from the ground electronic state ($X^1\Sigma_g^+$) to the excited electronic states $B^1\Sigma_u^+$ and $C^1\Pi_u$. At the relatively low kinetic temperatures experienced in the molecular region of the PN, only the ground vibrational state (v=0) of the ground electronic state will be effectively populated and hence the situation is somewhat simplified by only considering transitions from the rotational levels of the ground electronic-vibrational state.

A line in the Lyman band ($X^1\Sigma_g^+ \rightarrow B^1\Sigma_u^+$) will arise when there is a transition from a rotational level J in the ground electronic-vibrational state to a ro-vibrational state $v'J'$ in the excited electronic state B. Due to transition selection rules the value of ΔJ ($\Delta J = J' - J$) must be +1 or -1, i.e. only the P(J) and R(J) branches will be seen in the Lyman absorption band. Because of conservation of angular momentum in a $\Sigma \rightarrow \Sigma$ transition, $\Delta J = 0$ (the Q(J) branch) is not allowed. For the Lyman absorption band the model considers all the rotational levels of the ground electronic-vibrational state up to J=14 (and hence J'=15 is the maximum value of J' considered in the $B^1\Sigma_u^+$ state). It also considers all possible vibrational levels in the excited state up to v'=33.

For the Werner band ($X^1\Sigma_g^+ \rightarrow C^1\Pi_u$) all possible ro-vibrational transitions are considered from $v = 0, J$ to $v'J'$ in the excited electronic state where $0 \leq J \leq 14$,

$0 \leq J' \leq 15$ and $0 \leq v' \leq 10$. Due to the transition being $\Sigma \rightarrow \Pi$ a ΔJ=0 transition is allowed and hence the P(J), R(J) and Q(J) branches will all be present in the absorption spectrum.
Some of the transitions to excited electronic states will result in dissociation of the molecule. This very important topic is discussed later (§2.5.2.1). The data for wavelength, lifetime and oscillator strength of each UV transition in H_2 were taken from Abgrall and Roueff (1989). Values of the dissociation probabilities of ro-vibrational levels in excited electronic states were taken from Abgrall *et al.* (1992).

2.3.3 CO ultraviolet line absorption

The model incorporates UV transitions in CO from the ground vibrational state in the ground electronic state ($X^1\Sigma^+$) to ro-vibrational levels in excited electronic states. Excited vibrational states up to v'=3 are considered for the P(J) and R(J) branches (and Q(J) branch for a $\Sigma \rightarrow \Pi$ transition). The data for all CO ultraviolet transitions covering the 48 observed bands of the molecule - the wavelength, absorption oscillator strength, lifetime and dissociation probability of the upper state - have been taken from Eidelsberg *et al.* (1991).
The line oscillator strength $f_{0J,v'J'}$ for each line is obtained from the measured band oscillator strength $f_{v=0,v'}$ using the formula (Schadee 1967):

$$f_{0J,v'J'} = f_{v=0,v'}(\lambda_0/\lambda_{0J,v'J'})(S_J/(2J+1)) \tag{2.32}$$

$\lambda_{0J,v'J'}$ is the wavelength of the transition $v = 0, J \rightarrow v'J'$
λ_0 is the band origin (defined as the wavelength of the fictitious transition $v, J = 0 \rightarrow v', J' = 0$)
S_J is the Hönl-London factor for the transition

The S_J factor is given by the formulae

$$S_J = J,\ (J+1)$$

for a P, R branch respectively of a $\Sigma \rightarrow \Sigma$ transition

$$S_J = \frac{(J-1)}{2},\ \frac{(2J+1)}{2},\ \frac{(J+2)}{2}$$

for a P, Q, R branch respectively of a $\Sigma \rightarrow \Pi$ transition.

The model considers transitions from all rotational levels in the ground electronic-vibrational state up to J=15. As with H_2, transitions to excited electronic energy states of the molecule may cause dissociation and this is discussed later (§2.5.2.2).

2.3.4 Profile of the absorption lines

A line transition is characterised by a particular wavelength λ_0 and the absorption (or emission) line produced will exhibit a characteristic broadened profile centred around the wavelength λ_0. There are several causes of line broadening but the two most dominant processes are Doppler broadening and natural broadening.

2.3.4.1 Doppler broadening

The atoms and molecules in the nebula are undergoing constant random motion in all directions. If thermodynamic equilibrium amongst the species is assumed then the particle motions will be governed by a Maxwellian distribution of velocities characterised by a single gas temperature T. By using the Doppler formula which relates frequency shift to radial velocity it is possible to derive the spectral line intensity distribution due to thermal motion of the gas particles:

$$\phi_\nu^{\text{Doppler}}(\nu) = \frac{1}{\sqrt{2\pi}\sigma} \exp\left(-\frac{(\nu-\nu_0)^2}{2\sigma^2}\right) \tag{2.33}$$

ν_0 is the central frequency of the transition (Hz)
ν is the frequency under consideration (Hz)

The parameter σ is given by:

$$2\sigma^2 = \frac{\nu_0^2}{c^2}\left(\bar{V}^2 + \frac{2kT}{M}\right) = \frac{\nu_0^2}{c^2}\left(\bar{V}^2 + V_{\text{thermal}}^2\right) = \frac{\nu_0^2}{c^2}V_D^2 \tag{2.34}$$

T is the temperature of the gas (K)
M is the mass of the gas particle (g)
$\bar{V}$ is the mean turbulent velocity of material in the nebula (cm s^{-1})

V_{thermal} is the thermal Doppler velocity of the species, given by the expression $V_{\text{thermal}} = (2kT/M)^{1/2}$. The effective Doppler velocity V_D is a combination of the thermal Doppler velocity and the macroscopic turbulent velocity of the gas where $V_D = (\bar{V}^2 + V_{\text{thermal}}^2)^{1/2}$. The value of the gas turbulent velocity is a free parameter and a value of $\bar{V}$ = 1 km s^{-1} has been adopted for the model.

The Doppler profile has a full width to half maximum (FWHM) given by

$$\Delta\nu_D = 2(\log_e 2)^{\frac{1}{2}} \frac{\nu_0}{c} V_D \tag{2.35}$$

or equivalently, in terms of the wavelength:

$$\Delta\lambda_D = 2(\log_e 2)^{\frac{1}{2}} \frac{\lambda_0}{c} V_D \tag{2.36}$$

2.3.4.2 Natural broadening

The uncertainty principle implies that a molecular level will have a certain energy width. If the molecule remains in an excited state for a duration Δt then the spread in energy ΔE must satisfy $\Delta E \Delta t \sim \hbar$. The spontaneous decay of a molecule in an excited state j proceeds at a rate

$$\Gamma\,(\mathrm{s}^{-1}) = \sum_i \mathrm{A}_{ji} \tag{2.37}$$

A_{ji} is the Einstein coefficient for the spontaneous transition $j \rightarrow i$ (s^{-1})

The sum is over all states i of lower energy than state j. If radiation is present stimulated emission should be included in the sum. The coefficient of the wave function of state j is therefore of the form $e^{-\Gamma t/2}$ and leads to a decay of the electric field by the same factor. The emitted or absorbed spectrum is thus determined by the decaying sinusoidal type of electric field and hence the profile of the broadened line has the form

$$\phi_\nu^{\text{natural}}(\nu) = \frac{\Gamma/4\pi^2}{(\nu - \nu_0)^2 + (\Gamma/4\pi)^2} \tag{2.38}$$

and is evidently Lorentzian in form.

If both the upper and lower states of the transition are broadened then we have

$$\Gamma = \Gamma_u + \Gamma_l = \frac{1}{t_u} + \frac{1}{t_l} \tag{2.39}$$

t_u (t_l) is the mean lifetime of the molecule in the upper (lower) state (s)

For the intensity distribution governed by natural broadening the FWHM is given by

$$\Delta\nu_L = \frac{\Gamma}{2\pi} \tag{2.40}$$

or equivalently, in terms of wavelength:

$$\Delta\lambda_L = \frac{\lambda_0^2}{2\pi c}\Gamma \tag{2.41}$$

2.3.4.3 Combined Doppler and natural broadening

When the Doppler frequency shift $\Delta\nu_D$ is taken into account in calculating a Lorentz dispersion profile, combining equations (2.33) and (2.38) gives the overall spectral line intensity distribution function:

$$\phi_\nu(\nu) = \int_{-\infty}^{\infty} \frac{\Delta\nu_L \exp(-\Delta\nu^2/\Delta\nu_D^2)}{2\pi\sqrt{\pi}\Delta\nu_D[(\nu - \nu_0 - \Delta\nu)^2 + (\Delta\nu_L/2)^2]}\, d(\Delta\nu) \tag{2.42}$$

This result may be more compactly written by making use of the Voigt function (see e.g. Lang 1986):

$$H(a,b) = \frac{a}{\pi}\int_{-\infty}^{\infty} \frac{e^{-x^2}}{(b-x)^2 + a^2}\, dx \tag{2.43}$$

where

$$a = \frac{(\log_e 2)^{\frac{1}{2}}}{2}\frac{\Delta\nu_L}{\Delta\nu_D}$$

$$b = 2(\log_e 2)^{\frac{1}{2}}\frac{(\nu - \nu_0)}{\Delta\nu_D} \tag{2.44}$$

The line, broadened by thermal and natural processes, is now described as having a Voigt profile and the line intensity distribution is given by

$$\phi_\nu(\nu)\,(\mathrm{s}) = \frac{2(\log_e 2)^{\frac{1}{2}}}{\sqrt{\pi}\Delta\nu_D} H(a,b) \tag{2.45}$$

The form of equation (2.45) is chosen so that the intensity profile is normalised to unity:

$$\int_{\text{line}} \phi_\nu(\nu)\, d\nu = 1$$

The profile $\phi_\nu(\nu)$ may thus be thought of as a probability distribution; $\phi_\nu(\nu)d\nu$ represents the probability that, in making a line transition, the photon emitted (or absorbed) was in the frequency range ν to $\nu + d\nu$ where the probability is obviously peaked at the transition frequency ν_0.

2.3.5 Attenuation of radiation through spectral line absorption

Continuum absorption by dust and line absorption by H, H_2 and CO are the processes considered in the model whereby the outgoing radiation field is attenuated. Chapter 7 contains a full discussion of the assumed dust physical and optical properties and the consequent attenuating effect.

Let X be a species absorbing radiation through UV line absorption. In the context of the model X may represent atomic H in the ground state or H_2 or CO in a rotational level of the ground electronic-vibrational state. For each spectral line associated with species X the radiation field will be attenuated according to the formula:

$$\Phi(\lambda) = \Phi_0(\lambda) \exp\left(-\frac{\pi e^2}{m_e c} f_{0J,v'J'} \frac{\lambda^2}{c} \phi_\lambda(\lambda) N(\mathrm{X})\right) \tag{2.46}$$

$f_{0J,v'J'}$ is the absorption oscillator strength of the transition from $v = 0, J$ in the ground electronic state to the level $v'J'$ in an excited electronic state

$N(\mathrm{X})$ is the column density of species X (where X may represent H_2 or CO in a particular rotational level J) (cm^{-2})

$\phi_\lambda(\lambda)$ is the intensity distribution (Voigt profile) of the spectral line as a function of λ. The functions ϕ_ν and ϕ_λ are related by:

$$\phi_\lambda(\lambda) = \frac{c}{\lambda^2} \phi_\nu(\nu) \tag{2.47}$$

The quantity

$$\sigma_{0J,v'J'}(\nu)\,(\mathrm{cm}^2) = \left(\frac{\pi e^2}{m_e c}\right) f_{0J,v'J'} \phi_\nu(\nu) \tag{2.48}$$

represents the absorption cross-section for the transition $v = 0, J \rightarrow v'J'$ at the frequency ν. The Voigt function $\phi_\nu(\nu)$ is calculated in the model according to a numerical scheme to be found in the literature (Drayson 1976).

At each point in the nebula, by considering a thin slab of gas and dust, the equilibrium number densities of all the chemical species assumed to be present may be calculated (see Chapter 3). Since only a small portion of gas is being considered at any one point it is assumed the number densities of the species are constant within the slab and hence the column density of each species through the slab may be computed. This result may then be used in equation (2.46) to determine the attenuation of the UV field from spectral line absorption.

2.4 Photodissociation of H_2 and CO

Being the two most abundant molecular species the photodissociation of H_2 and CO plays a very important rôle in the chemical balance of the nebula. Chemical reactions with these molecules and their constituent atomic forms hydrogen, carbon and oxygen will dominate the chemical reaction network. Hence accurate modelling of the photodissociation process and a determination of the atomic/molecular transition region is necessary in order to produce reliable figures for the column densities of all the chemical species to compare with observations.

2.4.1 Photodissociation processes

The photodissociation of a diatomic molecule may proceed in various ways, as reviewed by van Dishoeck (1988). Figure 2.1 summarises the processes by which the molecule may dissociate and these may be categorised as direct photodissociation where absorption occurs directly into a repulsive potential or indirect photodissociation where the molecule is initially raised to a bound discrete excited state and consequently interacts with the continuum of a dissociating state.

Direct photodissociation (Figure 2.1(a)) is the simplest process and is the dominant route for a number of astrophysically important molecules such as H_2^+, CH^+ and H_2O. The cross-section for direct photodissociation is continuous as a function of wavelength and its shape reflects that of the vibrational wave function for the lower state.

Figure 2.1(b) illustrates the process of predissociation where the bound potential curve intersects the curve for a repulsive state of different symmetry. A transition may occur to a ro-vibrational level of the bound state such that the molecular wave function in this level is large at the corresponding point on the repulsive curve (generally near the intersection point). In this case there is a certain probability that curve-crossing will occur via a radiationless transition to the continuous curve thus causing dissociation of the molecule. The cross-section in this case consists of a set of discrete peaks broadened by the predissociation process. The photodissociation of the CO molecule proceeds by this route.

A molecule may also dissociate through coupled states photodissociation. In this process (Figure 2.1(c)) the bound level of an excited state couples with the continuum of a dissociative state of the same symmetry. The photodissociation of OH and CH proceeds in this manner. The cross-section generally consists of a continuous background on which is superposed a series of resonances, although the shape will depend on the details of the molecular structure.

Figure 2.1

Processes causing photodissociation of diatomic molecules
(from van Dishoeck 1988)

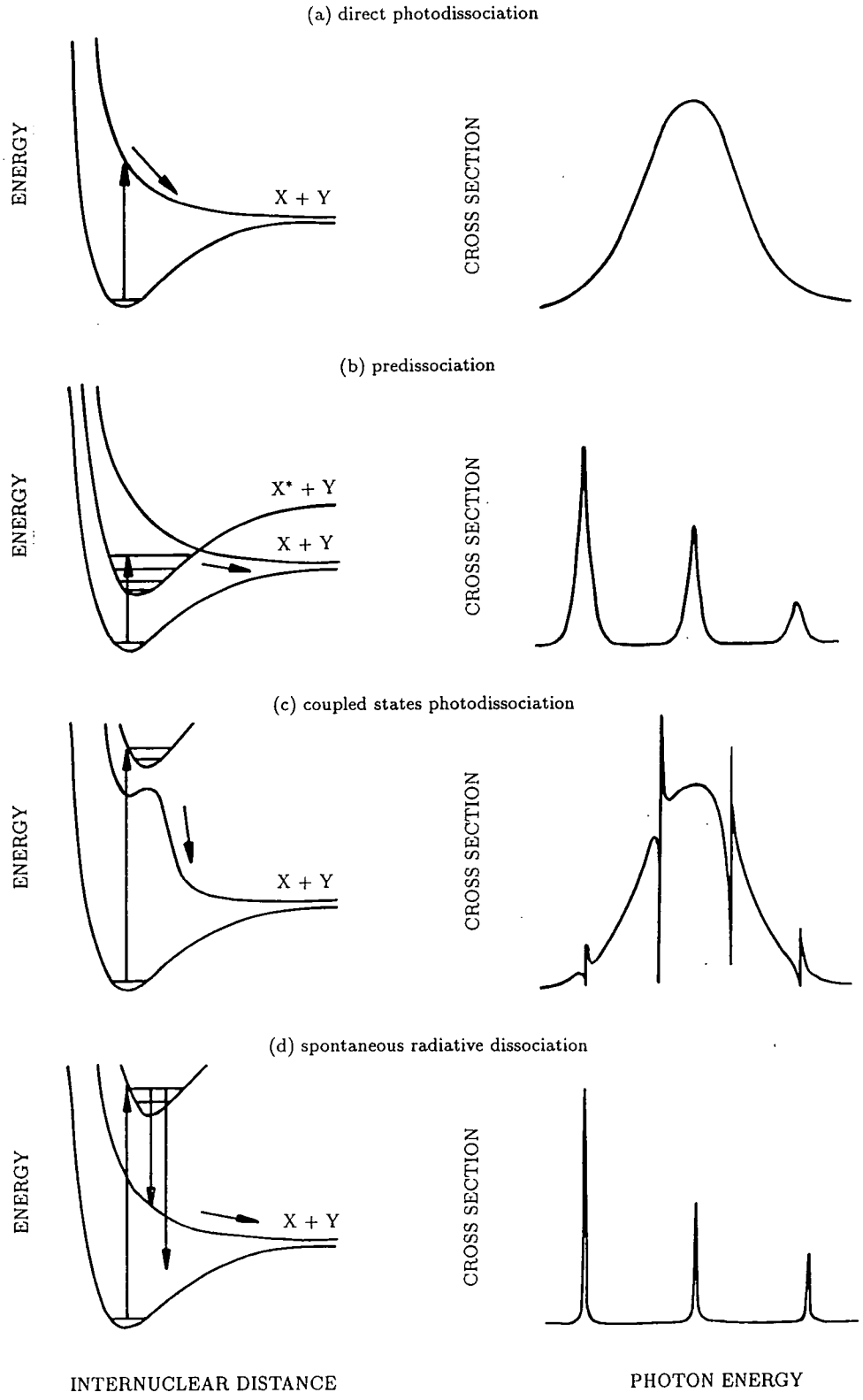

The last example of indirect photodissociation is when the bound excited state simply decays by spontaneous emission to a lower-lying continuum state (Figure 2.1(d)). This process represents the dissociation route for H_2, the most abundant molecule in the nebula. In this case the cross-section consists of a series of sharp, discrete peaks widened due to the natural radiative lifetimes of the upper levels.

2.4.2 Calculation of photodissociation rates

2.4.2.1 Photodissociation of H_2

The photodissociation of H_2 occurs through ultraviolet absorption in the discrete lines of the Lyman ($B^1\Sigma_u^+$ - $X^1\Sigma_g^+$) and Werner ($C^1\Pi_u$ - $X^1\Sigma_g^+$) band systems followed by spontaneous emission towards the vibrational continuum of the ground electronic state ($v > 14$ or with $J > 5$ for $v = 14$). Dalgarno *et al.* (1970) identified this continuous emission in laboratory spectra and recent observations have detected the emission in diffuse interstellar regions (Martin *et al.* 1990).
Each ro-vibrational level $v'J'$ in an excited electronic (B or C) state exhibits a certain probability $p^{\rm dis}_{v'J'}$ that subsequent spontaneous emission will occur to the vibrational continuum of the ground electronic state thus causing dissociation of the molecule. Values of $p^{\rm dis}_{v'J'}$ have been calculated by Abgrall *et al.* (1992) for the various ro-vibrational levels in the B and C excited states of H_2. The rate of photodissociation of H_2 is then given by:

$$\zeta^{\rm dis}_{\rm H_2}\,({\rm s}^{-1}) = \sum_{J=0}^{J_{\rm max}} \left(f_J \sum_E \sum_{v'J'} \zeta_{0J,v'J'} p^{\rm dis}_{v'J'} \right) \tag{2.49}$$

f_J is the fraction of H_2 molecules in rotational level J of the ground electronic-vibrational state
$\zeta_{0J,v'J'}$ is the rate of absorption in a particular line of the Lyman or Werner band from $v = 0, J$ in the ground state to $v'J'$ in the excited electronic state E (B or C state) (s^{-1})

Calculations are performed in the model to accurately determine the equilibrium rotational population f_J of the H_2 molecule (§4.1). The assumption is made that only the ground vibrational state ($v = 0$) of the molecule is effectively populated.
$\zeta_{0J,v'J'}$, the rate of line absorption, is given by the expression

$$\zeta_{0J,v'J'}\,({\rm s}^{-1}) = {\rm B}_{0J,v'J'} \int_{\lambda_{\rm H}}^{\infty} \Phi(\lambda) \frac{\lambda^2}{c} \phi_\lambda(\lambda)\, d\lambda \tag{2.50}$$

λ_H is the wavelength representing the Lyman limit of atomic hydrogen (λ_H = 912 Å)
$B_{0J,v'J'}$ is the Einstein coefficient for absorption in the line $v = 0, J$ to $v'J'$ in the excited electronic state E ($cm^3\ erg^{-1}\ s^{-2}$)
$\Phi(\lambda)$ is the local radiation field energy density ($erg\ cm^{-3}\ Å^{-1}$)
$\phi_\lambda(\lambda)$ is the normalised Voigt function for the transition $v = 0, J$ to $v'J'$ (§2.3.4.3) ($Å^{-1}$)

The Einstein B coefficient for absorption is related to the corresponding absorption oscillator strength by (e.g. McDaniel 1989):

$$B_{0J,v'J'} = \left(\frac{\pi e^2}{m_e c}\right) f_{0J,v'J'} \frac{\lambda_0}{h} \tag{2.51}$$

$f_{0J,v'J'}$ is the absorption oscillator strength for the transition $v = 0, J$ to $v'J'$
λ_0 is the wavelength of the transition

Values for the oscillator strengths and wavelengths of the relevant UV transitions in H_2 were taken from Abgrall and Roueff (1989). By taking into account all important contributions to the radiative transfer (UV line absorption by H, H_2 and CO and continuum absorption by dust grains) the function $\Phi(\lambda)$ is known at all points in the nebula. Since the Voigt function $\phi_\lambda(\lambda)$ can be calculated (§2.3.4.3) all the variables are known in order to calculate $\zeta_{0J,v'J'}$ from equation (2.50) and thus it is possible to compute the total photodissociation rate of H_2 at a point in the cloud from equation (2.49).

2.4.2.2 Photodissociation of CO

Letzelter *et al.* (1987) carried out high resolution spectroscopy on the CO molecule in the vacuum ultraviolet. Combining this with measurements of band oscillator strengths and fluorescence yields led to the conclusion that photodissociation proceeds through sharp predissociated lines rather than through a continuum. Using these experimental results along with data obtained by Eidelsberg and Rostas (1990) these workers calculated the parameters of all the relevant UV transitions in CO - wavelength, absorption oscillator strength and lifetime and dissociation probability of the upper level (Eidelsberg *et al.* 1991).
Exactly as in equation (2.49) for H_2, the rate of photodissociation of the CO molecule is given by:

$$\zeta_{CO}^{dis}\ (s^{-1}) = \sum_{J=0}^{J_{max}} \left(f_J \sum_E \sum_{v'J'} \zeta_{0J,v'J'} p_{v'J'}^{dis} \right) \tag{2.52}$$

$p^{\rm dis}_{v'J'}$ is equation (2.52) now obviously represents the dissociation probability for the CO molecule in the excited state $v'J'$.

As with H_2 detailed calculations are performed in the model to determine the equilibrium rotational population of CO so that the values of f_J in equation (2.52) are known. Again, the assumption is made that in the relatively cold nebular environment only the ground electronic-vibrational state is effectively populated. $\zeta_{0J,v'J'}$, the rate of line absorption for CO, is given by an expression as for equation (2.50):

$$\zeta_{0J,v'J'}\,({\rm s}^{-1}) = {\rm B}_{0J,v'J'} \int_{\lambda_{\rm H}}^{\infty} \Phi(\lambda) \frac{\lambda^2}{c} \phi_\lambda(\lambda)\, d\lambda \qquad (2.53)$$

$\phi_\lambda(\lambda)$ is equation (2.53) represents the normalised Voigt function appropriate to the CO molecule.

Chapter 3

Chemistry in the nebula

3.1 Chemical composition

The set of neutral and ionised atoms and molecules that are assumed to exist in the molecular region of the planetary nebula being modelled are listed in Appendix A. Only a fairly small minority of the molecular species listed have actually been positively detected in the PN environment. For the majority of species their existence in the nebula is at best very probable given our current knowledge of likely gas phase chemical routes, and at worst only speculative. The observational evidence for a selection of molecules is discussed below.

CO emission from planetary nebulae was first detected by Mufson *et al.* (1975) from NGC 7027. Since then this PN has proved to be a very rich source for molecular observation. H_2 and CO emission was detected from this nebula by Treffers *et al.* (1976). A number of other molecules have been detected in this nebula including HCN (Olofsson *et al.* 1982), ^{13}CO (Thronson and Mozurkewich 1983), C_3H_2 (Cox *et al.* 1987) and HCO^+ (Deguchi *et al.* 1990).

Moorhead *et al.* (1988) searched the spectrum of NGC 7027 for the R(0) line of the fundamental vibration-rotation band of the molecular ion HeH^+ with negative results. Thronson and Bally (1986) made a search for millimetre-wave emission from nine molecules in NGC 7027: CN, CS, C_2H, HC_3N, SiS, $C^{18}O$, SiCC, $^{13}CH_3OH$ and H_2CO. A search was also made for the J, K= (1,1) line of NH_3 and the $J = 21 \rightarrow 20$ transition of HC_7N at 1.3 cm. From this analysis only the $N = 1 \rightarrow 0$ line of CN was positively detected. To explain the non-detection of any CS or NH_3 lines Thronson and Bally suggested it may be the case that the density is so low in the molecular cloud of NGC 7027 that for CS and NH_3 the excitation of the molecules is insufficient for detection of the lines.

CO is the hardiest of molecules and has been detected and mapped in a large number of planetary nebulae. Forveille and Huggins (1991) mapped the $J = 2 \rightarrow 1$ emission of CO in five planetary nebulae: M1-7, M4-9, M2-51, NGC 7293 and VV 47. Bachiller *et al.* (1989) mapped the CO $J = 2 \rightarrow 1$ and $J = 1 \rightarrow 0$ emission of CO in the bipolar planetary nebula NGC 2346. They discovered the CO gas to have a clumped structure with the more prominent clumps concentrated on an expanding ring surrounding the central star. They also detected ^{13}CO, HCN, HNC and HCO^+ emissions from one of the clumps.

Huggins and Healy (1989) carried out a survey in the 230 GHz CO ($J = 2 \rightarrow 1$)

line in 100 planetary nebulae. Nineteen of the objects observed showed evidence of CO emission, primarily younger disk population objects formed from high-mass progenitor stars. Very strong radio emission from CO ($J = 1 \rightarrow 0$ and $J = 2 \rightarrow 1$) and weak emission from HCO^+ and ^{13}CO was detected from the very compact PN IRAS 21282+5050 by Likkel *et al.* (1988). This source is noted for having unusually strong features between 3 μm and 15 μm, now believed to be indicators of the presence of PAH (Polycyclic Aromatic Hydrocarbon) molecules (§5.1.1). Observations at the frequencies of the maser lines of H_2O and OH were made with no detection. These workers also report negative detection for the molecules HCN, H_2S and SO_2.

Molecular observations of PNe provide evidence of the history of the central star and imply that the AGB envelope is the direct precursor to the PN phase. OH maser emission is seen in oxygen-rich AGB envelopes, proto-PNe and young PNe as well as in Vy 2-2 and OH0.9+1.3 which have been mapped at high resolution (Shepherd *et al.* 1990).
A rich chemistry takes place in the thick envelopes of AGB stars and this is reflected in molecular observations of young PNe. Fourteen molecular species have been detected in the very young PN CRL 618 (e.g. Bujarrabal *et al.* 1988) where the molecular shell still retains some of the AGB characteristics. Fewer species are seen in more evolved objects but six (H_2, CO, HCN, HNC, CN and HCO^+) have now been detected in NGC 6072 and IC 4406 (Cox *et al.* 1992) where the central stars are now on their cooling tracks ($T_* \approx 10^5$ K) and the envelopes have developed well beyond the AGB phase.

3.1.1 Elemental abundances

Aller and Czyzak (1983) analysed image-tube scanner measurements and IUE data to establish the chemical composition of 41 planetary nebulae. The mean elemental abundances they deduced from this sample are shown below (relative to a value of unity for hydrogen). Their observations included many objects of high surface brightness and hence the chemical compositions reflect this bias.

H	1.00	S	1.00×10^{-5}
He	0.110	Ar	2.69×10^{-6}
C	7.76×10^{-4}	Na	1.51×10^{-6}
O	4.37×10^{-4}	Cl	1.66×10^{-7}
N	1.82×10^{-4}	Ca	1.07×10^{-7}

Ne	1.07×10^{-4}	K	8.91×10^{-8}

Based on observations made at the National Astrophysical Observatory (LNA) in Brazil, de Freitas Pacheco *et al.* (1992) analysed the chemical abundances of 33 southern planetary nebulae. The mean elemental abundances have been calculated from their reported data and are shown below, relative to a value of unity for hydrogen.

H	1.00	Ne	1.39×10^{-4} **
He	0.109	S	9.55×10^{-6} ***
O	6.40×10^{-4} *	Ar	3.75×10^{-6}
N	1.99×10^{-4}		

* Lower limit since observations of NGC 4361 (included in the mean) yielded O/H $\geq 1.90\times10^{-4}$

** Based on observations of 8 planetary nebulae. Lower limit since observation of NGC 4361 (included in the mean) yielded Ne/H $\geq 3.24\times10^{-5}$

*** Based on observations of 23 planetary nebulae

The data on individual nebulae from these workers displays the clear trend that N/O increases with He/H reflecting the enrichment in He and N due to the dredge-up episodes in the PN progenitor stars as proposed by theory (Renzini and Voli 1981; Peimbert 1992).

Chemical abundance analyses of individual nebulae are numerous in the literature. Based on 15 IUE spectra and on other observations, Harrington *et al.* (1982) constructed a detailed model of the PN NGC 7662. The model incorporated a stellar flux interpolated from LTE model atmosphere results and included radiation attenuation by dust where the grains were assumed to be graphitic. In order to obtain satisfactory agreement with the observed spectra from the nebula these workers found that the following elemental abundances were required.

H	1.0	Ne	7.0×10^{-5}
He	0.094	S	1.5×10^{-5}
C	6.2×10^{-4}	Si	6.0×10^{-6}
O	3.6×10^{-4}	Mg	8.0×10^{-7}
N	6.0×10^{-5}		

As these results show and theory suggests, the elements with pronounced abundances in nebulae are those involved in the CNO star cycle. However, radical

differences in the elemental composition of planetary nebulae do exist. Some objects are especially rich in nitrogen e.g. NGC 6302, NGC 2440 and HU1-2 (Aller *et al.* 1981; Marionni and Harrington 1981) while many observed PNe are especially rich in carbon. The CNO cycle favours nitrogen at the expense of carbon and current theory is that nitrogen-rich nebulae have conveyed the products of the CNO cycle to the surface. Carbon enrichment implies that helium burning products reached the surface. Observations of planetary nebulae frequently show excess of carbon in the nebular envelopes. Combining this with frequent observation of infrared emission implying solid carbon grains (§5.2.1) and that the spatial distribution of planetary nebulae resembles that of carbon stars gives credence to the theory that carbon stars are the immediate precursor to planetary nebulae. The popular theory is that a red giant star evolves then may change from an M star to a carbon star and then evolves into a planetary nebula. This theory is obviously not complete as not all PNe are observed to be carbon-rich although the C/O ratio is frequently enhanced, e.g. for the data of Aller and Czyzak above C/O= 1.78 and for Harrington *et al.* C/O= 1.72 for NGC 7662.

Although observations of chemical abundances in PNe seem to follow certain recurrent patterns there is clearly considerable flexibility in what values to adopt for elemental abundances. Since this model of the molecular shell of a planetary nebula employs results produced from a model of the ionised region of a planetary nebula (Stasińska, private communication), consistency between the two models with regard to elemental abundances is obviously desirable. The abundances used in the model are set out below. Iron is the representative metal in the model.

H	1.00	N	2.00×10^{-4}
He	0.100	S	1.00×10^{-5}
C	7.00×10^{-4}	Fe	3.00×10^{-7}
O	4.00×10^{-4}		

3.1.2 Initial chemical abundances

After being given the initial conditions relevant to the ionised/neutral interface the model solves the set of chemical reactions iteratively under the assumption of steady-state equilibrium at progressive stages through the nebula. It is required to supply data on the initial abundances of all the atomic and molecular species, neutral and ionised at the start of the molecular region.

The assumption is made that at the ionised/neutral interface photodissociation has destroyed the molecular species formed in and ejected from the precursor AGB

envelope and negligible amounts of the elements have re-formed into molecules; all the gas is atomic. The question as to whether the atomic form is predominantly neutral or ionised depends on the ionisation potential of the atom. Since hydrogen is by far the most abundant element in the nebula the approximation is made that all photons that can ionise hydrogen (i.e. with $\lambda < 912\,\text{Å}$) have been absorbed in this process in the ionised region. Hence atoms with an ionisation potential in excess of 13.6 eV (corresponding to $\lambda = \lambda_{\text{H}} = 912\,\text{Å}$) will be predominantly neutral at the interface whereas atoms with an ionisation potential below 13.6 eV will be predominantly singly ionised. Under this approximation carbon, sulphur and iron will exist in ionised form at the interface (having ionisation potentials of 11.26 eV, 10.36 eV and 7.87 eV respectively) and the other elements will exist in neutral form.

3.2 Chemical reactions

The model considers a chemical reaction set consisting of over one thousand two hundred reactions and these are set out in Appendix B with the associated rate coefficient for each reaction.

3.2.1 Reaction rate coefficients

The rapidity with which a particular reaction proceeds will depend on the abundances of the interacting species and on the rate coefficient associated with the reaction. Consider for example a particular molecule M being formed and destroyed by the following reactions (with corresponding rate coefficients shown in brackets):

$$\mathrm{A} + \mathrm{B} \rightarrow \mathrm{M} + \mathrm{N} \qquad (k_1 \ \mathrm{cm^3\ s^{-1}})$$

$$\mathrm{M} + \mathrm{X} \rightarrow \mathrm{Y} + \mathrm{Z} \qquad (k_2 \ \mathrm{cm^3\ s^{-1}})$$

$$\mathrm{M} + h\nu \rightarrow \mathrm{C} + \mathrm{D} \qquad (\zeta \ \mathrm{s^{-1}})$$

The rate of change of the number density of M, $n(\mathrm{M})$, is then given by:

$$\frac{dn(\mathrm{M})}{dt} = k_1 n(\mathrm{A}) n(\mathrm{B}) - k_2 n(\mathrm{M}) n(\mathrm{X}) - \zeta n(\mathrm{M}) \tag{3.1}$$

$n(\mathrm{P})$ is the number density of the general species P ($\mathrm{cm^{-3}}$)

Steady-state equilibrium occurs when $dn(\mathrm{M})/dt$=0.

The rate coefficients k_1 and k_2 are quantities which will functionally depend on the kinetic temperature of the interacting species which is assumed to be the same for all species (see discussion in Chapter 5). The coefficient ζ is for a photon process (ionisation for example) and will depend on the intensity of the local UV radiation field, the form of the spectrum and on the absorption cross-section of species M as a function of wavelength.

3.2.1.1 Computation of rate coefficients

Each atomic/molecular reaction is assumed to have a rate coefficient conforming to the general format:

$$k = \gamma \left(\frac{T}{300} \right)^{\alpha} \exp\left(-\frac{\beta}{T} \right) \tag{3.2}$$

k is the reaction rate coefficient ($cm^3\ s^{-1}$)
T is the gas kinetic temperature (K)

γ ($cm^3\ s^{-1}$), α and β (K) are parameters associated with the reaction chosen to make the value of k, as computed from equation (3.2), agree as closely as possible to the value of the rate coefficient as determined by quantum mechanical calculation or by experiment. Appendix B lists the values of α, β and γ appropriate to each reaction.
The pre-exponential factor T^{α} is in general a fairly slowly varying function of the kinetic temperature. It depends on the details of the collision such as the attractive long-range potential (Levine and Bernstein 1974) which in turn depends on the reacting species and whether they are electrically charged or not (§3.2.2).
Endothermic reactions and reactions with an activation energy will exhibit a non-zero value for the exponential factor β. If E is the endothermicity or activation energy of the reaction then the cross-section for the process will be zero unless the system possesses an energy $\geq E$. Due to the distribution of molecular speeds (assumed to be Maxwellian) this produces a rate coefficient of the form expressed in equation (3.2). If β ($\beta = E/k$) is such that $\beta \gg T$ then the rate coefficient will be negligible and unless the abundances of the interacting species are very high the reaction will not play a rôle in the chemistry. Exothermic ion-molecule reactions and some neutral reactions (usually involving radicals) do not exhibit activation energy barriers and hence tend to dominate the chemistry at low kinetic temperature.

The rate coefficient appropriate for a photoionisation process is defined by the following formula (e.g. van Dishoeck 1988):

$$\zeta\ (s^{-1}) = \frac{10^{-8}}{h} \int_{\lambda_H}^{\lambda_0} \lambda \Phi(\lambda) \sigma_\lambda \, d\lambda \qquad (3.3)$$

λ is wavelength (Å)
$\Phi(\lambda)$ is the local radiation field energy density (erg cm^{-3} $Å^{-1}$)
σ_λ is the photoionisation cross-section of the species under consideration as a function of wavelength (cm^2)

The integral in equation (3.3) extends from the Lyman limit of hydrogen λ_H to the threshold wavelength of the photoionisation process λ_0. If a species has an ionisation threshold below λ_H (e.g. H_2 which has an ionisation threshold of 805 Å) then ionisation will not occur in the nebula through absorption of UV radiation (although it can occur through other processes, primarily cosmic ray ionisation).

If photoionisation cross-section data is available in the literature then equation (3.3) is invoked in the model to compute the rate coefficient for the process at all points in the nebula, and if the cross-section data is reliable this represents the most accurate possible determination of the rate coefficient (see also §5.3.2).
If the threshold wavelength λ_0 is known for a particular photoionisation process but cross-section data is not available then the model assumes a 'standard' cross-section of 10^{-17} cm^2 between λ_H and λ_0 in order to estimate the photoionisation rate coefficient (see also Viala 1986).

For photodissociation processes (except the important cases of H_2 and CO) the rate coefficient is approximated by assuming an exponential decrease of an initial value due to absorption of radiation by dust grains:

$$\zeta\,(\mathrm{s}^{-1}) = \gamma(r)\zeta_0 \exp(-\beta\tau_V) \tag{3.4}$$

$\gamma(r)$ is a function of distance to take account of geometrical dilution
ζ_0 is the rate of the photodissociation reaction in the unattenuated interstellar radiation field (s^{-1})

The values of β taken for each photoreaction may be found in Appendix B.
The radiation field causing photoionisation and dissociation is being attenuated through dust absorption and because it is expanding away from the central star in a spherically symmetric way it is also being diluted in a $1/r^2$ manner. Hence calculation of rate coefficients for photoprocesses also includes multiplication by a global scaling parameter $\gamma(r)$ which is reduced on a $1/r^2$ basis.
Photodissociation is vital to the chemistry of the model and some justification is required to show that the simple exponential decay law for the photodissociation rate described above is sufficiently accurate. The values of the parameter β for the various photodissociated species will depend sensitively on how the dust grain opacity in the ultraviolet is modelled. This model of a PN has not assumed a 'standard' model of interstellar dust grains as other workers have done in the past because processes in the interstellar medium (e.g. supernovae shocks) are liable to alter the structure and size of the grains ejected from planetary nebulae (Hoare 1990). Instead the dust is modelled as amorphous carbon grains with a mean radius of 100 nm (Chapter 7). Because the grain model employed is not a standard model it is important to choose the values of β carefully; values applicable to absorption by interstellar grains are not necessarily applicable in this case.
The photoionisation cross-section of carbon was theoretically calculated by Hofmann *et al.* (1983) and this data is used in the model to calculate the rate according

to equation (3.3). Van Dishoeck (1988) reports values for ζ_0 and β for a number of important interstellar species which are photoionised or dissociated using dust grain models of Roberge *et al.* (1981). To see if the exponential law derived from this dust model is sufficiently accurate for use with the PN model presented here the photoionisation rate of carbon was calculated both ways through a modelled nebula with $n_{\rm H} = 1000$ cm^{-3} and total optical depth $\tau_V = 4$. The results are shown in Table 3.1.

Table 3.1
Comparison of photoionisation rate of carbon using 'exact' method and exponential formula

Optical depth τ_V	$\gamma(r)$	ζ (s^{-1})	
		'exact'	formula
0.0	10000	2.2×10^{-6}	2.2×10^{-6}
1.0	53.5	5.1×10^{-9}	4.0×10^{-9}
2.0	14.4	3.7×10^{-10}	3.7×10^{-10}
3.0	6.57	5.6×10^{-11}	5.7×10^{-11}
4.0	3.74	1.1×10^{-11}	1.1×10^{-11}

The formula reported by van Dishoeck for the photoionisation rate of carbon in an unattenuated interstellar radiation field is:

$$\zeta\,(\mathrm{s}^{-1}) = 2.2 \times 10^{-10} \exp(-1.07\tau_V)$$

and thus the formula rate has been calculated above according to:

$$\zeta\,(\mathrm{s}^{-1}) = \gamma(r) \times 2.2 \times 10^{-10} \exp(-1.07\tau_V)$$

The $\gamma(r)$ factor takes into account geometrical dilution of the radiation field which is expanding spherically outward from the star:

$$\gamma(r) = \gamma(r_0)\left(\frac{r_0}{r}\right)^2$$

where r_0 is the distance from the star to the ionised/neutral interface (at this point $\tau_V = 0.0$).

The $\gamma(r)$ factor also takes into account the fact that the radiation field in the modelled PN is far more intense than the interstellar radiation field (ISRF). This is incorporated in the value of $\gamma(r_0)$ which measures the ratio of the energy densities in the two different spectra:

$$\gamma(r_0) = \int_{\lambda_H}^{\lambda'} \Phi_0(\lambda)\, d\lambda \Big/ \int_{\lambda_H}^{\lambda'} \Phi_{ISRF}(\lambda)\, d\lambda$$

$\Phi_0(\lambda)$ is the energy density of the radiation field incident on the neutral region of the PN (§2.1) (erg cm^{-3} Å^{-1})
Φ_{ISRF} is the energy density of the mean interstellar radiation field (erg cm^{-3} Å^{-1})
λ_H is the Lyman limit of hydrogen

The upper limit λ' in the integrals was chosen to be 1500 Å as this then fully includes the spectrum of photoionising or dissociating radiation for most species of interest (e.g. the threshold wavelength for photoionisation of carbon is $\lambda_0 =$ 1101 Å). This choice of λ' also includes the very intense Lyα emission line at 1215 Å from atomic hydrogen in the ionised region (see Appendix D).
The mean ISRF in the wavelength region of interest has been estimated by many workers in the field. The ISRF used in the calculation of γ_0 must obviously be the same as that assumed by van Dishoeck in calculating the formulae for the photorates and this is the radiation field of Mathis *et al.* (1983). Using the function $\Phi_0(\lambda)$ calculated in Chapter 2 the value of γ_0 is very close to 10^4 (Table 3.1).
Examination of Table 3.1 shows that the rates calculated by 'exact' numerical integration and by the formula are extremely similar and using the formula for carbon photoionisation in the model would hardly introduce any error at all. This does not prove that similar formulae are as accurate in calculating photorates for other species but it does show that the grain characteristics modelled by Roberge *et al.* are sufficiently similar to the grain characteristics in this model that use of the simple exponential formula and the reported values of ζ_0 and β are justified for photodissociation processes where cross-section data is unavailable.

For the case of H_2 and CO calculations are performed in the model to determine the distribution of the molecules amongst the various rotational levels (see Chapter 4). Combining this with knowledge of absorption oscillator strengths and dissociation probabilities of excited ro-vibrational states enables a very accurate evaluation of the photodissociation rate of these two most important molecules at every point in the nebula (§2.5.2).

3.2.2 Varieties of chemical reaction

The varieties of reaction considered in the model are detailed below. Gas phase reactions alone are considered apart from the important case of hydrogen atoms interacting on the surface of dust grains to form the H_2 molecule. Rate coefficients for photoionisation and photodissociation processes are discussed in §3.2.1.1.

3.2.2.1 H_2 formation on dust grains

In order for two unbound hydrogen atoms with total energy E positive to form an H_2 molecule the system must lose energy in order for E to become negative. This may occur either through three-body collisions, the third body taking away the excess energy, or through radiative association. Transitions between the $^3\Sigma$ repulsive and $^1\Sigma$ attractive electronic potential curves of the molecule are forbidden to electric dipole radiation as they involve a change in the total spin quantum number. Further, radiative transitions involving the nuclear degrees of freedom are also forbidden as the H_2 molecule is homonuclear and does not possess a permanent dipole moment. Formation of H_2 by radiative association can in no way explain the observed high abundance of H_2 in nebulae or the interstellar medium. Three-body collisions involving two hydrogen atoms and a third molecule are extremely unlikely in the diffuse environment of the nebula and the current (and as yet only viable) theory for H_2 formation is by combination of two hydrogen atoms on a grain surface. The grain acts as a catalyst and plays the rôle of a third body in the reaction. The grain absorbs some of the formation energy of the molecule, the rest of the energy appearing as internal energy and translational kinetic energy of the H_2 molecule after being ejected from the grain surface (§5.3.4).
Hollenbach *et al.* (1971) studied quantitatively the formation of H_2 on grain surfaces. The rate of formation of H_2 molecules on grains can be written:

$$\left(\frac{dn(\mathrm{H_2})}{dt}\right)_{\mathrm{grain}} = \frac{1}{2}\gamma < v_{\mathrm{H}} >< n_d\sigma_d > n(\mathrm{H}) \qquad (3.5)$$

γ is a recombination coefficient
$< v_{\mathrm{H}} >$ is the mean thermal velocity of a hydrogen atom (cm s^{-1})
$< n_d\sigma_d >$ is the mean value of the absorption coefficient due to dust; n_d is the number density of dust grains and σ_d is the mean geometric cross-section of a dust grain (cm^{-1})
$n(\mathrm{H})$ is the number density of hydrogen atoms (cm^{-3})

The factor γ represents the fraction of H atoms striking a grain which eventually form a molecule. It will depend in a complicated manner on the properties of the grain surface, the gas and grain temperatures and on the interaction forces between H, H_2 and the grain surface.
Following Viala (1986) it is assumed that in the relatively low temperature conditions of the nebula the process has a maximum efficiency so that $\gamma = 1$.
Since a Maxwellian velocity distribution is assumed then (e.g. Mandl 1978):

$$< v_{\rm H} >= \left(\frac{8kT}{\pi m_{\rm H}}\right)^{\frac{1}{2}} \tag{3.6}$$

An expression for $< n_d \sigma_d >$ is derived in Chapter 5 (§5.2.3) in the context of photoelectric emission from dust grains. The expression is given by:

$$< n_d \sigma_d >= \frac{1.05 m_{\rm H} n_{\rm H} \Upsilon}{r_d \rho_d} \tag{3.7}$$

$m_{\rm H}$ is the mass of a hydrogen atom (g)
$n_{\rm H}$ is the number density of hydrogen nuclei ($\rm cm^{-3}$)
Υ is the mass ratio of dust to gas in the nebula
r_d is the mean radius of a dust grain (cm)
ρ_d is the mass density of the material composing the grains ($\rm g\ cm^{-3}$)

Substituting equations (3.6) and (3.7) into equation (3.5) we have:

$$\left(\frac{dn(\rm H_2)}{dt}\right)_{\rm grain} = 1.485 \frac{\gamma \Upsilon}{r_d \rho_d} \left(\frac{m_{\rm H} k}{\pi}\right)^{\frac{1}{2}} n_{\rm H} n({\rm H}) T^{1/2} \tag{3.8}$$

Values for Υ, r_d and ρ_d are derived in Chapter 7 based on assumptions about dust grain properties and nebular composition. These quantities have been assigned the following values (§7.1):

$$\Upsilon = 0.002$$

$$r_d = 100\ \rm nm$$

$$\rho_d = 1.8\ \rm g\ cm^{-3}$$

Substituting these values, and values for the physical constants, into equation (3.8) we have, assuming that $\gamma = 1$

$$\left(\frac{dn(\rm H_2)}{dt}\right)_{\rm grain} = 1.41 \times 10^{-18} n_{\rm H} n({\rm H}) T^{1/2} \tag{3.9}$$

for the rate of formation of H_2 molecules on dust grains.

3.2.2.2 Cosmic ray interactions

The flux of cosmic rays (primarily high energy protons) penetrating the nebula is a significant source of ionisation and dissociation of the molecular species. The ionisation caused by cosmic rays initiates some important chemical processes in the nebula. Indeed, photoionisation of H and H_2 the two most important species, cannot occur since no L_c radiation exists in the molecular region. For the carbon, oxygen and nitrogen chemistries to proceed effectively a certain fraction of hydrogen must be maintained in the ionised form of H^+ and H_2^+. With no possibility of photoionisation cosmic ray interactions provide the dominant route to these ions:

$$\mathrm{H} + \text{c.r.p.} \rightarrow \mathrm{H}^+ + e^- + \text{c.r.p.}$$

$$\mathrm{H_2} + \text{c.r.p.} \rightarrow \begin{cases} \mathrm{H_2^+} + e^- + \text{c.r.p.} \\ \mathrm{H^+} + \mathrm{H} + e^- + \text{c.r.p.} \\ \mathrm{H} + \mathrm{H} + \text{c.r.p.} \end{cases}$$

Accurate determination of the local interstellar flux of cosmic rays near the Earth is difficult because modulation by the solar wind leads to uncertainties in the measurements for proton energies below 100 MeV. Since this flux may well vary through the rest of the Galaxy anyway the ionisation rate of hydrogen ζ_0 is taken as a free parameter in the model. The canonical value chosen is based on a recent analysis by van Dishoeck and Black (1986) which suggests a typical primary hydrogen ionisation rate of $\zeta_0 = 4 \times 10^{-17}$ s^{-1}.
The rates of other cosmic ray induced processes relative to the ionisation rate of atomic hydrogen were taken primarily from Gredel *et al.* (1989) and Prasad and Huntress (1980). The flux of cosmic rays and consequent ionisation/dissociation rates are assumed uniform throughout the whole nebula which is a reasonable approximation according to the work of Cesarsky and Völk (1978).

3.2.2.3 Ion-molecule reactions

Because of the enhanced collision cross-section due to Coulomb attraction between the ion and the molecule reactions of this type will be of extreme importance in the reaction network. Laboratory studies of ion-molecule reactions show that in the majority of exothermic reactions, but not in all, the rate coefficient has a value practically independent of temperature and is usually of the order of 10^{-9} cm^3 s^{-1} (Duley and Williams 1984).

Classical theory provides some insight to the collision process. The ion induces a dipole in the (non-polar) molecule with a subsequent interaction energy of

$$E = -\frac{\alpha e^2}{2r^4} \tag{3.10}$$

α is the average polarisability of the molecule (cm^3)
e is the charge on the ion (C)
r is the ion-molecule distance (cm)

This problem can be treated with the standard theory of orbits with an r^{-5} attractive force. The theory shows that the critical impact parameter is:

$$b_0 = \left(\frac{4e^2\alpha}{\mu v^2}\right)^{\frac{1}{4}} \tag{3.11}$$

μ is the reduced mass of the ion-molecule system (g)
v is the relative velocity of the two species (cm s^{-1})

If the impact parameter $b > b_0$ the path of the ion is deflected and kinetic energy is exchanged but collision does not occur. If $b < b_0$ then the particles collide with considerable energy, up to a few eV, usually sufficient to surmount any activation energy barrier to the reaction. If $b = b_0$ the charged particle will end up orbiting the molecule.
The collision cross-section is thus $\sigma = \pi b_0^2$ and hence the reaction rate coefficient is

$$k = <\sigma v> = \pi < b_0^2 v> = \pi < \left(\frac{4e^2\alpha}{\mu v^2}\right)^{\frac{1}{2}} v> = 2\pi e\left(\frac{\alpha}{\mu}\right)^{\frac{1}{2}} \tag{3.12}$$

independent of velocity, i.e. independent of kinetic temperature.
This so-called Langevin coefficient depends only on the reduced mass μ and the polarisability α.
The mean polarisability of stable molecules do not tend to vary a great deal as shown in Table 3.2. Hence it is expected on classical grounds that rate coefficients for ion-molecule reactions should be independent of temperature and should be of the same order of magnitude for different reactions, as observed experimentally for a large number of cases.

Ion-molecule interactions tend to dominate the reactions initiating the complex chemistry in the nebula.

Table 3.2

Mean static polarisability α for a selection of stable molecules

Molecule	Polarisability α (cm^3)
H_2	0.79
N_2	1.76
O_2	1.58
CO	1.95
CN	2.59
H_2O	1.40

After formation of the CH_2^+ ion through radiative association the hydrocarbon chemistry proceeds through ion-molecule reactions with H_2:

$$CH_2^+ + H_2 \rightarrow CH_3^+ + H$$

which exhibits a rate coefficient of the order of 10^{-9} cm^3 s^{-1}.
CH_4^+ is not formed in this way however due to an activation barrier of over 30000 K. Instead slow radiative association forms CH_5^+:

$$CH_3^+ + H_2 \rightarrow CH_5^+ + h\nu$$

followed by ion-molecule reactions forming CH_4^+:

$$CH_5^+ + H \rightarrow CH_4^+ + H_2$$

Rapid recombination reactions then produce the corresponding neutral hydrocarbon molecules.
Once the basic hydrides and their ions are present subsequent reactions to create more complex hydrocarbons are possible. Cyclopropenylidene, C_3H_2, was first detected in planetary nebulae by Cox *et al.* (1987) in NGC 7027. The dominant synthesis is most probably ion-molecule reactions involving C^+ and acetylene followed by radiative association and recombination (Herbst *et al.* 1984):

$$C^+ + C_2H_2 \rightarrow C_3H^+ + H$$

$$C_3H^+ + H_2 \rightarrow C_3H_3^+ + h\nu$$

$$C_3H_3^+ + e^- \rightarrow C_3H_2 + H$$

Formation of the hydroxyl ion, OH^+ proceeds by combination of ionised oxygen and molecular hydrogen:

$$O^+ + H_2 \rightarrow OH^+ + H$$

where laboratory experiments have measured the rate coefficient to be approximately 1.2×10^{-9} cm^3 s^{-1}. Ionised oxygen itself is produced primarily through charge exchange between O and H^+ and by cosmic ray ionisation.
At sufficient distances from the central star the self-shielding effect of H_2 becomes effective and molecular hydrogen starts to become abundant. As this occurs, the reaction above proceeds efficiently to produce OH^+, to be followed by the reactions

$$OH^+ + H_2 \rightarrow H_2O^+ + H$$

$$H_2O^+ + H_2 \rightarrow H_3O^+ + H$$

which exhibit rate coefficients of the order of 10^{-9} cm^3 s^{-1}.
These ions may then rapidly undergo dissociative recombination to produce neutral OH and H_2. The production of the hydroxyl radical in this manner is very efficient and enables one particular gas phase route to CO:

$$C^+ + OH \rightarrow CO^+ + H$$

$$CO^+ + H_2 \rightarrow HCO^+ + H$$

$$HCO^+ + e^- \rightarrow CO + H$$

Ion-molecule reactions also play the leading rôle in the initiation of the nitrogen chemistry. After formation of the N^+ ion by cosmic ray ionisation or fast reactions with He^+ it may then take part in ion-molecule reactions with H_2 to produce heavier nitrogen-bearing species:

$$N^+ + H_2 \rightarrow NH^+ + H$$

$$NH^+ + H_2 \rightarrow NH_2^+ + H$$

$$NH_2^+ + H_2 \rightarrow NH_3^+ + H$$

$$NH_3^+ + H_2 \rightarrow NH_4^+ + H$$

The heavy ions thus produced can then undergo dissociative recombination with electrons to form the neutral species NH, NH_2 and NH_3.
The H_3^+ ion plays a pivotal rôle in the molecular evolution of the nebula because molecular hydrogen exhibits a very low proton affinity making the ion stable but very reactive. The ion is produced by combination of H_2 and the H_2^+ ion:

$$H_2^+ + H_2 \rightarrow H_3^+ + H$$

The small proton affinity of H_2 then enables fast proton transfer to other neutral atoms (C, O, S, Fe) and abundant molecules (CH, CO, C_2, CN, NH) to form H_2, exhibiting rate coefficients of the order of 10^{-9} cm^3 s^{-1}. However, this process has to compete with rapid H_3^+/e^- recombination which removes the ion from the gas.

3.2.2.4 Charge transfer reactions

Charge transfer reactions

$$A^+ + B \rightarrow A + B^+$$

will play a significant rôle in the nebular chemistry due to the large collision cross-section created by the Coulomb force between the ion and neutral.
If the energy of the collision is sufficiently high so that the collision duration $t_{\rm coll}$ is comparable to the electron transfer time $t_{\rm elec}$ then the probability of transfer is likely. For the reaction to occur it is also necessary for the Franck-Condon principle to be satisfied, i.e. during the electronic transition the nuclei must not move appreciably. If both criteria are met the reaction should occur and the rate coefficient can be estimated using equation (3.12). Thus rate coefficients should be of the order of 10^{-9} cm^3 s^{-1} and this is verified by experiment. If any of the criteria are not satisfied the rate coefficient is likely to be a lot smaller than the Langevin estimate.

The ionisation potentials of hydrogen and oxygen are almost exactly equal and hence the process of accidental resonance charge exchange

$$H^+ + O \rightarrow H + O^+$$

occurs efficiently even though being slightly endothermic (β= 227 K). H^+ is produced primarily by cosmic ray ionisation. This reaction is predicted to be the

dominant source of O^+ in the nebula close to the central star where the gas temperature is high enough to drive the reaction.
As the temperature drops with distance from the central star the endothermic reaction creating O^+ becomes ineffective and cosmic ray ionisation produces ionised oxygen.

3.2.2.5 Radiative association

Radiative association reactions

$$A + B \rightarrow AB + h\nu$$

generally exhibit very small rate coefficients where A and B may be atoms, molecules, radicals or their ions.
The criterion for radiative association between two species to occur is that there must exist at least two bound states of the molecule connected to the same ground state reacting particles, and the transitions between these bound states must be allowed which is why radiative association of two H atoms to form H_2 is forbidden. (§3.2.2.1).
If the species involved are both neutral the rate coefficient can be crudely estimated. The duration of the collision is typically about 10^{-14} s; in this time the system must radiate for stabilisation to occur. The Einstein transition probability for a strong transition is typically about 10^8 s^{-1} and hence the time for a transition is about 10^{-8} s. Hence the probability such a transition will occur is only about 10^{-6} per collision. The collision rate coefficient for neutrals is typically 10^{-11} cm^3 s^{-1} (§3.2.2.6) and thus a rate coefficient for radiative association of two neutrals is expected to be typically 10^{-17} cm^3 s^{-1} and quantum mechanical calculations produce results of this magnitude.
Because of the generally small rate coefficient associated with the reaction the process of radiative association normally only assumes importance when ion-molecule reactions between the reactants is not possible or exhibits a large activation barrier.
This is best illustrated by the hydrocarbon chemistry where the reaction

$$C^+ + H_2 \rightarrow CH_2^+ + h\nu$$

is the key reaction in the initiation of the hydrocarbon chemistry rather than the alternative ion-molecule reaction:

$$C^+ + H_2 \rightarrow CH^+ + H$$

which is endothermic by 0.39 eV.

Although the first reaction has a small rate coefficient ($\sim 5 \times 10^{-16}$ cm^3 s^{-1} at 100 K) it represents the primary route to formation of hydrocarbon molecules due to the fact carbon is primarily in ionised form at small optical depths in the nebula and self-shielding of the H_2 molecule rapidly becomes effective so that the abundance of molecular hydrogen quickly rises.

Radiative association also plays a part in the formation of heavier hydrocarbon species. After the ion-molecule reaction forming CH_3^+ from CH_2^+ and H_2, formation of CH_4^+ does not proceed in this way due to the large endothermicity of the reaction (over 30000 K). Indeed all CH_3^+/H_2 channels leading to two products are endothermic and the hydrocarbon chemistry proceeds by:

$$CH_3^+ + H_2 \rightarrow CH_5^+ + h\nu$$

Radiative association is also the primary route to formation of the hydroxyl radical (OH) at small optical depth:

$$O + H \rightarrow OH + h\nu$$

exhibiting a rate coefficient of 5×10^{-19} cm^3 s^{-1} (Black 1978). At higher optical depth dissociative recombination of H_2O^+ becomes a comparably fast creation channel for OH.

Experimental studies of radiative association reactions are very sparse because, unless the gas pressure is very low, the process must compete with ternary association. Thus theoretical treatment is essential in this area where the key problem is in calculation of the rate of radiative stabilisation of the collision complex (Bates and Herbst 1988).

3.2.2.6 Neutral exchange reactions

Neutral exchange reactions

$$A + BC \rightarrow AB + C$$

are of generally minor importance to the nebular chemistry. Rate coefficients have been measured for a variety of interacting species and a strong temperature dependence is often found, unlike the case for ion-molecule interactions.

Non-polar neutrals approaching each other will experience an attraction due to

the interaction between the dipoles mutually induced in the reactants. As they approach each other closely they form an activated complex (ABC)* in which all the atoms are closely interacting.

The motion of this system on the potential energy hypersurface is generally treated by solving the classical laws of motion. By studying a number of trajectories and by averaging the results it is possible to deduce rate coefficients. Such calculations give rate coefficients of the order of 10^{-11} cm^3 s^{-1} agreeing with the results of experiments. However, the dependence of the reaction rate on temperature varies widely between different reactions.

The reason that neutral reactions can behave so differently with respect to temperature is because of the existence of energy barriers on the potential energy hypersurface. If a barrier exists of height E (in energy) the probability to mount the barrier would be expected classically to be $\exp(-E/kT)$ and in general a neutral reaction is expected to have a rate coefficient of the form

$$k = AT^{1/2} \exp\left(-\frac{E}{kT}\right)$$

There is extensive coupling between the carbon and oxygen chemistry in the nebula, an important outcome of which is production of the CO molecule. Production of the OH radical and subsequent reaction with C^+ is one route to CO as described above. Neutral exchange reactions however play the dominant rôle in the production of CO:

$$O + CH \rightarrow CO + H$$

$$O + C_2 \rightarrow CO + C$$

$$C + OH \rightarrow CO + H$$

which exhibit rate coefficients of a few times 10^{-11} cm^3 s^{-1}. with a $T^{1/2}$ temperature dependence.

3.2.2.7 Radiative recombination

Radiative recombination provides a route for removal of atomic ions

$$A^+ + e^- \rightarrow A + h\nu$$

where the excess energy is released as radiation. The process may also occur for molecular ions but in this case dissociative recombination occurs and the excess

energy appears as kinetic energy of the products (§3.2.2.8).
Detailed quantum mechanical calculations show rate coefficients typically of the order of 10^{-12} cm^3 s^{-1} (Prasad and Huntress 1980).
The rate coefficient will invariably increase with decreasing kinetic temperature as the slower atomic speeds enables the strong Coulomb force to create a larger collision cross-section. Theoretical studies typically show a $T^{-\alpha}$ dependence on temperature where $\alpha \sim 0.6$ to 0.7.

3.2.2.8 Dissociative recombination

Positive molecular ions recombining with electrons result in dissociative recombination:

$$AB^+ + e^- \rightarrow A + B$$

The requirement for efficient dissociative recombination to occur is that there should be at least one of the many states of AB lying close to the initial state of AB^+. The molecule H_2^+ has no such repulsive potential energy curve close to the initial state and the reaction rate is indeed found to be very slow.
In order to calculate the rate coefficient it is necessary to calculate first the probability of electron capture by the ion and then to calculate the probability that dissociation will occur rather than autoionisation. Such calculations tend to show that if the species involved are governed by a Maxwellian distribution of energy then the rate coefficient should be large (about 10^{-7} cm^3 s^{-1}) and should exhibit a temperature dependence of $T^{-1/2}$. Some illustrative numbers are given below in Table 3.3 for rate coefficients measured at 100 K.

Dissociative recombination reactions are the primary route to formation of heavy neutral molecules after the corresponding ionised species have been created through ion-molecule reactions. In the hydrocarbon chemistry initial formation of the CH_2^+ ion and subsequent interaction with molecular hydrogen provides the route to ionised hydrocarbon molecules. Dissociative recombination reactions then rapidly produce the corresponding neutral hydrocarbons:

$$CH_2^+ + e^- \rightarrow CH + H$$

$$CH_3^+ + e^- \rightarrow \begin{cases} CH + H_2 \\ CH_2 + H \end{cases}$$

$$CH_4^+ + e^- \rightarrow \begin{cases} CH_3 + H \\ CH_2 + H_2 \end{cases}$$

Table 3.3

Dissociative recombination rate coefficients measured at 100 K

Molecule	Rate coefficient (10^{-7} cm^3 s^{-1})
CH^+	3.3
OH^+	1.4
NH^+	1.9
C_2^+	10
O_2^+	3.3
H_3^+	7.2
H_2O^+	13

$$CH_5^+ + e^- \rightarrow \begin{cases} CH + H_2 + H_2 \\ CH_2 + H_2 + H \\ CH_3 + H_2 \\ CH_4 + H \end{cases}$$

For the nitrogen chemistry it is a similar scenario. Reactions between nitrogen-bearing ionised molecules and H_2 produce heavy ions. These subsequently rapidly undergo dissociative recombination to form the various neutral species:

$$NH_4^+ + e^- \rightarrow \begin{cases} NH_3 + H \\ NH_2 + H_2 \end{cases}$$

$$NH_3^+ + e^- \rightarrow NH_2 + H$$

3.2.2.9 Negative ion reactions

With free electrons being present in the nebula radiative attachment may occur to form negative ions:

$$A + e^- \rightarrow A^- + h\nu$$

the most important example being the formation of the H^- ion. Because hydrogen is far more abundant than any other element only the H^- negative ion is considered in the model.

The H^- ion may be destroyed by a variety of processes. An incident photon may

remove the electron in the process of photodetachment:

$$H^- + h\nu \rightarrow H + e^-$$

Or it may react with another neutral species in the process of associative detachment:

$$H^- + A \rightarrow AH + e^-$$

Alternatively, it may undergo mutual neutralisation with a positive ionic species:

$$H^- + B^+ \rightarrow H + B$$

Rate coefficients for radiative attachment are likely to be a lot smaller than for the process of radiative recombination because the electron-neutral interaction is much weaker than the electron-positive ion interaction. Quantum mechanical calculations give rate coefficients of the order of 10^{-15} cm^3 s^{-1}. The important H-e^- radiative attachment process has a calculated rate coefficient of 3×10^{-16} cm^3 s^{-1} at 300 K with a T^{-1} temperature dependence (Prasad and Huntress 1980).
Because the electron-neutral interaction energy is usually low (0.755 eV in the case of H^-) photodetachment represents a very efficient process. Since the interaction energy is so low the electron-neutral separation will be large resulting in a large electric dipole. Thus the cross-section for photodetachment will be large and in the case of H^- is of the order of a few times 10^{-17} cm^2 (Doughty *et al.* 1966).
Because of the long-range Coulomb forces involved mutual neutralisation is invariably a rapid process. As the species H^- and B^+ approach each other, if a transition is possible from their potential curve to a neighbouring dissociative curve of the molecule HB, the reaction may occur. Laboratory measurements and theory agree that the rate coefficient tends to be large and exhibits a $T^{-1/2}$ dependence at low temperature with typical values being $\sim 10^{-6}\, T^{-1/2}$ cm^3 s^{-1}.

3.3 Solving the system of chemical equations

After calculating the local gas kinetic temperature (see Chapters 5 and 6) and the local ultraviolet radiation field spectrum (see Chapter 2) it is then possible to calculate the rate coefficients of every chemical reaction in the reaction network. Cosmic ray ionisation and dissociation is assumed to proceed at a rate independent of the gas temperature. For every chemical species considered in the model it is then possible to formulate an expression for the time rate of change of the number density:

$$\frac{dn(\mathrm{Z})}{dt} = \sum_i k_i n_i^{(1)} n_i^{(2)} - n(\mathrm{Z}) \sum_j k_j n_j^{(1)} - n(\mathrm{Z}) \sum_m \zeta_m \qquad (3.13)$$

$n(\mathrm{Z})$ is the number density of species Z (cm^{-3})
$n_i^{(1)}$, $n_i^{(2)}$ are the number densities of the species involved in reaction i (cm^{-3})
k_i is the rate coefficient of reaction i ($\mathrm{cm}^3\ \mathrm{s}^{-1}$)
ζ_m is a photon or cosmic ray induced ionisation or dissociation rate coefficient (s^{-1})

The first summation in equation (3.13) is over all gas-phase reactions that produce species Z. The second summation is over all gas-phase reactions that destroy species Z. The third summation is over all photon or cosmic ray interactions with species Z that tend to destroy the molecule.
With knowledge of the gas temperature and radiation field spectrum all the k's and ζ's are known. Under the assumption of steady-state equilibrium we have that $dn(\mathrm{Z})/dt = 0$ which then allows the set of differential equations to be reduced to a set of nonlinear algebraic equations of the general format:

$$F_1(n_1, n_2, \ldots, n_{N_\mathrm{s}}) = \sum_{i_1} k_{i_1} n_{i_1}^{(1)} n_{i_1}^{(2)} - n_1 \sum_{j_1} k_{j_1} n_{j_1}^{(1)} - n_1 \sum_{m_1} \zeta_{m_1} = 0$$

$$F_2(n_1, n_2, \ldots, n_{N_\mathrm{s}}) = \sum_{i_2} k_{i_2} n_{i_2}^{(1)} n_{i_2}^{(2)} - n_2 \sum_{j_2} k_{j_2} n_{j_2}^{(1)} - n_2 \sum_{m_2} \zeta_{m_2} = 0$$

and so on up to

$$F_{N_\mathrm{s}}(n_1, n_2, \ldots, n_{N_\mathrm{s}}) = \sum_{i_{N_\mathrm{s}}} k_{i_{N_\mathrm{s}}} n_{i_{N_\mathrm{s}}}^{(1)} n_{i_{N_\mathrm{s}}}^{(2)} - n_{N_\mathrm{s}} \sum_{j_{N_\mathrm{s}}} k_{j_{N_\mathrm{s}}} n_{j_{N_\mathrm{s}}}^{(1)} - n_{N_\mathrm{s}} \sum_{m_{N_\mathrm{s}}} \zeta_{m_{N_\mathrm{s}}} = 0$$

where there are N_s algebraic equations describing the time rate of change of the N_s chemical species in the reaction network.

From these N_s nonlinear equations it is required to determine the values of n_1, n_2, ..., n_{N_s} which satisfy all of them simultaneously. The numerical technique

employed is the Newton-Raphson method for nonlinear equations (e.g. Press *et al.* 1992).

Let the initial estimate of the vector of n values be denoted by $\mathbf{n}$. The assumption is made that the estimate is sufficiently close to the correct vector of n's so that we may write the vector of correct n values as $\mathbf{n} + \delta\mathbf{n}$ where $\delta\mathbf{n}$ is very small relative to $\mathbf{n}$. We may write $F_i(\mathbf{n} + \delta\mathbf{n})$ as a Taylor series about $\mathbf{n}$:

$$F_i(\mathbf{n} + \delta\mathbf{n}) = F_i(\mathbf{n}) + \sum_{j=1}^{N_s} \frac{\partial F_i}{\partial n_j} \delta n_j + O(\delta\mathbf{n}^2) \tag{3.14}$$

The matrix of partial derivatives in equation (3.14) is the Jacobian matrix $\mathbf{J}$ where

$$J_{ij} \equiv \frac{\partial F_i}{\partial n_j} \tag{3.15}$$

Hence in matrix notation:

$$\mathbf{F}(\mathbf{n} + \delta\mathbf{n}) = \mathbf{F}(\mathbf{n}) + \mathbf{J} \cdot \delta\mathbf{n} + O(\delta\mathbf{n}^2) \tag{3.16}$$

With the assumption that $\delta\mathbf{n}$ is very small we now truncate the Taylor series and ignore terms of order $\delta\mathbf{n}^2$ and higher. Setting $\mathbf{F}(\mathbf{n}+\delta\mathbf{n}) = \mathbf{0}$ then allows us to form a set of linear equations for the correction vector $\delta\mathbf{n}$ that move all the functions closer to zero simultaneously:

$$\mathbf{J} \cdot \delta\mathbf{n} = -\mathbf{F}(\mathbf{n}) \tag{3.17}$$

This matrix equation may be solved by LU decomposition (Press *et al.* 1992) to determine $\delta\mathbf{n}$. The correction vector is then added to the solution vector to produce a better estimate to the vector $\mathbf{n}$:

$$\mathbf{n}_{\text{new}} = \mathbf{n}_{\text{old}} + \delta\mathbf{n} \tag{3.18}$$

The 'better' set of number densities thus calculated are then used in recalculations of the kinetic temperature and ultraviolet radiation spectrum. Thus the reaction rate coefficients may be recomputed and a further improved set of number densities calculated. The process is iterated in this manner at each distance from the central star until convergence is achieved.

Chapter 4

Rotational equilibrium of diatomic molecules

At each point in the nebula the model performs calculations to determine the equilibrium rotational populations of the two abundant molecules H_2 and CO. The purpose of this is to enable accurate computation of the photodissociation rates of the two molecules (§2.5.2) and the contribution collisional excitation of the molecules makes to the cooling of the gas (§6.2). In the case of H_2 there is another reason for determining the distribution of the molecule amongst the various rotational levels.

Molecular hydrogen can exist in two forms, ortho- and para-H_2. In the former the nuclear spins are aligned resulting in a nuclear spin quantum number of I=1 representing a triplet state. In para-H_2 the spins are opposed and I=0 giving a singlet state. As the nuclei are identical fermions the nuclear wave function comprising vibration, rotation and spin components must be asymmetric under exchange of the protons. The ground vibrational state is invariant under this operation whereas the rotational function is multiplied by $(-1)^J$ where J is the rotational quantum number. The triplet spin function I=1 is symmetric under proton exchange and hence for ortho-H_2 only odd values of J are allowed. For para-H_2 only even values of J are allowed.

Para-H_2 exhibits substantially different physical characteristics to ortho-H_2. For example, the rate coefficient for collisional excitation of a species through interaction with H_2 will be different according to whether H_2 is in para- or ortho-form. Since H_2 is the most abundant molecule in the nebula this is an important consideration when, for example, considering cooling of the gas phase through fine-structure collisional excitation of an atom by H_2 (Chapter 6).

It is assumed in the model that only rotational levels in the ground vibrational state v=0 of the ground electronic state are effectively populated for both molecules. For the H_2 molecule for example the level $v = 1, J = 0$ lies at an energy 5988 K above the ground state $v = 0, J = 0$ and in the low temperature regime of the neutral region collisions and chemical reactions will produce a negligible population in excited vibrational states. Optical pumping of the molecules is very rapidly followed by radiative cascade to the ground electronic-vibrational state making the assumption of negligible populations in excited vibrational states justified.

In general the rotational populations of H_2 and CO will be governed by three processes: chemical reactions producing the molecule in rotational levels, collisions with other species tending to change the distribution amongst the rotational levels

and radiative processes, either optical pumping or spontaneous transitions in the ground electronic state. Thus, under the assumption of steady-state equilibrium, the rotational populations n_{0J} are obtained by solving the set of equations

$$\frac{dn_{0J}}{dt} = \left(\frac{dn_{0J}}{dt}\right)_{\text{chemistry}} + \left(\frac{dn_{0J}}{dt}\right)_{\text{collisions}} + \left(\frac{dn_{0J}}{dt}\right)_{\text{radiative}} = 0$$

4.1 Rotational equilibrium of H_2

For the specific case of H_2, expanding on the above discussion, it is possible to recognise six separate processes controlling the rotational population of the molecule and these are discussed below. In the following sections the convention is used that vJ, $v"J"$ and v^*J^* all refer to ro-vibrational states in the ground electronic state whereas $v'J'$ refers to a ro-vibrational state in an excited electronic state.

4.1.1 Formation on dust grains

As discussed previously (§3.2.2.1) the dominant route for formation of the H_2 molecule is by combination of two hydrogen atoms on a grain surface followed by ejection of the molecule into the gas phase with kinetic and internal energy. As discussed in Chapter 5 (§5.3.4) the assumption is made that the 4.5 eV of energy released in the formation of an H_2 molecule is divided equally between kinetic energy of the molecule, internal energy of the molecule and internal energy of the grain lattice. Hence, under this assumption, 1.5 eV of energy is available as internal vibration-rotation energy of the molecule.

Duley and Williams (1986) predict that, on amorphous silicates, H_2 forms vibrationally hot but rotationally cool. This general idea is assumed to hold for this model where the dust grains are taken to be composed of amorphous carbon (Chapter 7). Taking into account the triplet and singlet nature of ortho- and para-H_2, if we make the ansatz that the probability of formation of H_2 in ro-vibrational states is distributed as:

$$\begin{aligned} p_{vJ}^{\text{grain}} &= 0.25 \quad \text{for } v = 3, J = 0 \\ &= 0.75 \quad \text{for } v = 3, J = 1 \\ &= 0 \quad \text{for all other } vJ \text{ levels} \end{aligned}$$

Then each H_2 molecule is ejected with a mean internal energy of

$$E = \sum_{vJ} p_{vJ} \Delta E_{vJ} = 1.47 \text{ eV}$$

where ΔE_{vJ} is the energy of the level vJ with respect to the ground $v = 0, J = 0$ state.

This result is clearly consistent with the assumption of equipartition of the formation energy of H_2 amongst the three exit channels.

After being ejected from the grain in a vibrationally excited state the molecule will quickly cascade to a rotational level in the vibrational ground state $v = 0$. Thus the rate of formation of H_2 molecules in the state $v = 0, J$ is given by

$$\left(\frac{dn_{0J}}{dt}\right)_{H_2} = \left(\sum_{J" \geq J} p^{\text{grain}}_{0J"} C_{0J",0J} + \sum_{v"J"} p^{\text{grain}}_{v"J"} C_{v"J",0J}\right) k_g n(\text{H}) n_{\text{H}} \qquad (4.1)$$

n_{0J} is the number of H_2 molecules in the level $v = 0, J$ (cm^{-3})

p^{grain}_{vJ} is the probability of H_2 forming on a grain in the ro-vibrational state vJ

k_g is the rate coefficient for H_2 formation on grains ($\text{cm}^3\ \text{s}^{-1}$)

$n(\text{H})$ is the number density of atomic hydrogen (cm^{-3})

n_{H} is the number density of hydrogen nuclei (cm^{-3})

$C_{v"J",vJ}$ is a cascade coefficient from level $v"J"$ to level vJ

The quantity $k_g n(\text{H}) n_{\text{H}}$ represents the rate of formation of H_2 molecules on dust grains and has been derived previously (§3.2.2.1). The form of the rate coefficient k_g was also derived, given the assumptions about the dust characteristics in the nebula:

$$k_g\ (\text{cm}^3\ \text{s}^{-1}) = 1.41 \times 10^{-18} T^{\frac{1}{2}}$$

T is the gas temperature (K)

The quantity $C_{v"J",vJ}$ is a cascade coefficient and represents the probability that level $v"J"$ will decay to level vJ via all possible intermediate routes. This cascade coefficient can be obtained by summation over all possible intermediate levels v^*J^* provided that cascade coefficients for these intermediate levels $C_{v^*J^*,vJ}$ have already been computed.

If $P_{v"J",v^*J^*}$ is the probability that level $v"J"$ will decay directly to level v^*J^* then

$$P_{v"J",v^*J^*} = \frac{\text{A}_{v"J",v^*J^*}}{\sum_{vJ<v"J"} \text{A}_{v"J",vJ}} \qquad (4.2)$$

$\text{A}_{v"J",vJ}$ is the Einstein A coefficient for a spontaneous transition from level $v"J"$ to level vJ

Einstein A coefficients for the ground state of H_2 have been computed by Turner *et al.* (1977).

If we then adopt the convention

$$C_{vJ,vJ} = 1 \tag{4.3}$$

and

$$\mathrm{A}_{vJ,v"J"} = 0, \qquad P_{vJ,v"J"} = 0, \qquad C_{vJ,v"J"} = 0 \tag{4.4}$$

for all levels $v"J"$ lying above the initial state vJ (radiative decay always proceeds towards lower levels) then cascade coefficients can be computed from the recursion formula (Viala *et al.* 1988):

$$C_{v"J",vJ} = \sum_{v^*=v}^{v_{\max}} \sum_{J^*} P_{v"J",v^*J^*} C_{v^*J^*,vJ} \tag{4.5}$$

The summation over J is over all intermediate rotational levels from vJ up to $v"J"$. Thus, knowing the matrix $P_{v"J",vJ}$ from equation (4.2) the matrix $C_{v"J",vJ}$ may be constructed via equation (4.5) starting from the lowest level vJ using equation (4.3) and progressing upwards to the level $v"J"$.
In this way the set of cascade coefficients $C_{v"J",vJ}$ may be computed and used in equation (4.1) to determine $(dn_{0J}/dt)_{\mathrm{H_2}}$.

4.1.2 Spontaneous emission

Within the ground electronic-vibrational state spontaneous transitions between rotational levels will occur. Since the molecule has no permanent dipole moment only quadrupole emission with the selection rule $\Delta J = 0, \pm 2$ is allowed. Hexadecapole radiation ($\Delta J = \pm 4$) or higher make a negligible contribution to the equilibrium rotational population. Thus the rate of change of the number density of molecules in state $v = 0, J$ due to spontaneous emission is given by

$$\left(\frac{dn_{0J}}{dt}\right)_{\mathrm{H_2}} = n_{0,J+2}\mathrm{A}_{J+2,J} - n_{0J}\mathrm{A}_{J,J-2} \tag{4.6}$$

$\mathrm{A}_{J,J'}$ is the Einstein A coefficient for H_2 for the spontaneous rotational transition $J \rightarrow J'$ (s^{-1})

4.1.3 Optical pumping

Absorption of a UV photon by an H_2 molecule may cause a transition to a rovibrational state $v'J'$ in an excited electronic state (B or C) followed by radiative cascade through intermediate levels towards the ground electronic-vibrational

state. Thus the presence of an ultraviolet field will cause redistribution of the molecule amongst the rotational levels.

A molecule in any rotational state $v = 0, J$ may make a transition to any vibrational state v' in an excited electronic state E, the transition being described as a P(J), Q(J) or R(J) branch according to whether $\Delta J = J' - J$= -1, 0 or 1 respectively. If the molecule is excited from the ground state ($X^1\Sigma_g^+$) to the upper electronic level $B^1\Sigma_u^+$ selection rules demand, to ensure conservation of angular momentum, that a Q(J) transition is not allowed. For the $X^1\Sigma_g^+ \rightarrow C^1\Pi_u$ transition the P(J), Q(J) and R(J) branches will all be present.

Not all UV photon induced transitions result in radiative cascade back to the ground state. For each ro-vibrational level $v'J'$ in an excited electronic state there is a well-defined probability $p^{\rm dis}_{v'J'}$ that subsequent decay will occur to the vibrational continuum of the ground state thus causing dissociation of the molecule (§2.5.2.1).

Hence the rate at which the level $v = 0, J$ is populated through optical pumping from all rotational levels in the ground state followed by radiative cascade is given by:

$$\left(\frac{dn_{0J}}{dt}\right)_{\rm H_2} = \sum_{J"} n_{0J"} \sum_{E} \sum_{v'J'} \zeta_{0J",v'J'}(1 - p^{\rm dis}_{v'J'})\beta_{v'J',0J} \qquad (4.7)$$

where only transitions preserving the ortho/para character of the H_2 molecule are allowed (i.e. if J is even (odd) only even (odd) values of $J"$ are considered in the sum over $J"$).

The quantity $\zeta_{0J",v'J'}$ is the rate of absorption in a particular line of the Lyman or Werner band:

$$\zeta_{0J",v'J'}\,({\rm s}^{-1}) = {\rm B}_{0J",v'J'} \int_{\lambda_{\rm H}}^{\infty} \Phi(\lambda)\frac{\lambda^2}{c}\phi_\lambda^{0J",v'J'}(\lambda)\,d\lambda \qquad (4.8)$$

$\lambda_{\rm H}$ is the Lyman limit of atomic hydrogen ($\lambda_{\rm H} = 912\,$Å)
the other quantities in equation (4.8) are as defined previously (see equation (2.50))

The Einstein B coefficient for absorption is related to the corresponding absorption oscillator strength by:

$${\rm B}_{0J",v'J'} = \left(\frac{\pi e^2}{m_e c}\right) f_{0J",v'J'}\frac{\lambda_0}{h} \qquad (4.9)$$

$f_{0J",v'J'}$ is the absorption oscillator strength for the transition $v = 0, J"$ to $v'J'$
λ_0 is the wavelength of the transition

The quantity $\beta_{v'J',0J}$ is equation (4.7) is the total probability that a ro-vibrational level $v'J'$ in the excited electronic state E will decay to the level $v = 0, J$ of the ground state either directly or through radiative cascade within this state. It is given by the expression (Viala *et al.* 1988):

$$\beta_{v'J',0J} = P_{v'J',0J} + \sum_{v^*=1}^{v_{\max}} \sum_{J^*} P_{v'J',v^*J^*} a_{v^*J^*,0J} \tag{4.10}$$

$P_{v'J',v^*J^*}$ represents the probability that level $v'J'$ in an excited electronic state will decay directly to the level v^*J^* in the ground state and is given by the expression:

$$P_{v'J',v^*J^*} = \frac{\mathrm{A}_{v'J',v^*J^*}}{\sum_{v"J"} \mathrm{A}_{v'J',v"J"} + \sum_{v"J"} \mathrm{A}_{v'J',\mathrm{continuum}}} \tag{4.11}$$

$\mathrm{A}_{v'J',v"J"}$ is the Einstein A coefficient for the spontaneous transition from level $v'J'$ in an excited electronic state to level $v"J"$ in the ground state (s^{-1})
$\sum_{v"J"} \mathrm{A}_{v'J',\mathrm{continuum}}$ is the rate of radiative decay from the level $v'J'$ to the vibrational continuum of the ground state (s^{-1})

The rate of radiative decay

$$\mathrm{A}_{v'J'} = \sum_{v"J"} \mathrm{A}_{v'J',v"J"} + \sum_{v"J"} \mathrm{A}_{v'J',\mathrm{continuum}} \tag{4.12}$$

for levels $v'J'$ in excited electronic states of H_2 have been computed by Stephens and Dalgarno (1972).

The quantity $a_{v^*J^*,0J}$ is equation (4.10) is a cascade efficiency factor from level v^*J^* to level $0J$ as defined by Black and Dalgarno (1976) and tabulated in their paper for H_2. It is given by the expression

$$a_{v^*J^*,0J} = \sum_{v"=1}^{v^*} \sum_{J"} C_{v^*J^*,v"J"} P_{v"J",0J} \tag{4.13}$$

$C_{v^*J^*,v"J"}$ is a cascade coefficient (§4.1.1)
$P_{v"J",0J}$ is the probability of a direct radiative transition between levels $v"J"$ and $v = 0, J$ in the ground electronic state (see equation(4.2))

Thus all the factors are known or can be calculated to enable computation of the matrix $\beta_{v'J',0J}$. Calculation of $\zeta_{0J",v'J'}$ may proceed by employing equation (4.8) and with knowledge of the matrix $p^{\mathrm{dis}}_{v'J'}$ the calculation of equation (4.7) is made

possible. Values for the dissociation probabilities $p^{\rm dis}_{v'J'}$ for H_2 were taken from Abgrall *et al.* (1992).

Optical pumping will not only populate level $0J$ but will also cause depopulation of the level according to the formula:

$$\left(\frac{dn_{0J}}{dt}\right)_{H_2} = -n_{0J}\sum_E\sum_{v'J'}\zeta_{0J,v'J'} \tag{4.14}$$

Hence the total rate of change of the number density of H_2 molecules in the level $v=0, J$ due to optical pumping is given by combining equations (4.7) and (4.14):

$$\left(\frac{dn_{0J}}{dt}\right)_{H_2} = \sum_{J"} n_{0J"}\sum_E\sum_{v'J'}\zeta_{0J",v'J'}(1-p^{\rm dis}_{v'J'})\beta_{v'J',0J} - n_{0J}\sum_E\sum_{v'J'}\zeta_{0J,v'J'} \tag{4.15}$$

4.1.4 Chemical reactions

Exothermic chemical reactions producing H_2 may produce it in excited rotational levels. Similarly, reactions where H_2 is a reactant will destroy the rotationally excited molecule. The rate of change of the number density of H_2 molecules in level $v=0, J$ due to chemical reactions is given by:

$$\left(\frac{dn_{0J}}{dt}\right)_{H_2} = \sum_i k_i n_X n_Y p^i_{0J} - n_{0J}\sum_m k_m n_Z \tag{4.16}$$

n_X, n_Y are the number densities of reactants in reaction i forming the H_2 molecule ($\rm cm^{-3}$)
k_i is the rate coefficient for reaction i ($\rm cm^3\ s^{-1}$)
p^i_{0J} is the probability of forming H_2 in the level $v=0, J$ from reaction i
n_Z is the number density of a species reacting with H_2 so tending to destroy the molecule ($\rm cm^{-3}$)
k_m is the rate coefficient for reaction m ($\rm cm^3\ s^{-1}$)

The number densities of the various species and the reaction rate coefficients are known at each step in the iterative procedure (§3.4). The main difficulty arising from equation (4.16) is knowing (or estimating) the values of p^i_{0J}.
There is scant data on this subject of how H_2 is rotationally excited after being produced through chemical reactions. Consequently, values ascribed to p^i_{0J} can at best be only tenuous. The H_3^+ ion is a very reactive yet stable species because H_2 has a particularly low proton affinity (4.34 eV) and hence the ion will readily

transfer protons to most of the atoms and molecules in the gas. Proton transfer reactions in general exhibit a very large rate coefficient and in fact if allowed on energy grounds transfer will occur to the exclusion of all other exothermic channels, apart from some fast charge transfer reactions. Hence, since such proton transfer reactions tend to dominate the chemistry of H_2 production, it is reasonable to adopt values for p^i_{0J} appropriate to the general reaction:

$$H_3^+ + X \rightarrow H_2 + XH^+$$

In the minimum energetic state H_3^+ consists of two protons with spins parallel and one proton with spin anti-parallel. The formation of H_2 from H_3^+ involves removing one proton from the ion. Assuming that the ion is always in the minimum energy configuration the probability of leaving two protons with spins parallel (triplet state) is $\frac{1}{3}$ and of leaving two protons with spins anti-parallel (singlet state) is $\frac{2}{3}$. Thus there is a probability of $\frac{1}{3}$ of producing ortho-H_2 and a probability of $\frac{2}{3}$ of producing para-H_2. Assuming that the H_2 molecule is formed in the ground state then the values adopted for p^i_{0J} in the model are:

$$\begin{aligned} p^i_{0J} \quad &= \tfrac{2}{3} \qquad \text{for } v = 0, J = 0 \\ &= \tfrac{1}{3} \qquad \text{for } v = 0, J = 1 \\ &= 0 \qquad \text{for all other } vJ \text{ levels} \end{aligned}$$

4.1.5 Inelastic collisions

Inelastic collisions between molecular hydrogen and other species may cause a rotational transition in the H_2 molecule. Such collisions tend to preserve the ortho/para character of the molecule although interconversion between the two is possible, the dominant mechanism being collisions with thermal protons and H_3^+ (§4.1.6). Collisions may cause rotational excitation or de-excitation of the molecule and hence, if the ortho/para character is preserved the change in the rotational quantum number will be $\Delta J = \pm 2, \pm 4$ etc. The process of collisional excitation or de-excitation will have associated with it a rate coefficient which will depend on the colliding species, the gas kinetic temperature and the type of transition involved.

As a result of the Maxwellian velocity distribution among the gas particles, the relative populations of the various atomic and molecular energy levels will have some tendency to approach the values they would have in thermodynamic equilibrium. This tendency is particularly marked where transitions resulting from collisional

excitation and de-excitation dominate over photon processes. Under these conditions the rate coefficient for collisional excitation is connected to the rate coefficient for collisional de-excitation by a Boltzmann relationship (e.g. Osterbrock 1974a):

$$k_{ij} = k_{ji}\frac{g_j}{g_i}e^{-(E_j-E_i)/kT} \tag{4.17}$$

k_{ij} is the rate coefficient for collisional excitation from level i to level j ($\mathrm{cm^3\ s^{-1}}$)
k_{ji} is the rate coefficient for collisional de-excitation from level j to level i (with the same colliding species) ($\mathrm{cm^3\ s^{-1}}$)
g_i, g_j are the statistical weights (degeneracies) of levels i and j respectively
E_i, E_j are the energies of levels i and j respectively where $E_j > E_i$

The assumption is made that collisions do not cause vibrational excitation of the H_2 molecule from the $v = 0$ ground state. This is justified in the low temperature regime of the neutral region where the gas kinetic temperature will not exceed about 500 K whereas the $v = 1, J = 0$ state of the H_2 molecule lies at an energy equivalent of 5988 K above the $v = 0, J = 0$ state making collisionally induced vibrational transitions a negligible occurrence. Under this assumption the rate of change of the number density of H_2 molecules in the rotational state $v = 0, J$ due to collisions is given by

$$\left(\frac{dn_{0J}}{dt}\right)_{H_2} = \sum_{J"} n_{0J"} \sum_p k^p_{0J",0J} n_p - n_{0J} \sum_{J"} \sum_p k^p_{0J,0J"} n_p \tag{4.18}$$

$k^p_{0J",0J}$ is the rate coefficient for the rotational transition $0J" \rightarrow 0J$ for the case of H_2 colliding with species p; the collision may cause excitation or de-excitation of the molecule i.e. $J" < J$ or $J" > J$ ($\mathrm{cm^3\ s^{-1}}$)
n_p is the number density of species p ($\mathrm{cm^{-3}}$)

In the relatively low temperature environment of the neutral region the rate coefficients for $\Delta J = \pm 4$, ± 6 or higher are so much smaller than for $\Delta J = \pm 2$ that these transitions are neglected and hence under this approximation:

$$\begin{aligned}\left(\frac{dn_{0J}}{dt}\right)_{H_2} =& n_{0,J-2} \sum_p k^p_{0,J-2\rightarrow 0J} n_p + n_{0,J+2} \sum_p k^p_{0,J+2\rightarrow 0J} n_p - \\ & n_{0J}\left(\sum_p k^p_{0J\rightarrow 0,J-2} n_p + \sum_p k^p_{0J\rightarrow 0,J+2} n_p\right)\end{aligned} \tag{4.19}$$

4.1.5.1 H_2 - H collisions

Mandy and Martin (1993) calculated rates for H_2 excitation by H impact. However, their calculations are based on a quasi-classical treatment of the problem and have only been parameterised for the temperature range 600 K $< T <$ 10000 K.
Elitzur and Watson (1978b) used the surprisal analysis technique to find an analytic function representing approximately the cross-section for rotational de-excitation of the H_2 molecule by H impact. The cross-section obtained for a transition $J \rightarrow J'$ is given by (Levine *et al.* 1976):

$$\sigma(J \rightarrow J'; E) = R(2J'+1)\left(\frac{E/B - J'(J'+1)}{E/B - J(J+1)}\right)^{\frac{1}{2}} \exp\Big(-\theta(J, J', E)\Big) \qquad (4.20)$$

E is the total energy of the molecule (rotational plus barycentric kinetic energy)
B is the rotational constant of the H_2 molecule

For rotational excitation of the H_2 molecule Procaccia and Levine (1976) have shown that the function θ may be written

$$\theta(J, J', E) = \left(\theta_0 + \frac{\theta_1 E}{B}\right)\frac{|E_{J'} - E_J|}{E} \qquad (4.21)$$

where

$$\theta_0 = 5.01 \qquad \theta_1 = 0.1187$$

$E_J, E_{J'}$ are the energies of the rotational levels J and J' respectively, given by $E_J = BJ(J+1)$

For the rotational constant B of H_2 a value of 85.25 K was adopted and assumed to be constant for all rotational levels of the ground vibrational state.

The factor R in equation (4.20) is a normalisation constant expected to be independent of J, J' and E. For a $\Delta J = \pm 2$ transition equation (4.20) provides a good approximation for the cross-section for rotational excitation if R is taken to have the value (Elitzur and Watson 1978b):

$$R = 2.0 \times 10^{-16}\ \mathrm{cm}^2$$

To compute the rate coefficient for de-excitation $k_{J,J-2} = < \sigma(J \rightarrow J-2; E)v >$ it is required to integrate the expression from equation (4.20) over a Maxwell-Boltzmann distribution of velocities. This cannot be performed analytically but

the following expression provides an excellent approximation to the rate coefficient determined by numerical integration (Elitzur and Watson 1978b):

$$k_{J,J-2}\,(\mathrm{cm^3\ s^{-1}}) = <\sigma(J \rightarrow J';E)v> \approx 1.3\sigma(J \rightarrow J-2;E)\bar{v} \qquad (4.22)$$

where the expression on the RHS of equation (4.22) represents the expression in equation (4.20) with $J' = J - 2$. The total energy of the molecule (rotational plus barycentric kinetic energy) is given by

$$E = kT + BJ(J+1)$$

The quantity $\bar{v}$ in equation (4.22) is the mean thermal speed of an H_2 molecule assuming a Maxwell-Boltzmann distribution of velocities and is given by

$$\bar{v} = \left(\frac{8kT}{\pi\mu}\right)^{\frac{1}{2}} \qquad (4.23)$$

μ is the reduced mass of the H-H_2 system ($\mu = \frac{2}{3}m_{\mathrm{H}}$)

The rate coefficient for excitation due to H impact is, using equation (4.17):

$$k_{J-2,J}\,(\mathrm{cm^3\ s^{-1}}) = k_{J,J-2}\left(\frac{2J+1}{2J-3}\right)\exp\left(\frac{-2B(2J-1)}{kT}\right) \qquad (4.24)$$

The degeneracy of a particular rotational level of H_2 is given by:

$$g_J = (2J+1)(2I+1) \qquad (4.25)$$

where I is the nuclear spin quantum number; I=1 for ortho-H_2, I=0 for para-H_2. Since the collisions discussed in this section preserve the ortho/para character of the H_2 molecule the I-dependence in equation (4.24) drops out.

4.1.5.2 H_2 - H_2 collisions

Using the interaction potential of Meyer, Schaefer and Liu (1980, private communication) and the MOLSCAT computer code of Green and Hutson (1986), Danby *et al.* (1987) computed cross-sections for rotational transitions induced in collisions with H_2 molecules. By integrating the cross-sections over a Maxwellian distribution of velocities they deduced the corresponding rate coefficients for rotational de-excitation of the molecule as a function of kinetic temperature.

Table 4.1

Rate coefficients for rotational de-excitation of the H_2 molecule in collision with an H_2 molecule in the $v = 0, J = 0$ state

Temperature T (K)	Rate coefficient $J \rightarrow J-2$ (10^{-11} cm^3 s^{-1})					
	$2 \rightarrow 0$	$3 \rightarrow 1$	$4 \rightarrow 2$	$5 \rightarrow 3$	$6 \rightarrow 4$	$7 \rightarrow 5$
50	4.05 (-2)	2.21 (-2)	7.39 (-3)	2.36 (-3)	7.76 (-4)	2.70 (-4)
100	5.98 (-2)	3.59 (-2)	1.30 (-2)	4.42 (-3)	1.53 (-3)	5.61 (-4)
150	8.36 (-2)	5.47 (-2)	2.15 (-2)	7.79 (-3)	2.86 (-3)	1.11 (-3)
200	0.110	7.74 (-2)	3.27 (-2)	1.26 (-2)	4.88 (-3)	2.00 (-3)
250	0.138	0.103	4.65 (-2)	1.90 (-2)	7.74 (-3)	3.32 (-3)
300	0.167	0.132	6.28 (-2)	2.70 (-2)	1.15 (-2)	5.15 (-3)
350	0.198	0.163	8.16 (-2)	3.67 (-2)	1.63 (-2)	7.57 (-3)
400	0.230	0.196	0.103	4.81 (-2)	2.22 (-2)	1.06 (-2)
450	0.262	0.232	0.126	6.12 (-2)	2.92 (-2)	1.43 (-2)
500	0.296	0.269	0.151	7.60 (-2)	3.73 (-2)	1.88 (-2)

If a rotationally inelastic collision occurs between two hydrogen molecules either one or both may undergo a rotational transition. To simplify matters in the model it is assumed only one of the molecules is rotationally excited or de-excited, the other is scattered with no change in the rotational level. The further simplification is made that if the colliding partner is a para-H_2 molecule the rate coefficient used is the rate coefficient appropriate for the molecule in the J=0 rotational state. If the colliding partner is an ortho-H_2 molecule the rate coefficient is taken to be the rate coefficient for the molecule in the J=1 rotational state. This approximation has some justification in the fact that a large majority of the H_2 molecules will be in low J states (J=0 and J=1 in particular).

Rate coefficients for rotational de-excitation are reproduced in Tables 4.1 and 4.2 (Danby *et al.* 1987) for the two cases of J=0 and J=1 for the colliding partner. These rate coefficients have been fitted to a formula of the form:

$$k_{J,J-2}\,(\mathrm{cm}^3\ \mathrm{s}^{-1}) = A(J)T^{B(J)}$$

Table 4.2

Rate coefficients for rotational de-excitation of the H_2 molecule in collision with an H_2 molecule in the $v = 0, J = 1$ state

Temperature T (K)	Rate coefficient $J \rightarrow J-2$ (10^{-11} cm^3 s^{-1})					
	$2 \rightarrow 0$	$3 \rightarrow 1$	$4 \rightarrow 2$	$5 \rightarrow 3$	$6 \rightarrow 4$	$7 \rightarrow 5$
50	6.40 (-2)	2.13 (-2)	8.11 (-3)	2.60 (-3)	8.57 (-4)	3.02 (-4)
100	9.67 (-2)	3.62 (-2)	1.45 (-2)	4.93 (-3)	1.70 (-3)	6.31 (-4)
150	0.137	5.67 (-2)	2.42 (-2)	8.73 (-3)	3.20 (-3)	1.25 (-3)
200	0.181	8.18 (-2)	3.70 (-2)	1.42 (-2)	5.48 (-3)	2.25 (-3)
250	0.227	0.111	5.30 (-2)	2.14 (-2)	8.70 (-3)	3.74 (-3)
300	0.275	0.143	7.20 (-2)	3.06 (-2)	1.30 (-2)	5.81 (-3)
350	0.323	0.178	9.39 (-2)	4.17 (-2)	1.84 (-2)	8.53 (-3)
400	0.373	0.216	0.119	5.47 (-2)	2.51 (-2)	1.19 (-2)
450	0.423	0.256	0.146	6.98 (-2)	3.30 (-2)	1.61 (-2)
500	0.473	0.297	0.176	8.68 (-2)	4.22 (-2)	2.11 (-2)

Note: a (b) implies a$\times 10^{\text{b}}$

Table 4.3

Values of $A(J)$ and $B(J)$ to compute the rotational de-excitation coefficient of H_2 in collision with H_2 ($v = 0, J = 0$)

$J \rightarrow J-2$	$A(J)$	$B(J)$	$J \rightarrow J-2$	$A(J)$	$B(J)$
$2 \rightarrow 0$	9.107 (-15)	0.923	*9 $\rightarrow$ 7	1.259 (-20)	2.34
$3 \rightarrow 1$	1.852 (-15)	1.16	*10 $\rightarrow$ 8	1.796 (-21)	2.50
$4 \rightarrow 2$	2.195 (-16)	1.41	*11 $\rightarrow$ 9	2.563 (-22)	2.65
$5 \rightarrow 3$	2.765 (-17)	1.63	*12 $\rightarrow$ 10	3.656 (-23)	2.80
$6 \rightarrow 4$	3.988 (-18)	1.82	*13 $\rightarrow$ 11	5.217 (-24)	2.94
$7 \rightarrow 5$	6.604 (-19)	2.00	*14 $\rightarrow$ 12	7.443 (-25)	3.08
*8 $\rightarrow$ 6	8.825 (-20)	2.17	*15 $\rightarrow$ 13	1.062 (-25)	3.22

Table 4.4

Values of $A(J)$ and $B(J)$ to compute the rotational de-excitation coefficients of H_2 in collision with H_2 ($v = 0, J = 1$)

$J \rightarrow J-2$	$A(J)$	$B(J)$	$J \rightarrow J-2$	$A(J)$	$B(J)$
$2 \rightarrow 0$	1.486 (-14)	0.921	*9 $\rightarrow$ 7	1.208 (-20)	2.35
$3 \rightarrow 1$	1.443 (-15)	1.22	*10 $\rightarrow$ 8	1.680 (-21)	2.51
$4 \rightarrow 2$	2.177 (-16)	1.44	*11 $\rightarrow$ 9	2.336 (-22)	2.66
$5 \rightarrow 3$	2.882 (-17)	1.64	*12 $\rightarrow$ 10	3.249 (-23)	2.81
$6 \rightarrow 4$	4.235 (-18)	1.83	*13 $\rightarrow$ 11	4.519 (-24)	2.95
$7 \rightarrow 5$	7.407 (-19)	2.00	*14 $\rightarrow$ 12	6.284 (-25)	3.08
*8 $\rightarrow$ 6	8.687 (-20)	2.19	*15 $\rightarrow$ 13	8.739 (-26)	3.22

Note: a (b) implies $a \times 10^b$

(* extrapolated from lower order data)

$A(J)$ and $B(J)$ are coefficients depending on J only

The values of $A(J)$ and $B(J)$ up to J=15 are displayed in Tables 4.3 and 4.4 for the two cases of the colliding partner being in the rotational state J=0 and J=1.

The corresponding rate coefficient for excitation may be computed from $k_{J,J-2}$ via equation (4.17) and is given by equation (4.24).

4.1.5.3 H_2 - He collisions

Collisions with He atoms will make a minor contribution to the rotational equilibrium of H_2 since He is considerably less abundant than hydrogen in the nebula. Using results given by Schaefer (Schaefer, private communication), Flower has produced rate coefficients for rotational de-excitation of H_2 by He according to the formula (Flower, private communication):

$$k_{J,J-2}\,(\mathrm{cm}^3\ \mathrm{s}^{-1}) = T^{A(J)} \times 10^{B(J)}$$

$A(J)$ and $B(J)$ are coefficients depending on J only

Values of $A(J)$ and $B(J)$ are reproduced in Table 4.5 below.

Rate coefficients for excitation may be computed from the de-excitation rate coefficients using equation (4.24).

Table 4.5

Values of $A(J)$ and $B(J)$ to compute the rate coefficient for rotational de-excitation of H_2 through collisions with He

J	$A(J)$	$B(J)$	J	$A(J)$	$B(J)$
2	1.210	-14.46	9	2.394	-20.02
3	1.568	-15.56	10	2.394	-20.31
4	1.852	-16.62	11	2.394	-20.47
5	2.124	-17.67	12	2.394	-20.47
6	2.255	-18.33	13	2.394	-20.47
7	2.362	-19.07	14	2.394	-20.47
8	2.394	-19.61	15	2.394	-20.47

4.1.6 Ortho-H_2/para-H_2 interconversion through collisions

As a first approximation ortho-H_2 and para-H_2 may be regarded as two separate chemical species with different physical characteristics with no interconversion between the two. However, processes to convert ortho- to para-H_2 and vice-versa do exist (Dalgarno *et al.* 1973) and the dominant mechanism for interconversion are collisions between the H_2 molecule and either thermal protons or the H_3^+ ion (Flower 1990). The interaction must be a nuclear spin-changing collision and occurs when one of the protons in the H_2 molecule is interchanged with a proton of opposite spin from the collision partner. At the low temperatures in the neutral region collisions causing a rotational transition with $\Delta J = \pm 3$, ± 5 or higher are negligible and are ignored in the model. Under this approximation of $\Delta J = \pm 1$ only the rate of change of the number density of H_2 molecules in rotational level J due to collisions causing ortho/para conversion is given by:

$$\left(\frac{dn_{0J}}{dt}\right)_{H_2} = n_{0,J+1}\sum_p k^p_{0,J+1\rightarrow 0J} n_p + n_{0,J-1}\sum_p k^p_{0,J-1\rightarrow 0J} n_p - n_{0J}\left(\sum_p k^p_{0J\rightarrow 0,J+1} n_p + \sum_p k^p_{0J\rightarrow 0,J-1} n_p\right) \quad (4.26)$$

$k^p_{0J\rightarrow 0J'}$ is the rate coefficient for a rotational transition $J \rightarrow J'$ through collisions with species p

n_p is the number density of species p

Table 4.6

Values of k_0 and ΔE_0 to compute the rate coefficient for rotational de-excitation of H_2 in collision with H^+

J	k_0 (10^{-10} cm^3 s^{-1})	ΔE_0 (K)
1	2.024	3.841
2	9.575	2.124
3	2.729	2.890
4	7.910	1.706
5	2.246	2.518
6	6.223	1.439
7	1.828	2.240
8	4.974	1.567

Gerlich (1990) calculated state to state rate coefficients for the interconversion of ortho/para H_2 through collisions with thermal protons. Using the frozen nuclear spin (FNS) approximation the cross-sections $\sigma_{JJ'}(E)$ for the rotational transitions were calculated as a function of the translational kinetic energy E. The rate coefficients were then computed by numerical integration over a Maxwell-Boltzmann distribution of translational energies. Gerlich fitted the calculated rate coefficients to a formula of the type:

$$k_{J,J-1}(T) = k_0 \exp(-\Delta E_0/kT) \tag{4.27}$$

The values of k_0 and ΔE_0 reported by Gerlich for rotational de-excitation $J \rightarrow J-1$ are reproduced in Table 4.6.

Gerlich does not report values of k_0 and ΔE_0 for values of J above J=8 and consequently a constant value of $k_{J,J-1}$=3.0×10^{-10} cm^3 s^{-1} is estimated for the levels J=9 to J=15 based on the data published.

The rate coefficient for rotational de-excitation through collisions with H_3^+ are assumed to be the same as for H^+.

4.2 Rotational equilibrium of CO

Due to a lack of theoretical or experimental data on cascade probabilities for the CO molecule it is not possible to take into account optical pumping of CO when calculating the distribution of the molecule amongst the rotational levels. With this omission in the computations just three separate processes are considered in the equilibrium calculations: spontaneous radiative decay in the ground electronic-vibrational state, formation of rotationally excited CO through chemical reactions and collisions between CO and other abundant species causing rotational excitation or de-excitation.

4.2.1 Spontaneous emission

Unlike H_2, CO exhibits a permanent dipole moment and hence electric dipole transitions with $\Delta J = \pm 1$ are allowed. These will dominate over magnetic dipole and lower order transitions and the approximation is made that spontaneous transitions with $\Delta J = \pm 2$ or higher make a negligible contribution to the rotational equilibrium of the molecule. Under this dipole approximation the rate of change of the number density of molecules in state $v = 0, J$ due to spontaneous emission is given by:

$$\left(\frac{dn_{0J}}{dt}\right)_{\mathrm{CO}} = n_{0,J+1}\mathrm{A}_{J+1,J} - n_{0J}\mathrm{A}_{J,J-1} \tag{4.28}$$

$\mathrm{A}_{J,J'}$ is the Einstein A coefficient for CO for the spontaneous rotational transition $J \rightarrow J'$ (s^{-1})

4.2.2 Chemical reactions

Exothermic chemical reactions with CO as a product may produce it in excited rotational states. The equation governing the rate of change of the number density of CO molecules in level $v = 0, J$ due to chemical reactions is, exactly as for H_2:

$$\left(\frac{dn_{0J}}{dt}\right)_{\mathrm{CO}} = \sum_i k_i n_X n_Y p^i_{0J} - n_{0J}\sum_m k_m n_Z \tag{4.29}$$

n_X, n_Y are the number densities of reactants in reaction i forming the CO molecule (cm^{-3})
k_i is the rate coefficient for reaction i ($\mathrm{cm}^3\ \mathrm{s}^{-1}$)
p^i_{0J} is the probability of forming CO in the level $v = 0, J$ from reaction i
n_Z is the number density of a species reacting with CO to form other products

(cm^{-3})
k_m is the rate coefficient for reaction m $(\mathrm{cm}^3\ \mathrm{s}^{-1})$

As with the corresponding case of H_2 formation the problem with equation (4.29) is knowing or estimating the p^i_{0J}. In the case of CO, due to the lack of experimental or theoretical work in this area, the assumption is made that formation into any of the rotational levels of the ground electronic-vibrational state are equally likely. Thus we have:

$$p^i_{0J} = \frac{1}{J_{\max}} \tag{4.30}$$

$J_{\max}$ is the highest rotational level in the ground state considered in the equilibrium calculations.

4.2.3 Inelastic collisions

Collisions between CO and other abundant species may cause rotational transitions in the molecule. The rate coefficients for excitation and de-excitation are connected by the Boltzmann relationship as for H_2 (see equation (4.17)). As with H_2, the approximation is made that collisionally induced vibrational transitions out of the ground $v = 0$ vibrational state are a negligible occurrence.
CO is a heavy molecule and hence has a small rotational constant ($B = 5.53$ K) so that many rotational levels are accessible through collisions even at fairly low kinetic temperatures. For simplicity, the model only considers collisions causing transitions with $\Delta J = \pm 1$ or ± 2 but it should be borne in mind that although the approximation of considering $\Delta J = \pm 2$ only for collisionally induced transitions in H_2 is justified due to the large rotational constant of this molecule the approximation is not very accurate for the case of CO. Optical pumping is not considered in the rotational equilibrium of CO and ignoring collisionally induced rotational transitions with $\Delta J = \pm 3$ or higher will not contribute a great deal to the error introduced by omitting optical pumping altogether. Because of these large approximations made for the equilibrium calculations of CO it would be inconsistent to produce detailed formulae for the rate coefficients for collisional de-excitation. Hence to simplify the calculations (and due to the fact data on de-excitation rate coefficients for CO over the temperature range in the nebula are very sparse in the literature) the rate coefficients are assumed not to depend on the kinetic temperature, only on the rotational transition involved.
Under the approximation of only considering transitions with $\Delta J = \pm 1$ or ± 2 the rate of change of the number density of CO molecules in the state $v = 0, J$ due to

collisions is given by:

$$\left(\frac{dn_{0J}}{dt}\right)_{\mathrm{CO}} = n_{0,J-1}\sum_p k^p_{0,J-1\rightarrow 0J}n_p + n_{0,J-2}\sum_p k^p_{0,J-2\rightarrow 0J}n_p + n_{0,J+1}\sum_p k^p_{0,J+1\rightarrow 0J}n_p + n_{0,J+2}\sum_p k^p_{0,J+2\rightarrow 0J}n_p - n_{0J}\left(\sum_p k^p_{0J\rightarrow 0,J-1}n_p + \sum_p k^p_{0J\rightarrow 0,J-2}n_p + \sum_p k^p_{0J\rightarrow 0,J+1}n_p + \sum_p k^p_{0J\rightarrow 0,J+2}n_p\right) \quad (4.31)$$

$k_{0J",0J}$ is the rate coefficient for the rotational transition $0J" \rightarrow 0J$ for the case of CO colliding with species p ($\mathrm{cm^3\ s^{-1}}$)
n_p is the number density of species p ($\mathrm{cm^{-3}}$)

4.2.3.1 CO - H collisions

Green and Thaddeus (1976) used the close-coupling method (Arthurs and Dalgarno 1960) to calculate the cross-sections for rotational de-excitation of the CO molecule through collisions with H and He.

Table 4.7
Rate coefficients for rotational de-excitation of CO in collision with H

J	Rate coefficient $k_{J,J'}$ (10^{-11} $\mathrm{cm^3\ s^{-1}}$)		J	Rate coefficient $k_{J,J'}$ (10^{-11} $\mathrm{cm^3\ s^{-1}}$)	
	$J \rightarrow J-1$	$J \rightarrow J-2$		$J \rightarrow J-1$	$J \rightarrow J-2$
1	0.644		*9	0.6	0.6
2	1.03	0.441	*10	0.6	0.6
3	1.09	0.614	*11	0.6	0.6
4	1.09	1.01	*12	0.6	0.6
5	0.918	1.03	*13	0.6	0.6
6	0.868	1.08	*14	0.6	0.6
7	0.682	0.851	*15	0.6	0.6
*8	0.6	0.6			

(* estimated from lower order data)

By taking an average of $v\sigma_{J,J'}(v)$ over a Maxwell-Boltzmann distribution of relative velocities v they determined the de-excitation rate coefficients as a function of temperature up to a maximum temperature of 100 K. This is well below the maximum temperature in the molecular region of the PN predicted by the model. An average has been taken over all the data reported by Green and Thaddeus and this mean rate coefficient is assumed to be sufficiently accurate for all temperatures experienced in the nebula.

The rate coefficients thus calculated for the CO-H system are shown in Table 4.7. Green and Thaddeus only report results up to rotational level J=7. Mean rate coefficients for J=8 and higher have been estimated, based on the results for lower J values.

4.2.3.2 CO - H_2 collisions

Based on an *ab initio* calculation of the CO-H_2 interaction potential Flower and Launay (1985) carried out quantum mechanical coupled channel calculations to determine the cross-sections for rotational de-excitation of CO in collision with ortho- and para-H_2. They determined the corresponding rate coefficients by integrating the cross-sections over a Maxwellian distribution of velocities.

Table 4.8

Rate coefficients for rotational de-excitation of CO in collision with para-H_2

J	Rate coefficient $k_{J,J'}$ (10^{-11} cm^3 s^{-1})		J	Rate coefficient $k_{J,J'}$ (10^{-11} cm^3 s^{-1})	
	$J \rightarrow J-1$	$J \rightarrow J-2$		$J \rightarrow J-1$	$J \rightarrow J-2$
1	3.8		9	7.3	10.5
2	5.5	4.3	10	7.4	9.2
3	6.2	7.1	11	6.9	10.3
4	6.8	8.6	*12	6.0	9.0
5	7.0	9.5	*13	6.0	9.0
6	7.8	10.5	*14	6.0	9.0
7	9.3	10.8	*15	6.0	9.0
8	8.1	11.2			

Table 4.9

Rate coefficients for rotational de-excitation of CO in collision with ortho-H_2

J	Rate coefficient $k_{J,J'}$ (10^{-11} cm^3 s^{-1})		J	Rate coefficient $k_{J,J'}$ (10^{-11} cm^3 s^{-1})	
	$J \rightarrow J-1$	$J \rightarrow J-2$		$J \rightarrow J-1$	$J \rightarrow J-2$
1	5.1		*9	7.0	11.0
2	7.1	6.9	*10	7.0	11.0
3	7.3	10.8	*11	7.0	11.0
4	7.3	12.0	*12	7.0	11.0
5	7.4	13.0	*13	7.0	11.0
6	6.7	14.0	*14	7.0	11.0
*7	7.0	11.0	*15	7.0	11.0
*8	7.0	11.0			

(* estimated from lower order data)

The values for $k_{J,J-1}$ and $k_{J,J-2}$ they report have been averaged over the values quoted in the paper (10 K to 250 K for collisions with para-H_2 and 10 K to 100 K for collisions with ortho-H_2) and the resulting figure assumed to be sufficiently accurate at all temperatures in the nebula.
The results are shown in Tables 4.8 and 4.9.

Flower and Launay only report values of the rate coefficients up to J=11 for para-H_2 and J=6 for ortho-H_2. Values of the temperature-averaged rate coefficients have been estimated for higher values of J.

4.2.3.3 CO - He collisions

Green and Thaddeus (1976) computed rate coefficients for the rotational de-excitation of CO in collision with H and He (§4.2.3.1). They calculated values for the temperature range 5 K to 100 K. Their results have been averaged over temperature and the result assumed to be sufficiently accurate for all temperatures in the nebula. The temperature-averaged results are reported in Table 4.10.

Table 4.10

Rate coefficients for rotational de-excitation of the CO molecule in collision with He

J	Rate coefficient $k_{J,J'}$ (10^{-11} cm^3 s^{-1})		J	Rate coefficient $k_{J,J'}$ (10^{-11} cm^3 s^{-1})	
	$J \rightarrow J-1$	$J \rightarrow J-2$		$J \rightarrow J-1$	$J \rightarrow J-2$
1	2.3		*9	3.0	5.0
2	3.5	2.7	*10	3.0	5.0
3	3.2	4.8	*11	3.0	5.0
4	2.8	5.5	*12	3.0	5.0
5	2.9	5.9	*13	3.0	5.0
6	3.0	6.4	*14	3.0	5.0
*7	3.0	5.0	*15	3.0	5.0
*8	3.0	5.0			

(* estimated from lower order data)

Green and Thaddeus only report values up to J=6. Values for the rate coefficient for J=7 and higher have been estimated, based on the data reported.

4.3 Solving the system of equations

For each rotational level J of H_2 or CO we have a set of expressions contributing to dn_{0J}/dt. These expressions must be summed to yield the total time rate of change of n_{0J}. For H_2 the relevant expressions are equations (4.1), (4.6), (4.15), (4.16), (4.19) and (4.26) and for CO equations (4.28), (4.29) and (4.31). Thus for each rotational level J we have an expression of the form:

$$\frac{dn_{0J}}{dt} = a_{J0}n_{00} + a_{J1}n_{01} + a_{J2}n_{02} + ... + a_{JJ_{\max}}n_{0J_{\max}} + k_{0J} - k'n_{0J} \qquad (4.32)$$

n_{0J} is the fraction of molecules in the state $v = 0, J$
$a_{JJ'}$ are the coefficients of the $n_{0J'}$'s (s^{-1})
k_{0J} is the rate of creation of the molecule in the state $v = 0, J$ through chemical reactions (s^{-1})
k' is the total rate of destruction of the molecule through chemical reactions (s^{-1})

The term k_{0J} in equation (4.32) arises because formation of the molecule through chemical reactions (and on dust grains for H_2) does not depend on the current rotational population of the molecule.
There are $J_{\max} + 1$ equations similar to equation (4.32) which describe dn_{0J}/dt for each level from $J = 0$ to $J = J_{\max}$. Under the assumption of steady-state equilibrium we have $dn_{0J}/dt = 0$ for each rotational level. The resulting set of inhomogeneous equations may be written in matrix form:

$$\mathbf{A}.\mathbf{x} = -\mathbf{k} \qquad (4.33)$$

$\mathbf{A}$ is the matrix of $a_{JJ'} - \delta_{JJ'}k'$ values (where $\delta_{JJ'}$ is the Kronecker delta symbol)
$\mathbf{x}$ is the vector of the n_{0J}'s
$\mathbf{k}$ is the vector of k_{0J} values

The technique of matrix LU decomposition is employed to solve equation (4.33) for $\mathbf{x}$ (Press *et al.* 1992) and hence determine the rotational population of H_2 and CO at each point in the nebula.

Chapter 5

Heating processes in the nebula

The kinetic temperature of the gas in the neutral envelope in a steady state is determined by the condition that the total kinetic energy gained per unit volume per second, which is denoted by Γ, is equal to the corresponding energy lost per unit volume per second, denoted by Λ. In general, both Γ and Λ will depend on the kinetic temperature T as well as on other gas parameters. The value of T at which these two functions are equal will represent the local equilibrium temperature.
For purposes of modelling, it is assumed that all the chemical species at some point in the nebula have the same kinetic temperature. This simplifying assumption is in fact a very good approximation. Electrons produced by photoionisation have an initial distribution of energies that depends on the form of the radiation spectrum and the photoionisation cross-section. However, the cross-section for elastic scattering collisions between electrons is quite large, of the order $4\pi(e^2/mv^2)^2 \approx 10^{-13}$ cm^2 (Osterbrock 1974a) and these collisions tend to set up a Maxwell-Boltzmann energy distribution. The recombination cross-sections involved in the nebula are so much smaller that, to a very good approximation, the electron energy distribution function is Maxwellian and therefore all atomic processes occur at rates fixed by the local temperature defined by the Maxwellian.

Heating of the gas in the nebula is achieved through a variety of processes. At the interface between the ionised and the molecular region, even though all L_c radiation (radiation with $\lambda < 912$ Å) has been used in the ionisation of hydrogen, there still exists an extremely strong ultraviolet field, several thousand times as strong as the interstellar field. Because of this, photoejection of electrons from dust grains is predicted to be an important heating process at low values of optical depth τ_V. There is enough evidence now, through observations of IR features in the emission spectrum, to support the idea of PAH disc molecules being present in the molecular domain of planetary nebulae. Photoionisation of such molecules is included in the thermal processes and proves to be the dominant source of heating at low τ_V.
As the optical depth increases these processes cease to be the dominant source of heating and other physical effects take over, primarily heat evolution through chemical reactions and photoionisation of other molecular species.

5.1 Thermal effect of PAH molecules

5.1.1 Evidence for the existence of PAH molecules in the nebular environment

For a number of years infrared observations of PNe have yielded, amongst other data, several bright emission bands lying between 3μm and 12μm. The central wavelengths of the six brightest features lie at 3.3μm, 3.4μm, 6.2μm, 7.7μm, 8.6μm and 11.3μm. The widths of the lines are less than 1μm or between 3% to 10% of their wavelength.

Gillett *et al.* (1973) first observed the IR features in the PN NGC 7027 and since at the time no generally accepted explanation was devised, the bands became known as unidentified infrared emission features (UIF). The bands are commonly associated with PNe, e.g. Martin (1987) carried out low resolution spectroscopy and narrow band photometry on 12 planetary nebulae and discovered the 3.3μm feature to be present in all 12. However, UIF are not exclusively associated with PNe, but seem to occur wherever there exists a close source of strong UV radiation.

Sellgren (1984) discovered continuum IR emission between 1.2μm and 4.8μm from reflection nebulae, and attributed the radiation to quantum heating of very small grains. Leger and Puget (1984) suggested that the grains could be composed of carbon and that very small carbon grains in a hydrogen rich environment should be considered as polycyclic aromatic hydrocarbons (PAHs). Using coronene ($C_{24}H_{12}$) they demonstrated that most of the observed UIF can be produced from thermal emission of PAHs. The data of Martin (1987) supported the view that the 3.3μm feature is caused by emission from PAHs. The 3.4μm feature is not so definite, although it is related to the 3.3μm feature and hence probably to PAH emission as well. Martin also reports that both these features are correlated to the 11.3μm feature and to the far infrared flux, although only the 3.3μm feature is correlated to the 3.8μm continuum excess radiation and to the carbon abundance.

The first definite detection of a hydrocarbon molecule in a planetary nebula was made by Cox *et al.* (1987). They detected the 18.3 and 21.6 GHz transitions of cyclopropenylidene (C_3H_2) towards PN NGC 7027. They report that the molecule appears to originate in the dense neutral region just bordering the ionisation front. If the chemistry of C_3H_2 is linked with the formation of aromatic species in this nebula, the fact that the molecule is primarily arising from the neutral interface contiguous to the ionised region is consistent with the spatial distribution of the

IR emission features in NGC 7027. Allamandola *et al.* (1989) consider a possible chemical pathway from acetylene (C_2H_2) to PAH molecules.

Allamandola *et al.* (1989) compared the IR emission spectrum from the Orion Bar with the absorption spectra of three PAH species, chrysene ($C_{18}H_{12}$), pyrene ($C_{16}H_{10}$) and coronene ($C_{24}H_{12}$) and found a fairly good general resemblance between the two. Comparison of the interstellar IR spectra with the spectra of PAHs (singly or in mixtures) generally produce a good overall resemblance but fail to match in the details such as band positions, relative intensities or profiles across the entire mid-IR. The resemblance suggests PAH species are responsible but they are probably a mixture of molecules which are larger than those normally studied in the laboratory and may well be ionised, dehydrogenated and perhaps electronically excited.

Stein and co-workers have carried out extensive theoretical studies of organic molecule growth from carbon atoms and have shown that aromatic hydrocarbons are the most thermodynamically favourable form of hydrocarbon in the temperature range of several hundred to nearly 3000°C (Stein 1978; Stein and Brown 1987). At temperatures above 3000°C polyacetylenes are favoured (Stein and Fahr 1985).

Other models for the IR emission bands have been proposed in the past as follows: (1) infrared fluorescence from UV-pumped, vibrationally excited small molecules frozen on 0.1μm sized grains at low ($\approx$ 10 K) temperatures (Allamandola and Norman 1978); (2) equilibrium thermal emission from small (0.01μm) grains at 300 K, coated with an unspecified polymeric material (Dwek *et al.* 1980); (3) equilibrium thermal emission from characteristic groups on aromatic-like moieties present at the surface of small carbon grains (Duley and Williams 1981). There are drawbacks with all these alternative models that make them incompatible with other theory and observations. The PAH hypothesis produces no such disagreement and the body of evidence supporting this view is now very strong. Apart from the overall resemblance of the IR band spectrum to the vibrational spectrum expected from PAH-like species (Allamandola *et al.* 1987) other recent observations tend to favour an aromatic hydrocarbon origin as well. Cohen *et al.* (1986) have shown that the fraction of total IR luminosity radiated by the 7.7μm feature in PNe is strongly correlated with the nebular C/O ratio.
Because the source of the IR bands must be produced in the nebula under extremely harsh conditions, they must be extremely stable and carbon-rich, two characteristics completely consistent with the PAH hypothesis. Cohen *et al.* also

show that while there is variation among the relative IR band intensities among different objects, they are correlated, implying that a single class of chemical species is responsible for all the infrared emission features.

These observational results, combined with other recent theoretical and laboratory measurements strongly suggest that PAH molecules are responsible for the observed characteristic IR emission features and are hence present in the nebular environment.

5.1.2 Theory behind photoelectric heating effect

The ionisation rate for a neutral PAH can be written as:

$$R_{\rm ion}\,({\rm s}^{-1}) = \frac{10^{-8}}{h}\int_{\lambda_{\rm H}}^{\lambda_{\rm IP}} \lambda\Phi(\lambda)\sigma_{\rm ion}(\lambda)\,d\lambda \tag{5.1}$$

$\lambda_{\rm H}$ is the Lyman limit of atomic hydrogen ($\lambda_{\rm H} = 912\,$Å)
$\lambda_{\rm IP}$ is the wavelength corresponding to the ionisation potential of the molecule (Å)
$\Phi(\lambda)$ is the radiation field energy density (erg cm^{-3} Å^{-1})
$\sigma_{\rm ion}(\lambda)$ is the photoionisation cross-section (cm^2)
h is Planck's constant (erg s)

The recombination rate for a PAH cation is:

$$k_{\rm rec} = < v\sigma_{\rm rec}(v) > \tag{5.2}$$

$k_{\rm rec}$ is the recombination rate for the process (cm^3 s^{-1})
v is the speed of an electron (cm s^{-1})
$\sigma_{\rm rec}(v)$ is the recombination cross-section for an electron (cm^2)

Since it is assumed the electrons have a Maxwell-Boltzmann speed distribution (see earlier), the average is taken over a Maxwellian distribution:

$$< v\sigma_{\rm rec}(v) >= 4\pi\left(\frac{m_e}{2\pi kT}\right)^{3/2}\int_0^\infty [v\sigma_{\rm rec}(v)]v^2\exp\left(\frac{-m_e v^2}{2kT}\right)dv \tag{5.3}$$

where the symbols have their usual meanings (e.g. Mandl 1978)

For a spherical molecule bearing a single positive charge we have (Spitzer 1978):

$$\sigma_{\rm rec}^{(3)}(v,a) = Y_s\sigma_0(1 + 2eU(a)/m_e v^2) \tag{5.4}$$

a is the radius of the molecule
$\sigma_0 = \pi a^2$ is the geometrical cross-section of the molecule
Y_s is the sticking probability for recombination of an electron on the molecule
m_e is the electron mass
the mean electrostatic potential at $r = a$ is $U(a) = e/a$

However, PAHs are planar objects, not spherical, and they can be viewed as disks with a radius given by $a = 0.9 N_c^{1/2}$ Å (Omont 1986) where N_c is the number of carbon atoms in the molecule. Taking into account this planar shape and hence the fact the cross-section depends on the direction from which the electron approaches the disk, the cross-section is reduced by a factor $Y_{\rm rec} = 0.80$ (Verstraete *et al.* 1990) so that:

$$\sigma_{\rm rec}^{(2)}(v) = Y_{\rm rec} Y_s \sigma_0 (1 + 2eU(a)/m_e v^2) \tag{5.5}$$

the superscripts (2) and (3) refer to 2 and 3 dimensional objects respectively.

Henceforward the assumption is made that $Y_s = 1$ (d'Hendecourt and Leger 1987; Omont 1986).

After averaging, one can write:

$$k_{\rm rec} = Y_{\rm rec} \sigma_0 (1 + eU(a)/kT)(8kT/\pi m_e)^{1/2} \tag{5.6}$$

Now $\sigma_0 = \pi a^2 = 0.81 \pi N_c$ using the above relation. Hence substituting for the values of the constants gives:

$$k_{\rm rec}\ ({\rm cm^3 s^{-1}}) = 1.28 \times 10^{-10} N_c T^{1/2} (1 + \phi) \tag{5.7}$$

where, since $U(a) = e/a = e/(0.9 N_c^{1/2})$, the parameter ϕ is defined as:

$$\phi = eU(a)/kT = 1.85 \times 10^5 / (N_c^{1/2} T) \tag{5.8}$$

Hence the ionisation balance is stated as:

$$n({\rm PAH^0}) R_{\rm ion} = n({\rm PAH^+}) n_e k_{\rm rec} \tag{5.9}$$

n_e is the number density of electrons (cm^{-3})
$n({\rm PAH^0})$ is the number density of neutral PAH molecules (cm^{-3})
$n({\rm PAH^+})$ is the number density of PAH cations (cm^{-3})

The ionisation fraction is:

$$\beta = n(\mathrm{PAH}^+)/n_{\mathrm{PAH}} = R_{\mathrm{ion}}/(R_{\mathrm{ion}} + n_e k_{\mathrm{rec}}) \tag{5.10}$$

n_{PAH} is the total number density of PAH molecules (cm^{-3})

The mean heat input to the gas results from the net balance between the energy gain from photoejected electrons and the energy loss due to electrons recombining with ions:

$$Q = (1-\beta)\int_{\lambda_{\mathrm{H}}}^{\lambda_{\mathrm{IP}}} \lambda c\Phi(\lambda)\sigma_{\mathrm{ion}}(\lambda)\gamma(\lambda)\Big(\frac{1}{\lambda} - \frac{1}{\lambda_{\mathrm{IP}}}\Big)\, d\lambda \;\; - \;\; n_e\beta < \frac{1}{2}m_e v^2 v\sigma_{\mathrm{rec}}(v) > \tag{5.11}$$

$\gamma(\lambda)$ is the coefficient for the repartition of the available energy (E-IP) between the kinetic energy of the ejected electron and the energy that remains in the ion as excitation energy. The assumption is now made that $< \gamma(\lambda) > = 0.5$ and that this mean value may be used in equation (5.11) without loss of accuracy. This value for $< \gamma(\lambda) >$ is inferred from measurements of photoionisation on benzene (Terenin and Villessov 1964).
The Maxwell averaged recombined energy is:

$$E_{\mathrm{rec}} = n_e\beta < \frac{1}{2}m_e v^2 v\sigma_{\mathrm{rec}}(v) >= kT\beta R_{\mathrm{rec}} f(T, N_c) \tag{5.12}$$

Since $\beta R_{\mathrm{rec}} = \beta n_e k_{\mathrm{rec}} = (1-\beta)R_{\mathrm{ion}}$ from equation (5.10) we have:

$$E_{\mathrm{rec}} = (1-\beta)R_{\mathrm{ion}} kT f(T, N_c) \tag{5.13}$$

The function f is defined as:

$$f(T, N_c) = (2+\phi)/(1+\phi) \tag{5.14}$$

If $< E_e >$ is the mean energy of the ejected photoelectron then

$$< E_e > \ (\mathrm{erg}) \ = \frac{1}{2}R_{\mathrm{ion}}^{-1}\int_{\lambda_{\mathrm{H}}}^{\lambda_{\mathrm{IP}}} \lambda c\Phi(\lambda)\sigma_{\mathrm{ion}}(\lambda)\Big(\frac{1}{\lambda} - \frac{1}{\lambda_{\mathrm{IP}}}\Big)\, d\lambda \tag{5.15}$$

λ is wavelength (Å)
$\Phi(\lambda)$ is radiation field energy density ($\mathrm{erg\ cm^{-3}\ \AA^{-1}}$)
$\sigma_{\mathrm{ion}}(\lambda)$ is photoionisation cross-section (cm^2)
c is the speed of light ($\mathrm{cm\ s^{-1}}$)
R_{ion} is the ionisation rate (s^{-1})

the factor of 1/2 comes from assuming a value of $\gamma(E) =< \gamma(E) > = 0.5$ over the entire range.

Hence the heat input per PAH molecule can be expressed as:

$$Q = (1 - \beta)R_{\rm ion}[< E_e > -f(T, N_c)kT] \tag{5.16}$$

So the total rate of heating due to PAH molecules is given by:

$$\Gamma_{\rm PAH}\ ({\rm erg\ cm^{-3}\ s^{-1}}) = n_{\rm PAH}(1 - \beta)R_{\rm ion}[< E_e > -f(T, N_c)kT] \tag{5.17}$$

$n_{\rm PAH}$ is the PAH abundance ($\rm cm^{-3}$)

Hence, knowledge of $\sigma_{\rm ion}(\lambda)$ and $\Phi(\lambda)$ would enable the calculation of $R_{\rm ion}$ and $< E_e >$ and hence $\Gamma_{\rm PAH}$ at every point in the nebula. A primary task of the model is to solve the radiative transfer equation in the nebula (Chapter 2) and thus the radiation energy density $\Phi(\lambda)$ is known at every point in the cloud. Chapter 2 discusses the form of the radiation field $\Phi_0(\lambda)$ incident on the nebula. Estimates are also required for N_c and $n_{\rm PAH}$.

Near-IR emission from the interstellar medium attributed to PAHs suggest a fairly large mean molecular size, $N_c \approx 80$ (Leger *et al.* 1989). Rouan *et al.* (1992) analysed the observed intensity ratio $I(11.3\mu{\rm m})/I(3.3\mu{\rm m})$ from reflection nebulae and computed mean PAH characteristics based on laboratory data of known PAH molecules. They discovered a value of $N_c \sim 78$. Allamandola *et al.* (1989) analysed observations of the IR spectra from the PN NGC 7027 and compared the intensities of the 11.3 μm feature and the 3.3 μm feature. They deduced that the range of carbon atom numbers in PAH molecules in the nebula was approximately 35 to 90.
Based on this evidence a value of $N_c = 80$ is used in the model. Verstraete *et al.* (1990) use the fact that the ionisation cross-section is proportional to the number of carbon atoms to determine the cross-section for an N_c=80 PAH molecule. The data from this paper on $\sigma_{\rm ion}(\lambda)$ for an N_c=80 PAH molecule is used in the model for numerical integration purposes.

According to the so-called liquid drop model the classical expression for the ionisation potential of a particle is given by (Smith 1961; Moskovitz 1991; Bakes and Tielens 1993):

$${\rm IP} = W + (Z + \frac{1}{2})\frac{e^2}{C} \tag{5.18}$$

W is the work function of the bulk material
Z is the charge on the particle (in units of the electronic charge)
C is the capacitance of the particle

Being in the shape of a thin circular disk, the capacitance of a PAH molecule of radius a is given by:

$$C = \frac{2a}{\pi} \tag{5.19}$$

The work function of an infinite graphitic sheet is 4.4 eV (Smith 1961; Gallegos 1968) and hence the ionisation potential of a PAH molecule is given by:

$$\text{IP (eV)} = 4.4 + (Z + \frac{1}{2})\frac{25.1}{N_c^{1/2}} \tag{5.20}$$

Substituting a value of N_c=80 gives a value for the ionisation potential of a neutral PAH molecule of IP = 5.8 eV (i.e. $\lambda_{\rm IP}$ = 2138 Å).

If the fraction of carbon locked up in PAH molecules is f_c then the number density of molecules is given by:

$$n_{\rm PAH} = n({\rm C}) f_c / N_c \tag{5.21}$$

n(C) is the total abundance of carbon atoms (cm^{-3})

Allamandola *et al.* (1989) analysed the observed values for the fraction of the IR flux in the emission features and in the dust continuum for the PN NGC 7027 and derived a value of ~0.06 for the ratio between the two. By calculating an upper limit for the average peak UV absorption cross-section of PAHs per carbon atom they derived a lower limit to the fraction of carbon locked up in PAHs of 0.5%. An upper limit to the fraction was estimated by using a conservative lower limit to the UV absorption cross-section per C atom which produced a value of 5%. Tielens *et al.* (1987) report that an analysis of the emission mechanism of PAHs in the interstellar medium produces an estimate of the fraction of carbon locked up in the molecules of about 1% and hence a value of f_c = 0.01 is used in the model.

5.2 Thermal effect of dust grains

5.2.1 Evidence for dust grains in the nebular environment

The presence of dust grains in the gaseous envelope of a planetary nebula is today unquestioned. The evidence for grains, in the form of absorption features and infrared thermal emission, cannot lead to any other conclusion. Since the discovery by Gillett *et al.* (1967) of 10μm emission from NGC 7027, which was greatly in excess of the expected free-free and line fluxes, IR measurements taken of many planetary nebulae show that in general there is an infrared continuum that is from 10 to 100 times stronger in the 5μm - 18μm region than the extrapolated free-free and bound-free continua. This is shown below in Table 5.1 in which the 11μm fluxes for some PNe are compared with the radio-frequency fluxes at 10 GHz, a frequency at which the nebulae are optically thin (from Osterbrock 1974a).

Table 5.1
Infrared and radio-frequency continuum fluxes of PNe

Nebula	πF_ν (11μm) (f u)	πF_ν (10 GHz) (f u)
NGC 6543	54	0.71
NGC 6572	28	1.23
NGC 7009	10	0.63
NGC 7027	320	6.3
NGC 7662	3	0.54
IC 418	33	1.4

Note: 1 f u = 1 flux unit = 10^{-23} erg cm^{-2} Hz^{-1} s^{-1}

Narrow band-width measurements show that most of the infrared radiation has a continuous spectrum except for a few emission lines that have been detected in several planetary nebulae. These lines make only a small contribution to the broad-band-measured IR fluxes, and the fluxes listed have been corrected for them and refer to the continuum only.

Krishna Swamy *et al.* (1968) interpreted the initial IR observations of NGC 7027 as being due to emission from small graphite particles heated by resonantly trapped

Lyα photons. It was not possible to say whether the grains were inside the ionised zone or the neutral shell. They suggested that the grains could have originated in the envelope of a precursor red giant star, which is now the accepted solution.

Terzian and Saunders (1972) calculated the expected IR flux distributions assuming the grains resided in the neutral shell and predicted a mean grain temperature of ~85 K, with fluxes peaking at ~35 μm. The 10 - 18 μm observations of Cohen and Barlow (1974) did not support this prediction, yielding mean colour temperatures of ~190 K. However, it later became clear that the broad-band observations of PNe at 10μm were yielding too high 10 - 18 μm colour temperatures. Furthermore, later work by Telesco and Harper (1977) on airborne far-infrared observations showed that ground-based 10 - 20 μm observations sample a hotter dust component than 30 - 100 μm observations.

Telesco and Harper (1977) found that their FIR data for NGC 7027 could be fitted by a 95 K blackbody with a λ^{-2} emissivity. Classical Mie theory predicts such an emissivity law for small graphite particles. McCarthy *et al.* (1978) obtained 15 - 40 μm spectrophotometry of NGC 7027 and found that a 90 K blackbody with λ^{-2} emissivity produced the best fit. Moseley (1980) observed thirteen PNe at four wavelengths between 37 and 108 μm. The flux distributions were generally similar to that of NGC 7027 and the mean colour temperature was 80 K (for λ^{-2} emissivity).

The IR observations of NGC 7027 suggest a λ^{-2} emissivity, for which graphite seems appropriate. However, after determination of the FIR constants of graphite by Philipp (1977), Forrest *et al.* (1980) have pointed out that, if appropriate for small grains, this would predict a λ^{-3} emissivity beyond 20μm. Conversely, Koike *et al.* (1980) have experimentally found a λ^{-1} emissivity for small amorphous carbon grains.

Aside from infrared emission there exists plenty of other evidence to support the idea of dust in PNe. Osterbrock (1974b) pointed out that if significant dust existed in the ionised region of a planetary nebula, it would produce asymmetric emission line profiles since the red wing, originating from the far side of the nebula, would suffer more extinction than the blue wing. Since an asymmetric distribution of gas could give rise to spurious results if only a single profile were analysed, Osterbrock compared the profiles of three Balmer lines. For normal extinction laws, the effect of internal extinction would be most pronounced on the profile with the shortest rest wavelength. However, the Hα, Hβ and Hγ lines of NGC 7027 showed no

noticeable differences in their profiles and Osterbrock set a conservative upper limit of $\tau(\mathrm{H}\beta) < 0.6$.

Hicks *et al.* (1976) analysed the less thermally broadened [OIII] λ5007 profile at various points on NGC 7027. A red/blue asymmetry was found, consistent with a non-uniform gas distribution or $\tau_{\mathrm{int}}(\lambda5007) \sim 0.34$. However, as pointed out by Hicks *et al.*, this effect could also be produced by a non-uniform distribution of external dust across the face of an inclined spheroidal nebula, preferentially extinguishing the emission from one side. NGC 7027 is known to have such an asymmetric distribution of external dust, which seems to be associated with the dense molecular CO envelope.
Doughty and Kaler (1982) analysed the observations of seven PNe carried out by O. C. Wilson. They compared both short and long wavelength lines in order to eliminate the effects of asymmetric gas distributions. For NGC 7027 they derived $\tau(\mathrm{H}\beta) = 0.15$, assuming that the dust is internal.

Bohlin *et al.* (1975) obtained the first UV spectrum of NGC 7027 and found that the CIV λ1549 resonance doublet was a factor of three weaker, relative to [CIII] λ1909 than predicted by model nebula calculations. They ascribed the discrepancy to dust absorption of the resonantly scattered CIV photons and derived a radial dust optical depth in the ionised zone of $\tau_d(\lambda1549) \sim 0.2$, using the resonance line transfer results of Panagia and Ranieri (1973). Their nebular model had an ionised hydrogen column density of $N_{\mathrm{H}} = 1.9\times10^{21}$ cm^{-2} and they noted that this column density, combined with a normal interstellar reddening law and colour excess ratio $N_{\mathrm{H}}/E_{B-V} = 5.4\times10^{21}$ cm^{-2} mag^{-1}, would predict $\tau_d(\lambda1549) = 2.6$, so that the dust within the ionised zone must be depleted by a factor of ten if it has normal interstellar reddening characteristics.
Harrington *et al.* (1982) carried out an analysis of the optical and UV spectrum of NGC 7662 and by using the resonance line transfer results of Hummer and Kunasz (1980) they derived an internal dust optical depth of $\tau_d(\lambda1549) = 0.08$-$0.13$.

The presence of dust grains in the planetary nebula environment is today an established fact. The debatable issue is what exactly the grains are composed of and how this is related to other physical aspects of the nebula.
Observation shows that the composition of the dust varies between nebulae. The standard picture of dust formation today is, as logic would suggest, that the C/O ratio determines the type of grain formed. In oxygen-rich environments CO molecules should lock up all the carbon atoms, leaving only oxygen-rich grains such as silicates to form. In carbon-rich environments the locking up of oxygen in

CO molecules would allow carbon-rich grains such as silicon carbide, graphite and amorphous carbon to condense. Observations of C/O ratios in PNe confirm this picture as shown in Table 5.2 below.

Table 5.2

Infrared emission features and nebular C/O abundance ratios

Nebula	Feature	C/O	Reference
IC 4997	silicate	0.4	Seaton (1983)
He 2-131	silicate	0.3	Seaton (1983)
M 1-26	silicate	0.5	Seaton (1983)
IC 418	SiC	1.3	Seaton (1983)
NGC 6572	SiC	1.1	Seaton (1983)
IC 2501	SiC	0.9	Seaton (1983)
NGC 5315	11.3μm	2.5	Torres-Peimbert and Pena (1981)
BD+30^{0}3639	11.3μm	$\geq$2.8	Torres-Peimbert and Pena (1981)
NGC 7027	11.3μm	3.5	Shields (1978)

The nebulae with silicate emission all have C/O < 0.5. The nebulae with strong SiC emission all have C/O very close to unity and are all consistent with C/O > 1 when the small contribution from C locked up in SiC is allowed for. The nebulae with strong features in the 3 - 12 μm range (attributed to aromatic hydrocarbons) all have C/O > 2.

The nebular model presented here has a C/O ratio of 1.75 and hence the physical processes that involve dust are modelled with the assumption that the grains are composed of amorphous carbon (Chapter 7).

5.2.2 Calculation of dust temperature in the nebula

For a spherical dust grain of radius a, equating the radiative energy emitted by the grain to the energy absorbed by the grain gives the following expression for the dust grain temperature (Hollenbach *et al.* 1991) where the grain is assumed to radiate as a black body:

$$4\pi a^2 \int_0^\infty Q_{\rm abs}(\nu)\pi B_\nu(T_d)\,d\nu = \pi a^2 \int_0^{\nu_{\rm H}} Q_{\rm abs}(\nu)F(\nu)\,d\nu + 4\pi a^2 \int_0^\infty Q_{\rm abs}(\nu)\pi J_d(\nu)\,d\nu \quad (5.22)$$

T_d is the temperature of the dust grain
$B_\nu(T_d)$ is the Planck function at the temperature T_d
$F(\nu)$ is the local FUV flux in the nebula
$J_d(\nu)$ is the mean intensity of the re-emitted infrared radiation from the grains
$Q_{\rm abs}(\nu)$ is the dust absorption efficiency
$\nu_{\rm H}$ is the frequency of the Lyman limit of atomic hydrogen

The dust absorption efficiency depends on the refractive index of the grain material which is a function of wavelength. If the assumption is made that the grains are spherical then the absorption efficiency may be calculated using Mie scattering theory. The results of such calculations are tabulated in Chapter 7 (§7.2) using values of refractive index for amorphous carbon taken from the literature.
For the purposes of the present calculation $Q_{\rm abs}$ is approximated according to the following scheme (see §7.2 for derivation of formulae):

$$\begin{aligned} Q_{\rm abs}(\nu) &= m_1\nu && \text{for } \nu \le \nu_0 \\ Q_{\rm abs}(\nu) &= c_2 - m_2\nu && \text{for } \nu_0 < \nu \le \nu_1 \\ Q_{\rm abs}(\nu) &= c_3 - m_3\nu && \text{for } \nu > \nu_1 \end{aligned} \tag{5.23}$$

where $\nu_0 = 6.00 \times 10^{14}$ Hz, $\nu_1 = 1.05 \times 10^{15}$ Hz
$m_1 = 2.767 \times 10^{-15}$
$c_2 = 1.740, \quad m_2 = 1.333 \times 10^{-16}$
$c_3 = 1.817, \quad m_3 = 1.990 \times 10^{-16}$

The UV radiation field from the central star will be much stronger than the infrared continuum emitted by the grains. This, combined with the fact that the dust absorption efficiency $Q_{\rm abs}(\nu)$ is very small at IR wavelengths means that the contribution to dust grain heating from the IR continuum is negligible compared to the effect of the UV flux and hence the second integral on the RHS of equation (5.22) can be ignored.
Thus, the equation of energy balance reads:

$$4\pi a^2 \int_0^\infty Q_{\rm abs}(\nu)\pi B_\nu(T_d)\,d\nu \;=\; \pi a^2 \int_0^{\nu_{\rm H}} Q_{\rm abs}(\nu)F(\nu)\,d\nu \tag{5.24}$$

The Planck function $B_\nu(T_d)$ is given by:

$$B_\nu(T_d) = \frac{2h\nu^3}{c^2}\frac{1}{e^{h\nu/kT_d}-1} \qquad \text{erg cm}^{-2}\,\text{s}^{-1}\,\text{Hz}^{-1}\,\text{sr}^{-1} \tag{5.25}$$

The integral on the LHS of equation (5.24) is thus:

$$\mathrm{I}_1 = 4\pi a^2 \int_0^\infty Q_{\mathrm{abs}}(\nu) \frac{2\pi h\nu^3}{c^2} \frac{1}{e^{h\nu/kT_d} - 1}\, d\nu \tag{5.26}$$

Hence:

$$\mathrm{I}_1 = \frac{8\pi^2 h a^2}{c^2}(\mathrm{J} + \mathrm{K} + \mathrm{L})$$

Where:

$$\mathrm{J} = m_1 \int_0^{\nu_0} \frac{\nu^4}{e^{h\nu/kT_d} - 1}\, d\nu$$

$$\mathrm{K} = c_2 \int_{\nu_0}^{\nu_1} \frac{\nu^3}{e^{h\nu/kT_d} - 1}\, d\nu - m_2 \int_{\nu_0}^{\nu_1} \frac{\nu^4}{e^{h\nu/kT_d} - 1}\, d\nu$$

$$\mathrm{L} = c_3 \int_{\nu_1}^{\infty} \frac{\nu^3}{e^{h\nu/kT_d} - 1}\, d\nu - m_3 \int_{\nu_1}^{\infty} \frac{\nu^4}{e^{h\nu/kT_d} - 1}\, d\nu$$

Making the substitution $x = h\nu/kT_d$ we arrive at:

$$\mathrm{J} = m_1 \left(\frac{kT_d}{h}\right)^5 \int_0^\alpha \frac{x^4}{e^x - 1}\, dx \tag{5.27}$$

$$\mathrm{K} = c_2 \left(\frac{kT_d}{h}\right)^4 \int_\alpha^\beta \frac{x^3}{e^x - 1}\, dx - m_2 \left(\frac{kT_d}{h}\right)^5 \int_\alpha^\beta \frac{x^4}{e^x - 1}\, dx \tag{5.28}$$

$$\mathrm{L} = c_3 \left(\frac{kT_d}{h}\right)^4 \int_\beta^\infty \frac{x^3}{e^x - 1}\, dx - m_3 \left(\frac{kT_d}{h}\right)^5 \int_\beta^\infty \frac{x^4}{e^x - 1}\, dx \tag{5.29}$$

Where $\alpha = h\nu_0/kT_d$, $\beta = h\nu_1/kT_d$.

The integral $\int_0^\alpha x^4/(e^x - 1)\, dx$ is evaluated in Appendix G.
The result is:

$$\int_0^\alpha \frac{x^4}{e^x - 1}\, dx = 24\zeta(5) - \sum_{n=1}^{\infty} \frac{e^{-n\alpha}}{n} \left(\frac{24}{n^4} + \frac{24\alpha}{n^3} + \frac{12\alpha^2}{n^2} + \frac{4\alpha^3}{n} + \alpha^4\right) \tag{5.30}$$

Where $\zeta(n)$ is the Riemann zeta function, defined as:

$$\zeta(n) = \sum_{k=1}^{\infty} \frac{1}{k^n}$$

From tables, $\zeta(5) = 1.0369$ approximately.

For integral J the parameter α in equation (5.30) is given by $\alpha = h\nu_0/kT_d$ and hence the infinite series will become more important as T_d increases. The dust

temperature in the neutral shell is predicted never to exceed about a hundred kelvin and so to see whether the infinite series makes a significant contribution to equation (5.30) an upper limit of $T_d = 100$ K is used:

$$\alpha_{\min} \approx \frac{6.6 \times 10^{-27} \times 6.00 \times 10^{14}}{1.3 \times 10^{-16} \times 100} \approx 300$$

So the first term in the infinite series will have a factor of $\sim e^{-300}$ which will be multiplied by a factor of $\sim (300)^4$. The exponential factor is far more important and makes the term utterly negligible in comparison to $24\zeta(5)$. Subsequent terms in the series will be even more negligible. Hence the result for integral J is effectively:

$$\mathrm{J} = 24 m_1 \left(\frac{kT_d}{h}\right)^5 \zeta(5) \tag{5.31}$$

The integral $\int_0^\alpha x^3/(e^x - 1)\,dx$ is also calculated in Appendix G.
The result is:

$$\int_0^\alpha \frac{x^3}{e^x - 1}\,dx = 6\zeta(4) - \sum_{n=1}^{\infty} \frac{e^{-n\alpha}}{n}\left(\frac{6}{n^3} + \frac{6\alpha}{n^2} + \frac{3\alpha^2}{n} + \alpha^3\right) \tag{5.32}$$

Hence the integral K may be written:

$$\mathrm{K} = c_2 \left(\frac{kT_d}{h}\right)^4 \int_\alpha^\beta \frac{x^3}{e^x - 1}\,dx - m_2 \left(\frac{kT_d}{h}\right)^5 \int_\alpha^\beta \frac{x^4}{e^x - 1}\,dx \tag{5.33}$$

Which may be expanded into a sum of four infinite series using equations (5.30) and (5.32). The same reasoning can be applied here as to whether the four infinite series are significant. In comparison with the result for integral J they represent a negligible contribution. Exactly similar reasoning can be applied to integral L which makes an insignificant contribution to the overall sum.
Hence the result for the integral on the LHS of equation (5.24) is:

$$\mathrm{I}_1 = \frac{192 m_1 \pi^2 h a^2}{c^2} \left(\frac{kT_d}{h}\right)^5 \zeta(5) \tag{5.34}$$

A simple fifth-power expression for T_d.

The integral on the RHS of equation (5.24) is:

$$\mathrm{I}_2 = \pi a^2 \int_0^{\nu_\mathrm{H}} Q_{\mathrm{abs}}(\nu) F(\nu)\,d\nu$$

Converting this to an integral over wavelength:

$$\mathrm{I}_2 = \pi c a^2 \int_{\lambda_\mathrm{H}}^{\infty} Q_{\mathrm{abs}}(\lambda)\Phi(\lambda)\, d\lambda \tag{5.35}$$

where $\lambda_\mathrm{H} = 912\,\text{Å}$.

$Q_{\mathrm{abs}}(\lambda)$ is the dust absorption efficiency as a function of wavelength
$\Phi(\lambda)$ is the radiation field energy density (erg cm^{-3} Å^{-1})

Hence, equating the integrals I_1 and I_2:

$$192 m_1 h \left(\frac{\pi a}{c}\right)^2 \left(\frac{kT_d}{h}\right)^5 \zeta(5) \;=\; \pi c a^2 \int_{\lambda_\mathrm{H}}^{\infty} Q_{\mathrm{abs}}(\lambda)\Phi(\lambda)\, d\lambda \tag{5.36}$$

Including the effect of the 2.73 K microwave background radiation yields the following expression for T_d:

$$T_d = \left(\frac{c^3 h^4}{192 m_1 \pi k^5 \zeta(5)} \int_{\lambda_\mathrm{H}}^{\infty} Q_{\mathrm{abs}}(\lambda)\Phi(\lambda)\, d\lambda \;+\; (2.73)^5\right)^{0.2}$$

Inserting numerical values for the constants gives:

$$T_d\,(\mathrm{K}) \;=\; \left(5.975 \times 10^{17} \int_{\lambda_\mathrm{H}}^{\infty} Q_{\mathrm{abs}}(\lambda)\Phi(\lambda)\, d\lambda \;+\; (2.73)^5\right)^{0.2} \tag{5.37}$$

By performing numerical integration over the radiation field energy density, the integral in equation (5.37) may be evaluated and hence the dust temperature at each point in the nebula may be computed.

5.2.3 Theory behind photoelectric emission from dust grains

After absorption of a FUV photon, a dust grain may emit a photoelectron. The kinetic energy of the electron will be the difference between the photon energy and the work function of the grain, which in general will depend on the charge on the grain. The difference between this input of kinetic energy to the gas and the effective cooling when electrons (with typical energy $\sim kT$) recombine with dust grains represents a net heating of the gas.

The charge on a dust grain may be found by equating the rate of ejection of electrons from a grain to the rate of recombination of electrons with a dust grain (Spitzer 1968):

$$\int_{\nu_0}^{\nu_\mathrm{H}} \sigma_d(\nu) Y c \frac{F(\nu)}{h\nu}\, d\nu = \sigma_d \left(1 + \frac{h\nu_0 - h\nu_d}{kT}\right) n_e v_e \tag{5.38}$$

$\sigma_d(\nu)$ is the photoabsorption cross-section of a grain
σ_d is the geometrical cross-section of a grain
Y is the photoelectric emission efficiency
$v_e = (2kT/m_e)^{1/2}$ is the r.m.s. speed of an electron
$F(\nu)$ is the local radiation field energy density

The upper limit on the integral, $\nu_{\rm H}$, is the frequency of the Lyman limit since there are no L_c photons. The lower limit, ν_0, is the frequency corresponding to the energy barrier that electrons have to overcome before leaving the grain.
The value of ν_0 incorporates the effect of charge on the grains:

$$h\nu_0 = h\nu_d + V_0 \tag{5.39}$$

$h\nu_d$ is the threshold photoelectric energy of the neutral dust material
V_0 is the electrostatic potential of the grain

The factor $1 + (h\nu_0 - h\nu_d)/kT$ in equation (5.38) takes account of enhanced recombination when the grains are positively charged ($\nu_0 > \nu_d$).

$\sigma_d(\nu)$ is, of course, given by $Q_{\rm abs}(\nu)\sigma_d$ where $Q_{\rm abs}(\nu)$ is the radiation absorption efficiency factor for the dust grains. Chapter 7 contains the results of calculations of $Q_{\rm abs}(\nu)$ but for the present calculation it is sufficient to assume that $Q_{\rm abs}(\nu) = 1.4$ over the relevant frequency range (§7.2).
If it is also assumed that Y is independent of frequency (Feuerbacher and Fitton 1972) then equation (5.38) becomes:

$$1.4Yc\int_{\nu_0}^{\nu_{\rm H}} \frac{F(\nu)}{h\nu}\,d\nu = n_e\left(1 + \frac{h\nu_0 - h\nu_d}{kT}\right)\left(\frac{2kT}{m_e}\right)^{1/2} \tag{5.40}$$

Converting to an integral over wavelength and defining the parameter $x = \nu_0/\nu_{\rm H}$ we have:

$$1.4 \times 10^8 \frac{Y}{h}\int_{\lambda_{\rm H}}^{\lambda_{\rm H}/x} \lambda\Phi(\lambda)\,d\lambda = n_e\left(\frac{kT + h\nu_0 - h\nu_d}{kT}\right)\left(\frac{2kT}{m_e}\right)^{1/2} \tag{5.41}$$

$\Phi(\lambda)$ is the radiation field energy density (erg cm^{-3} Å^{-1})

Rearranging this equation we have:

$$1.4 \times 10^8 \frac{YkT}{hn_e}\left(\frac{m_e}{2kT}\right)^{\frac{1}{2}}\int_{\lambda_{\rm H}}^{\lambda_{\rm H}/x} \lambda\Phi(\lambda)\,d\lambda = kT + h\nu_0 - h\nu_d \tag{5.42}$$

Defining the parameters x_k and x_d such that:

$x_k = kT/h\nu_{\rm H}$

$x_d = \nu_d/\nu_{\rm H}$

we then have:

$$1.4 \times 10^8 \frac{YkT}{h^2 \nu_{\rm H} n_e} \left(\frac{m_e}{2kT}\right)^{\frac{1}{2}} \int_{\lambda_{\rm H}}^{\lambda_{\rm H}/x} \lambda \Phi(\lambda)\, d\lambda = x_k + x - x_d \qquad (5.43)$$

Following de Jong (1977) the photoelectric yield Y is taken to be 0.1 since, using this value, the observed cooling rates in diffuse clouds can be theoretically balanced by photoelectric heating, the main heating mechanism in such low density interstellar objects (Pottasch *et al.* 1979). The photoelectric threshold for neutral grain material is taken to be $h\nu_d = 6$ eV for the same reason (de Jong, 1980). Hence the value of x_d is:

$$x_d = \frac{h\nu_d}{h\nu_{\rm H}} = \frac{6\ {\rm eV}}{13.6\ {\rm eV}} = 0.44$$

Now $x_k = kT/h\nu_{\rm H}$, hence

$$x_k = \frac{T}{1.58 \times 10^5}$$

Substituting values for the constants in equation (5.43) gives:

$$2.4328 \times 10^7 \frac{YT^{1/2}}{n_e} \int_{\lambda_{\rm H}}^{\lambda_{\rm H}/x} \lambda \Phi(\lambda)\, d\lambda - (x_k + x - x_d) = 0 \qquad (5.44)$$

Hence it is required to solve the following equation for x:

$$\mathcal{F}(x) = \gamma \int_{\lambda_{\rm H}}^{\lambda_{\rm H}/x} \lambda \Phi(\lambda)\, d\lambda - (x_k + x - x_d) = 0 \qquad (5.45)$$

where $\gamma = 2.4328 \times 10^7 YT^{1/2}/n_e$.

The value of x will lie somewhere between the limits $x \rightarrow x_d - x_k$ (the grains are neutral) and $x \rightarrow 1$ (the grains attain their maximum charge). The Bisection Method is used in the model (Press *et al.* 1992) to determine the value of x satisfying equation (5.45).

The net heat input to the gas results from the balance between energy input from photoejected electrons and energy loss due to electrons recombining with dust grains:

$$\begin{aligned} \Gamma_{\rm grain}\ ({\rm erg\ cm^{-3}\ s^{-1}}) = & \int_{\nu_0}^{\nu_{\rm H}} Q_{\rm abs}(\nu)(n_d \sigma_d) Y c F(\nu) g(\nu) \frac{(h\nu - h\nu_0)}{h\nu}\, d\nu \\ & - n_e n_d < \frac{1}{2} m_e v^2 v \sigma_{\rm rec}(T) > \end{aligned} \qquad (5.46)$$

n_d is the number density of dust grains (cm^{-3})
σ_d is the geometrical cross-section of a dust grain (cm^2)
$Q_{abs}(\nu)$ is the photoabsorption efficiency factor
$g(\nu)$ is the kinetic energy partition function
m_e is the mass of an electron (g)
v is the speed of an electron (cm s^{-1})
$\sigma_{rec}(T)$ is the recombination cross-section for an electron recombining with a dust grain (cm^2)

Strictly speaking, Q_{abs} is a function of frequency as calculated in Chapter 7. However, for the purposes of this calculation the approximation is made that $Q_{abs} = 1.4$ over the relevant frequency range (§7.2).
$g(\nu)$ represents the fraction of the available energy imparted to the photoejected electron. The remainder of the energy is dissipated in the excitation energy of the grain. There is evidence to suggest that at high photon energies $g(\nu) \approx 0.5$. The experimental support comes from studies of the benzene, coronene and ovalene molecules (d'Hendecourt and Leger 1987) and bulk graphite (Feuerbacher *et al.* 1973). This quantity is uncertain but, with the evidence cited, a value of $g(\nu)$=0.5 is assumed for the model (c.f. equation (5.11) and the discussion of the energy repartition coefficient for photoionisation of PAH molecules).

Hence, converting to an integral over wavelength gives

$$\Gamma_{grain} = 0.7 < n_d\sigma_d > Yc\int_{\lambda_H}^{\lambda_H/x} \Phi(\lambda)\left(1 - \frac{\lambda}{\lambda_0}\right) d\lambda - n_e n_d < \frac{1}{2}m_e v^2 v\sigma_{rec}(T) > \tag{5.47}$$

$< n_d\sigma_d >$ is the mean value of the absorption coefficient due to dust (cm^{-1})

The recombination cross-section $\sigma_{rec}(T)$ is given by the expression as in equation (5.38):

$$\sigma_{rec}(T) = \sigma_d\left(1 + \frac{h\nu_0 - h\nu_d}{kT}\right) \tag{5.48}$$

Using the definitions of x_k, x and x_d this may be written

$$\sigma_{rec}(T) = \frac{\sigma_d}{T}\left(\frac{hc}{k\lambda_H}\right)(x_k + x - x_d) \tag{5.49}$$

Hence the Maxwell averaged recombined energy is

$$< \frac{1}{2}m_e v^2 v\sigma_{rec}(T) >= 4\pi\left(\frac{m_e}{2\pi kT}\right)^{\frac{3}{2}}\int_0^\infty \frac{1}{2}m_e v^5\sigma_{rec}(T)\exp\left(-\frac{m_e v^2}{2kT}\right) dv \tag{5.50}$$

Using equation (5.49) this becomes:

$$< \frac{1}{2} m_e v^2 v \sigma_{\rm rec}(T) >= \frac{1}{\sqrt{2\pi}} \left(\frac{m_e}{kT}\right)^{\frac{5}{2}} \left(\frac{hc}{\lambda_{\rm H}}\right) \sigma_d(x_k + x - x_d) \int_0^\infty v^5 \exp\left(-\frac{m_e v^2}{2kT}\right) dv \tag{5.51}$$

The value of the integral is

$$\mathrm{I} = \int_0^\infty v^5 \exp\left(-\frac{m_e v^2}{2kT}\right) dv = \left(\frac{2kT}{m_e}\right)^3$$

So that

$$< \frac{1}{2} m_e v^2 v \sigma_{\rm rec}(T) >= \left(\frac{32kT}{\pi m_e}\right)^{\frac{1}{2}} \left(\frac{hc}{\lambda_{\rm H}}\right) \sigma_d(x_k + x - x_d) \tag{5.52}$$

Using the fact that $\lambda_0 = \lambda_{\rm H}/x$ and combining equations (5.47) and (5.52) we have for the heating rate due to photoejection of electrons from dust grains the following expression:

$$\begin{aligned} \Gamma_{\rm grain}\ (\mathrm{erg\ cm^{-3}\ s^{-1}}) \ =& 0.7 < n_d \sigma_d > Yc \int_{\lambda_{\rm H}}^{\lambda_{\rm H}/x} \Phi(\lambda) \left(1 - x\frac{\lambda}{\lambda_{\rm H}}\right) d\lambda \\ & - \left(\frac{32kT}{\pi m_e}\right)^{\frac{1}{2}} \left(\frac{hc}{\lambda_{\rm H}}\right) n_e < n_d \sigma_d > (x_k + x - x_d) \end{aligned} \tag{5.53}$$

The number density of dust grains can be computed if a value for the mass ratio of dust to gas in the nebula is estimated. Chapter 7 contains a full discussion of what to take for this parameter with the conclusion that a constant value of $\Upsilon = \rho_{\rm dust}/\rho_{\rm gas} = 0.002$ is suitable. Hence the number density of dust grains is given by:

$$n_d\,(\mathrm{cm^{-3}}) = \frac{\rho_{\rm gas} \Upsilon}{m_d} \tag{5.54}$$

$\rho_{\rm gas}$ is mass density of gas (g cm^{-3})
m_d is the mass of one dust grain (g)

The mass of a dust grain is given by:

$$m_d\,(\mathrm{g}) = \frac{4}{3} \pi r_d^3 \rho_d \tag{5.55}$$

r_d is the mean grain radius (cm)
ρ_d is the grain mass density (g cm^{-3})

Chapter 7 discusses what values to take for r_d and ρ_d. Since the dust is modelled as amorphous carbon grains a density of 1.8 g cm^{-3} is appropriate. Based on

observational evidence a mean grain radius of $r_d = 100$ nm is employed for the model.

If $n_{\rm H}$ is the number density of hydrogen nuclei, i.e. $n_{\rm H} = n({\rm H}) + 2n({\rm H_2})$ then the mass density of the gas is given by:

$$\rho_{\rm gas} = m_{\rm H}(n_{\rm H} + 4 \times 0.1 \times n_{\rm H}) \tag{5.56}$$

$m_{\rm H}$ is the mass of one hydrogen atom

The simplicity of equation (5.56) arises from ignoring the tiny mass contribution from elements other than hydrogen or helium. The second term in brackets arises from the fact that $m_{\rm He} \approx 4 \times m_{\rm H}$ and the helium abundance is 10% relative to hydrogen.

Hence:

$$\rho_{\rm gas} = 1.4 m_{\rm H} n_{\rm H} \tag{5.57}$$

So combining the above expressions, we have for the grain number density:

$$n_d = \frac{3 \times 1.4 \times m_{\rm H} n_{\rm H} \Upsilon}{4\pi r_d^3 \rho_d} \tag{5.58}$$

Since $\sigma_d = \pi r_d^2$ then combining this with the expression for n_d yields

$$< n_d \sigma_d >= \frac{3 \times 1.4 \times m_{\rm H} n_{\rm H} \Upsilon}{4 r_d \rho_d} \tag{5.59}$$

To summarise, the rate of heating due to photoejection of electrons from dust grains is given by

$$\begin{aligned} \Gamma_{\rm grain}\ ({\rm erg\ cm^{-3}\ s^{-1}}) \ =& 0.7 < n_d \sigma_d > Yc \int_{\lambda_{\rm H}}^{\lambda_{\rm H}/x} \Phi(\lambda) \left(1 - x\frac{\lambda}{\lambda_{\rm H}}\right) d\lambda \\ & - \left(\frac{32kT}{\pi m_e}\right)^{\frac{1}{2}} \left(\frac{hc}{\lambda_{\rm H}}\right) n_e < n_d \sigma_d > (x_k + x - x_d) \end{aligned} \tag{5.60}$$

where

$$< n_d \sigma_d >= 1.05 \frac{m_{\rm H} n_{\rm H} \Upsilon}{r_d \rho_d}$$

and x is the solution to the equation

$$2.4328 \times 10^7 \frac{Y T^{1/2}}{n_e} \int_{\lambda_{\rm H}}^{\lambda_{\rm H}/x} \lambda \Phi(\lambda)\, d\lambda - (x_k + x - x_d) = 0$$

5.2.4 Thermal equilibrium between gas and dust

If there is a difference between the gas kinetic temperature T and the dust temperature T_d then there will in general be a flow of heat energy from the hotter component to the colder, which will depend on the difference in temperature as well as other parameters. This will result in a net heating/cooling of the gas phase.
The net heating rate per unit volume may be written (Burke and Hollenbach 1983):

$$\Gamma_{\rm gas-gr} = 2kn_{\rm H} < n_d\sigma_d > \left(\frac{8kT}{\pi m_{\rm H}}\right)^{1/2} \bar{\alpha}_T(T_d - T) \qquad (5.61)$$

$n_{\rm H}$ is the number density of hydrogen nuclei ($\rm cm^{-3}$)
n_d is the number density of dust grains ($\rm cm^{-3}$)
σ_d is the geometrical cross-section of a dust grain ($\rm cm^2$)
$m_{\rm H}$ is the mass of a hydrogen atom (g)
$\bar{\alpha}_T$ is the mean thermal accommodation coefficient

Most of these parameters are known. The value of $< n_d\sigma_d >$ has been computed previously when looking at photoelectric emission from grains. It is given by:

$$< n_d\sigma_d >= \frac{3 \times 1.4 \times m_{\rm H} n_{\rm H} \Upsilon}{4 r_d \rho_d} \qquad (5.59)$$

The thermal accommodation coefficient α_T is defined when the rate at which gas molecules strike the surface of a grain is equal to the rate at which molecules bounce off and evaporate from the grain surface. It is defined as follows:

$$F_e = F_c \alpha_T (2kT - 2kT_d) \qquad (5.62)$$

F_e is the flux of energy transferred from the gas to the grain surface (erg $\rm cm^{-2}$ $\rm s^{-1}$)
F_c is the flux of gas molecules ($\rm cm^{-2}$ $\rm s^{-1}$)

F_c is defined as follows:

$$F_c = n v_T/4 = n(kT/2\pi m)^{1/2} \qquad (5.63)$$

and obviously represents the flux of gas particles of number density n, thermal speed v_T and mass m.

The value of α_T=1 when an incident gas molecule becomes thermalised ('accommodates') with the surface and leaves with an average kinetic energy of $2kT_d$. In general, $\alpha_T < 1$ because particles interacting with the grain surface do not completely accommodate. The value of α_T must always satisfy $0 \leq \alpha_T \leq 1$.

The value of $\bar{\alpha}_T$ will depend on the material composing the grains, the molecular species interacting with the surface and the gas temperature in a fairly complicated way. Since the model assumes a carbon-rich environment (C/O = 1.75) the dust is modelled as amorphous carbon grains. By assuming the number density of helium atoms is $0.1n_{\rm H}$ and ignoring heavier elements, Burke and Hollenbach computed values of $\bar{\alpha}_T$ for a variety of grain compositions and gas/grain temperatures in an astrophysical environment. The results for the case of graphite particles are shown in Figure 5.1. Burke and Hollenbach do not compute values of $\bar{\alpha}_T$ for amorphous carbon and hence the values for graphite are used in the model with the presumption that this will not introduce unacceptably large errors.

Figure 5.1
Average accommodation coefficient $\bar{\alpha}_T$ vs gas temperature for interstellar gas incident on graphite particles
(from Burke and Hollenbach 1983)

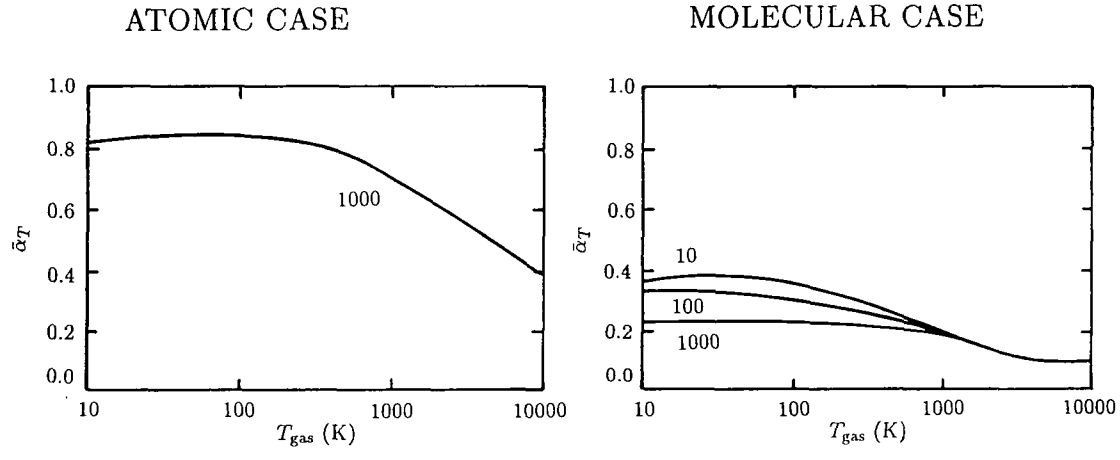

Two limiting cases of interstellar gas are distinguished - purely atomic and purely molecular hydrogen. The number next to each curve represents the grain surface temperature in kelvin.

Since the gas kinetic temperature in the neutral region never exceeds about 500 K it can be seen from the graphs that, for both the atomic and molecular case, over the region 10 K < T < 500 K the value of $\bar{\alpha}_T$ is practically constant (for a given grain surface temperature). Hence, to simplify matters, the value of $\bar{\alpha}_T$ is

assumed independent of the gas temperature.

Of course, the model does not presume that the gas is in either purely atomic or purely molecular form and so some expression must be sought to extrapolate the value of $\bar{\alpha}_T$ to the usual situation of a hydrogen atomic/molecular mix. The value of the accommodation coefficient is lower for the molecular case primarily because $n(\mathrm{H_2}) = 0.5 n_{\mathrm{H}}$ and that $v_{\mathrm{T}}(\mathrm{H_2}) = 0.707 v_{\mathrm{T}}(\mathrm{H})$ where v_{T} is the average thermal speed of the species.

Hence a suitable expression for $\bar{\alpha}_T$ which has the right limiting form for a purely atomic/purely molecular hydrogen gas is:

$$\bar{\alpha}_T = 0.8 \times \Big(n(\mathrm{H}) + 0.707 n(\mathrm{H_2})\Big)/n_{\mathrm{H}} \tag{5.64}$$

n_{H} is the number density of hydrogen nuclei i.e. $n_{\mathrm{H}} = n(\mathrm{H}) + 2n(\mathrm{H_2})$

From this expression it can be seen that when the gas is purely atomic (i.e. $n(\mathrm{H_2}) = 0$) then $\bar{\alpha}_T = 0.8$. When the gas is purely molecular (i.e. $n(\mathrm{H}) = 0$) then $\bar{\alpha}_T = 0.28$, and in general the value of the average accommodation coefficient lies between these two limits. What equation (5.64) does not take into account is the fact that the value of $\bar{\alpha}_T$ also depends on the grain surface temperature. However, this is a fairly slight effect (as can be seen from Figure 5.1) and is ignored for simplification.

5.3 Heating due to chemical reactions

5.3.1 Thermal effect of atomic/molecular interactions

Every chemical species has associated with it a standard enthalpy of formation. This represents the enthalpy of the reaction forming the species from the constituent elements in some standard state (298 K and 1 atm pressure). Because enthalpy (H) is a state function, ΔH for a given overall process will be independent of the path taken. This principle is known as Hess' Law of constant heat summation, and it enables ΔH for any chemical reaction to be computed, so long as the standard enthalpies of the reactants and products are known.
For example, for a chemical reaction A + B $\rightarrow$ C + D the enthalpy of this reaction would be given by:

$$\Delta H^0_{298} = \Delta H^0_{f,298}(A) + \Delta H^0_{f,298}(B) - \Delta H^0_{f,298}(C) - \Delta H^0_{f,298}(D)$$

$\Delta H^0_{f,298}$ is the standard enthalpy of formation (at 298 K and 1 atm pressure)
This definition uses the convention that positive enthalpy implies an exothermic reaction and negative enthalpy implies an endothermic reaction.

In general, the enthalpy of any chemical reaction is given by:

$$\Delta H^0_{298} = \sum_{\text{reactants}} n_r \Delta H^0_{f,298} - \sum_{\text{products}} n_p \Delta H^0_{f,298} \qquad (5.65)$$

Hence, knowing the enthalpies of formation of all the chemical species in the model will enable the heat evolved from each chemical reaction to be computed.

For a particular chemical reaction A + B $\rightarrow$ C + D, the contribution this reaction makes to the heating per unit volume is then given by:

$$\Gamma_{\text{reaction}} = n(A)n(B)k\Delta H \qquad (5.66)$$

n(A) is the number density of species A (as for B) (cm^{-3})
k is the rate coefficient for the process (cm^3 s^{-1})
ΔH is the enthalpy of the reaction (erg)

In this way, knowing the enthalpies of formation of all the chemical species enables one to determine the contribution the reactions make to the overall heating of the gas.

Appendix A lists all the chemical species used in the model with their associated enthalpies of formation.

5.3.2 Heat input from photoionisation reactions

When a photon of energy $h\nu$ is absorbed by a molecule followed by ejection of an electron, the electron has an initial kinetic energy of $h(\nu - \nu_0)$ where ν_0 is the threshold frequency for photoionisation. The photoelectron is rapidly thermalised and thus contributes to the overall heating of the gas. For a species X at a particular point in the nebula the contribution to the heating of the gas (per unit volume per unit time) due to photoionisation is given by:

$$\Gamma_{\text{photoionisation}} = n(\text{X}) \int_{\lambda_\text{H}}^{\lambda_0} \Phi(\lambda) \lambda c \sigma_\lambda(\text{X}) \left(\frac{1}{\lambda} - \frac{1}{\lambda_0} \right) d\lambda \qquad (5.67)$$

c is the speed of light (cm s^{-1})
λ_H is the Lyman limit of atomic hydrogen ($\lambda_\text{H} = 912$ Å)
λ_0 is the threshold wavelength for the photoionisation process ($\lambda_0 = c/\nu_0$) (Å)
$n(\text{X})$ is the number density of species X (cm^{-3})
$\Phi(\lambda)$ is the local radiation field energy density (erg cm^{-3} Å^{-1})
$\sigma_\lambda(\text{X})$ is the photoionisation cross-section for species X as a function of λ (cm^2)

Theoretically, knowledge of the energy spectrum of radiation and the photoionisation cross-section (as a function of wavelength) would thus enable accurate computation of the contribution to the heating of the gas made by photoionisation of species X. For species for which cross-section data is available in the literature this is exactly how the model computes the heating effect (see also the discussion on computation of photorate coefficients, §3.2.1.1). Numerical integration is employed to calculate equation (5.67) for every photo-reacting species with data on σ_λ. These computations must obviously be carried at each point in the nebula as the spectrum of radiation energy will change with distance from the star.
Data on photoionisation cross-sections does not exist for every species considered in the model and for these cases some approximation must be made to calculate their contribution to the gas heating. If the threshold wavelength for photoionisation is known for a species but cross-section data is unavailable then the approximation is made that the cross-section is constant between λ_H and λ_0 and has the value $\sigma_\lambda = 10^{-17}$ cm^2 (see also §3.2.1.1).
For some species data may not exist for cross-section or threshold wavelength. In these cases the assumption made is that such a photoionisation reaction always

reacts with a photon of energy 13.0 eV and that this mean photon energy remains constant throughout the nebula. Since the specific enthalpies of the ionised and neutral atom are known it is then a simple task of subtracting the difference in enthalpies (which represents the ionisation potential of the neutral form) from the energy of the ionising photon to determine the energy imparted to the ejected electron.

5.3.3 Heat input from cosmic ray interactions

Cosmic rays (principally protons) represent a potentially large source of energy input to the nebula. Cosmic ray particles (CRPs) of relatively low energy (2 to 10 MeV) are most effective in ionising and heating the gas. The most recent analysis of ionisation and molecular abundances in diffuse clouds suggests a typical hydrogen ionisation rate of $\zeta = 7 \times 10^{-17}$ s^{-1} (van Dishoeck and Black 1986). This corresponds to a primary ionisation rate of $\zeta_0 = \zeta/(1+\phi) = 4 \times 10^{-17}$ s^{-1}, where $\phi \approx 0.7$ is the correction for secondary ionisations. A value of $\zeta_0 = 4 \times 10^{-17}$ s^{-1} is used in the model as the primary hydrogen ionisation rate.
An accurate determination of the heating rate due to CRPs is very complicated and must by necessity involve detailed knowledge of the energy spectrum of the cosmic rays. In a neutral molecular gas the mean energy input per primary ionisation (including secondary processes) probably lies in the range 5.7 to 7.3 eV, the higher value applying at densities $n_{\rm H} \sim 10^4$ cm^{-3} (Cravens and Dalgarno 1978). The model thus assumes an energy input of 6 eV per cosmic ray interaction.

Hence for each individual CRP-molecule interaction the heating rate per unit volume will be:

$$\Gamma_{\rm CRP}^{(i)} = n({\rm X}_i)\zeta_0\gamma_i \times (6\,{\rm eV}) \tag{5.68}$$

$n({\rm X}_i)$ is the number density of ${\rm X}_i$, the interacting molecule (cm^{-3})
ζ_0 is the hydrogen ionisation rate (s^{-1})
γ_i is the ionisation rate of species ${\rm X}_i$ relative to the ionisation rate of H

The overall contribution to the heating of the gas by cosmic ray reactions is thus:

$$\Gamma_{\rm CRP} = \sum_i \Gamma_{\rm CRP}^{(i)} = \zeta_0 \times (6\,{\rm eV}) \times \sum_i n({\rm X}_i)\gamma_i \tag{5.69}$$

5.3.4 Thermal effect of H_2 formation on grains

Radiative association of two hydrogen atoms to form the molecule is forbidden by dipole selection rules and it is now believed that H_2 is formed primarily on grain surfaces. Other processes for the formation of the molecule do exist, for example the gas phase route involving the H^- ion:

$$H + e^- \rightarrow H^- + h\nu$$

$$H^- + H \rightarrow H_2 + e^-$$

which represents the fastest possible gas phase route to formation of the molecule. However the rate of this reaction does not usually compete with grain surface synthesis of H_2 and formation on grains is by far the dominant process.
When two hydrogen atoms collide and stick to a grain surface they may diffuse across the surface, meet and react to form the H_2 molecule. The molecule is then ejected with considerable kinetic, vibrational and rotational energy thus contributing to the overall heating of the gas. Each formation of the H_2 molecule releases 4.5 eV, but the way this energy is divided between kinetic energy of the molecule, internal energy of the molecule and internal energy of the grain lattice is unknown. Because of this uncertainty the logical step is, following Black and Dalgarno (1976), to assume equipartition of energy between the three exit channels. Thus each hydrogen molecule is assumed to be released with 1.5 eV of translational kinetic energy.

Hence the total heating rate per unit volume from H_2 formation on grains is given by:

$$\Gamma_{H_2-\text{grain}} = n_H n(H) k_g \times \frac{1}{3}\Delta E \tag{5.70}$$

n_H is the number density of hydrogen nuclei i.e. $n_H = n(H) + 2n(H_2)$ (cm^{-3})
$n(H)$ is the number density of hydrogen atoms (cm^{-3})
k_g is the reaction rate coefficient ($cm^3\ s^{-1}$)
ΔE is the total energy liberated by the reaction (erg)

The rate coefficient k_g for the formation of H_2 on grains is given by

$$k_g = 1.41 \times 10^{-18} T^{\frac{1}{2}}$$

and is derived in Chapter 3, given the assumptions about the grain properties in the nebula.

Chapter 6

Cooling processes in the nebula

The cooling of the gas in the nebula is achieved through a number of physical processes all stemming from the underlying process of conversion of kinetic energy of gas particles to radiative energy which may subsequently escape from the nebula. The cooling of the gas is dominated by two processes: collisional excitation of species exhibiting fine structure levels where the energy difference above the ground level is similar to the kinetic energies of the colliding species and rotational excitation of the abundant molecules H_2 and CO. It is these two cooling processes that are considered in the model.

6.1 Energy loss by collisionally induced fine structure transitions

6.1.1 General theory

A very important source of radiative cooling is collisional excitation of the low-lying levels of common atoms and ions such as C, C^+ and O. These species play an important rôle in cooling because they have fine structure energy levels with excitation potentials of the order of kT. An electron, atom or molecule colliding with such a species may excite it to a fine structure level from which it will subsequently decay back to the ground state, emitting a photon of appropriate energy. Such an inelastic collision leaves the colliding particle with less kinetic energy than before the impact and, through subsequent elastic scattering collisions, this loss is imparted to the gas as a whole which consequently becomes cooler.

To compute cooling rates due to fine structure excitation the rate coefficient for the collisional process is required (§3.2.1). This rate coefficient k_{ij} ($cm^3\ s^{-1}$) for the fine structure transition from level i to level j in the target particle will be different for different colliding species and will also generally be a function of the gas kinetic temperature.

Collisions are not just inelastic however; they can also be superelastic where the particle collides with the target particle which is initially in the upper level j. The collision may cause de-excitation of the target particle to level i and the colliding species leaves with more kinetic energy than before the impact. This reverse collisional reaction will also have associated with it a rate coefficient k_{ji} ($cm^3\ s^{-1}$). The rate coefficients for excitation and de-excitation are related by a Boltzmann

relationship (§4.1.5):

$$k_{ij} = k_{ji}\frac{g_j}{g_i}e^{-(E_j-E_i)/kT} \tag{6.1}$$

k_{ij} is the rate coefficient for collisional excitation from level i to level j (cm^3 s^{-1})
k_{ji} is the rate coefficient for collisional de-excitation from level j to level i (with the same target and colliding species) (cm^3 s^{-1})
g_i, g_j are the statistical weights (degeneracies) of levels i and j respectively
E_i, E_j are the energies of levels i and j respectively, where $E_j > E_i$

6.1.2 Evaluation of the rate coefficients

Evaluation of k_{ij} and k_{ji} requires knowledge of the corresponding cross-section for the processes which are obtained through quantum mechanical calculations. The cross-section $\sigma_{ij}(u)$ will, in general, be a function of the relative speed u between the colliding species. Consider the target particle moving with a relative speed u through field particles with a number density n_f. The probability that the target particle, initially in state i, performs a transition to a state j as the result of a collision in the time interval dt is given by $n_f u\sigma_{ij}(u)dt$. The rate coefficient k_{ij} is the mean value of this transition probability per unit density of field particles, averaged over a Maxwellian distribution for u:

$$k_{ij} =< u\sigma_{ij}(u) >= 4\pi\left(\frac{\mu}{2\pi kT}\right)^{\frac{3}{2}}\int_0^\infty u^3\sigma_{ij}(u)e^{\mu u^2/2kT}\,du \tag{6.2}$$

μ is the reduced mass of the system of colliding particles, i.e.
$1/\mu = 1/m_1 + 1/m_2$
where m_1 and m_2 are the masses of the colliding species
T is the kinetic temperature of the gas

Equivalently, in terms of the impact energy E:

$$k_{ij} = \frac{1}{(\pi\mu)^{1/2}}\left(\frac{2}{kT}\right)^{\frac{3}{2}}\int_0^\infty E\sigma_{ij}(E)e^{-E/kT}\,dE \tag{6.3}$$

6.1.3 Calculation of cooling rates

With knowledge of the excitation and de-excitation rate coefficients for all the important collisional processes, the rate of cooling due to radiative de-excitation

from fine structure levels may be computed.
The collision rates are related simply to the rate coefficients:

$$C_{ij}^{Y_p}\ (s^{-1}) = k_{ij}^{Y_p} n(Y_p) \tag{6.4}$$

Y_p denotes the particle striking the target particle
$n(Y_p)$ is the number density of species Y_p (cm^{-3})

If more than one particle is involved in inducing fine structure transitions in the target particle X then the total collision rate is given by:

$$C_{ij} = \sum_p k_{ij}^{Y_p} n(Y_p) \tag{6.5}$$

The Einstein A coefficient, A_{ji}, is the probability of spontaneous decay from level j to level i per atom in level j per unit time. If $n(X)$ is the *total* number density of the target particle X then the rate of cooling due to radiative de-excitation from level j to level i is given by:

$$\Lambda_{ji}(X)\ (erg\ cm^{-3}\ s^{-1}) = \hbar\omega_{ij} f_j n(X) A_{ji} \tag{6.6}$$

$\hbar\omega_{ij}$ is the photon energy liberated in the transition (erg)
f_j is the fraction of target particles in the excited state j
A_{ji} is the Einstein A coefficient for spontaneous decay from level j to level i (s^{-1})

Formulae for f_j may be calculated by applying the condition of stationarity, i.e.

Number of transitions into level i per unit time	=	Number of transitions out of level i per unit time

Appendix F sets out the results when applying this criterion to two and three level multiplets and the outcome of this algebra is shown below for convenience.
For a two level multiplet, the fraction of atoms in the excited (upper) state is given by:

$$f_2^{(2)} = \frac{C_{12}}{C_{12} + C_{21} + A_{21}} \tag{6.7}$$

For a three level multiplet, application of these conditions yields the following formulae for atoms in the upper two excited states:

$$f_2^{(3)} = \frac{(C_{12} + C_{13})(A_{32} + C_{32}) + C_{12}(A_{31} + C_{31})}{\alpha + \beta + \gamma} \tag{6.8}$$

$$f_3^{(3)} = \frac{C_{13}(A_{21} + C_{21}) + C_{23}(C_{12} + C_{13})}{\alpha + \beta + \gamma} \tag{6.9}$$

Where α, β and γ are defined as:

$$\alpha = (C_{32} + A_{32})(C_{12} + C_{13} + A_{21} + C_{21})$$

$$\beta = C_{12}(A_{31} + C_{31} + C_{23})$$

$$\gamma = (C_{23} + C_{21} + A_{21})(C_{31} + A_{31} + C_{13})$$

6.1.4 Theory of excitation of C^+

The ground state of C^+ is $2s^2 2p\ ^2P_{\frac{1}{2}}$. The $^2P_{\frac{3}{2}}$ level of C^+ lies at a slightly higher energy. If the lower level, $^2P_{\frac{1}{2}}$, is denoted by 1 and the upper level, $^2P_{\frac{3}{2}}$, is denoted by 2 then the energy difference between them is ΔE_{12}= 0.008 eV or, expressing the energy as an equivalent temperature (by dividing by Boltzmanns constant k), ΔE_{12}= 92.0 K. This energy difference is such that that fine structure excitation of C^+ by collisions with other species will occur frequently since the kinetic temperature of the gas in the nebula is of the same order as the energy difference. Because of this, collisional excitation of C^+ will be an important cooling process.
The Einstein A coefficient for spontaneous decay $^2P_{\frac{3}{2}} \rightarrow ^2P_{\frac{1}{2}}$ for the C^+ ion is 2.29×10^{-6} s^{-1} (Flower 1990).

6.1.4.1 C^+ - e^- collisions

For excitation caused by electron collision it is usual to express the cross-section in terms of a dimensionless collision strength Ω_{ij} as follows (e.g. Spitzer 1978):

$$\sigma_{ij}(v_e) = \frac{\pi}{g_i}\left(\frac{\hbar}{m_e v_e}\right)^2 \Omega_{ij}(v_e) \tag{6.10}$$

m_e is the mass of the electron
v_e is the speed of the electron
g_i is the degeneracy of the initial level

The collision strength can be thought of as the particle equivalent of oscillator strength. By using the condition of detailed balance in thermodynamic equilibrium it can be shown that $\Omega_{ij} = \Omega_{ji}$.

Since the ion velocity is generally negligible, the electron velocity v_e has been substituted for the relative velocity. By using equations (6.10) and (6.2) it can be shown that, if Ω_{ij} is constant, the rate coefficient for collisional de-excitation is related to the collision strength by:

$$k_{ji} = \left(\frac{2\pi}{k}\right)^{\frac{1}{2}} \frac{\hbar^2}{m_e^{3/2}} \frac{\Omega_{ji}}{g_j\sqrt{T}} \tag{6.11}$$

Inserting values for the physical constants yields:

$$k_{ji} = \frac{8.629 \times 10^{-6}}{g_j\sqrt{T}} \Omega_{ji} \tag{6.12}$$

However, Ω_{ji} will generally not be a constant and a Maxwell-averaged value of the collision strength, Υ_{ji}, should be used in equation (6.12)

$$\Upsilon_{ji} =< \Omega_{ji}(E) >= \int_0^\infty \Omega_{ji}(E) e^{-E/kT}\, d(E/kT) \tag{6.13}$$

Hence

$$k_{ji}\,(\mathrm{cm^3\ s^{-1}}) = \frac{8.629 \times 10^{-6}}{g_j\sqrt{T}} \Upsilon_{ji} \tag{6.14}$$

Equation (6.1) relates the rate coefficients for collisional excitation and de-excitation so that, for collisional excitation:

$$k_{ij}\,(\mathrm{cm^3\ s^{-1}}) = \frac{8.629 \times 10^{-6}}{g_i\sqrt{T}} \Upsilon_{ji} e^{-\Delta E/kT} \tag{6.15}$$

For the C^+ ion the lower level (1), $^2P_{\frac{1}{2}}$, has a degeneracy $g_1=(2J+1) = 2$. For the upper level of the multiplet (2), $^2P_{\frac{3}{2}}$, this has a degeneracy of $g_2=(2J+1) = 4$. Hence the rate coefficients for collisional excitation and de-excitation of the fine structure levels of C^+ by electrons are given by:

$$k_{21}\,(\mathrm{cm^3\ s^{-1}}) = \frac{8.629 \times 10^{-6}}{4\sqrt{T}} \Upsilon_{21}$$

$$k_{12}\,(\mathrm{cm^3\ s^{-1}}) = \frac{8.629 \times 10^{-6}}{2\sqrt{T}} \Upsilon_{21}\, e^{-92.0/T}$$

Hayes and Nussbaumer (1984) calculated values of the effective collision strength Υ_{ij} for the C^+-e^- system for a range of kinetic temperatures. Their results are shown over the page.

The middle column of the table shows the results of Hayes and Nussbaumer. The far right column represents a formula fit to their results as follows:

$$\Upsilon\,(^2\mathrm{P}_{\frac{1}{2}} - ^2\mathrm{P}_{\frac{3}{2}}) = 1.80 + 6 \times 10^{-5} T \qquad (6.16)$$

As can be seen from the table, Υ is a very slowly varying function of kinetic temperature. Above 1000 K the formula does not agree well with the calculations. However, the range of kinetic temperatures relevant to the model is up to about 500 K, for which the formula is adequate. Hence equation (6.16) is used in the model to estimate Υ_{12} for the C^+-e^- collision reaction.

Table 6.1
Values of the effective collision strength for the C^+-e^- system

Temperature T (K)	$\Upsilon(^2\mathrm{P}_{\frac{1}{2}} - ^2\mathrm{P}_{\frac{3}{2}})$	Υ (formula)
0	1.80	1.80
500	1.82	1.83
1000	1.87	1.86
2000	2.03	1.92
3000	2.26	1.98

6.1.4.2 C^+ - H collisions

In the nebular environment, the fine structure excitation of C^+ may also be influenced by collisions with atomic or molecular hydrogen.
For the atomic hydrogen case the relevant reaction is:

$$\mathrm{C}^+(^2\mathrm{P}_{\frac{1}{2}}) + \mathrm{H}(^2\mathrm{S}_{\frac{1}{2}}) \rightarrow \mathrm{C}^+(^2\mathrm{P}_{\frac{3}{2}}) + \mathrm{H}(^2\mathrm{S}_{\frac{1}{2}})$$

Launay and Roueff (1977a) studied this reaction and made a full quantum calculation of the excitation cross-section using the close-coupling formalism of Mies (1973). The cross-section for collisional excitation and the cross-section for collisional de-excitation between two levels in an atom are related, through detailed balance, by the following expression:

$$g_i(E - E_i)\sigma_{ij} = g_j(E - E_j)\sigma_{ji} \qquad (6.17)$$

g_i, g_j are the degeneracies of levels i and j respectively
E_i, E_j are the energies of levels i and j respectively
E is collision impact energy relative to the ground state of the atom

Hence, for the C^+-H system the cross-section for de-excitation is related to the cross-section for excitation by:

$$\sigma_{21}(T_E) = \frac{1}{2}\frac{T_E}{(T_E - 92.0)}\sigma_{12}(T_E) \tag{6.18}$$

where $T_E = E/k$

The results obtained for the de-excitation cross-section are shown over the page, where the incident kinetic energy is relative to the $J = \frac{1}{2}$ ground state of C^+.

From these values of σ_{21} rate coefficients for the de-excitation process may be computed by taking a Maxwell average of $u\sigma_{21}(u)$ where u is the relative speed between the two species. From equation (6.3) this is given by:

$$k_{21} = \frac{1}{(\pi\mu)^{1/2}}\left(\frac{2}{kT}\right)^{\frac{3}{2}}\int_0^\infty E\sigma_{21}(E)e^{-E/kT}\,dE$$

μ is the reduced mass of the C^+-H system.

Equivalently, if we define $T_E = E/k$ then we get, inserting values for the physical constants:

$$k_{21}\,(\mathrm{cm^3\ s^{-1}}) = \frac{1.875 \times 10^{-8}}{(\mu T^3)^{1/2}}\int_0^\infty T_E\sigma_{21}(T_E)e^{-T_E/T}\,dT_E \tag{6.19}$$

Numerical integration yields the values of k_{21} at various kinetic temperatures using the cross-section data of Launay and Roueff. The results are shown in Table 6.3.

Only kinetic temperatures up to 500 K are considered since the prediction of the model is that the gas temperature in the molecular domain of the planetary nebula will not exceed this value. Hence polynomial/power fits to data for rate coefficients are only valid below 500 K, and this applies to all further curve-fitting to rate coefficient data.

These data values for k_{21} can be satisfactorily modelled using a simple power expression in T:

$$k_{21}\,(\mathrm{cm^3\ s^{-1}}) = 6.746 \times 10^{-10}\,T^{0.0455}$$

Table 6.2

De-excitation cross-section as a function of collision energy for the C^+-H system

Incident kinetic energy E/k (K)	Cross-section $\sigma(^2P_{\frac{3}{2}} \rightarrow ^2 P_{\frac{1}{2}})$ (a_0^2)
93	1930
95	1110
100	681
125	337
150	284
175	245
200	212
250	173
300	154
400	130
600	100
800	89.3
1000	79.8
3000	56.2

Note: a_0 = Bohr radius = 5.292 $\times 10^{-9}$ cm.

This expression gives a fit to the data curve with a correlation coefficient of R=0.9486.

The rate coefficient for collisional excitation, k_{12}, is related to k_{21} through equation (6.1). Hence for fine structure collisional excitation of C^+ by H the rate coefficient is given by the following expression:

$$k_{12}\,(\mathrm{cm^3\ s^{-1}}) = 3.373 \times 10^{-10}\, T^{0.0455}\, e^{-92.0/T}$$

Table 6.3

Rate coefficient for collisional de-excitation for the C^+-H system as a function of kinetic temperature

Temperature T (K)	Rate coefficient $k_{21}(^2P_{\frac{3}{2}} \rightarrow ^2 P_{\frac{1}{2}})$ (10^{-10} cm^3 s^{-1})	Temperature T (K)	Rate coefficient $k_{21}(^2P_{\frac{3}{2}} \rightarrow ^2 P_{\frac{1}{2}})$ (10^{-10} cm^3 s^{-1})
5	7.36	140	8.35
10	7.80	160	8.39
20	7.96	180	8.43
30	8.03	200	8.47
40	8.08	240	8.54
50	8.12	280	8.62
60	8.16	320	8.70
70	8.19	360	8.78
80	8.22	400	8.85
90	8.24	440	8.92
100	8.27	480	8.97
120	8.31	520	9.01

6.1.4.3 C^+ - H_2 collisions

Collisions with molecular hydrogen will also contribute to the fine structure excitation of C^+. Flower and Launay (1977) studied this reaction, taking into account the H_2 rotational angular momentum for the calculations. They considered the C^+ ion as a frozen C^{2+} core with a 2p valence electron and the H_2 molecule as a rigid rotator. Using the basis sets $J = (0, 2)$ for para-H_2 and $J = (1, 3)$ for ortho-H_2 they calculated the C^+ fine structure excitation cross-section. Using the relationship from equation (6.17) the cross-section for de-excitation may be computed from the excitation cross-section and is given by equation (6.18). The results obtained for the de-excitation cross-section are set out in Table 6.4, where the impact energy is given relative to the $J = \frac{1}{2}$ ground state of C^+.

Rate coefficients for collisional de-excitation may then be computed by integrating over a Maxwellian distribution (see equation (6.3)). The results are set out in

Table 6.4

De-excitation cross-section as a function of collision energy for the C^+-H_2 system

Barycentric energy E/k (K)	Cross-section $\sigma(^2P_{\frac{3}{2}} \rightarrow {}^2P_{\frac{1}{2}})$ (a_0^2)		Barycentric energy E/k (K)	Cross-section $\sigma(^2P_{\frac{3}{2}} \rightarrow {}^2P_{\frac{1}{2}})$ (a_0^2)	
	Basis: (0,2)	Basis: (1,3)		Basis: (0,2)	Basis: (1,3)
94	811	1300	210	140	167
97	454	797	250	133	153
100	421	614	300	124	134
105	340	460	360	111	121
112	277	378	440	91.7	116
120	221	319	550	78.7	103
135	231	272	750	69.5	94.0
150	188	242	*1000	61.1	85.9
165	172	209	*1500	47.0	74.0
180	155	195	*2000	34.5	63.4

(* extrapolated from published data)

Table 6.5.

This data for the de-excitation rate coefficients can be modelled using a power expression in T.

For the C^+ - para-H_2 system:

$$k_{21}\,(\mathrm{cm^3\ s^{-1}}) = 2.179 \times 10^{-10}\, T^{0.1366}$$

with a correlation coefficient of R=0.9545.

For the C^+ - ortho-H_2 system:

$$k_{21}\,(\mathrm{cm^3\ s^{-1}}) = 3.460 \times 10^{-10}\, T^{0.0925}$$

with a correlation coefficient of R=0.9698.

The rate coefficients for fine structure excitation may be found using equation (6.1) and are hence given by the following expressions.

Table 6.5

Rate coefficient for collisional de-excitation for the C^+-H_2 system as a function of kinetic temperature

Temperature T (K)	Rate coefficient $k_{21}(^2P_{\frac{3}{2}} \rightarrow ^2P_{\frac{1}{2}})$ (10^{-10} cm^3 s^{-1})		Temperature T (K)	Rate coefficient $k_{21}(^2P_{\frac{3}{2}} \rightarrow ^2P_{\frac{1}{2}})$ (10^{-10} cm^3 s^{-1})	
	Basis: (0,2)	Basis: (1,3)		Basis: (0,2)	Basis: (1,3)
5	2.74	4.20	140	4.44	5.37
10	3.15	4.54	160	4.49	5.46
20	3.48	4.73	180	4.54	5.54
30	3.67	4.82	200	4.57	5.62
40	3.81	4.89	240	4.62	5.76
50	3.93	4.94	280	4.66	5.88
60	4.02	5.00	320	4.67	5.97
70	4.11	5.05	360	4.66	6.03
80	4.18	5.10	400	4.64	6.07
90	4.24	5.14	440	4.60	6.07
100	4.29	5.19	480	4.55	6.06
120	4.37	5.28	520	4.48	6.02

For the C^+ - para-H_2 system:

$$k_{12}\,(\mathrm{cm^3\ s^{-1}}) = 1.090 \times 10^{-10}\, T^{0.1366}\, e^{-92.0/T}$$

For the C^+ - ortho-H_2 system:

$$k_{12}\,(\mathrm{cm^3\ s^{-1}}) = 1.730 \times 10^{-10}\, T^{0.0925}\, e^{-92.0/T}$$

6.1.5 Theory of excitation of C

The ground state of the neutral carbon atom is $1s^2 2s^2 2p^2\ ^3P_0$. In the ^3P state the atom has a triplet of J values (J=0,1 or 2) with the J=1 and J=2 states lying at a slightly higher energy. If the states J=0,1,2 are labelled 1,2,3 respectively (for

consistency with previous nomenclature) then the fine structure energy splitting is as follows: ΔE_{12}= 23.0 K, ΔE_{23}= 39.0 K and ΔE_{13}= 62.0 K where the energy difference is expressed as an equivalent temperature. This energy splitting is of such a magnitude that cooling due to collisional excitation with electrons and abundant atoms will be important.

The Einstein A coefficients for spontaneous decay from the excited levels are: $A_{21} = 7.93 \times 10^{-8}$ s^{-1}, $A_{32} = 2.65 \times 10^{-7}$ s^{-1} and $A_{31} = 1.71 \times 10^{-14}$ s^{-1} (Nussbaumer and Rusca 1979). Since the triplet of states all have the same parity emission of electric dipole radiation cannot occur and the transitions $J = 1 \rightarrow 0$ and $J = 2 \rightarrow 1$ occur through magnetic dipole emission. However, selection rules forbid magnetic dipole emission for $J = 2 \rightarrow 0$ (since $\Delta J = 0, \pm 1$ for a magnetic dipole transition), and hence this decay proceeds through electric quadrupole emission which is why the Einstein A coefficient is several orders of magnitude smaller.

6.1.5.1 C - e$^-$ collisions

Johnson *et al.* (1987) used the relativistic R-matrix programs of Scott and Taylor (1982) to calculate the fine structure cross-section of carbon due to collisions with electrons. The theory behind fine structure excitation by electron impact has been discussed (§6.1.4.1) where the C^+-e^- system was considered. The theory relates the de-excitation rate coefficient to the effective collision strength (the collision strength averaged over a Maxwellian velocity distribution):

$$k_{ji}\,(\mathrm{cm}^3\ \mathrm{s}^{-1}) = \frac{8.629 \times 10^{-6}}{g_j\sqrt{T}}\Upsilon_{ji} \tag{6.14}$$

From their values of the inelastic cross-section, Johnson *et al.* computed values for the effective collision strength Υ_{ji} for a range of kinetic temperatures. They fitted their results to the form

$$\ln(\Upsilon_{ji}) = a_0 + a_1X + a_2X^2 + a_3X^3 + a_4X^4 \tag{6.20}$$

where $X = \ln(T)$

The coefficients quoted for this formula are set out in Table 6.6, which are valid for kinetic temperatures less than 1000 K.

The degeneracies of the levels in the triplet are $g_1 = 1$, $g_2 = 3$ and $g_3 = 5$. Hence the rate coefficients for collisional de-excitation of C by e$^-$ impact are given by

$$k_{21}\,(\mathrm{cm}^3\ \mathrm{s}^{-1}) = \frac{8.629 \times 10^{-6}}{3\sqrt{T}}\Upsilon_{21}$$

Table 6.6

Coefficients for the formula approximation to the effective collision strength

Coefficient	Transition		
	$^3P_0 - ^3P_1$	$^3P_0 - ^3P_2$	$^3P_1 - ^3P_2$
a_0	-9.251	-7.697	-7.439
a_1	-7.738 (-1)	-1.307	-5.744 (-1)
a_2	3.612 (-1)	6.976 (-1)	3.583 (-1)
a_3	-1.509 (-2)	-1.113 (-1)	-4.182 (-2)
a_4	-6.563 (-4)	7.053 (-3)	2.353 (-3)

Note: a (b) implies $a \times 10^b$

$$k_{32}\,(\mathrm{cm^3\ s^{-1}}) = \frac{8.629 \times 10^{-6}}{5\sqrt{T}}\Upsilon_{32}$$

$$k_{31}\,(\mathrm{cm^3\ s^{-1}}) = \frac{8.629 \times 10^{-6}}{5\sqrt{T}}\Upsilon_{31}$$

where Υ_{21}, Υ_{32} and Υ_{31} are the effective collision strengths for the three possible transitions, to be computed by the formula above.

Equation (6.1) relates the excitation to the de-excitation rate coefficient and hence the excitation rate coefficients for the three transitions are given by the following expressions

$$k_{12}\,(\mathrm{cm^3\ s^{-1}}) = \frac{8.629 \times 10^{-6}}{\sqrt{T}}\Upsilon_{21}\,e^{-23.0/T}$$

$$k_{23}\,(\mathrm{cm^3\ s^{-1}}) = \frac{8.629 \times 10^{-6}}{3\sqrt{T}}\Upsilon_{32}\,e^{-39.0/T}$$

$$k_{13}\,(\mathrm{cm^3\ s^{-1}}) = \frac{8.629 \times 10^{-6}}{\sqrt{T}}\Upsilon_{31}\,e^{-62.0/T}$$

6.1.5.2 C - H collisions

Launay and Roueff (1977b) studied the impact of hydrogen atoms on carbon atoms, causing fine structure excitation in the carbon atom according to the following reaction:

$$\mathrm{C}(^3\mathrm{P}_J) + \mathrm{H}(^2\mathrm{S}_{\frac{1}{2}}) \rightarrow \mathrm{C}(^3\mathrm{P}_{J'}) + \mathrm{H}(^2\mathrm{S}_{\frac{1}{2}})$$

where $(J, J') = (0,1)$, $(0,2)$ or $(1,2)$

Table 6.7

Rate coefficient for collisional de-excitation of C by H as a function of kinetic temperature

Temperature T (K)	Rate coefficient $J \rightarrow J'$ (10^{-11} cm^3 s^{-1})			Temperature T (K)	Rate coefficient $J \rightarrow J'$ (10^{-11} cm^3 s^{-1})		
	$1 \rightarrow 0$	$2 \rightarrow 0$	$2 \rightarrow 1$		$1 \rightarrow 0$	$2 \rightarrow 0$	$2 \rightarrow 1$
10	15.3	9.85	23.7	50	15.6	9.40	26.4
12	15.6	9.47	23.8	60	15.6	9.33	26.9
14	15.8	9.55	23.8	70	15.6	9.31	27.4
16	16.0	9.54	24.0	80	15.7	9.29	27.8
18	16.0	9.52	24.1	90	15.8	9.32	28.2
20	16.0	9.50	24.3	100	15.9	9.33	28.7
22	16.0	9.51	24.4	120	16.2	9.42	29.5
24	16.1	9.51	24.6	160	16.6	9.75	31.0
26	16.0	9.49	24.8	200	16.9	10.2	32.4
28	16.0	9.48	24.9	250	17.2	10.8	34.2
30	15.9	9.48	25.1	300	17.6	11.4	35.8
33	15.9	9.46	25.2	350	17.9	11.9	37.4
36	15.8	9.46	25.5	400	18.3	12.4	38.9
40	15.7	9.42	25.8	450	18.7	12.9	40.3
45	15.7	9.44	26.1	500	19.0	13.4	41.7

They used the close-coupling quantal treatment of Mies (1973) to calculate the excitation cross-section as a function of impact energy for the three possible transitions. They report values for the excitation rate coefficients from which the de-excitation rate coefficients have been calculated using equation (6.1). Data for the de-excitation rate coefficients are given in Table 6.7.

This data is satisfactorily approximated by employing third-order polynomial curve fits according to:

$$k_{ji} = m_0 + m_1 T + m_2 T^2 + m_3 T^3$$

The coefficients m_0 to m_3 for the three possible transitions are given by the fol-

lowing:

k_{21} : $m_0 = 1.509 \times 10^{-10}$
$m_1 = 1.415 \times 10^{-13}$
$m_2 = -3.228 \times 10^{-16}$
$m_3 = 4.050 \times 10^{-19}$

with a correlation coefficient of R=0.8990

k_{32} : $m_0 = 2.316 \times 10^{-10}$
$m_1 = 6.461 \times 10^{-13}$
$m_2 = -1.049 \times 10^{-15}$
$m_3 = 1.010 \times 10^{-18}$

with a correlation coefficient of R=0.9996

k_{31} : $m_0 = 9.685 \times 10^{-11}$
$m_1 = -9.421 \times 10^{-14}$
$m_2 = 7.369 \times 10^{-16}$
$m_3 = -8.089 \times 10^{-19}$

with a correlation coefficient of R=0.9977

The rate coefficients for collisional excitation may then be calculated by employing equation (6.1).

6.1.5.3 C - H_2 collisions

By utilising the COLMOL program of Launay (1977), Schröder *et al.* (1991) computed the cross-section for fine structure excitation of carbon through collisions with the H_2 molecule. The H_2 molecule was represented by the $J = (0, 2)$ rotational states (in para form) and by $J = (1, 3)$ (in ortho form). The cross-section for transitions induced by ortho-H_2 are generally smaller than for para-H_2. For para-H_2 in its ground state (J=0), the internuclear axis has no preferential orientation and hence collisions perpendicular to and collinear with the intermolecular axis are equally probable. Conversely, the ground state of ortho-H_2 (J=1) is such that a preferred direction of the internuclear axis can be adopted. The energetically preferred approach is that in which the internuclear and intermolecular axes are collinear and hence the cross-section tends to be smaller for collisions with ortho-H_2, at low energies.
Schröder *et al.* compute rate coefficients for fine structure de-excitation by integrating the cross-sections over a Maxwellian velocity distribution. Their data are

Table 6.8

Rate coefficient for collisional de-excitation of C by para-H_2 as a function of kinetic temperature

Temperature T (K)	Rate coefficient $J \rightarrow J'$ (10^{-10} cm^3 s^{-1})			Temperature T (K)	Rate coefficient $J \rightarrow J'$ (10^{-10} cm^3 s^{-1})		
	$1 \rightarrow 0$	$2 \rightarrow 0$	$2 \rightarrow 1$		$1 \rightarrow 0$	$2 \rightarrow 0$	$2 \rightarrow 1$
10	0.96	0.96	1.75	140	0.66	0.84	1.79
20	1.00	0.99	1.84	160	0.66	0.84	1.81
30	0.91	0.97	1.84	180	0.67	0.84	1.84
40	0.83	0.95	1.81	200	0.67	0.85	1.88
50	0.77	0.92	1.79	250	0.69	0.87	1.96
60	0.73	0.90	1.77	300	0.71	0.88	2.04
70	0.70	0.89	1.76	350	0.72	0.91	2.12
80	0.69	0.87	1.75	400	0.74	0.93	2.19
90	0.67	0.86	1.75	450	0.75	0.95	2.26
100	0.67	0.86	1.75	500	0.76	0.96	2.32
120	0.66	0.85	1.77				

shown in Tables 6.8 and 6.9, as a function of gas kinetic temperature.
The $J = 1 \rightarrow 0$ transition is forbidden, to first order, in collisions of C(^{3}P$_J$) with H_2. The magnitude of the corresponding rate coefficient depends on the degree of indirect collisional coupling $J = 1 \rightarrow 2 \rightarrow 0$. As can be seen from Tables 6.8 and 6.9 indirect coupling is significant for the $J = 1 \rightarrow 0$ transition, whose rate coefficient is not much smaller than for $J = 2 \rightarrow 0$.

This data can be represented by employing third-order polynomial curve fits according to:

$$k_{ji} = m_0 + m_1 T + m_2 T^2 + m_3 T^3$$

The coefficients for the polynomial for the three possible transitions with ortho- and para-H_2 are given by the following:

For para-H_2 collisions:

k_{21} : $m_0 = 1.001 \times 10^{-10}$

$m_1 = -4.804 \times 10^{-13}$

Table 6.9

Rate coefficient for collisional de-excitation of C by ortho-H_2 as a function of kinetic temperature

Temperature T (K)	Rate coefficient $J \rightarrow J'$ (10^{-10} cm^3 s^{-1})			Temperature T (K)	Rate coefficient $J \rightarrow J'$ (10^{-10} cm^3 s^{-1})		
	$1 \rightarrow 0$	$2 \rightarrow 0$	$2 \rightarrow 1$		$1 \rightarrow 0$	$2 \rightarrow 0$	$2 \rightarrow 1$
10	0.73	0.52	0.92	140	0.70	0.73	1.63
20	0.81	0.58	1.05	160	0.71	0.75	1.70
30	0.80	0.60	1.13	180	0.71	0.77	1.76
40	0.78	0.62	1.19	200	0.71	0.79	1.82
50	0.76	0.63	1.25	250	0.73	0.83	1.96
60	0.74	0.64	1.30	300	0.74	0.87	2.08
70	0.73	0.65	1.35	350	0.76	0.91	2.18
80	0.72	0.67	1.39	400	0.77	0.94	2.28
90	0.71	0.68	1.43	450	0.79	0.97	2.37
100	0.71	0.69	1.48	500	0.80	1.00	2.45
120	0.71	0.71	1.55				

$$m_2 = 1.901 \times 10^{-15}$$
$$m_3 = -2.101 \times 10^{-18}$$

with a correlation coefficient of R=0.9299

k_{31} :
$$m_0 = 1.010 \times 10^{-10}$$
$$m_1 = -2.223 \times 10^{-13}$$
$$m_2 = 8.645 \times 10^{-16}$$
$$m_3 = -8.841 \times 10^{-19}$$

with a correlation coefficient of R=0.9711

k_{32} :
$$m_0 = 1.831 \times 10^{-10}$$
$$m_1 = -1.596 \times 10^{-13}$$
$$m_2 = 1.124 \times 10^{-15}$$
$$m_3 = -1.228 \times 10^{-18}$$

with a correlation coefficient of R=0.9913

For ortho-H_2 collisions:

k_{21} : $m_0 = 8.011 \times 10^{-10}$
$m_1 = -1.264 \times 10^{-13}$
$m_2 = 5.012 \times 10^{-16}$
$m_3 = -5.001 \times 10^{-19}$

with a correlation coefficient of R=0.8541

k_{31} : $m_0 = 5.387 \times 10^{-11}$
$m_1 = 1.789 \times 10^{-13}$
$m_2 = -3.128 \times 10^{-16}$
$m_3 = 2.832 \times 10^{-19}$

with a correlation coefficient of R=0.9971

k_{32} : $m_0 = 9.216 \times 10^{-11}$
$m_1 = 6.705 \times 10^{-13}$
$m_2 = -1.291 \times 10^{-15}$
$m_3 = 1.136 \times 10^{-18}$

with a correlation coefficient of R=0.9990

By using equation (6.1) the corresponding rate coefficients for collisional excitation may be computed.

6.1.5.4 C - He collisions

Helium is the second most abundant chemical species in the nebula after hydrogen, and fine structure excitation of carbon through inelastic collisions with helium atoms will provide a minor contribution to the cooling of the gas. Staemmler and Flower (1991) performed SCF + CEPA computations of the $^3\Sigma^-$ and $^3\Pi$ potentials for the interaction between C(^{3}P) and He(^{1}S). Using the COLMOL program of Launay (1977) they deduced the fine structure excitation cross-section for the collision reaction

$$C(^3P_J) + He(^1S_0) \rightarrow C(^3P_{J'}) + He(^1S_0)$$

where (J, J') = (0,1), (0,2) or (1,2)

Using equation (6.17) the de-excitation cross-section may then be computed and these are set out in Table 6.10, as reported by these workers.

Table 6.10

De-excitation cross-section as a function of collision energy for the C-He system

Barycentric energy E/k (K)	Cross-section $\sigma(J \rightarrow J')$ (a_0^2)			Barycentric energy E/k (K)	Cross-section $\sigma(J \rightarrow J')$ (a_0^2)		
	$1 \rightarrow 0$	$2 \rightarrow 0$	$2 \rightarrow 1$		$1 \rightarrow 0$	$2 \rightarrow 0$	$2 \rightarrow 1$
25	5.39			140	6.76	24.3	43.5
30	7.82			160	6.38	21.7	39.1
40	9.75			180	6.14	19.6	35.8
50	14.1			200	5.97	18.0	33.3
60	23.8			300	5.60	13.3	26.3
65	19.3	122	215	400	5.45	11.6	24.2
70	15.5	67.9	120	600	5.20	11.4	25.3
80	11.6	47.2	83.4	800	4.99	12.2	27.3
90	9.73	38.9	68.6	1000	4.85	12.4	27.9
100	8.63	34.0	59.9	*1500	4.65	12.6	28.3
120	7.41	28.0	49.7	*2000	4.59	12.8	28.5

(* extrapolated from published data)

The cross-section is given as a function of the barycentric collision energy E, relative to the J=0 ground state of C.

De-excitation rate coefficients may then be computed as a function of the gas kinetic temperature by taking an average of $\sigma(J \rightarrow J')v$ over a Maxwellian velocity distribution for v. The results of this calculation are set out in Table 6.11.

The data for the de-excitation rate coefficients can be accurately modelled by employing logarithmic and power fits to the gas temperature as follows:

$$k_{21}\ (\mathrm{cm^3\ s^{-1}}) = -1.666 \times 10^{-12} + 9.804 \times 10^{-12} \log_{10}(T)$$

with a correlation coefficient of R=0.9923

$$k_{31}\ (\mathrm{cm^3\ s^{-1}}) = 2.212 \times 10^{-11} + 1.284 \times 10^{-11} \log_{10}(T)$$

Table 6.11

Rate coefficient for collisional de-excitation of C by He as a function of kinetic temperature

Temperature T (K)	Rate coefficient $J \rightarrow J'$ (10^{-11} cm^3 s^{-1})			Temperature T (K)	Rate coefficient $J \rightarrow J'$ (10^{-11} cm^3 s^{-1})		
	$1 \rightarrow 0$	$2 \rightarrow 0$	$2 \rightarrow 1$		$1 \rightarrow 0$	$2 \rightarrow 0$	$2 \rightarrow 1$
5	0.421	3.30	5.82	140	1.85	4.59	8.87
10	0.835	3.89	6.87	160	1.90	4.67	9.16
20	1.34	4.19	7.40	180	1.96	4.77	9.46
30	1.52	4.29	7.62	200	2.01	4.87	9.78
40	1.59	4.34	7.76	240	2.11	5.09	10.4
50	1.63	4.37	7.86	280	2.21	5.31	11.0
60	1.65	4.39	7.96	320	2.29	5.51	11.6
70	1.68	4.40	8.05	360	2.36	5.69	12.1
80	1.70	4.42	8.15	400	2.41	5.84	12.5
90	1.72	4.44	8.25	440	2.45	5.95	12.8
100	1.74	4.46	8.36	480	2.47	6.03	13.0
120	1.80	4.52	8.60	520	2.49	6.08	13.2

with a correlation coefficient of R=0.9492

$$k_{32}\,(\mathrm{cm}^3\ \mathrm{s}^{-1}) = 3.987 \times 10^{-11}\, T^{0.1799}$$

with a correlation coefficient of R=0.9636

By utilising equation (6.1) the rate coefficients for collisional excitation by He impact may be computed.

6.1.6 Theory of excitation of O

The ground state of the neutral oxygen atom is $1s^2 2s^2 2p^4\ {}^3P_2$. The ^{3}P level of oxygen represents an inverted triplet where the J=2 state lies at a lower energy than the J=0 or 1 states, as compared to the ^{3}P ground state of carbon which

forms a normal triplet with J=0 having the lowest energy. If the states J=2,1,0 are labelled 1,2,3 for consistency then the fine structure energy splitting in the ^{3}P level is as follows: ΔE_{12}= 228.0 K, ΔE_{23}= 98.0 K and ΔE_{13}= 326.0 K.
The Einstein A coefficients for spontaneous decay from the fine structure levels are: $A_{21} = 8.95 \times 10^{-5}$ s^{-1}, $A_{32} = 1.70 \times 10^{-5}$ s^{-1} and $A_{31} = 1.00 \times 10^{-10}$ s^{-1} (Tielens and Hollenbach 1985).

6.1.6.1 O - e$^-$ collisions

Berrington (1988) used the R-matrix method to calculate the collision strengths for a range of energies for fine structure excitation of oxygen by electron impact. The rate coefficient for collisional de-excitation is related to the collision strength through equation (6.14):

$$k_{ji}\,(\mathrm{cm}^3\ \mathrm{s}^{-1}) = \frac{8.629 \times 10^{-6}}{g_j\sqrt{T}}\Upsilon_{ji}$$

where Υ_{ji} is the collision strength for the transition averaged over a Maxwellian velocity distribution.

Table 6.12 shows the results Berrington reports for the effective collision strength for the three possible fine structure transitions in oxygen, for different values of the gas kinetic temperature.

This data is adequately modelled by employing third order polynomial fits according to:

$$\Upsilon_{ji} = m_0 + m_1 T + m_2 T^2 + m_3 T^3$$

The coefficients to the polynomial for the different transitions are as follows:

Υ_{21} : $m_0 = 1.920 \times 10^{-5}$
$m_1 = 4.476 \times 10^{-7}$
$m_2 = 1.755 \times 10^{-10}$
$m_3 = -6.292 \times 10^{-15}$

with a correlation coefficient of R=1.0000

Υ_{32} : $m_0 = 4.154 \times 10^{-4}$
$m_1 = 1.363 \times 10^{-5}$
$m_2 = -8.041 \times 10^{-9}$
$m_3 = 3.715 \times 10^{-12}$

with a correlation coefficient of R=0.9999

Table 6.12

Values of the effective collision strength for the O-e^- system

Temperature T (K)	Effective collision strength Υ_{ji}		
	$^3P_2 - ^3P_1$	$^3P_2 - ^3P_0$	$^3P_1 - ^3P_0$
*0	4.00 (-4)	2.00 (-4)	2.00 (-5)
50	1.08 (-3)	5.42 (-4)	4.05 (-5)
100	1.74 (-3)	8.22 (-4)	6.62 (-5)
200	2.82 (-3)	1.28 (-3)	1.16 (-4)
500	5.69 (-3)	2.51 (-3)	2.86 (-4)
1000	9.72 (-3)	4.11 (-3)	6.36 (-4)

(* extrapolated from published data)
Note: a (b) implies a $\times 10^b$

Υ_{31} : $m_0 = 2.217 \times 10^{-4}$
$m_1 = 6.179 \times 10^{-6}$
$m_2 = -4.156 \times 10^{-9}$
$m_3 = 1.866 \times 10^{-12}$

with a correlation coefficient of R=1.0000

These formulae for Υ_{ji} enable the de-excitation rate coefficients to be computed. Equation (6.1) may then be used to calculate the corresponding excitation rate coefficients for fine structure transitions in O due to electron impact.

6.1.6.2 O - H collisions

Using the close-coupling formalism of Mies (1973), Launay and Roueff (1977b) studied the fine structure excitation of oxygen by atomic hydrogen impact. They report rate coefficients for excitation of the O atom, from which the de-excitation rate coefficients may be computed using equation (6.1) and this data is shown in Table 6.13 as a function of gas kinetic temperature.

The data for the de-excitation rate coefficients may be modelled using third order

Table 6.13

Rate coefficients for collisional de-excitation of O by H impact

Temperature T (K)	Rate coefficient k_{ji} (10^{-11} cm^3 s^{-1})		
	$^3P_1 \rightarrow ^3P_2$	$^3P_0 \rightarrow ^3P_2$	$^3P_0 \rightarrow ^3P_1$
5	*1.50	*0.600	*5.70
10	*2.00	*0.800	*6.00
50	*5.50	*2.30	8.31
100	9.12	*4.00	10.6
150	12.6	5.71	12.3
200	15.5	7.40	13.8
250	18.1	9.03	15.1
300	20.5	10.5	16.3
350	22.6	11.9	17.5
400	24.5	13.3	18.6
450	26.4	14.7	19.7
500	28.1	15.9	20.8

(* extrapolated from published data)

polynomial curve fits:

$$k_{ji} = m_0 + m_1 T + m_2 T^2 + m_3 T^3$$

The coefficients m_0 to m_3 for the three possible transitions are as follows:

k_{21} : $m_0 = 1.092 \times 10^{-11}$

$m_1 = 9.154 \times 10^{-13}$

$m_2 = -1.120 \times 10^{-15}$

$m_3 = 7.396 \times 10^{-19}$

with a correlation coefficient of R=1.0000

k_{31} : $m_0 = 4.247 \times 10^{-12}$

$m_1 = 3.735 \times 10^{-13}$

$m_2 = -1.253 \times 10^{-16}$

$$m_3 = -4.536 \times 10^{-21}$$

with a correlation coefficient of R=1.0000

k_{32} : $m_0 = 5.476 \times 10^{-11}$
$m_1 = 5.941 \times 10^{-13}$
$m_2 = -1.068 \times 10^{-15}$
$m_3 = 9.916 \times 10^{-19}$

with a correlation coefficient of R=0.9998

By employing equation (6.1) the rate coefficients for fine structure excitation of O by H impact may be calculated.

6.1.6.3 O - H_2 collisions

Jaquet *et al.* (1992) performed SCF+CEPA calculations for the O-H_2 interaction potential and used these results to compute cross-sections and rate coefficients for the O fine structure transitions induced by impact with para- and ortho-H_2. For the calculations para-H_2 was represented by the rotational basis set J=(0,2) and ortho-H_2 by J=(1,3).
Because the $J = 0 \rightarrow 1$ transition is forbidden to first order and indirect collisional coupling $J = 1 \rightarrow 2 \rightarrow 0$ is weak in the O-H_2 system (as opposed to the C-He system), the calculations showed that $\sigma(J = 0 \rightarrow 1) \ll \sigma(J = 1 \rightarrow 2)$, $\sigma(J = 0 \rightarrow 2)$ over the entire energy range and hence the transition rate coefficient for $J = 0 \rightarrow 1$ was very small relative to the other transitions.
The rate coefficients for de-excitation of $O(^3P_J)$ by H_2 are given in Tables 6.14 and 6.15 as a function of gas temperature, as reported by Jaquet *et al.*

The data for de-excitation rate coefficients may be accurately approximated by employing third order polynomial curve fits according to:

$$k_{ji} = m_0 + m_1 T + m_2 T^2 + m_3 T^3$$

The coefficients m_0 to m_3 appropriate to the different possible transitions are given below

For para-H_2 collisions:
k_{21} : $m_0 = 7.084 \times 10^{-11}$
$m_1 = 9.508 \times 10^{-13}$
$m_2 = -2.021 \times 10^{-15}$

Table 6.14

Rate coefficients for collisional de-excitation of O by para-H_2

Temperature T (K)	Rate coefficient $J \rightarrow J'$ (10^{-10} cm^3 s^{-1})			Temperature T (K)	Rate coefficient $J \rightarrow J'$ (10^{-10} cm^3 s^{-1})		
	$1 \rightarrow 2$	$0 \rightarrow 2$	$0 \rightarrow 1$		$1 \rightarrow 2$	$0 \rightarrow 2$	$0 \rightarrow 1$
*10	0.80	0.50	0.002	180	1.86	2.90	0.045
20	0.89	1.11	0.004	200	1.93	3.01	0.052
40	1.04	1.90	0.008	250	2.07	3.23	0.071
60	1.21	2.05	0.012	300	2.19	3.41	0.090
80	1.36	2.21	0.016	350	2.29	3.56	0.111
100	1.49	2.37	0.021	400	2.37	3.68	0.131
120	1.60	2.52	0.026	450	2.45	3.78	0.152
140	1.69	2.66	0.032	500	2.51	3.87	0.173
160	1.78	2.79	0.038				

(* extrapolated from published data)

$$m_3 = 1.690 \times 10^{-18}$$

with a correlation coefficient of R=0.9998

k_{31} :
$$m_0 = 4.726 \times 10^{-11}$$
$$m_1 = 2.539 \times 10^{-12}$$
$$m_2 = -7.536 \times 10^{-15}$$
$$m_3 = 7.749 \times 10^{-18}$$

with a correlation coefficient of 0.9785

k_{32} :
$$m_0 = 1.038 \times 10^{-13}$$
$$m_1 = 1.325 \times 10^{-14}$$
$$m_2 = 7.348 \times 10^{-17}$$
$$m_3 = -6.264 \times 10^{-20}$$

with a correlation coefficient of R=1.0000

For ortho-H_2 collisions:

Table 6.15

Rate coefficients for collisional de-excitation of O by ortho-H_2

Temperature T (K)	Rate coefficient $J \rightarrow J'$ (10^{-10} cm^3 s^{-1})			Temperature T (K)	Rate coefficient $J \rightarrow J'$ (10^{-10} cm^3 s^{-1})		
	$1 \rightarrow 2$	$0 \rightarrow 2$	$0 \rightarrow 1$		$1 \rightarrow 2$	$0 \rightarrow 2$	$0 \rightarrow 1$
*10	0.72	0.53	0.004	180	1.75	2.81	0.058
20	0.80	0.94	0.009	200	1.83	2.94	0.066
40	0.95	1.77	0.017	250	1.99	3.21	0.087
60	1.11	1.90	0.020	300	2.14	3.44	0.110
80	1.25	2.06	0.025	350	2.26	3.64	0.135
100	1.37	2.23	0.030	400	2.37	3.80	0.159
120	1.48	2.38	0.036	450	2.47	3.95	0.185
140	1.58	2.54	0.043	500	2.57	4.08	0.210
160	1.67	2.68	0.050				

(* extrapolated from published data)

k_{21} : $m_0 = 6.348 \times 10^{-11}$
$m_1 = 8.800 \times 10^{-13}$
$m_2 = -1.675 \times 10^{-15}$
$m_3 = 1.383 \times 10^{-18}$

with a correlation coefficient of R=0.9999

k_{31} : $m_0 = 6.695 \times 10^{-11}$
$m_1 = 1.982 \times 10^{-12}$
$m_2 = -4.987 \times 10^{-15}$
$m_3 = 4.842 \times 10^{-18}$

with a correlation coefficient of R=0.9885

k_{32} : $m_0 = 5.995 \times 10^{-13}$
$m_1 = 1.753 \times 10^{-14}$
$m_2 = 7.304 \times 10^{-17}$
$m_3 = -5.275 \times 10^{-20}$

with a correlation coefficient of R=0.9999

Equation (6.1) enables the corresponding rate coefficients for excitation of O to be computed from these values of the de-excitation rate coefficients.

6.1.6.4 O - He collisions

Monteiro and Flower (1987) studied the fine structure excitation of O through impact with He according to:

$$O(^3P_J) + He(^1S) \rightarrow O(^3P_{J'}) + He(^1S)$$

They used the CEPA potential for the interaction between O and He, as developed by Staemmler and Jaquet (1985). To solve the scattering equations a modified form of the code MOLSCAT of Green and Hutson (1986) was employed and the fine structure excitation and de-excitation cross-sections subsequently computed. The rate coefficients $< \sigma(v)v >$ were derived for a Maxwellian distribution of velocities v, and for a range of gas kinetic temperatures.
The results for the de-excitation rate coefficients are shown below in Table 6.16.

Table 6.16
Rate coefficients for collisional de-excitation of O by He impact

Temperature T (K)	Rate coefficient k_{ji} (10^{-10} cm^3 s^{-1})		
	$^3P_0 \rightarrow ^3P_1$	$^3P_0 \rightarrow ^3P_2$	$^3P_1 \rightarrow ^3P_2$
*10	3.42×10^{-4}	0.0596	0.0492
*50	4.60×10^{-3}	0.329	0.226
100	0.0144	0.578	0.380
200	0.0460	0.992	0.615
300	0.0855	1.32	0.809
400	0.128	1.60	0.996
500	0.171	1.85	1.17
600	0.215	2.06	1.31

(* extrapolated from published data)

Because of the selection rule forbidding, to first order, the $J = 0 \rightarrow 1$ fine structure transition of O by He impact the cross-section for the process is much reduced relative to the $J = 0 \rightarrow 2$ and $J = 1 \rightarrow 2$ transitions. This is reflected in the results for the rate coefficients where the coefficient for $J = 0 \rightarrow 1$ is about an order of magnitude smaller than the other two, for all gas temperatures.
As before, third order polynomial curves provide accurate fits to the rate coefficient data:

$$k_{ji} = m_0 + m_1 T + m_2 T^2 + m_3 T^3$$

The polynomial coefficients for the three de-excitation transitions are given below:

k_{21} : $m_0 = 1.246 \times 10^{-12}$
$m_1 = 4.038 \times 10^{-13}$
$m_2 = -5.692 \times 10^{-16}$
$m_3 = 4.323 \times 10^{-19}$

with a correlation coefficient of R=0.9994

k_{31} : $m_0 = 1.810 \times 10^{-13}$
$m_1 = 6.454 \times 10^{-13}$
$m_2 = -8.411 \times 10^{-16}$
$m_3 = 5.657 \times 10^{-19}$

with a correlation coefficient of R=0.9998

k_{32} : $m_0 = -1.010 \times 10^{-13}$
$m_1 = 8.965 \times 10^{-15}$
$m_2 = 8.470 \times 10^{-17}$
$m_3 = -6.639 \times 10^{-20}$

with a correlation coefficient of R=0.9999.
A further constraint on k_{32} is that $k_{32} = \max(k_{32}, 5.0 \times 10^{-15})$

The rate coefficients for excitation may be computed from the de-excitation rate coefficients by using equation (6.1).

6.2 Energy loss by collisionally induced rotational transitions

Cooling through radiative decay of a CO or H_2 molecule from a rotational level to a lower-lying rotational level will obviously depend on the equilibrium population of the rotational levels and the processes by which the molecules were rotationally excited in the first place. Detailed calculations are performed by the model taking into account the different physical processes involved to compute the equilibrium fraction of molecules in each rotational level of the ground electronic-vibrational state (Chapter 4), after which the cooling effect of collisionally induced rotational transitions may be calculated using the methods described in this section.

6.2.1 H_2 rotational transitions

The H_2 molecule acts as a cooling agent of the nebular gas through collisional excitation of rotational energy levels which subsequently decay back to the ground state, emitting far infrared radiation. The process is effective because the difference in energy between the lowest lying rotational states is of the same order as the kinetic temperature of the gas (several hundred kelvin) and because the H_2 molecule is so abundant, at sufficiently large distances from the central star where the radiation field is heavily diluted and attenuated.

As discussed in Chapter 4 molecular hydrogen can exist in two forms; ortho- and para-H_2. For the former, only odd values of J are allowed and for the latter, only even values of J. In general there is very little inter-conversion between the two forms. Radiative processes cannot change one form to another and the dominant process for conversion is collisions with thermal protons (§4.1.6).
Because H_2 exists in these two separate states radiative de-excitation of the rotationally excited H_2 molecule can only occur through $J \rightarrow J-2$, $J \rightarrow J-4$ and so on. The radiation emitted in such a decay, due to the relevant selection rules, must be electric quadrupole (or higher). Since a $J \rightarrow J-4$ transition requires the emission of hexadecapole radiation with a virtually negligible Einstein coefficient, only the $J \rightarrow J-2$ transitions emitting electric quadrupole radiation are considered.
If the upper rotational levels of the H_2 molecule were populated purely by collisional excitation and radiative de-excitation dominated over collisional de-excitation the rate of cooling due to this process would be:

$$\Lambda_{\mathrm{H_2\ rotation}}\ (\mathrm{erg\ cm^{-3}\ s^{-1}}) = n(\mathrm{H_2}) \sum_{J=2}^{J_{\max}} f_J \mathrm{A}_{J,J-2} \Delta E_{J,J-2} \qquad (6.21)$$

$n(H_2)$ is the number density of H_2 molecules (cm^{-3})
f_J is the fraction of H_2 molecules (in the ground electronic and vibrational state) in the rotational state J
$A_{J,J-2}$ is the Einstein coefficient for spontaneous emission from $J \rightarrow J-2$ (s^{-1})
$\Delta E_{J,J-2}$ is the energy difference between the rotational levels J and $J-2$ (erg)

The premise that the upper rotational levels are populated purely through collisional excitation is false. Other processes exist in the nebular environment to rotationally excite the H_2 molecule, as discussed in Chapter 4 (§4.1). If all possible processes for rotational excitation (collisions and optical pumping) and de-excitation (radiative decay and collisions) are taken into account, the rate of cooling due to rotational excitation is reduced from the result given by equation (6.21) according to the formula:

$$\Lambda_{H_2\ \mathrm{rotation}}\ (\mathrm{erg\ cm^{-3}\ s^{-1}}) = n(H_2) \sum_{J=2}^{J_{\max}} f_J A_{J,J-2} \Delta E_{J,J-2} - n(H_2) \sum_{J}^{J_{\max}} \sum_{J"}^{J_{\max}} f_{J"} \zeta_{J",J} \Delta E_{J",J} \tag{6.22}$$

$\zeta_{J",J}$ is the rate at which rotational level J is populated through optical pumping from rotational level $J"$ in the ground electronic and vibrational state.
$\zeta_{J",J}$ is given by the expression (§4.1.3):

$$\zeta_{J",J}\ (\mathrm{s^{-1}}) = \sum_{E} \sum_{v'J'} \zeta_{0J",v'J'} (1 - p^{\mathrm{dis}}_{v'J'}) \beta_{v'J',0J} \tag{6.23}$$

$\zeta_{0J",v'J'}$ is the rate of absorption in the line $0J" \rightarrow v'J'$ where $0J"$ is a rotational level in the ground electronic and vibrational state and $v'J'$ is a ro-vibrational level in the excited electronic state E (representing a B or C state) (s^{-1})
$p^{\mathrm{dis}}_{v'J'}$ is the probability that the state $v'J'$ will decay to the vibrational continuum of the ground state hence causing dissociation of the molecule
$\beta_{v'J',0J}$ is the probability that the ro-vibrational level $v'J'$ in the excited electronic state E will decay to the rotational state J in the ground electronic and vibrational state, either through a direct transition or indirectly through radiative cascade within the ground electronic state

Chapter 4 (§4.1.3) contains a full discussion of optical pumping of the H_2 molecule and derives suitable expressions for $\zeta_{0J",v'J'}$ and $\beta_{v'J',0J}$ which may be computed and used in equation (6.22).

6.2.2 CO rotational transitions

The cooling of the gas due to collisional excitation of rotational levels of the CO molecule followed by radiative decay is taken into account by adopting the photon escape probability formalism of Federman *et al.* (1979). If it is assumed that collisions with other species is the unique process for excitation of rotational levels in the ground electronic- vibrational state and that radiative decay is the unique process for de-excitation then the rate of cooling due to rotational transitions in the molecule is given by:

$$\Lambda_{\mathrm{CO\ rotation}}\ (\mathrm{erg\ cm^{-3}\ s^{-1}}) = n(\mathrm{CO}) \sum_{J=1}^{J_{\max}} f_J \mathrm{A}_{J,J-1} \Delta E_{J,J-1} p_J \qquad (6.24)$$

$n(\mathrm{CO})$ is the number density of CO molecules ($\mathrm{cm^{-3}}$)
f_J is the fraction of CO molecules in rotational level J of the ground electronic-vibrational state
$\mathrm{A}_{J,J-1}$ is the Einstein coefficient for spontaneous decay from rotational level J to level $J-1$ ($\mathrm{s^{-1}}$)
$\Delta E_{J,J-1}$ is the energy difference between levels J and $J-1$ (erg)
p_J is the probability that the photon emitted in the radiative decay $J \rightarrow J-1$ will eventually escape from the nebula hence contributing to the cooling of the gas

Unlike the $\mathrm{H_2}$ molecule, the CO molecule has a permanent dipole moment and hence electric dipole transitions are allowed (i.e. a transition $J \rightarrow J-1$). These transitions will dominate over lower order transitions such as electric quadrupole and magnetic dipole and so only these transitions are considered in the cooling rate. Although allowed (electric dipole) radiation is emitted in the process of rotational decay of the CO molecule, because the Einstein A coefficient for a dipole transition in general has a λ^{-3} dependence on wavelength, the A coefficient for a rotational transition (generally in the microwave region of the spectrum) will in fact be fairly small. For the CO molecule the Einstein spontaneous coefficient is of the order of 10^{-8} $\mathrm{s^{-1}}$ for low J levels to 10^{-4} $\mathrm{s^{-1}}$ for higher levels. A typical rate coefficient for collisional de-excitation is of the order of 10^{-11} $\mathrm{cm^3\ s^{-1}}$ at the kinetic temperatures typical in the nebula so the rate at which the CO molecule is rotationally de-excited through collisions with an abundant species, for example H ($\sim 10^3$ $\mathrm{cm^{-3}}$) is comparable to the Einstein coefficient for low J values. For high J values the assumption of ignoring collisional de-excitation is justified but it should be borne in mind that the assumption employed in the model of ignoring collisional de-excitation of the rotationally excited CO molecule is not strictly accurate for low J values.

Following Federman *et al.* (1979) and Hollenbach *et al.* (1971) the probability p_J may be calculated approximately by assuming the photons emitted in the 2π steradians back into the nebula will definitely not escape whereas the photons emitted in the 2π steradians towards the outer edge of the nebula have a certain probability of escaping, given by:

$$p_J = p_D + p_R \tag{6.25}$$

where

$$p_D(\tau) = \frac{2}{\sqrt{\pi}} \int_{-\infty}^{\infty} \exp(-t^2 - \tau e^{-t^2})\, dt$$

$$p_R(\tau) = \left(\frac{r}{t_1}\right) \frac{\mathrm{erf}(u_1)}{u_1} \tag{6.26}$$

These expressions are derived by assuming plane-parallel geometry in the cloud.

The function $\mathrm{erf}(x)$ is the error function defined by the integral

$$\mathrm{erf}(x) = \frac{2}{\sqrt{\pi}} \int_0^x e^{-t^2}\, dt$$

The parameters u_1 and t_1 are given by

$$u_1 = \frac{(\tau r)^{\frac{1}{2}}}{t_1} \qquad t_1 = 3.02(1000r)^{-0.064} \tag{6.27}$$

r is the ratio of the Doppler and natural widths of the $J \rightarrow J-1$ transition line shape (§2.3.4)

$$r = \frac{\gamma}{\sqrt{\pi}\beta} \tag{6.28}$$

where

$$\gamma = \frac{\Gamma}{4\pi} \qquad \beta = \frac{V_D}{\lambda_0} \tag{6.29}$$

Γ is the reciprocal of the mean lifetime of the upper rotational level (Γ=$A_{J,J-1}$ in the dipole approximation) (s^{-1})
V_D is the effective Doppler velocity of the CO molecule (§2.3.4.1) (cm s^{-1})
λ_0 is the wavelength of the transition $J \rightarrow J-1$ (cm)

τ in equations (6.26) represents the optical depth from the position of the CO molecule under consideration to the outer edge of the nebula. This optical depth is given by:

$$\tau = \tau' - \tau_0 \tag{6.30}$$

τ' is the *total* optical depth at the line centre through the nebula
τ_0 is the optical depth at the centre of the line at the position of the CO molecule

The optical depth τ_0 is given by:

$$\tau_0 = N(\mathrm{CO}_{J-1})\sigma(\lambda_0) \tag{6.31}$$

$N(\mathrm{CO}_{J-1})$ is the column density of CO in the rotational level $J-1$ (cm^{-2})
$\sigma(\lambda_0)$ is the cross-section of the molecule for absorption at the line centre where $\lambda = \lambda_0$ (cm^2)

Using equation (2.48) the absorption cross-section at the line centre is given by

$$\sigma(\lambda_0) = \left(\frac{\pi e^2}{m_e c}\right) f_{J-1,J} \frac{\lambda_0^2}{c} \phi_\lambda(\lambda_0) \tag{6.32}$$

$f_{J-1,J}$ is the absorption oscillator strength for the transition $J-1 \rightarrow J$
$\phi_\lambda(\lambda_0)$ is the value of the normalised Voigt function at the line centre
the other symbols have the same meaning as before.

Using the relationship between absorption oscillator strength and the corresponding Einstein A coefficient for spontaneous emission (e.g. McDaniel 1989) we have

$$\mathrm{A}_{J,J-1} = \frac{8\pi^2 e^2}{m_e \lambda_0^2 c} \frac{g_{J-1}}{g_J} f_{J-1,J} \tag{6.33}$$

g_J is the statistical weight (degeneracy) of rotational level J; $g_J = (2J+1)$

Hence

$$f_{J-1,J} = \left(\frac{2J+1}{2J-1}\right) \frac{m_e \lambda_0^2 c}{8\pi^2 e^2} \mathrm{A}_{J,J-1} \tag{6.34}$$

Substituting this expression for $f_{J-1,J}$ into equation (6.32) gives

$$\sigma(\lambda_0) = \left(\frac{2J+1}{2J-1}\right) \frac{\lambda_0^4}{8\pi c} \phi_\lambda(\lambda_0) \mathrm{A}_{J,J-1} \tag{6.35}$$

Now using the definition of the Voigt function $\phi_\nu(\nu)$ (§2.3.4.3) we have

$$\phi_\nu(\nu_0) = \frac{2(\log_e 2)^{\frac{1}{2}}}{\sqrt{\pi}\Delta\nu_D} H(a,0) = \frac{2(\log_e 2)^{\frac{1}{2}} a}{\pi^{\frac{3}{2}}\Delta\nu_D} \int_{-\infty}^{\infty} \frac{e^{-x^2}}{x^2 + a^2}\, dx \tag{6.36}$$

where

$$a = \frac{(\log_e 2)^{\frac{1}{2}}}{2} \frac{\Delta\nu_L}{\Delta\nu_D}$$

$\Delta\nu_L$ is the natural width of the line due to the intrinsic lifetime of the upper level
$\Delta\nu_D$ is the Doppler width of the line due to the gas temperature

The integral in equation (6.36) may be solved (Gradshteyn and Ryzhik 1980) to yield:

$$\phi_\nu(\nu_0) = \frac{2(\log_e 2)^{\frac{1}{2}} e^{a^2}}{\sqrt{\pi}\Delta\nu_D}\mathrm{erfc}(a) \tag{6.37}$$

where $\mathrm{erfc}(x)$ is the complementary error function defined by the integral

$$\mathrm{erfc}(x) = \frac{2}{\sqrt{\pi}}\int_x^\infty e^{-t^2}\,dt = 1 - \mathrm{erf}(x)$$

Now $\Delta\nu_D \gg \Delta\nu_L$ i.e. Doppler broadening is much more important than natural line broadening. In the situation being modelled, a typical value of the ratio $\Delta\nu_L/\Delta\nu_D$ is $\sim 10^{-10}$. Consequently the parameter a is also very small and to an extremely good approximation we can say $\mathrm{erfc}(a)$=1 and also e^{a^2}=1. Hence we then have the result:

$$\phi_\nu(\nu_0) = \frac{2(\log_e 2)^{\frac{1}{2}}}{\sqrt{\pi}\Delta\nu_D} \tag{6.38}$$

Hence, using the definition of $\Delta\nu_D$ from equation (2.35) and the relationship between the functions $\phi_\nu(\nu)$ and $\phi_\lambda(\lambda)$ from equation (2.47) we have:

$$\tau_0(J) = N(\mathrm{CO}_{J-1})\sigma(\lambda_0) = N(\mathrm{CO}_{J-1})\left(\frac{2J+1}{2J-1}\right)\frac{\lambda_0^3}{8\pi^{\frac{3}{2}}V_D}\mathrm{A}_{J,J-1} \tag{6.39}$$

To compute the optical depth $\tau'(J)$ i.e. the total optical depth at the centre of the line through the whole cloud it is required to run the model once using an escape probability of unity for all the CO rotational transitions (this will overestimate the effect of CO rotational cooling). The total optical depth through the nebula may then be derived from the computed values of the column densities of the rotational levels of CO using exactly the same formula as in equation (6.39):

$$\tau'(J) = N_0(\mathrm{CO}_{J-1})\left(\frac{2J+1}{2J-1}\right)\frac{\lambda_0^3}{8\pi^{\frac{3}{2}}V_D}\mathrm{A}_{J,J-1} \tag{6.40}$$

$N_0(\mathrm{CO}_{J-1})$ is the total column density of the CO molecule in rotational state $J-1$ through the nebula (cm^{-2})

This procedure is performed several times as an iterative process as altering the total optical depth at the line centre will change the cooling effect of CO rotational excitation which in turn will affect the equilibrium kinetic temperature of the gas,

upon which the rotational population of the CO molecule depends.
Once computed, the values of $\tau'(J)$ may then be used in equation (6.30) to compute more accurately the cooling effect of rotational excitation of CO.

Hence, to summarise, the cooling effect of rotational excitation of the CO molecule by collisions with other species is given by:

$$\Lambda_{\text{CO rotation}} = n(\text{CO}) \sum_{J=1}^{J_{\max}} f_J \Delta E_{J,J-1} \text{A}_{J,J-1} p_J$$

where p_J, the probability that the emitted photon escapes from the nebula, is given by:

$$p_J = p_D(\tau) + p_R(\tau)$$

and

$$p_D(\tau) = \frac{2}{\sqrt{\pi}} \int_{-\infty}^{\infty} \exp(-t^2 - \tau e^{-t^2})\, dt$$

$$p_R(\tau) = \left(\frac{r}{t_1}\right) \frac{\text{erf}(u_1)}{u_1}$$

where

$$\tau(J) = \tau'(J) - \tau_0(J)$$

$$\tau_0(J) = N(\text{CO}_{J-1}) \left(\frac{2J+1}{2J-1}\right) \frac{\lambda_0^3}{8\pi^{\frac{3}{2}} V_D} \text{A}_{J,J-1}$$

$$\tau'(J) = N_0(\text{CO}_{J-1}) \left(\frac{2J+1}{2J-1}\right) \frac{\lambda_0^3}{8\pi^{\frac{3}{2}} V_D} \text{A}_{J,J-1}$$

To compute $p_R(\tau)$ for small values of the argument u_1 ($u_1 \leq 0.01$) the error function is approximated by expanding the exponential integrand as a truncated Taylor series. For large values of the argument ($u_1 > 0.01$) the error function is calculated by employing a rational approximation to be found in the literature (Abramowitz and Stegun 1965).
Calculation of $p_D(\tau)$ is achieved by employing numerical approximations to the integral applicable to the various different ranges of values of τ (le Bourlot, private communication).

Chapter 7

Dust properties

The evidence for dust grains in the planetary nebula environment has been outlined in Chapter 5 on gas heating processes. This chapter discusses the grain characteristics adopted for the model.

Dust represents the dominant source of opacity in the nebula by which the outgoing UV radiation field is attenuated. The grains extinguish the starlight by scattering or by absorption of high-energy photons followed by subsequent emission in the infra-red. Dust grains also play an important rôle in the thermal balance of the nebula through interaction with the radiation field and with the gas particles and this aspect has been discussed in Chapter 5.

7.1 Dust characteristics

7.1.1 Amount of dust in the nebula

Planetary nebulae are thought to be the major source of recycled interstellar matter and the dust to gas ratio ejected into the interstellar medium (ISM) will obviously depend on the dust to gas ratio in the nebula. As reviewed by Bode (1988) the value of Υ in PNe is thought to be only about 0.001 where Υ is the ratio of dust mass per unit volume in the nebula to gas mass per unit volume, i.e. $\Upsilon = \rho_{\rm dust}/\rho_{\rm gas}$. This may be compared to the value of $\Upsilon \approx 0.01$ estimated for red giant stars (Knapp 1985), the precursor phase of PNe, or the canonical value for the dust/gas ratio in the diffuse ISM, $\sim$0.006 derived from observations of the colour excess of stars and theoretical extinction cross-sections of dust grains (Spitzer 1978).

In the harsh conditions of the ionised region of the planetary nebula Υ is likely to have a smaller value than the neutral region because of chemical sputtering due to surface reactions with impinging hydrogen atoms and ions which would tend to destroy the dust grains (Barlow and Silk 1977). Hence it is reasonable to suppose that the value of Υ in the molecular domain of the nebula is likely to be higher than the overall estimate of $\sim$0.001.

Hoare *et al.* (1992) have modelled the dust emission from the carbon rich PNe NGC 7027 and BD+30°3639 utilising their own JCMT sub-mm and mm-wavelength photometry as well as the IRAS and shorter wavelength infrared data. They estimated a dust to gas mass ratio of 7×10^{-4} in the ionised region based on the observed attenuation of the CIV 1550 Å resonantly scattered line. For the

neutral region around NGC 7027, Hoare *et al.* estimated a dust to gas mass ratio of $\Upsilon = 1.5 \times 10^{-3}$, not significantly different from the ratio derived for the ionised zone considering the uncertainties reported by these workers associated with the CO-based neutral mass estimate.
For the model presented in this work a canonical value of $\Upsilon = 0.002$ is employed, a value assumed to be constant throughout the nebula.

7.1.2 Grain size

Workers in the area of stellar and interstellar dust modelling often assume a grain size distribution. To explain the features of the interstellar extinction curve Mathis, Rumpl and Nordsieck (1977) produced a model of the interstellar dust comprising several different materials and with a power-law distribution of particle size following $n(r_d) \propto r_d^{-3.5}$ where r_d is the radius of a spherical dust grain. This power law was found to apply to all the materials in the model. The sizes of graphite particles in the model varied from about 5 nm to about 1000 nm. Such a grain size distribution was subsequently used by Hoare (1990) to model the dust content of two carbon-rich planetary nebulae.
To explain the observed power radiated by dust in the ISM Désert *et al.* (1990) produced a model consisting of three grain components - 2 dimensional PAH molecules, very small grains and big grains. The very small grains were modelled as graphite particles with a power law size distribution between radius limits of 1.2 nm and 15 nm. The big grains were modelled as carbon-coated silicates with a size distribution between radii of 15 nm and 110 nm.
Cohen *et al.* (1984) produced a model of the dust content of the planetary nebula IC 3568. In order to fit the observations of the infra-red spectrum from the nebula they found the model required grains with absorption properties like those of amorphous carbon with a mean radius of 15 nm.
Based on the evidence gleaned from these previous models and their comparison with observed IR spectra the current model assumes a mean grain radius of r_d= 100 nm. A grain size distribution is not employed in the model. Because of the paucity of data on grain size and variation in nebulae this could at best be only an informed estimate and, with other uncertainties existing elsewhere in the model, such detail was regarded as unjustified.

7.1.3 Grain composition

The program models a carbon-rich planetary nebula (C/O = 1.75) and hence the dust grains are assumed to be carbon-based. In the past graphite has long been

thought of as the material from which stellar and interstellar carbon grains are composed, in particular because it was thought to be the origin of the 2175 Å feature in the interstellar extinction curve. Objections to pure graphite have recently been put forward and amorphous carbon has emerged as possibly a better candidate (Mathis 1986; Bussoletti *et al.* 1987).

In modelling the dust content of the PNe IC 418 and NGC 7662, Hoare (1990) deduced that the likely source of the far-IR continuum emission was probably grains composed of amorphous carbon with a component of pure graphite. In a similar vein, Cohen *et al.* (1984) found that to fit the IR observations of the PN IC 3568 the optical properties of the grains had to fit those of amorphous carbon.

Hoare *et al.* (1992) modelled the dust emission from NGC 7027 and BD+30°3639 using both graphite and amorphous carbon models. For both PNe they found that their graphite grain models were unable to produce enough sub-mm flux but that an acceptable fit could be obtained with amorphous carbon models. However, the amorphous carbon model of NGC 7027 was unable to account for an ubiquitous prominent feature peaking at 30 - 35 μm which has previously been observed in the spectra of carbon stars and IC 418 (Moseley and Silverberg 1986). A carbonaceous origin for this feature would seem likely given the fact that it has only been observed in carbon rich objects. Temperature spiking in small grains has been suggested as the cause of this short-wavelength excess but the topic remains open.

Some of the features in the infrared spectra obtained from PNe may be taken as evidence of the presence of amorphous carbon particles. The emission bands at 6.2μm, 7.7 μm and 11.3μm observed in many PNe (§5.1.1) are also evident as broad features in the extinction curve of amorphous carbon particles (Koike *et al.* 1980; Borghesi *et al.* 1983).

The convincing evidence accumulated to date for the presence of PAH molecules in the neutral regions of PNe (§5.1.1) also lends theoretical weight to believing that amorphous carbon is the dominant constituent of the carbon grains. Once formed, the PAH molecules can become the building blocks of amorphous carbon particles (Allamandola *et al.* 1989). Soot formation occurs in terrestrial sources when the aromatic molecules in the soot-forming region become large enough that condensation processes can occur when they collide (Miller *et al.* 1984) and this must also be the nucleation process for amorphous carbon particles produced in the vicinity of stars. Interstellar amorphous carbon particle growth probably proceeds by the kinetic growth of PAH clusters (several PAH molecules combined together in a semi-random three-dimensional orientation). The degree of 'amorphicity' or lack of three-dimensional regularity is built in by the kinetic growth process and

the most stable geometries of the various PAH clusters.

If the hypothesis of grain growth by coagulation of PAH molecules is correct it is probable that the grains will exhibit small-scale crystalline structure but overall will be of an amorphous character i.e. a polycrystalline carbon structure similar to soot will result. In the temperature and density conditions of the molecular shell condensation of carbon and hydrogen atoms to form PAH molecules is favoured over other crystalline forms such as polyacetylenes (§5.1.1). These PAH molecules may then cluster to form the much larger polycrystalline soot particle. Truly amorphous carbon particles can be formed when only a few condensation nuclei are formed in a rapidly condensing gas, a situation not encountered in the relatively diffuse, expanding nebula. This hypothesis is given credence by the observational high abundance of PAH molecules with large carbon numbers in planetary nebulae (§5.1.1). Any differences in physical and optical properties between amorphous carbon and polycrystalline carbon are too subtle to be of importance with the current state of knowledge (Tielens and Allamandola 1987) although future theory and observation may reveal differences in physical characteristics that prove to be significant.

It is possible to argue that energetic processes occurring within the amorphous carbon particle may tend to convert the structure to a more crystalline graphite-like structure. However, complete graphitisation would require several thousand degree temperatures sustained for several hours throughout the particle (Marchand 1987), a situation that would certainly not arise in the molecular region of the nebula.

Based on this evidence and the theoretical considerations the dust in this model is assumed to be composed of amorphous carbon exhibiting isotropic optical properties with a corresponding mass density of $\rho_d = 1.8$ g cm^{-3} (Hoare 1990). The results obtained with these assumed dust properties will certainly be considerably different than if standard interstellar graphite grain properties were used. In Chapter 8 the results obtained with amorphous carbon particles are presented but these are compared with results obtained by assuming physical and optical properties of graphite.

7.2 Grain optical properties

If the complex refractive index of the grain material is known as a function of wavelength and the grains are assumed to be spherical then Mie scattering theory may be employed to calculate cross-sections for extinction, scattering and absorption of radiation. If the radius of the spherical grain is a then we may define efficiency factors for scattering, absorption and extinction in terms of the corresponding cross-sections $C_{\rm sca}$, $C_{\rm abs}$ and $C_{\rm ext}$ as follows:

$$Q_{\rm sca} = C_{\rm sca}/\pi a^2$$

$$Q_{\rm abs} = C_{\rm abs}/\pi a^2$$

$$Q_{\rm ext} = Q_{\rm sca} + Q_{\rm abs} = C_{\rm ext}/\pi a^2$$

The scattering properties of the sphere at a wavelength λ may be determined by the following parameters:

$$x = 2\pi a/\lambda$$

$$m = n - ik = \sqrt{K - 2i\sigma\lambda/c}$$

n, k are the refractive and absorptive indices respectively
K is the dielectric constant
σ is the conductivity of the grain material

The Mie formulae give us (Mie 1908; Wickramasinghe 1973):

$$Q_{\rm sca} = \frac{2}{x^2}\sum_{n=1}^{\infty}(2n+1)\left[|a_n|^2 + |b_n|^2\right]$$

$$Q_{\rm ext} = \frac{2}{x^2}\sum_{n=1}^{\infty}(2n+1)\ {\rm Re}(a_n + b_n)$$

$$Q_{\rm abs} = Q_{\rm ext} - Q_{\rm sca} \qquad (7.1)$$

where

$$a_n = \frac{x\psi_n'(y)\psi_n(x) - y\psi_n'(x)\psi_n(y)}{x\psi_n'(y)\zeta_n(x) - y\zeta_n'(x)\psi_n(y)}$$

$$b_n = \frac{y\psi_n'(y)\psi_n(x) - x\psi_n'(x)\psi_n(y)}{y\psi_n'(y)\zeta_n(x) - x\zeta_n'(x)\psi_n(y)} \qquad (7.2)$$

with $y = mx$.
Note that primes denote differentiation with respect to the argument.

The functions $\psi_n(z)$ and $\zeta_n(z)$ occurring in equations (7.2) are the Ricatti-Bessel functions, defined in terms of the spherical Bessel functions of the first kind by:

$$\psi_n(z) = \left(\frac{\pi z}{2}\right)^{\frac{1}{2}} J_{n+\frac{1}{2}}(z)$$

$$\zeta_n(z) = \left(\frac{\pi z}{2}\right)^{\frac{1}{2}} \left(J_{n+\frac{1}{2}}(z) + i(-1)^n J_{-(n+\frac{1}{2})}(z)\right) \tag{7.3}$$

By employing the usual recurrence relation for Bessel functions:

$$2J'_\nu(z) = J_{\nu-1}(z) - J_{\nu+1}(z)$$

the derivatives of the Ricatti-Bessel functions become:

$$\psi'_n(z) = \frac{1}{2}\left(\frac{\pi}{2z}\right)^{\frac{1}{2}} \left(J_{n+\frac{1}{2}}(z) + zJ_{(n-1)+\frac{1}{2}}(z) - zJ_{(n+1)+\frac{1}{2}}(z)\right)$$

$$\zeta'_n(z) = \psi'_n(z) + \frac{1}{2}i(-1)^n\left(\frac{\pi}{2z}\right)^{\frac{1}{2}} \left(J_{-(n+\frac{1}{2})}(z) + zJ_{-((n+1)+\frac{1}{2})}(z) - zJ_{-((n-1)+\frac{1}{2})}\right) \tag{7.4}$$

The FORTRAN program GRAIN in Appendix C has been written to compute the efficiency factors of a spherical grain at a given wavelength given the radius of the grain and the complex refractive index of the material at this wavelength.

Values for the complex refractive index of amorphous carbon have been published in the literature and these are shown in Table 7.1.

By using the program GRAIN the values for the efficiency factors for scattering, absorption and extinction have been calculated for a spherical grain of amorphous carbon of radius r_d = 100 nm. This data is shown in Table 7.2.

The model requires values for $Q_{\rm abs}$ extending over the wavelength range 912 Å to 3000 Å for calculations concerned with the dust temperature (§5.2.2) and these may be approximated by employing a fourth- order polynomial fit to the data (where λ is in Å):

$$Q = m_0 + m_1\lambda + m_2\lambda^2 + m_3\lambda^3 + m_4\lambda^4$$

For $Q_{\rm abs}$ the coefficients m_0 to m_4 are given by:

Table 7.1

The complex refractive index of amorphous carbon as a function of wavelength

Wavelength λ (Å)	n	k	Reference
919	1.37	0.93	
954	1.45	0.89	
992	1.53	0.85	
1033	1.59	0.79	Williams and Arakawa (1972)
1078	1.65	0.73	(glassy carbon)
1127	1.71	0.67	
1181	1.78	0.58	
1240	1.81	0.45	
1250	1.94	0.52	
1333	1.95	0.47	
1428	1.94	0.43	
1538	1.88	0.42	
1667	1.86	0.42	
1818	1.88	0.44	Duley (1984)
2000	1.92	0.48	(amorphous carbon solid)
2222	2.00	0.52	
2500	2.16	0.55	
2857	2.28	0.59	
3333	2.32	0.63	
4000	2.32	0.64	

$m_0 = -0.14019$

$m_1 = 2.4189 \times 10^{-3}$

$m_2 = -1.3977 \times 10^{-6}$

$m_3 = 3.7599 \times 10^{-10}$

$m_4 = -3.7549 \times 10^{-14}$

which gives a correlation coefficient to the data of R=0.9978

Table 7.2

Efficiency factors for scattering, absorption and extinction for an amorphous carbon grain of radius 100 nm as a function of wavelength

Wavelength λ (Å)	Q_{sca}	Q_{abs}	Q_{ext} $(Q_{sca}+Q_{abs})$	Albedo A_λ (Q_{sca}/Q_{ext})	τ_λ/τ_V
919	1.32	1.17	2.49	0.53	0.793
954	1.30	1.19	2.50	0.52	0.804
992	1.29	1.22	2.51	0.52	0.807
1033	1.28	1.24	2.52	0.51	0.819
1078	1.27	1.26	2.53	0.50	0.831
1127	1.26	1.29	2.55	0.50	0.837
1181	1.26	1.31	2.57	0.49	0.852
1240	1.24	1.35	2.59	0.48	0.867
1250	1.28	1.33	2.60	0.49	0.862
1333	1.27	1.36	2.62	0.48	0.877
1428	1.25	1.40	2.64	0.47	0.892
1538	1.24	1.43	2.67	0.46	0.911
1667	1.27	1.47	2.73	0.46	0.931
1818	1.29	1.49	2.79	0.46	0.952
2000	1.33	1.51	2.84	0.47	0.960
2222	1.37	1.56	2.92	0.47	0.987
2500	1.38	1.58	2.96	0.47	1.00
2857	1.45	1.60	3.05	0.48	1.02
3333	1.56	1.70	3.25	0.48	1.09
4000	1.60	1.62	3.23	0.50	1.06

Values for the absorption efficiency factor Q_{abs} are also required as a function of frequency for the dust temperature calculation (§5.2.2). This data may easily be derived from Table 7.2 by converting the wavelength to frequency. For the purpose of computing the dust temperature the data can be approximated by the following formulae:

For $\nu \leq 6.00 \times 10^{14}$ Hz:	$Q_{\rm abs} = 2.767 \times 10^{-15}\nu$
For 6.00×10^{14} Hz $< \nu \leq 1.05 \times 10^{15}$ Hz:	$Q_{\rm abs} = 1.740 - 1.333 \times 10^{-16}\nu$
For $\nu > 1.05 \times 10^{15}$ Hz:	$Q_{\rm abs} = 1.817 - 1.990 \times 10^{-16}\nu$

7.2.1 Attenuation of the radiation field

In a small slab of the nebula, of unit cross-sectional area and depth dr (in the direction of propagation of the radiation), there are $n_d\,dr$ dust particles (where n_d is the number density of grains). Each grain offers an extinction cross-section of $Q_{\rm ext}(\lambda)\pi r_d^2$ where r_d is the radius of a grain. Hence the fraction of the photon flux removed from the stream of outgoing photons (which is equal to the fraction of the radiation energy density removed) is given by:

$$\frac{d\Phi(\lambda)}{\Phi(\lambda)} = -Q_{\rm ext}(\lambda)n_d\pi r_d^2\,dr$$

This equation assumes all the light scattered by the particle is scattered out of the forward direction, so that scattering is as effective as absorption in attenuating the photon flux. At the other extreme, if *all* the scattered light were assumed to be scattered into the forward direction, i.e. a strictly forward scattering phase function were assumed for the grains then only absorption would contribute to the attenuation of the photon flux and hence:

$$\frac{d\Phi(\lambda)}{\Phi(\lambda)} = -Q_{\rm abs}(\lambda)n_d\pi r_d^2\,dr \;=\; -(1-A_\lambda)Q_{\rm ext}(\lambda)n_d\pi r_d^2\,dr$$

A_λ is the albedo of the grain, defined as $A_\lambda = Q_{\rm sca}/Q_{\rm ext}$

The assumption of enhanced forward scattering is somewhat consistent with observations of scattering of galactic light from interstellar grains at UV wavelengths. The true amount of forward scattering will lie somewhere between the two extremes. Strictly forward scattering will overestimate the radiation intensity at large distances from the star and to compensate for this and to take the scattering by dust into account (if only approximately), it is assumed the radiation field will be attenuated by dust according to:

$$\frac{d\Phi(\lambda)}{\Phi(\lambda)} = -(1-A_\lambda)^{\frac{1}{2}}Q_{\rm ext}(\lambda)n_d\pi r_d^2\,dr$$

Values for the albedo of amorphous carbon grains as a function of wavelength are tabulated in Table 7.2 where it is seen that they do not vary greatly from a value of 0.5.

If n_d is not a function of distance from the star (as is the case in this constant hydrogen nuclei number density model) then this equation is easily solved to yield:

$$\Phi(\lambda) = \Phi_0(\lambda) \exp(-(1 - A_\lambda)^{\frac{1}{2}} r Q_{\rm ext}(\lambda) n_d \pi r_d^2) \tag{7.5}$$

$\Phi_0(\lambda)$ is the value of the radiation field energy density at some initial point (erg cm^{-3} Å^{-1})
r is the distance in a direction away from the central star (cm)

A formula for the number density of dust grains has already been derived in Chapter 5 (equation (5.58)) and is given by:

$$n_d = \frac{1.05 m_{\rm H} n_{\rm H} \Upsilon}{\pi r_d^3 \rho_d}$$

where the symbols have the same meaning as before.

Hence the optical depth τ_λ, due to extinction by dust grains, and defined via the equation:

$$\Phi(\lambda) = \Phi_0(\lambda) e^{-\tau_\lambda}$$

is given by

$$\tau_\lambda = \frac{1.05 m_{\rm H} n_{\rm H} \Upsilon}{r_d \rho_d} (1 - A_\lambda)^{\frac{1}{2}} Q_{\rm ext}(\lambda) r \tag{7.6}$$

The fact that this is a constant hydrogen nuclei density model means that the optical depth at a given wavelength is directly proportional to the distance r.
The ratio of optical depth at wavelength λ to τ_V (the optical depth at the visual wavelength) is given by

$$\frac{\tau_\lambda}{\tau_V} = \frac{(1 - A_\lambda)^{\frac{1}{2}} Q_{\rm ext}(\lambda)}{(1 - A_{\lambda_V})^{\frac{1}{2}} Q_{\rm ext}(\lambda_V)} \tag{7.8}$$

where λ_V represents the visual (V) wavelength (λ_V= 5550 Å).

Although the data is not reproduced in Table 7.1, Duley reports values of refractive index for amorphous carbon up to a wavelength of 10000 Å. Using this data, a value of extinction efficiency at the V wavelength has been calculated as $Q_{\rm ext}(\lambda_V)$= 2.97 with an albedo of A_{λ_V}= 0.474. The final column of Table 7.2 contains the values of the function $\tau_\lambda/\tau_V = (1 - A_\lambda)^{1/2} Q_{\rm ext}(\lambda)/(1 - A_{\lambda_V})^{1/2} Q_{\rm ext}(\lambda_V)$ as a function of wavelength.
Hence the attenuation of radiation due to extinction by dust grains is given by:

$$\Phi(\lambda) = \Phi_0(\lambda) \exp(-\tau_\lambda) = \Phi_0(\lambda) \exp\left(-\left(\frac{\tau_\lambda}{\tau_V}\right)\tau_V\right) \tag{7.9}$$

The values of τ_λ/τ_V are well approximated by employing a fourth-order polynomial fit to the range 912 Å $< \lambda <$ 3000 Å (where λ is in Å):

$$\tau_\lambda/\tau_V = m_0 + m_1\lambda + m_2\lambda^2 + m_3\lambda^3 + m_4\lambda^4$$

The coefficients m_0 to m_4 are as follows:

$m_0 = 0.60950$
$m_1 = 1.1730 \times 10^{-4}$
$m_2 = 1.7228 \times 10^{-7}$
$m_3 = -1.0324 \times 10^{-10}$
$m_4 = 1.6189 \times 10^{-14}$
which gives a fit to the data with a correlation coefficient of R=0.9994.

The values of τ_λ/τ_V predicted by utilising the refractive index data in the literature are very unlike the corresponding function for graphite. In the case of crystalline carbon the function rises sharply in the ultraviolet so that there is far more extinction at small wavelengths than in the visible range of the spectrum. Use of the refractive index data for amorphous carbon actually predicts less absorption in the UV than at visible wavelengths (Table 7.2). Observations of extinction of starlight by interstellar grains indeed shows far greater extinction at small wavelengths ('reddening') and also shows a peak in the extinction curve at around 2200 Å. By making judicious choices for the sizes and shapes of the graphite grains this feature can also be reproduced by theoretical models (Spitzer 1978) which is why carbon-rich interstellar grains are commonly thought to be composed of graphite. Choosing between the amorphous and crystalline forms of carbon particles will obviously have a pronounced effect on the final predicted molecular column densities. Photoionisation and photodissociation will affect the nebular chemistry far deeper into the gas cloud in the case of amorphous carbon because the ultraviolet field from the central star undergoes far less extinction. In Chapter 8 results are presented for the amorphous carbon case and are compared with the results obtained using graphitic grain properties (Mathis *et al.* 1983).

Chapter 8

Results and observations

The model was run using various values for the (constant) hydrogen nuclei number density. Values from $n_{\rm H} = 10^3$ cm^{-3} to $n_{\rm H} = 10^4$ cm^{-3} were used in steps of 10^3 cm^{-3}. The criterion for deciding at what optical depth to terminate execution and calculate column densities was to match the predicted absolute column density of a given molecule to a value computed from observations of a planetary nebula. Bachiller *et al.* (1989) made observations of the young PN NGC 2346 and mapped the CO $J = 2 \rightarrow 1$ (and $J = 1 \rightarrow 0$) emission from the nebula. By making judicious estimates for the two parameters $n({\rm H_2})$ and $T_{\rm gas}$ to explain the observed $2 \rightarrow 1$ and $1 \rightarrow 0$ intensities in the nebula these workers were then able to derive an estimate for the CO column density in the nebula, $N({\rm CO})$. The value of $N({\rm CO})$ thus computed obviously varies with position in the nebula but they found typical values of $N({\rm CO})$ reached 7×10^{15} cm^{-2}, although the CO column density averaged over the entire nebula was less than this by about a factor of two. The value utilised for comparison with the model is the value Bachiller *et al.* derived towards one clump in the nebula (clump C in the paper). Thus the edge of the modelled nebula is assumed to have been reached when the computed value of $N({\rm CO})$ reaches 3.8×10^{15} cm^{-2}. This means that in general the model run will be stopped at different distances (and different optical depths) from the central star for the various values of $n_{\rm H}$ considered. As the value of the assumed $n_{\rm H}$ increases the linear distance for termination of the run decreases and the optical depth increases (due to the increased grain opacity).

The result of these runs was the discovery that the abundances of the various species relative to $n_{\rm H}$ as a function of optical depth/distance did not vary a great deal over the range of values taken for $n_{\rm H}$ both quantitatively and in an overall qualitative picture of abundance variations. From the ten values of $n_{\rm H}$ used computational results are shown for two representative densities of $n_{\rm H} = 1000$ cm^{-3} and 5000 cm^{-3}. Figs. 8.7 to 8.18 show abundance variations, temperature distribution, dissociation probabilities and thermal rates through the nebula for a hydrogen nuclei density of 1000 cm^{-3}. Figs. 8.19 to 8.30 show the corresponding results for $n_{\rm H} = 5000$ cm^{-3}. Table 8.1 displays the column densities of all the chemical species in the neutral shell for both densities of 1000 cm^{-3} and 5000 cm^{-3}.

8.1 Model results

The first thing to notice about the two sets of results is the overall similarity in the abundance variations, albeit occurring on a different distance (and optical depth) scale. The discussion below concentrates on the results obtained for $n_{\rm H}$ = 1000 cm^{-3} but is directly applicable to the results for $n_{\rm H}$ = 5000 cm^{-3}.

In Fig. 8.7 are shown the abundances of the important H/He bearing species (and the electron abundance). Atomic hydrogen is the most abundant form of hydrogen below an optical depth of $\tau_V \approx 1.4$ (approximately one third of the way through the nebula). The self-shielding effect of H_2 line absorption starts to become effective at about $\tau_V = 0.6$ and the photodissociation rate drops considerably (Fig. 8.14). Self-shielding in the low-lying ortho levels of H_2 (J=1,3) is predicted to occur an appreciable distance before the process becomes effective for the low-lying para levels (J=0,2) (Fig. 8.2). Thus the rapid rise in the abundance of H_2 at $\tau_V \approx 0.6$ occurs through selective photodissociation, ortho-H_2 becoming much more abundant than para-H_2 in this region (Fig. 8.1).
Near the ionised/neutral interface the chemistry of H_2 is completely dominated by formation on dust grains and photodissociation through UV line absorption and this remains true a considerable way through the nebula, up to about half the total thickness of the molecular shell. In this regime, under the assumption of static equilibrium, the abundance of the hydrogen molecule is described by the relation:

$$k_g n({\rm H}) n_{\rm H} = \zeta_{\rm H_2} n({\rm H_2}) \tag{8.1}$$

where $\zeta_{\rm H_2}$ is the photodissociation rate of the molecule and

$$k_g = 1.41 \times 10^{-18} T^{1/2} \ {\rm cm^3 \ s^{-1}} \tag{8.2}$$

(see §3.2.2.1).
Since $n_{\rm H}$=1000 cm^{-3} and is assumed constant we have

$$\frac{n({\rm H_2})}{n({\rm H})} = 1.41 \times 10^{-15} \frac{\sqrt{T}}{\zeta_{\rm H_2}} \tag{8.3}$$

Figs. 8.13 and 8.14 show the gas temperature variation and the photodissociation rate of H_2 through the nebula. It is clear that whereas the value of $\sqrt{T}$ drops by less than an order of magnitude below $\tau_V = 2$, the value of $\zeta_{\rm H_2}$ drops by about ten orders of magnitude over the same region. This is the reason why such a rapid increase in $n({\rm H_2})/n({\rm H})$ is observed in Fig. 8.7.

Figs. 8.3 and 8.4 demonstrate why self-shielding is so effective in protecting molecular hydrogen from dissociation at large optical depths. Fig. 8.3 shows the ultraviolet spectrum (900 Å to 1300 Å) computed at an optical depth of $\tau_V = 0.5$, before the H/H_2 transition region at $\tau_V \approx 1.4$. The Lyman absorption lines of atomic hydrogen (e.g. a, b, c, d, e in the figure) are saturated but the absorption lines of H_2 have had very little effect. Fig. 8.4 shows the UV spectrum at an optical depth of $\tau_V = 2.0$ where it is easily seen that the H_2 absorption lines are already saturated and there is very little radiation left of the wavelengths required to optically pump the molecule from where dissociation may occur through spontaneous radiative decay (§2.4.1). This far into the nebula line absorption by molecular hydrogen has effectively removed all the dissociating radiation and H_2 is the dominant hydrogen-bearing species (Fig. 8.7).

In the outer half of the cloud the gas temperature has dropped considerably to about 15 K primarily due to the fact that heating from photoionisation of dust grains and PAH molecules is no longer important (Fig. 8.15). The attenuation of the ultraviolet field also means that photodissociation is no longer the dominant destruction route for H_2 in this region of the nebula. Cosmic ray dissociation and ionisation of the molecule, assumed to occur at a constant rate throughout the nebula (§3.2.2.2), is now comparable to the photodissociation process. However, far from the central star it is ion-molecule reactions with abundant ions which control the destruction of H_2, principally through the radiative association reaction

$$C^+ + H_2 \rightarrow CH_2^+ + h\nu \tag{8.4}$$

occurring at a rate of 7.3×10^{-16} cm^3 s^{-1} at 15 K (Marquette *et al.* 1989). Although this is a small rate coefficient the consistently high abundance of ionised carbon (Fig. 8.8) ensures that the reaction retains its central position in the chemistry of the hydrogen molecule.

Although the low temperature characterising the outer half of the nebula is favourable for recombination reactions producing H_2, the formation process on dust grains remains the dominant route to creation of the molecule. Even though the rate coefficients are extremely large (of the order of 10^{-6} cm^3 s^{-1} at 15 K) dissociative recombination remains of secondary importance because of the low abundance of the main contributing species (H_3^+ and CH_2^+). At optical depths above $\tau_V \approx 2$ the abundance of H_2 is thus described approximately by the relation:

$$k_g n(\mathrm{H}) n_{\mathrm{H}} = k' n(C^+) n(H_2) \tag{8.5}$$

where k' is the rate coefficient associated with equation (8.4).
At $\tau_V = 4$ the gas temperature is $T \approx 11$ K (Fig. 8.13) and the value of k' is approximately 8×10^{-16} cm^3 s^{-1} (Marquette *et al.* 1989) and since $n(C^+) \approx 0.4$ cm^{-3} at the exterior edge of the nebula (Fig. 8.8) we have that

$$\frac{n(H_2)}{n(H)} \approx 15$$

at an optical depth of $\tau_V = 4$ (see Fig. 8.7).
The model presented here does not include the effect of interstellar photodissociating radiation incident on the exterior of the nebula. If this were included it would have the effect of photodissociating H_2 at the outer edge of the neutral region, the efficiency of the process decreasing toward the central star. Thus in reality photodissociation of the hydrogen molecule (as well as other species) is likely to retain the importance of an effective destruction mechanism throughout most of, if not all of, the molecular cloud. Instead of the simple H/H_2 transition region predicted by the model it is thus more likely that in reality there would be a shell of molecular material surrounded on the interior and exterior by shells of atomic material as pointed out by many workers in the field (e.g. Gussie *et al.* 1994). This subject of the omission of an external interstellar radiation field is further discussed in §8.2.
The ionised forms of hydrogen exhibit different abundance variations through the nebula. The abundance of H^+ falls with distance from the central star but the abundances of H_2^+ and H_3^+ rise (although always remaining at negligible levels of abundance relative to molecular hydrogen). At the ionised/neutral interface the abundance of H^+ is controlled by cosmic ray ionisation of H and radiative recombination. Charge exchange with oxygen is also important and represents the dominant route to formation of O^+, even though the reaction in question displays an endothermicity of 232 K. The two reactions in question are

$$O^+ + H \rightarrow O + H^+ \tag{8.8}$$

$$H^+ + O \rightarrow H + O^+ - 232\,K \tag{8.9}$$

exhibiting rate coefficients of $k_1 = 6 \times 10^{-10}$ and $k_2 = 7 \times 10^{-10} \exp(-232/T)$ cm^3 s^{-1} respectively.
As the gas temperature drops rapidly (Fig. 8.13) the endothermicity of reaction (8.9) means that very little O^+ is created to drive reaction (8.8) and cosmic ray ionisation and recombination quickly become the sole controlling factors for the H^+

abundance. At an optical depth of $\tau_V = 1.0$ for example the equation governing the abundance of H^+ is (Prasad and Huntress 1980):

$$0.46\zeta_0 n(\mathrm{H}) = 3.61 \times 10^{-12}\left(\frac{T}{300}\right)^{-0.75} n(\mathrm{H}^+)n(e^-)$$

At $\tau_V = 1.0$ the temperature is $T \approx 25K$ (Fig. 8.13) and $n(e^-) \approx 0.8$ cm^{-3} so that, with a value of $\zeta_0 = 4 \times 10^{-17}$ s^{-1}, we have

$$\frac{n(\mathrm{H}^+)}{n(\mathrm{H})} \approx 10^{-6}$$

At the H/H_2 transition region ($\tau_V \approx 1.4$) H^+ is still being produced by cosmic ray ionisation and thus the abundance of H^+ falls correspondingly with the drop in the abundance of H.

As the temperature drops further and the abundances of other molecules increases, H^+ tends to be destroyed in charge exchange reactions with hydrocarbon species (CH, CH_2, C_2H) occurring with a Langevin rate of about 10^{-9} cm^3 s^{-1} and with other carbon-bearing species (CS, C_2). Far from the central star temperature-dependent reactions between ionised helium and H_2 become more important in the creation of the molecule. As the gas temperature drops in the outer half of the cloud the abundance of H^+ then becomes a balance between creation through He^+/H_2 combination, which becomes more rapid at lower temperatures, and destruction through reactions with hydrocarbon molecules which are generally becoming more abundant with distance from the central star (Fig. 8.9).

The recombination rate of H_2^+ is very small (about 10^{-8} cm^3 s^{-1} at 15 K) and actually plays a negligible rôle in the chemistry of the molecule. The chemistry of the ion is fairly simple. Before the H/H_2 transition region charge transfer with atomic hydrogen destroys the molecule:

$$\mathrm{H}_2^+ + \mathrm{H} \rightarrow \mathrm{H}_2 + \mathrm{H}^+ \qquad (8.11)$$

with a rate coefficient of $k = 6.4 \times 10^{-10}$ cm^3 s^{-1} (Karpas *et al.* 1979).

After the transition region the H atom abstraction reaction with H_2 becomes dominant:

$$\mathrm{H}_2^+ + \mathrm{H}_2 \rightarrow \mathrm{H}_3^+ + \mathrm{H} \qquad (8.12)$$

where $k = 2.1 \times 10^{-9}$ cm^3 s^{-1} (Prasad and Huntress 1980).

Throughout the entire nebula production of H_2^+ is through cosmic ray ionisation of H_2 with a rate of $0.93\zeta_0$ s^{-1} where ζ_0 is the cosmic ray ionisation rate of atomic

hydrogen (Prasad and Huntress 1980). The value of ζ_0 is 4×10^{-17} s^{-1} in the model (§3.2.2.2) and thus the abundance of H_2^+ is predicted to mirror the abundance of H_2 where

$$\frac{n(H_2^+)}{n(H_2)} \approx 6 \times 10^{-11}$$

where hydrogen is practically all in atomic form ($\tau_V < 1.4$) and

$$\frac{n(H_2^+)}{n(H_2)} \approx 4 \times 10^{-11}$$

where H_2 is the dominant hydrogen-bearing species.

The chemistry of H_3^+ is linked to the chemistry of H_2^+ through equation (8.12). This reaction is the dominant creation mechanism for H_3^+ as well as the destruction route for H_2^+. The very low proton affinity of H_2 (4.34 eV) means that H_3^+ reacts readily with neutrals to produce H_2. However, the abundances of the neutral collision partners (C, O, N, S in particular) are not sufficient to compete with dissociative recombination of the molecule:

$$H_3^+ + e^- \rightarrow \begin{cases} H_2 + H \\ H + H + H \end{cases} \tag{8.13}$$

with a rate coefficient of $k = 2.6 \times 10^{-7}(T/300)^{-0.5}$ cm^3 s^{-1} and a branching ratio of 58% and 42% respectively.

Since the electron abundance is fairly constant throughout the nebula the expectation is that the abundance of H_3^+ should rise more steeply than H_2 and H_2^+ before the three species reach their maximum abundances as can be seen in Fig. 8.7.

Beyond the H/H_2 transition region, equating the rates of formation and destruction gives:

$$2.1 \times 10^{-9} n(H_2^+) n(H_2) = \frac{4.5 \times 10^{-6}}{\sqrt{T}} n(H_3^+) n(e^-) \tag{8.14}$$

In the H_2 dominated region of the nebula $n(H_2^+)/n(H_2) \approx 4 \times 10^{-11}$ (see above) and the electron density is practically constant with $n(e^-) \approx 0.5$ cm^{-3} (Fig. 8.7). In this regime we thus have

$$\frac{n(H_3^+)}{n(H_2)} \approx 4 \times 10^{-14} n(H_2) \sqrt{T} \tag{8.15}$$

Since practically all hydrogen is molecular and $T \approx 15$ K this yields

$$\frac{n(H_3^+)}{n(H_2)} \approx 7 \times 10^{-11}$$

Helium is a very inert species and the only way it is destroyed in the nebula is through cosmic ray ionisation; photoionisation does not occur as the ionisation potential of the atom (24.6 eV) lies above the Lyman limit of atomic hydrogen. Association of the atom with H^+ and H_2^+ to form HeH^+ exhibit utterly negligible rate coefficients. Radiative recombination of He^+ creates the neutral form at low optical depth and since this becomes more rapid with a decrease in temperature the abundance of He^+ falls initially. Beyond the H/H_2 transition region the ion-molecule reaction between He^+ and H_2 to create H^+, H and He becomes the main destruction route for He^+. At a temperature of 15 K this reaction has a rate coefficient of about 2.3×10^{-13} cm^3 s^{-1} (Böhringer and Arnold 1986). Helium has a cosmic ray ionisation rate of one half that of hydrogen (Prasad and Huntress 1980) so that at optical depths greater than ~ 1.4 we have

$$0.5\zeta_0 n(\mathrm{He}) \approx 2.3 \times 10^{-13} n(\mathrm{He^+}) n(\mathrm{H_2}) \tag{8.16}$$

where ζ_0 (s^{-1}) is the cosmic ray ionisation rate of atomic hydrogen (§3.2.2.2). Hence, since practically all the hydrogen is in molecular form

$$\frac{n(\mathrm{He^+})}{n(\mathrm{He})} \approx 2 \times 10^{-7}$$

at optical depths beyond the H/H_2 transition region (Fig. 8.7).
Hydrogen is entirely in neutral form throughout the molecular shell and C^+ is by far the most abundant ionised species through the process of photoionisation (see below). Thus the electron abundance mirrors the abundance of C^+ at every point in the nebula and $n(C^+) \approx n(e^-)$ for all optical depths.

Fig. 8.8 displays the predicted abundances of the carbon-bearing species. Atomic carbon has an ionisation potential of 11.3 eV ($\lambda = 1101$Å) and hence photoionisation plays the major rôle in the C/C^+ balance in the nebula. Ion-molecule and radiative association reactions between C^+ and hydrogen (atomic and molecular) occur with very small rate coefficients and in fact recombination of the ion is the dominant destruction route throughout the whole cloud.
Hofmann *et al.* (1983) made theoretical calculations of the photoionisation cross-section of carbon. Between the photoionisation limit ($\lambda = 1101$Å) and the Lyman limit of hydrogen ($\lambda = 912$Å) the cross-section is predicted to be practically constant with a value of $\sigma \approx 1.7 \times 10^{-17}$ cm^2.
Near the central star the intense ultraviolet field ensures that photoionisation of

carbon is extremely rapid, gas phase reactions being totally negligible. The photoionisation rate is given by (§3.2.1.1)

$$\zeta\,(\mathrm{s}^{-1}) = \frac{10^{-8}}{h}\int_{\lambda_{\mathrm{H}}}^{\lambda_0} \lambda\Phi(\lambda)\sigma_\lambda\, d\lambda \tag{8.17}$$

where the symbols have the same meaning as before.

A rough calculation enables the order of magnitude of the rate to be computed. In the wavelength range of interest the radiation spectrum is simply a section of the Planck spectrum from the star (with a black body temperature of $T_* = 10^5$ K) combined with a small number of emission lines from the ionised region. The CIII ($2s^2\,{}^1\mathrm{S} - 2p\,{}^1\mathrm{P^o}$) line at 977 Å is the principal contribution, but there are also contributions from CII (1037 Å), NII (1085 Å) and NIII (992 Å) (see Appendix D). Being at the tail-end of the 10^5 K Planck spectrum the energy density in this range is fairly constant and at $\lambda = 1000$Å has the value of $\Phi(\lambda = 1000\text{Å}) \approx 5\times10^{-13}$ erg cm^{-3} Å^{-1} (§2.1.1). Taking this as a constant value in equation (8.17) and using $\sigma_\lambda \approx 1.7\times10^{-17}$ cm^2 gives the photoionisation rate of carbon at the ionised/neutral interface as approximately

$$\zeta \approx 2.5\times10^{-6}\,\mathrm{s}^{-1} \tag{8.18}$$

Equating the rate of photoionisation of carbon to the rate of recombination of the ion gives

$$\zeta n(\mathrm{C}) = kn(\mathrm{C}^+)n(e^-) \tag{8.19}$$

where $k = 4.4\times10^{-12}(T/300)^{-0.61}$ (Prasad and Huntress 1980) is the rate of the C^+/e^- recombination.

Very near the ionised/neutral interface the gas temperature is about $T \approx 130K$ (Fig. 8.13) and the electron abundance is $n(e^-) \approx 0.8$ cm^{-3} (Fig. 8.7) so that

$$\frac{n(\mathrm{C})}{n(\mathrm{C}^+)} \approx 2\times10^{-6}$$

The UV field from the central star is so intense that, notwithstanding the large attenuation through H_2 line absorption and continuum absorption by dust grains, photoionisation of carbon remains the dominant destruction route of the atom throughout the entire cloud and the $\mathrm{C/C}^+$ balance is everywhere determined solely by photoionisation and recombination. At an optical depth of $\tau_V = 4$ for example the photoionisation rate is computed to be $\zeta = 1.1\times10^{-11}$ s^{-1} compared to to a C^+/e^- recombination rate of approximately 3.3×10^{-11} cm^3 s^{-1}. Thus the $\mathrm{C/C}^+$ ratio at this optical depth is predicted to be

$$\frac{n(\mathrm{C})}{n(\mathrm{C}^+)} \approx \frac{3.3\times10^{-11}\times0.3}{1.1\times10^{-11}} \approx 1$$

where $n(e^-) \approx 0.3$ cm^{-3} at $\tau_V = 4$. As can be seen in Fig. 8.7 this is the ratio predicted by the model.

The primary reason why photoionisation maintains a C^+/C ratio greater than unity throughout almost the whole cloud is in the way the optical properties of the dust are modelled. The dust is assumed to be amorphous carbon based rather than a crystalline form (e.g. graphite) and, by using optical properties of amorphous carbon reported in the literature (Williams and Arakawa 1972; Duley 1984), the absorption properties of such dust in the visible and ultraviolet may be computed (§7.2). These calculations show that there is comparable absorption in the UV region relative to the visible region (Table 7.2) as compared to graphitic dust models which predict much greater absorption in the UV region compared to the visible (e.g. Mathis *et al.* 1983). Thus in the case of amorphous carbon the values of τ_λ/τ_V (where V is the visible wavelength at 5550 Å) are much lower for UV wavelengths. Hence the ultraviolet photon field is not as heavily attenuated as in the graphite dust case with the consequence that photoionisation (and photodissociation) rates are kept at high values throughout the nebula. The effects of using a graphite dust model are presented and discussed in §8.3.

The photodissociation rate of the CO molecule remains very high (relative to the H_2 photodissociation rate) throughout the whole nebula (Fig. 8.14) and is the primary destruction route of the molecule even at large optical depths. There are basically two reasons for the large $\zeta(CO)/\zeta(H_2)$ ratio in the nebula: there is much more hydrogen in the nebula than carbon or oxygen and hence self-shielding in the UV absorption lines is much more effective in the case of H_2, and the fact that recent experiments on photodissociation of CO seem to predict a photodissociation probability of 100% for practically all ro-vibrational levels in excited electronic states (Eidelsberg *et al.* 1991). In other words if a CO molecule is optically pumped to an excited electronic state it will almost certainly subsequently dissociate (through the process of predissociation, §2.4.1) and this is reflected in the predicted photodissociation rate of CO which is for most of the time several orders of magnitude higher than the corresponding rate for H_2.

The chemistry of the carbon monoxide molecule is of course inextricably linked to the carbon and oxygen chemistries. Initially this is through the ion-molecule reaction:

$$C^+ + OH \rightarrow H^+ + CO \qquad (8.20)$$

where OH is produced by radiative association of hydrogen and oxygen.

In the outer half of the cloud neutral reactions, often of minor importance in the

nebular chemistry, actually play the vital rôle in the production of CO. Neutral carbon makes a minor contribution here:

$$C + OH \rightarrow CO + H \tag{8.21}$$

However, because C^+ remains the dominant form of carbon rather than the neutral atom (except near the edge of the nebula) and the abundance of the hydroxyl radical remains small this reaction is of secondary importance to reactions involving oxygen and carbon-bearing molecules:

$$O + CH \rightarrow CO + H \tag{8.22}$$

$$O + CN \rightarrow CO + N \tag{8.23}$$

$$O + C_2 \rightarrow CO + C \tag{8.24}$$

All these reactions exhibit rate coefficients of a few times 10^{-11} cm^3 s^{-1} with a $T^{1/2}$ temperature dependence.

For example, at the outer edge of the nebula the photodissociation rate of CO is computed to be about 10^{-12} s^{-1} (Fig. 8.14). Since the reaction between O and CN exhibits a small reaction barrier of 50 K (an estimated temperature dependence; le Bourlot, private communication) the dominant CO producing reactions at this distance are equations (8.22) and (8.24) which exhibit rates of approximately 10^{-11} cm^3 s^{-1} at the temperature of the gas. Thus equating the rates of formation and destruction of the molecule yields the ratio of CO to O at the outer edge of the cloud as:

$$\frac{n(CO)}{n(O)} \approx \frac{10^{-3} \times 10^{-11}}{10^{-12}} \approx 0.01$$

where $n(C_2) \approx 7 \times 10^{-4}$ and $n(CH) \approx 4 \times 10^{-4}$ cm^{-3} at $\tau_V = 4.5$.

As discussed previously (§2.1) the components of the radiation field incident on the neutral region are calculated without including the attenuating properties of dust grains in the ionised region. Dust is certainly a component of the ionised region as well as the neutral region although likely to be less abundant because of sputtering of the grains by the UV field in the ionised region (Barlow and Silk 1977). Using JCMT observations Hoare *et al.* (1992) estimate that the dust to gas mass ratio in the ionised zone of NGC 7027 is approximately half the ratio in the neutral zone. If this is a typical scenario then neglecting dust attenuation in the ionised shell will lead to a considerable overestimate of the radiation field incident on the neutral shell. The consequences of utilising a properly attenuated field are

obvious. Photoionisation and photodissociation rates would be much smaller leading to, for example, an increased $n(\mathrm{C})/n(\mathrm{C}^+)$ ratio through the nebula, a much earlier H/H_2 transition region and the probability of predicting far more CO. The effect of dust attenuation in the ionised region is looked at in more detail in §8.3 where the results of using an attenuated incident radiation field are shown and compared with PN observations.

With the model in its current form the results show that the assumed total column density of CO (chosen to match observations of NGC 2346) is insufficiently large to encompass the $\mathrm{C}^+/\mathrm{C}/\mathrm{CO}$ transition region. In a directly analogous fashion to the case of hydrogen eventually the absorption lines of CO would become saturated and, coupled with the fact photoionisation of carbon would eventually become ineffective, the carbon monoxide molecule would be predicted to become the dominant carbon-bearing species as models of interstellar clouds have demonstrated in the past (e.g. le Bourlot *et al.* 1993). Thus it would seem from these results that the molecular shell of NGC 2346, and other PNe if this represents a typical object, are too small to incorporate the full carbon transition to CO. This conclusion is reinforced when it is noted that the model does not take into account interstellar photodissociating radiation incident on the exterior of the nebula which would destroy CO and increase the abundance of C^+ near the exterior edge of the cloud, the effect becoming less important as the central star is approached. The effect of the ISRF would be to suppress the production of CO (as well as other molecules) at large distances from the star thus reducing further the probability of the full $\mathrm{C}^+/\mathrm{C}/\mathrm{CO}$ transition taking place in the molecular shell.

Diatomic carbon (C_2) is predicted by the model to be a very abundant molecule and hence important to the nebular chemistry; it plays a vital rôle in the production of CO in the outer half of the cloud (equation (8.24)). The steep increase in the abundance of C_2 below $\tau_V = 1.4$ arises through rapid dissociative recombination of $\mathrm{C}_2\mathrm{H}^+$:

$$\mathrm{C}_2\mathrm{H}^+ + e^- \rightarrow \mathrm{C}_2 + \mathrm{H} \tag{8.25}$$

balanced by photodissociation of the molecule.

$\mathrm{C}_2\mathrm{H}^+$ itself is created by $\mathrm{C}^+/\mathrm{CH}_2$ combination and so a necessary condition for the production of C_2 is that the hydrocarbon chemistry has to have been initiated. This occurs when H_2 becomes sufficiently abundant to drive the reaction producing CH_2^+ (see below) which can then subsequently react with H_2 to form large hydrocarbon molecules and recombine to create the neutral forms. Hence the abundance of C_2 continues to rise steeply until molecular hydrogen has reached

the maximum abundance (at about $\tau_V = 1.4$). From this point since the abundance of C_2H^+ slowly rises and dissociative recombination becomes more effective with decreasing gas temperature the abundance of C_2 continues to rise. Very far from the star reactions between C_2 and S^+, O and N become more important in removing the molecule as photodissociation becomes ineffective.

The predicted profile of the hydrocarbon abundances is shown in Fig. 8.9. The hydrocarbon chemistry cannot proceed until H_2 becomes sufficiently abundant to take part in the reaction scheme. However, the formation of CH^+ can occur slowly through radiative association:

$$C^+ + H \rightarrow CH^+ + h\nu \tag{8.26}$$

with a rate coefficient of 7×10^{-17} cm^3 s^{-1} (Viala 1986).
The formation of larger hydrocarbon molecules cannot proceed in the absence of H_2 since further reactions with atomic hydrogen produces ionised carbon and H_2:

$$CH^+ + H \rightarrow C^+ + H_2$$

Thus at small optical depths the methylidine ion is the only hydrocarbon species exhibiting a non-negligible number density. Very close to the star the ion is photodissociated but recombination rapidly becomes the destruction route of the ion:

$$CH^+ + e^- \rightarrow C + H \tag{8.27}$$

where $k = 2.9 \times 10^{-7}(T/300)^{-0.5}$ cm^3 s^{-1}.
Thus at small optical depths the abundance of the ion is controlled by the equation

$$\frac{5 \times 10^{-6}}{\sqrt{T}} n(CH^+)n(e^-) = 7 \times 10^{-17} n(C^+)n(H)$$

since $n(C^+) \approx n(e^-)$ this yields (with T=60 K)

$$\frac{n(CH^+)}{n(H)} \approx 10^{-10}$$

Once molecular hydrogen has formed in sufficient quantity the hydrocarbon chemistry proper may proceed. The vital step in the initiation of the chemistry is the radiative association reaction

$$C^+ + H_2 \rightarrow CH_2^+ + h\nu \tag{8.28}$$

rather than the binary reaction

$$C^+ + H_2 \rightarrow CH^+ + H \tag{8.29}$$

which is endothermic by 0.39 eV (representing a barrier of 4500 K). This reaction plays no part in the nebular chemistry although shock wave heating of the gas to drive reaction (8.29) has been suggested in the past to explain the large amounts of CH^+ observed in interstellar clouds (Flower 1989).

After the formation of CH_2^+ further reactions with H_2 produce larger hydrocarbon species:

$$CH_2^+ + H_2 \rightarrow CH_3^+ + H$$

$$CH_3^+ + H_2 \rightarrow CH_5^+ + h\nu$$

CH_4^+ is stepped over in the chain of reactions since the reaction

$$CH_3^+ + H_2 \rightarrow CH_4^+ + H$$

exhibits an activation barrier of over 30000 K and is entirely suppressed in the nebula. The molecule is formed through the reaction

$$CH_5^+ + H \rightarrow CH_4^+ + H_2$$

However, the barrier to this reaction (2200 K) coupled with the fact that atomic hydrogen is no longer abundant ensures that the abundances of CH_4^+ (and CH_5^+ which is formed by slow radiative association) are very small with consequently negligible column densities (Table 8.1).

The corresponding neutral hydrocarbon species are then formed through rapid dissociative recombination of the ions:

$$CH_2^+ + e^- \rightarrow CH + H$$

$$CH_3^+ + e^- \rightarrow \begin{cases} CH_2 + H \\ CH + H_2 \end{cases}$$

$$CH_4^+ + e^- \rightarrow \begin{cases} CH_2 + H_2 \\ CH_3 + H \end{cases}$$

$$CH_5^+ + e^- \rightarrow \begin{cases} CH + H_2 + H_2 \\ CH_2 + H_2 + H \\ CH_3 + H_2 \\ CH_4 + H \end{cases}$$

For example, mid-way through the neutral shell the CH_2^+ molecule is formed through equation (8.28) with a rate of about 7×10^{-16} cm^3 s^{-1} (at 15 K) balanced by recombination and combination with H_2 to form CH_3^+. These occur with rates of 2×10^{-6} (at 15 K) and 7×10^{-10} cm^3 s^{-1} respectively. Thus in static equilibrium the expectation is that

$$\frac{n(CH_2^+)}{n(C^+)} \approx \frac{7 \times 10^{-16} n(H_2)}{7 \times 10^{-10} n(H_2) + 2 \times 10^{-6} n(e^-)}$$

Practically all hydrogen is in molecular form at this optical depth and $n(e^-) \approx 0.6$ cm^{-3} (Fig. 8.7) so that

$$\frac{n(CH_2^+)}{n(C^+)} \approx 2 \times 10^{-7}$$

in the outer half of the cloud.

The synthesis of cyclopropenylidene (C_3H_2) is bound up with the chemistry of acetylene (C_2H_2) and occurs through the following chain of reactions:

$$C^+ + C_2H_2 \rightarrow C_3H^+ + H \tag{8.30}$$

$$C_3H^+ + H_2 \rightarrow C_3H_3^+ + h\nu \tag{8.31}$$

$$C_3H_3^+ + e^- \rightarrow \begin{cases} C_3H_2 + H \\ C_2H_2 + CH \end{cases} \tag{8.32}$$

Destruction of C_3H_2 and C_2H_2 initially proceeds through photodissociation and reaction (8.32) represents the primary formation route to both molecules so that the ratio of the abundances of these two molecules is simply determined by the ratio of their respective photodissociation rates.

At an optical depth of $\tau_V = 2.5$ the photodissociation rates of C_3H_2 and C_2H_2 are computed to be approximately 1.8×10^{-9} and 3×10^{-9} s^{-1} respectively and thus, at this distance from the central star

$$\frac{n(C_3H_2)}{n(C_2H_2)} \approx 1.7$$

as can be seen in Fig. 8.9.

According to the data of van Dishoeck (1988) the rate of decrease of the photodissociation rates of the two molecules are very similar functions of optical depth (in the regime of the mean interstellar radiation field) and thus the abundance ratio remains fairly constant. However, as the photodissociation rate of C_2H_2 drops reaction (8.30) eventually becomes a more rapid destruction route for the molecule

occurring at a constant rate of 2.2×10^{-9} cm^3 s^{-1} (Anicich and Huntress 1986). Thus the abundance ratio $n(C_3H_2)/n(C_2H_2)$ rises since the destruction of C_3H_2 still proceeds through photodissociation.

Fig. 8.10 displays the predicted abundances of the major nitrogen bearing species. Since the photoionisation potentials of N and CN are 14.6 eV and 14.5 eV respectively, photoionisation plays a negligible rôle in the nitrogen chemistry as opposed to the vital rôle it plays in the carbon chemistry. In fact it is predicted that neutral atomic nitrogen is by far the dominant species throughout the molecular shell with the $n(N^+)/n(N)$ ratio never exceeding 2×10^{-5}.
The cyanogen radical (CN) is the primary result of the coupling of the nitrogen and hydrocarbon chemistries. The fact that CN exists at small optical depths is due to the presence of CH^+, the only hydrocarbon species that exists in the absence of molecular hydrogen. The reaction

$$N + CH^+ \rightarrow CN + H^+ \tag{8.34}$$

efficiently produces CN while CH^+ is the most abundant hydrocarbon species (Fig. 8.9). As molecular hydrogen increases in abundance eventually reactions with neutral CH assume dominance at an optical depth of about $\tau_V = 1$. Since C_2 is also rapidly increasing in abundance in this region (Fig. 8.8) CN is produced by the two neutral exchange reactions

$$N + CH \rightarrow CN + H \tag{8.35}$$

$$N + C_2 \rightarrow CN + C \tag{8.36}$$

The N/C_2 reaction exhibits a $T^{1/2}$ temperature dependence, but with the temperatures characteristic of the nebula the rates of the two reactions are similar ($\sim 10^{-11}$ cm^3 s^{-1}).
Photodissociation of the molecule is the primary destruction route for the first half of the cloud and since the abundances of CH and C_2 are rising, n(CN) displays a rapid increase beyond $\tau_V \approx 1$. At about $\tau_V = 3.5$ the abundance of CN becomes sufficiently high to control the $n(N^+)/n(N)$ ratio. Up to this point cosmic ray ionisation and recombination had been the determining factors. Now however the rapid ion-molecule reaction

$$He^+ + CN \rightarrow N^+ + C + He \tag{8.37}$$

takes over the production of N^+. Thus the abundance of N^+, which had been falling due the increased efficacy of recombination at lower gas temperatures, starts to level off. CN also now provides the main destruction route for N^+, through charge exchange:

$$N^+ + CN \rightarrow CN^+ + N$$

although other reactions are important in removing N^+ (charge exchange with CO and C_2 and reactions with H_2).

Photodissociation of the CN molecule remains the most effective removal mechanism throughout the cloud but in the outer half of the nebula the ultraviolet field has become attenuated to the extent that cosmic ray dissociation also becomes an important destruction route. Gredel *et al.* (1989) theoretically predict a very large cosmic ray photodissociation efficiency for the molecule - $\zeta \approx 21200\zeta_0$ where ζ_0 is the cosmic ray induced photoionisation rate of atomic hydrogen (this assumes a mean dust grain albedo of $< A_\lambda >= 0.5$, see §7.2).

The rates of equations (8.35) and (8.36) are approximately 2×10^{-11} and 10^{-11} cm^3 s^{-1} respectively (at a temperature of T=15 K). Thus at the exterior edge of the cloud we have

$$(4.4 \times 10^{-12} + 21200\zeta_0)n(CN) = \Big(2n(CH) + n(C_2)\Big) \times 10^{-11} n(N)$$

where, using the data of van Dishoeck (1988), the photodissociation rate of CN is predicted to be $\zeta = 4.4 \times 10^{-12}$ s^{-1} at $\tau_V = 4.5$.

A value of 4×10^{-17} s^{-1} is assumed for ζ_0 in the model. Since $n(CH) \approx 3 \times 10^{-4}$ cm^{-3} and $n(C_2) \approx 6 \times 10^{-4}$ cm^{-3} in this region we have

$$\frac{n(CN)}{n(N)} \approx 0.002$$

near the exterior edge of the nebula.

Like the hydrocarbon chemistry, the production of NH, NH_2 and larger molecules proceeds efficiently through ion-molecule reactions involving H_2. The reaction between C^+ and H_2 to create CH^+ is endothermic by 0.4 eV (see above) and the hydrocarbon chemistry is initiated by slow radiative association to form CH_2^+. This is not so for the nitrogen reaction scheme and NH^+ is formed by

$$N^+ + H_2 \rightarrow NH^+ + H \qquad (8.38)$$

Subsequent reactions with molecular hydrogen can then form NH_2^+, NH_3^+ and NH_4^+. Rapid dissociative recombination forms the neutral counterparts. However,

the density of NH molecules is consistently low throughout the nebula and thus the abundance of ammonia (NH_3) is predicted to be almost negligible - the abundance ratio $n(NH_3)/n(N)$ nowhere exceeds 10^{-11}. Thronson and Bally (1986) made a search for emission lines of ammonia from the PN NGC 7027 with negative results.
Hydrogen cyanide (HCN) and hydrogen isocyanide (HNC) have both been observed in a number of planetary nebulae (e.g. Cox *et al.* 1992). The route to formation of HCN proceeds by production of the ionised form mainly through the reaction

$$CH_2^+ + N \rightarrow HCN^+ + H \tag{8.39}$$

which can take place efficiently after the hydrocarbon chemistry has been initiated (at $\tau_V \approx 0.5$). With the ionised molecule being present, HCN can then form through very rapid charge exchange involving atomic hydrogen:

$$HCN^+ + H \rightarrow HCN + H^+ \tag{8.40}$$

which exhibits a rate of about 10^{-8} cm^3 s^{-1} (based on the rate for the reverse charge transfer reaction, Anicich and Huntress 1986).
Reaction (8.40) is so rapid, especially below $\tau_V = 1.4$ where hydrogen is practically all atomic, that it is even faster than HCN^+/e^- recombination. Since nitrogen is primarily atomic and CH_2^+ is produced effectively in the hydrocarbon chemistry, reactions (8.39) and (8.40) provide an efficient scheme to produce HCN.
Photodissociation destroys the molecule below $\tau_V \approx 2.5$ but as the radiation field weakens reactions with C^+ take over to remove the molecule:

$$C^+ + HCN \rightarrow C_2N^+ + H \tag{8.41}$$

where $k = 3.4 \times 10^{-9}$ cm^3 s^{-1}.
As the abundance of H drops through the H/H_2 transition zone the neutral reaction

$$N + CH_2 \rightarrow HCN + H \tag{8.42}$$

becomes important in the production of HCN so that near the exterior edge of the cloud the abundance of the molecule is controlled by the equation

$$3.4 \times 10^{-9} n(C^+) n(HCN) = 4 \times 10^{-12} n(N) n(CH_2) + 10^{-8} n(HCN^+) n(H)$$

where $k = 4 \times 10^{-12}$ cm^3 s^{-1} is the rate of the temperature-dependent reaction (8.42) at $\tau_V = 4$ (Prasad and Huntress 1980). The abundance of HCN^+ at this point in the cloud is approximately 2×10^{-11} cm^{-3} so that

$$n(HCN) \approx 3 \times 10^{-8} \text{ cm}^{-3}$$

at $\tau_V = 4$, using the values of $n(\mathrm{H})$, $n(\mathrm{C}^+)$, $n(\mathrm{CH_2})$ and $n(\mathrm{N})$ from Figs. 8.7, 8.8 and 8.10.

The mechanisms that remove HCN are the same mechanisms that remove its isomeric partner HNC. However, production of this molecule is dominated by electronic recombination:

$$\mathrm{H_2CN^+ + e^- \rightarrow HNC + H} \tag{8.43}$$

There is also interconversion between the two forms primarily through collisions with thermal protons:

$$\mathrm{H^+ + HNC \rightleftharpoons H^+ + HCN} \tag{8.44}$$

However, the conversion HCN→HNC exhibits an energy barrier of 7850 K and is entirely suppressed in the nebula so that HCN is formed at the expense of HNC. Thus HCN is always more abundant than HNC with a correspondingly larger column density. Predicted column density ratios $N(\mathrm{HNC})/N(\mathrm{HCN})$ are in fact in very good agreement with observations of planetary nebulae (§8.2) giving credence to believing the reactions and chemical rates employed in the model regarding these species are relatively complete and correct. Conversely, predictions of $N(\mathrm{CN})/N(\mathrm{HCN})$ are orders of magnitude higher than observations; survival of HCN from the AGB phase of the central star to the PN phase may provide an explanation for this discrepancy (§8.2).

Fig. 8.11 shows the predicted abundances of the major oxygen bearing species. Neutral atomic oxygen is the most abundant species in the nebula due to the incapacity of the photon field to ionise the atom (the photoionisation threshold of oxygen is 910.5 Å which lies just below the Lyman limit cut-off at 911.7 Å). The production of the hydroxyl radical (OH) can proceed by rapid ion-molecule reactions. However, the abundances of the ions in question (primarily $\mathrm{SH^+}$ and $\mathrm{CH_2^+}$) are too low to compete with slow radiative association of oxygen and hydrogen

$$\mathrm{O + H \rightarrow OH} + h\nu \tag{8.45}$$

with a rate of 5×10^{-19} cm^3 s^{-1}.

Although the abundance of $\mathrm{CH_2^+}$ does increase significantly, following the general trend of hydrocarbon species as $\mathrm{H_2}$ becomes abundant (Fig. 8.9), this ion reacts with diatomic oxygen to form OH and $\mathrm{O_2}$ is not present in sufficient amounts to affect the OH chemistry. The radiative association reaction is the dominant production route throughout the nebula although at large optical depths dissociative

recombination of H_2O^+ becomes comparable. Below about $\tau_V = 2.5$ photodissociation of the molecule is the dominant removal mechanism and the photodissociation rate is computed to be approximately 1.5×10^{-6} s^{-1} at the ionised/neutral interface. Thus at this point in the cloud the predicted $n(\mathrm{OH})/n(\mathrm{O})$ ratio is

$$\frac{n(\mathrm{OH})}{n(\mathrm{O})} \approx \frac{5 \times 10^{-19} n(\mathrm{H})}{1.5 \times 10^{-6}}$$

since hydrogen is all in atomic form in this region we have

$$\frac{n(\mathrm{OH})}{n(\mathrm{O})} \approx 3 \times 10^{-10}$$

as can be seen in Fig. 8.11.

With increasing distance from the star the photodissociation rate of the molecule drops exponentially and thus the abundance rises. At $\tau_V = 1.4$ the abundance of atomic hydrogen falls as it undergoes the transition to molecular hydrogen (Fig. 8.7) and thus the density of OH, which is still being produced by O/H radiative association falls. Beyond this point photodissociation continues to be the destruction route for the molecule until, at $\tau_V \approx 2.5$, ion-molecule reactions with C^+ become more effective than photodissociation in removing the molecule:

$$\mathrm{C^+ + OH} \rightarrow \begin{cases} \mathrm{CO^+ + H} \\ \mathrm{H^+ + CO} \end{cases} \tag{8.46}$$

which proceeds at an approximately constant rate.

In the outer half of the nebula the abundance of ionised water is sufficiently high so that recombination of this ion provides a rate of production of OH comparable to O/H radiative association. Since recombination in general proceeds more rapidly at lower gas temperatures the abundance of the hydroxyl radical increases with optical depth.

The presence of OH is necessary for the production of diatomic oxygen through the neutral exchange reaction

$$\mathrm{O + OH} \rightarrow \mathrm{O_2 + H} \tag{8.47}$$

which exhibits a rate that increases with decreasing temperature (Smith 1988). Photoionisation and photodissociation are both effective in removing O_2 at small optical depths so that significant creation of the molecule is suppressed until the temperature is low enough for reaction (8.47) to proceed efficiently. As with the

OH molecule, photodissociation is the destruction route for O_2 until $\tau_V \approx 2.5$ when reactions with ionised carbon become more effective:

$$C^+ + O_2 \rightarrow \begin{cases} CO^+ + O \\ O^+ + CO \end{cases} \tag{8.48}$$

occurring with a Langevin rate of about 10^{-9} cm^3 s^{-1} and a branching ratio of 38% and 62% respectively.

Since the radical-radical reaction (8.47) has a rate that rises as the gas temperature falls the ratio $n(O_2)/n(OH)$ increases towards the exterior of the cloud. According to the experiments of Smith (1988) the rate of reaction (8.47) is adequately described by $k = 3.1 \times 10^{-11}(T/300)^{-0.36}$ cm^3 s^{-1}. Thus at the exterior edge of the cloud where $T \approx 10$ K we have

$$\frac{n(O_2)}{n(OH)} \approx \frac{10^{-10} n(O)}{10^{-9} n(C^+)}$$

Near the exterior edge of the cloud $n(O) \approx n(C^+)$ (Figs. 8.8 and 8.11) so that, in this region of the nebula

$$\frac{n(O_2)}{n(OH)} \approx 0.1$$

The formyl ion (HCO^+) belongs to that small group of molecules which have been positively identified within a number of planetary nebulae and have had column densities calculated (Cox *et al.* 1992; Bachiller *et al.* 1989). The model however predicts only a small amount of HCO^+ to be present in the molecular region; the column density ratio is predicted to be $N(HCO^+)/N(CO) \approx 10^{-6}$ whereas observations typically show a ratio of a few times 10^{-4} (Cox *et al.* 1992). It is interesting to note however that observations of evolved carbon stars that have not yet made it to the stage of planetary nebulae show much lower ratios. Johansson *et al.* (1984) derived an upper limit for the ratio $N(HCO^+)/N(CO)$ in IRC+10°216 to be 4×10^{-6}. The considerable discrepancy with PN observations has a possible explanation in that shock waves, not included in this model, would provide chemical conditions well suited to the production of this particular molecule (see discussion in §8.2).

After being primarily destroyed by photodissociation close to the central star, dissociative recombination of HCO^+ takes over at higher optical depths to return atomic hydrogen and CO to the gas. Carbon monoxide has a fairly low proton affinity (6.20 eV) and hence HCO^+ reacts readily with a number of neutral species to produce CO. These reactions generally tend to occur with a Langevin rate of a few times 10^{-9} cm^3 s^{-1}. However, the high electron abundance in the molecular

gas and the rapidity of the recombination reaction effectively relegates these ion-molecule reactions to secondary importance.
Carbon monoxide plays a rôle in the formation of HCO^+ through reactions with H_3^+ which, since H_2 has a lower proton affinity than CO, readily transfers a proton to the molecule:

$$H_3^+ + CO \rightarrow HCO^+ + H_2 \tag{8.49}$$

which is thought to be the main route to formation of HCO^+ in the interstellar medium. However, most H_3^+ is destroyed by dissociative recombination before reacting with CO and for this reaction to be important the ionisation rate of H_2 by cosmic ray particles (which can subsequently react with H_2 to form H_3^+) has to be very large, of the order of 10^{-13} s^{-1} (Cox *et al.* 1992). This is however incompatible with current theory and observations which predict a much smaller ionisation rate of the order of 10^{-17} s^{-1}.
The dominant reaction producing the molecule is predicted to be the chemi-ionisation reaction between CH and atomic oxygen:

$$CH + O \rightarrow HCO^+ + e^- \tag{8.50}$$

which exhibits a rate coefficient of approximately 6×10^{-12} cm^3 s^{-1} at 20 K and a temperature dependence of roughly $T^{0.44}$.
Thus the density of HCO^+ molecules reflects the rise in abundance of CH as hydrogen undergoes the transition to molecular form (at $\tau_V \approx 1.4$). Even though HCO^+/e^- recombination becomes more rapid at lower temperatures and reaction (8.50) becomes slower, the rise in the abundance of CH enables $n(HCO^+)$ to increase with optical depth. The resultant column density of HCO^+ is, however, lower than observations of PNe would tend to suggest and this discrepancy is discussed in §8.2.

The major sulphur and iron bearing species have their abundance profiles displayed in Fig. 8.12. Like carbon, neutral sulphur has an ionisation potential (10.4 eV) that makes it susceptible to photoionisation in the neutral region and, just as in the case of carbon, it is photoionisation and recombination that control the S/S^+ ratio throughout the cloud. Chapman and Henry (1972) theoretically calculated the photoionisation cross-section of the sulphur atom from the far ultraviolet to the threshold wavelength at $\lambda_0 = 1197$Å and deduced a fairly flat function of wavelength with $\sigma_\lambda \sim 6 \times 10^{-17}$ cm^2. The S^+/e^- recombination rate is described by $k = 3.9 \times 10^{-12}(T/300)^{-0.63}$ cm^3 s^{-1} (Prasad and Huntress 1980). Using the cross-section data of Chapman and Henry the model predicts a photoionisation

rate of 1.2×10^{-5} s^{-1} at the ionised/neutral interface. Thus, in this region where $T \approx 130$ K (Fig. 8.13) we have

$$1.2 \times 10^{-5} n(\mathrm{S}) = 6.6 \times 10^{-12} n(\mathrm{S}^+) n(e^-)$$

and hence, since $n(e^-) \approx n(\mathrm{C}^+) \approx 0.7$ cm^{-3}

$$\frac{n(\mathrm{S})}{n(\mathrm{S}^+)} \approx 4 \times 10^{-7}$$

With increasing distance from the star the photoionisation rate falls and eventually, at about $\tau_V = 3$, charge exchange with C^+ becomes the dominant removal mechanism for the neutral sulphur atom:

$$\mathrm{C}^+ + \mathrm{S} \rightarrow \mathrm{S}^+ + \mathrm{C} \tag{8.51}$$

occurring with a Langevin rate of about 10^{-9} cm^3 s^{-1} (Prasad and Huntress 1980). Since $n(\mathrm{C}^+) \approx n(e^-)$ in the nebula the S/S$^+$ ratio near the exterior edge of the cloud is simply given by the ratio of the rate of the recombination reaction to the rate of reaction (8.51):

$$\frac{n(\mathrm{S})}{n(\mathrm{S}^+)} \approx \frac{3 \times 10^{-11}}{1.5 \times 10^{-9}} \approx 0.02$$

Photodissociation plays the dominant rôle in the chemistry of the carbon monosulphide molecule (CS). This is the main destruction route of the molecule even at large optical depths but the formation of the molecule depends on dissociative recombination. The HCS^+ ion is formed primarily through the reaction

$$\mathrm{S}^+ + \mathrm{CH_2} \rightarrow \mathrm{HCS}^+ + \mathrm{H} \tag{8.52}$$

and once the hydrocarbon chemistry is initiated through $\mathrm{C}^+/\mathrm{H_2}$ reactions and $\mathrm{CH_2}$ becomes abundant this reaction can proceed efficiently since ionised sulphur is present in large numbers. Thus as the abundances of $\mathrm{CH_2}$ and HCS^+ increase the CS molecule starts to be produced by the rapid recombination reaction

$$\mathrm{HCS}^+ + e^- \rightarrow \mathrm{CS} + \mathrm{H} \tag{8.53}$$

Photodissociation is the destruction route of the molecule at all points in the nebula and thus, even past the H/$\mathrm{H_2}$ transition zone where the abundances of $\mathrm{CH_2}$

and hence HCS^+ level off, $n(CS)$ continues to rise rapidly. The reason for the continued steep rise in the abundance of CS is that recombination of HCS^+ becomes more efficient at lower temperatures while the photodissociation rate of the molecule continues to fall sharply with distance.

The reason why the radiation field remains intense enough so that photodissociation of the molecule dominates even at large optical depth is the same reason for the consistently high C^+/C ratio. The modelled dust grain opacity in the ultraviolet (applicable to amorphous carbon particles) is far less than the opacity that would be seen with crystalline carbon particles (see discussion above).

The model predicts that a large amount of CS would be formed in the molecular region - the column density ratio is predicted to be $N(CS)/N(CO) \approx 1.4 \times 10^{-2}$ (see Table 8.1). It would thus appear that CS would be a promising candidate in a search for emission lines from planetary nebulae. Thronson and Bally (1986) made such a search in the very well studied PN NGC 7027, with the expectation of readily detecting the molecule since carbon and sulphur are both sufficiently abundant in the nebula to warrant such a search (Shields 1978). The fact that the CS molecule was not readily detected was something of a surprise, the most likely reason being that the excitation conditions in the molecular region of NGC 7027 are unfavourable for molecular emission. This is unlike the case of the carbon star IRC+10°216 where CS emission is readily observed and the derived $N(CS)/N(CO)$ column density ratio has been derived to be approximately $3\text{-}6\times10^{-4}$ (Thronson and Bally 1986 and references therein). However, even this figure falls short of the predicted $N(CS)/N(CO)$ ratio by more than an order of magnitude. It is apparent from the results that, compared with molecular observations of PNe, the model is predicting far too much carbon being incorporated into the molecules CN, CS and, to a lesser extent, CO (relative to HCN). Possible reasons for this are discussed in §8.2.

The chemistry of iron is also dominated by photoionisation and recombination at small optical depths. Lombardi *et al.* (1978) experimentally measured the photoionisation cross-section of neutral iron at 1540 Å to be 5×10^{-18} cm^2. For the purposes of the model this value of σ_λ is assumed to be approximately valid for all wavelengths between λ_H and the threshold wavelength of iron at $\lambda_0 = 1575$Å. Thus the Fe/Fe^+ ratio displays the same trend as the S/S^+ ratio. The fact that the photoionisation cross-section of iron is about an order of magnitude smaller than that of sulphur and that the charge exchange reaction between iron and C^+:

$$C^+ + Fe \rightarrow Fe^+ + C \qquad (8.53)$$

displays a rate coefficient ($k = 2.6 \times 10^{-9}$ cm^3 s^{-1}) almost twice that of reaction (8.51) means that reaction (8.53) becomes the destruction route for iron (at $\tau_V \approx 1.4$) a long distance before the same transition occurs for sulphur (at $\tau_V \approx 3$, see above). At the exterior edge of the cloud Fe^+/e^- recombination is creating neutral iron and charge exchange with ionised carbon is destroying the atom so that the Fe/Fe^+ ratio at $\tau_V = 4$ is given by, since $n(C^+) \approx n(e^-)$:

$$\frac{n(\mathrm{Fe})}{n(\mathrm{Fe}^+)} \approx \frac{3 \times 10^{-11}}{2.6 \times 10^{-9}} \approx 0.01$$

where $k = 3 \times 10^{-11}$ cm^3 s^{-1} is the rate of the Fe^+/e^- recombination reaction at T=10 K (Prasad and Huntress 1980).

Figs. 8.15 and 8.16 show the heating and cooling rates in the nebula due to the various different thermal processes. Fig. 8.13 displays the temperature profile through the molecular cloud required to balance the heating and cooling rates.
As can be seen in Fig. 8.15 photoionisation of PAH molecules is the dominant heating process at optical depths less than about $\tau_V = 1.7$. The rate of heating due to the photoelectric effect on dust grains is consistently less than the PAH rate by a factor of two or three. This is except near the ionised/neutral interface where the grain heating effect is much lower and rises to a maximum at about $\tau_V = 0.3$. The physical reason for this peak in the heating rate is that close to the central star the grains are highly positively charged and the heating rate is thus suppressed. With increasing distance from the star the grains become more neutral and the heating rate increases. When the ratio of neutral grains to charged grains reaches a maximum the only factor remaining to affect the rate is the rapid decrease in the number of UV photons, primarily due to H_2 line absorption (as well as geometrical dilution of the radiation field). Thus from this point onwards the grain photoelectric heating rate decreases with distance from the star. About half way through the cloud the prediction of the model is that heating through exothermic chemical reactions and photoreactions becomes predominant. Formation of H_2 on dust grains makes a negligible contribution to the heating of the gas. The assumption made in the model is that on average one third of the H_2 formation energy (4.5 eV) transfers to kinetic energy of the ejected molecule (§5.3.4). It is clear from Fig. 8.15 that even if this assumed energy branching ratio were a gross underestimate the contribution from PAH and grain heating by photoionisation would still dominate.
Workers in the field of chemical and thermal modelling of interstellar clouds have often predicted that H_2 formation on grains is a major contribution to the rate

of gas heating (e.g. le Bourlot *et al.* 1993). However, the obvious difference here is that the UV radiation field is produced by a star in very close proximity to the cloud whereas work on interstellar clouds employ models of the much weaker general interstellar background radiation field. In the environment of a planetary nebula photoionisation would be expected to make the dominant contribution to gas heating as demonstrated by the results.

Fig. 8.16 displays the fact that the cooling of the gas is, as expected, dominated by collisionally induced fine structure transitions in C^+ (§6.1.4) until the point is reached where neutral carbon becomes sufficiently abundant (Fig. 8.8) that it assumes the rôle in the dominant cooling process. The energy splitting between the ground state and the fine structure states ($^3P_1$ and $^3P_2$) in neutral carbon (23 K and 62 K respectively) are smaller than the fine structure splitting in C^+ (92 K between the $^2P_{\frac{1}{2}}$ and $^2P_{\frac{3}{2}}$ states). In the low temperature outer half of the molecular shell neutral carbon becomes the predominant cooling agent even while C^+ is more abundant by about a factor of two (at $\tau_V \approx 3.2$).

Although fine structure transitions in oxygen play a minor rôle close to the star it rapidly becomes a negligible contribution. The energy splitting between the ground state ($^3P_2$) and the fine structure states ($^3P_1$, $^3P_0$) that lie above it are too high (228 K, 326 K respectively) for these states to becomes appreciably occupied (§6.1.6). The situation is slightly different for the case of a more dense gas ($n_H = 5000$ cm^{-3}). The higher gas density implies a higher number density of PAH molecules and dust grains which consequently raises the heating rate (Fig. 8.27). To achieve thermal balance a higher gas temperature is needed in order to collisionally populate the fine structure states sufficiently so that the required energy loss through spontaneous radiative decay is achieved. This higher temperature (over 300 K at the ionised/neutral interface) enables the fine structure states of oxygen to become appreciably occupied so that it makes an important contribution to the gas cooling (Fig. 8.28). However, as in the case of the lower density cloud model, the gas cools rapidly with distance from the star and thus cooling through transitions in oxygen becomes negligible even at small optical depths into the cloud.

Rotational transitions in H_2 and CO remain a negligible cooling process throughout the entire cloud. Close to the central star this is because the density of H_2 and CO molecules is extremely low (Figs. 8.7 and 8.8). However, even after hydrogen is primarily in molecular form ($\tau_V \geq 1.4$), the processes still make a negligible contribution. For the denser gas considered in this analysis rotationally exciting

collisions are more frequent and cooling by this process makes a minor contribution at large distances from the central star (Fig. 8.28). For the case of CO this is easily explained by considering the two controlling factors. Far from the star where the UV field is heavily attenuated the photodissociation rate of the molecule has fallen (Fig. 8.26) and the abundance consequently rises so there is more CO to take part in collisional cooling. Secondly, the further away from the star the molecule is the closer it is to the exterior edge of the nebula and the probability that the photon emitted in the rotational transition will escape from the nebula is consequently higher, thus producing an increased rate of cooling (§6.2.2).
The moment of inertia of the CO molecule is much higher than the H_2 molecule because of the much heavier constituent atoms. Consequently the energy splitting between the rotational states is much less in the case of carbon monoxide since it is inversely proportional to the moment of inertia I:

$$E_J = \frac{\hbar^2}{2I} J(J+1)$$

For CO the $J = 1$ ($v = 0$) level lies at just (the energy equivalent of) 5.5 K above the $J = 0$ ($v = 0$) level. For H_2 the energy splitting between the same states is 170.5 K. Thus in the low temperature regime far from the star collisionally induced rotational transitions in H_2 are infrequent and cooling by CO dominates even though molecular hydrogen is much more abundant (by a factor of about 10^5). This is exacerbated by the fact the hydrogen molecule has no permanent dipole moment and thus collisions must preserve the ortho/para character of the molecule. A molecule in the $J = 0$ state can only be excited to the $J = 2$ state (or higher) and this lies 509.9 K above the ground state. Reactions in which proton transfer takes place (e.g. with H^+ or H_3^+) are capable of inducing a $\Delta J = \pm 1$ transition in the molecule but these reaction partners are far less abundant than the major collision partners (H, H_2, He, CO).

Figs. 8.17 and 8.18 show the predicted distribution amongst the rotational levels of H_2 and CO. The general expected trend is displayed in the graphs. In the relatively high temperature, UV intense regime near the ionised/neutral interface collisions and optical pumping tend to cause significant populations of high lying rotational states, e.g. J=1, 3 and 5 for the H_2 molecule. Away from the star where the radiation field is no longer capable of optically pumping the molecule and the temperature is very low the higher levels tend to become depopulated and the $J = 0$ and $J = 1$ levels tend to dominate the distribution. It is worth looking in more detail at the distribution of the H_2 rotational levels with optical depth as

this is given a full analysis in the model.

At low optical depths ($\tau_V \leq 0.3$) self-shielding has not yet become effective for the molecule and the ortho-H_2 photodissociation rate is approximately the same as the para-H_2 photodissociation rate (Fig. 8.2 below). The abundances of H^+ and H_3^+ are negligible (Fig. 8.7) and hence ortho-/para-H_2 interconversion through collisions with these species is an unimportant process (§4.1.6). Since optical pumping preserves the ortho/para character of the molecule the ortho to para ratio in this regime is determined from the assumptions made about formation on dust grains. It is assumed that creation of the molecule produces an ortho/para ratio equal to the ratio of the statistical weights (§4.1.1) and hence in the unshielded environment near the ionised/neutral interface it is predicted that $n(H_2\text{-o})/n(H_2\text{-p}) \approx 3$ (Fig. 8.1 below).

At an optical depth of about $\tau_V = 0.4$ self-shielding starts to become effective and the H_2 photodissociation rate drops rapidly with distance (Fig. 8.14). However, ortho-H_2 ($J = 1$) is shielded before para-H_2 ($J = 0$) (Fig. 8.2) and since the variation is exponential the ortho photodissociation rate becomes much smaller than the para photodissociation rate. Thus there is a very large peak in the ortho/para ratio in the cloud extending over an optical depth of ~ 0.5 (Fig. 8.1).

Beyond an optical depth of $\tau_V \approx 1.4$ self-shielding has become very effective in the absorption lines and the photodissociation rate of H_2 has become extremely small and is no longer the dominant destruction mechanism of the molecule (Figs. 8.4 and 8.14). In this regime there are basically three processes that control the ortho/para ratio. Creation of the molecule is still dominated by formation on grain surfaces. Collisions with thermal protons are effective in interconverting the two species and destruction of the molecule is now dominated by gas phase chemistry involving abundant species.

The chemistry can be generalised to six reactions (with rates given to the right of each reaction):

$$\begin{aligned}
H + H + \text{grain} &\rightarrow H_2(p) + \text{grain} && k_g \\
H + H + \text{grain} &\rightarrow H_2(o) + \text{grain} && 3k_g \\
H_2(p) + H^+ &\rightarrow H_2(o) + H^+ && k_1 \\
H_2(o) + H^+ &\rightarrow H_2(p) + H^+ && k_2 \\
C^+ + H_2(p) &\rightarrow CH_2^+ + h\nu && k_3 \\
C^+ + H_2(o) &\rightarrow CH_2^+ + h\nu && k_3
\end{aligned}$$

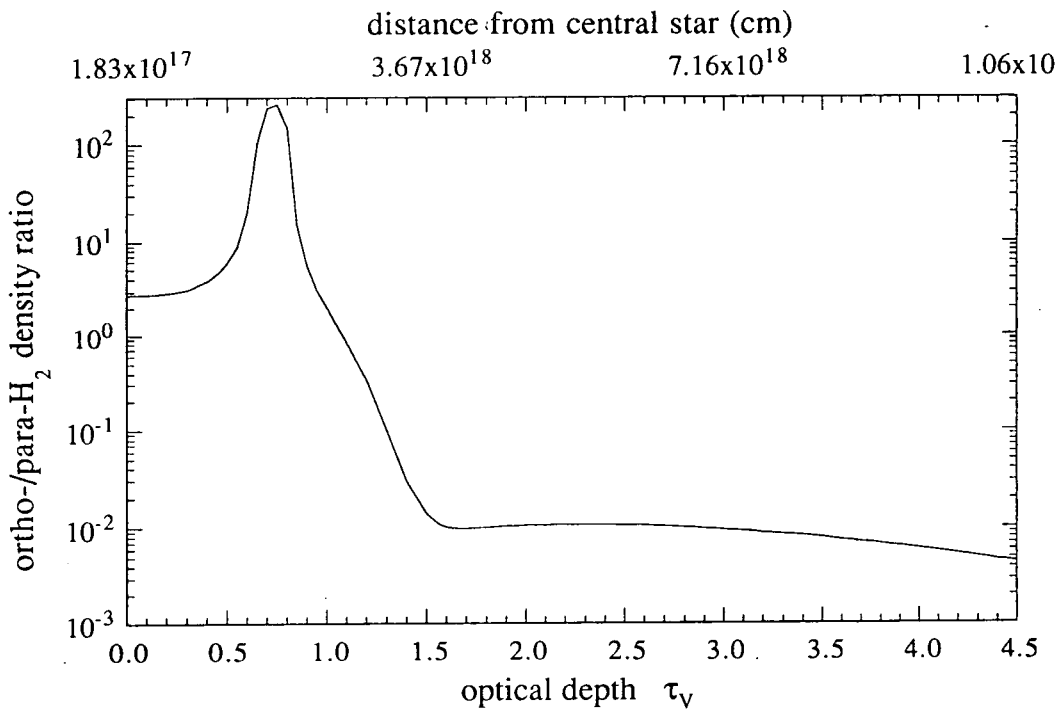

FIG. 8.1 - The ortho-/para-H_2 density ratio in the nebula as a function of optical depth and distance for a gas density of $n_{\rm H} = 1000$ cm^{-3}.

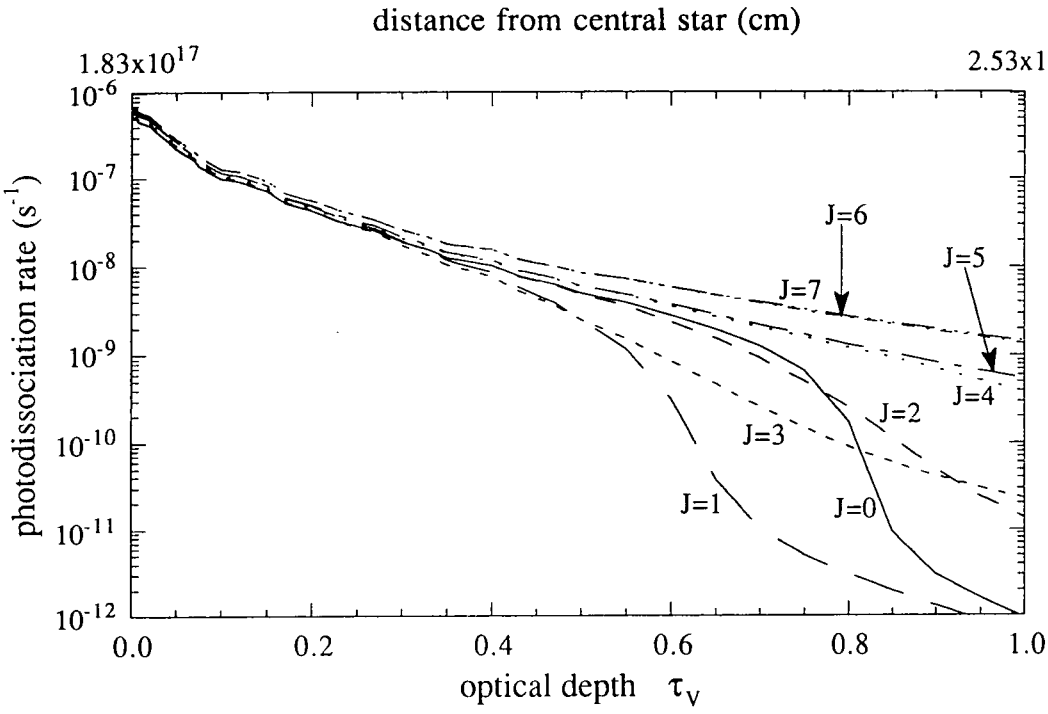

FIG. 8.2 - The photodissociation rate of the H_2 molecule in rotational levels $0 \leq J \leq 7$ $(v = 0)$ at optical depths $\tau_V \leq 1.0$ for a gas density of $n_{\rm H} = 1000$ cm^{-3}.

$k_1 \ll k_2$ for optical depths above $\tau_V \sim 1.5$ because the energy splitting between the $J = 0$ and $J = 1$ levels (170.5 K) must be overcome but the temperature characterising the Maxwellian distribution of molecular speeds is less than 20 K (Fig. 8.13). Thus the ratio k_1/k_2 is $9e^{-170.5/T} \approx 10^{-3}$ at 20 K and $\approx 10^{-7}$ at 10 K very near the exterior edge of the nebula. The ion-molecule reaction involving C^+ and H_2 is the dominant destruction route for the molecule at large optical depths where the rate coefficient is assumed to be the same for both ortho and para interactions and is given by the expression

$$k_3 = 1.25 \times 10^{-15} T^{-0.2} \quad \text{cm}^3\ \text{s}^{-1} \tag{8.54}$$

With the assumption of steady-state equilibrium the above expression yields, after some algebra, an ortho-/para-H_2 ratio of

$$\frac{n(\text{H}_2 - \text{o})}{n(\text{H}_2 - \text{p})} = \frac{3k_3 n(\text{C}^+) - 2k_1 n(\text{H}^+)}{k_3 n(\text{C}^+) + 4k_2 n(\text{H}^+)} \tag{8.55}$$

Beyond $\tau_V = 1.5$ the ratio $n(C^+)/n(H^+)$ is practically constant with a value of approximately 4×10^3 (Figs. 8.7 and 8.8). Thus

$$\frac{n(\text{H}_2 - \text{o})}{n(\text{H}_2 - \text{p})} \approx \frac{1.2 \times 10^4 k_3 - 2k_1}{4 \times 10^3 k_3 + 4k_2} \tag{8.56}$$

k_1 is negligible at the temperatures characterising the nebula at large optical depths ($T \approx 15$ K). Further, k_2 is much larger than k_3 and the whole expression simplifies to

$$\frac{n(\text{H}_2 - \text{o})}{n(\text{H}_2 - \text{p})} \approx 3 \times 10^3 \frac{k_3}{k_2} \tag{8.57}$$

At T=15 K $k_3 \approx 7 \times 10^{-16}$ cm^3 s^{-1} (equation 8.54) and $k_2 \approx 2 \times 10^{-10}$ cm^3 s^{-1} (see §4.1.6). Thus beyond $\tau_V \approx 1.5$ the predicted ortho/para ratio is

$$\frac{n(\text{H}_2 - \text{o})}{n(\text{H}_2 - \text{p})} \approx 10^{-2}$$

Fig. 8.1 displays the ortho-/para-H_2 ratio predicted by the model (for the case of $n_H = 1000$ cm^{-3}) through the entire nebula.

The reason for the fall in the $n(H_2 - o)/n(H_2 - p)$ ratio below the predicted value of 0.01 at large optical depths is because taking $n(C^+)/n(H^+)$ as constant in the above analysis is an approximation. In fact, as can be seen in Figs. 8.7 and 8.8, the abundance of C^+ falls and the abundance of H^+ increases slightly above $\tau_V \approx 2.5$

so that the ortho-/para-H_2 ratio subsequently decreases below the value derived above.

Figs. 8.3 to 8.6 show the computed effect of dust continuum absorption and UV line absorption by H_2, H and CO on the modelled ultraviolet spectrum. Fig. 8.3 displays the complete UV spectrum (900 Å to 1300 Å) at an optical depth of $\tau_V = 0.5$ into the molecular shell. At this point in the nebula the H/H_2 transition region has not been reached and the absorption lines of H_2 and CO have had little attenuating effect on the radiation field. Atomic hydrogen is the predominant absorbing species in the Lyman series of lines. The Lyα line (a) at 1215.7 Å is the most obvious feature of the spectrum and the Voigt profile of the line can be seen clearly, the line broadening occurring through a combination of random thermal motion and natural broadening (§2.3.4). Other lines in the series can be identified - Lyβ (b) at 1025.7 Å, Lyγ (c) at 972.5 Å, Lyδ (d) at 949.7 Å and Lyϵ (e) at 937.8 Å. Although the absorption lines of H dominate the spectrum at this optical depth other lines can be seen, e.g. H_2 X$(v = 0, J = 1) \rightarrow$ C$(v' = 0, J' = 1)$ (f) at 1009.8 Å. This line is already fairly prominent because most of the molecular hydrogen is in the $J = 1$ rotational state at small optical depth (Fig. 8.17) and thus optical pumping from this level is more frequent than from lesser populated levels.
Emission lines, arising from recombination of electrons and highly ionised atoms in the ionised region of the planetary nebula, can also be identified in the spectrum. The most obvious case is the CIII ($2s^2\,{}^1S - 2p\,{}^1P^o$) line (g) at 977 Å. Models of the ionised region of a PN predict this line to exhibit one of the largest intensities of all the emission lines in the far ultraviolet (Stasińska, private communication). Because this CIII emission line happens not to fall near an absorption line of H_2 it actually remains very prominent even at much larger optical depths (Fig. 8.4). Other prominent emission lines identifiable in the spectrum include a NIII line (h) at 992 Å and a NV line (i) at 1240 Å.
Because the underlying continuum represents the tail-end of a 10^5 K Planck spectrum from the central star it is a very flat function of wavelength, only decreasing slowly at lower frequencies. Beyond the Lyα absorption line the energy density of the spectrum increases because of the contribution of the hydrogen two-photon continuum which exists for wavelengths $\lambda > 1215.7$Å (§2.1.2).
Fig. 8.4 shows the same wavelength range of the spectrum at an optical depth of $\tau_V = 2.0$. This is well past the H/H_2 transition region at $\tau_V \approx 1.4$ (Fig. 8.7) and the effects of H_2 line absorption are obvious, most of the lines being completely saturated.

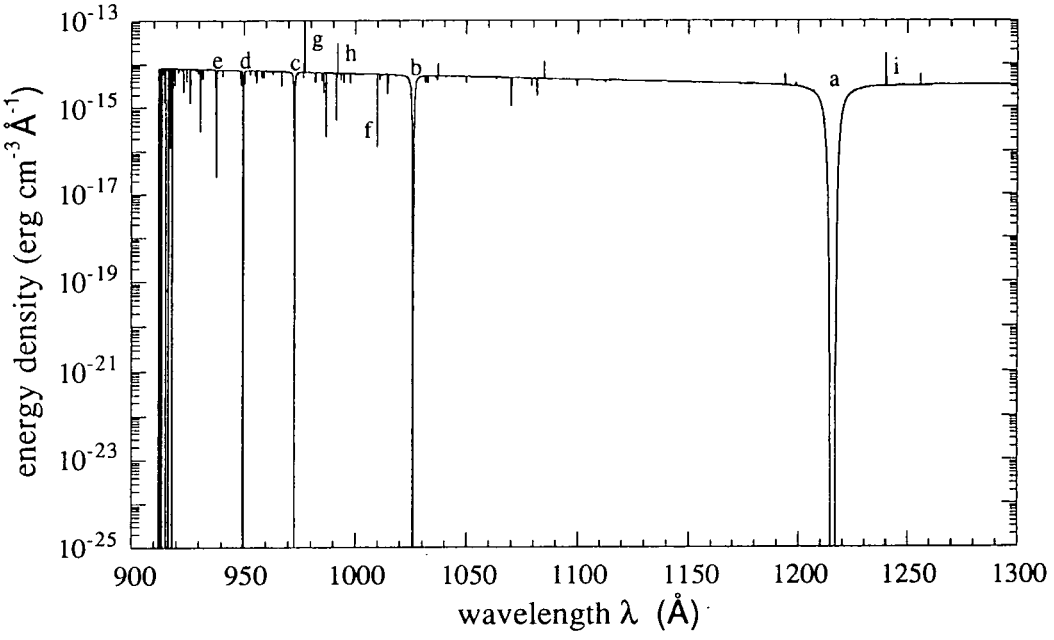

FIG. 8.3 - The UV spectrum of radiation (900 Å to 1300 Å) at an optical depth of $\tau_V = 0.5$ into a nebula with a gas density of $n_{\rm H} = 1000$ cm^{-3}.

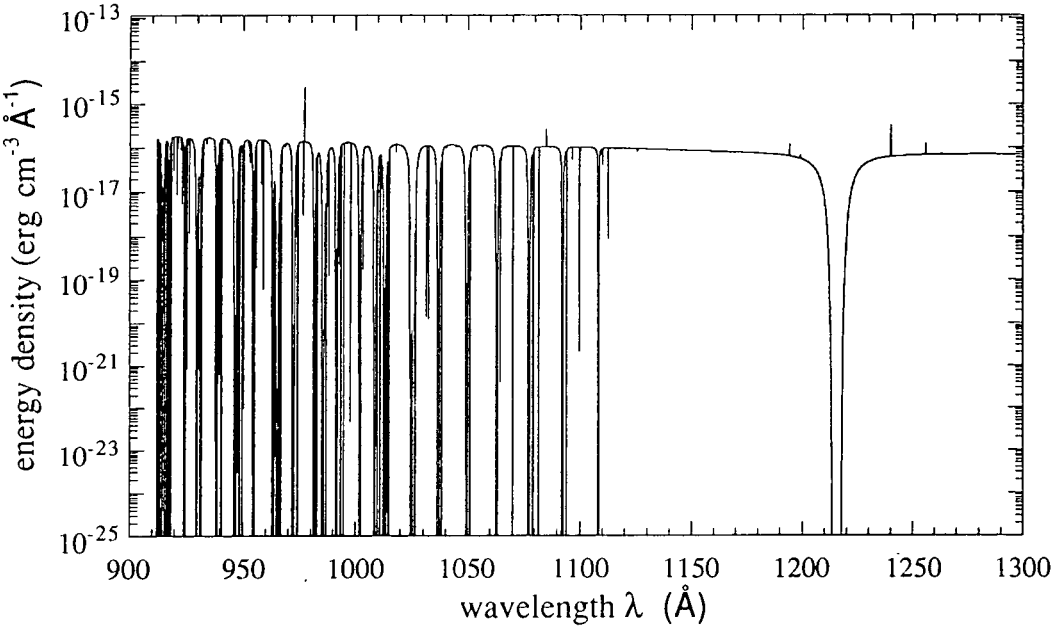

FIG. 8.4 - The UV spectrum of radiation (900 Å to 1300 Å) at an optical depth of $\tau_V = 2.0$ into a nebula with a gas density of $n_{\rm H} = 1000$ cm^{-3}.

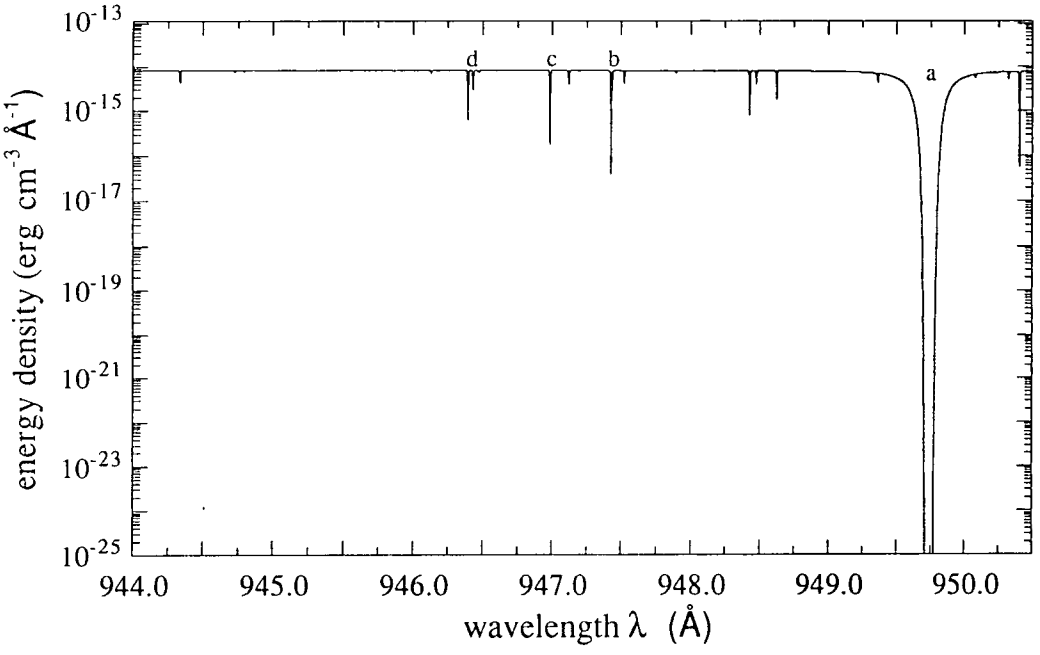

FIG. 8.5 - Section of the UV spectrum (944.0 Å to 950.5 Å) at an optical depth of $\tau_V = 0.5$ into a nebula with a gas density of $n_{\rm H} = 1000$ cm^{-3}.

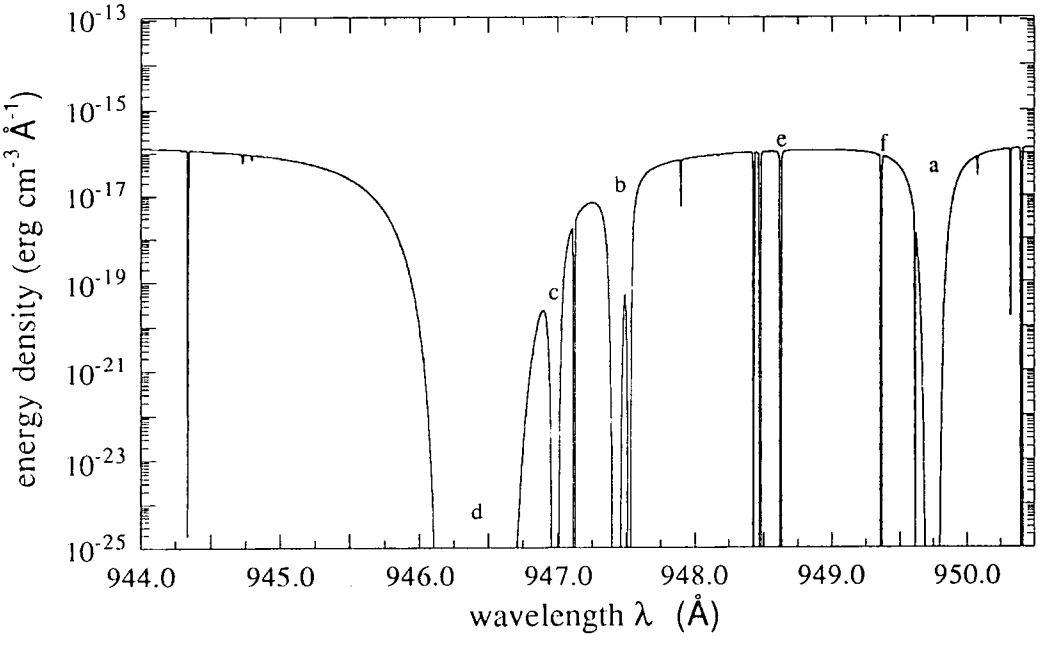

FIG. 8.6 - Section of the UV spectrum (944.0 Å to 950.5 Å) at an optical depth of $\tau_V = 2.0$ into a nebula with a gas density of $n_{\rm H} = 1000$ cm^{-3}.

Continuum absorption by dust grains has attenuated the energy density in the spectrum by about two orders of magnitude from Fig. 8.3. The attenuation by dust is fairly constant over the whole spectrum and is an artifact of the assumed composition and optical properties of the grains. Modelling the grains as amorphous carbon particles produces a very flat $E(\lambda, V)$ curve (§7.2) where $E(\lambda, V)$=A_λ-A_V. This may be compared to interstellar dust properties based on observations of starlight which indicate a steeply increasing $E(\lambda, V)$ function in the ultraviolet and a peak in the selective extinction at about 2200 Å (Spitzer 1978). This evidence strongly suggests that grains in the interstellar medium are graphite based as calculations using Mie theory with the properties of graphite provide an increasing $E(\lambda, V)$ curve in the UV and the peak at 2200 Å. However, the shape and position of the peak is highly sensitive to the assumed grain size and shape which is difficult to reconcile with the observed constancy of the UV peak in most observed stars. There exist other possible candidates to explain the 2200 Å bump as well; certain silicates or irradiated quartz can be made to reproduce this section of the selective extinction curve (Savage 1975).

Thus modelling the dust as amorphous carbon produces far less extinction in the ultraviolet than would a graphite particle model. The effects of this - a large C^+/C (and S^+/S) ratio throughout the entire nebula, an H/H_2 transition region occurring at a higher optical depth and so forth, have previously been discussed in this Chapter. It is obviously of great interest to compare the results obtained from the model with results obtained if 'standard' interstellar graphite particles are assumed and this comparison is performed in §8.3.

Figs. 8.5 and 8.6 show a small section of the radiation spectrum (944.0 Å to 950.5 Å) at the same two values of optical depth to show in more detail line broadening and the effect of line overlap. In Fig. 8.5, at an optical depth of $\tau_V = 0.5$, the H Lyδ line (a) at 949.74 Å is obvious whereas all the other absorption features belong to H_2. At this optical depth into the cloud practically all the molecular hydrogen is in the $J = 1$ or $J = 3$ rotational state (Fig. 8.17) and hence identifiable H_2 absorption lines in Fig. 8.5 primarily arise from optical pumping from these levels, the H_2 population in levels $J > 3$ being negligible in comparison. The H_2 $X(v = 0, J = 1) \rightarrow C(v' = 3, J' = 1)$ line (b) at 947.43 Å is fairly prominent already, as is the H_2 $X(v = 0, J = 1) \rightarrow B(v' = 14, J' = 2)$ line (c) at 946.98 Å and the H_2 $X(v = 0, J = 1) \rightarrow C(v' = 3, J' = 2)$ line (d) at 946.39 Å. A weaker line is visible at a slightly higher wavelength to this last feature representing absorption from the $v = 0, J = 0$ state via the transition H_2 $X(v = 0, J = 0) \rightarrow C(v' = 3, J' = 1)$.

Fig. 8.6 shows the same section of the spectrum at an optical depth of $\tau_V = 2.0$; line

broadening and the effects of line overlap are obvious. The features (b), (c) and (d) described above are clearly seen as broadened and now saturated lines. At this optical depth into the nebula almost all the molecular hydrogen is in the $v = 0, J = 0$ state and the H_2 $X(v = 0, J = 0) \rightarrow C(v' = 3, J' = 1)$ line (d) at 946.43 Å is extremely strong and has blended completely with the H_2 $X(v = 0, J = 1) \rightarrow C(v' = 3, J' = 2)$ line at 946.39 Å.

Weak features are identifiable from levels with $J = 2$. The H_2 $X(v = 0, J = 2) \rightarrow C(v' = 3, J' = 2)$ line (e) at 948.62 Å can be seen as well as, for example, the H_2 $X(v = 0, J = 2) \rightarrow B(v' = 14, J' = 1)$ line (f) at 949.36 Å. However, at optical depths $\tau_V > 0.5$ there is very little H_2 in the $J = 2$ level (Fig. 8.17) and these features fail to become significantly broadened.

Table 8.1

Total column densities of chemical species through the nebula

Species X	Column density $N(\mathrm{X})/N_{\mathrm{H}}$	
	$n_{\mathrm{H}} = 1000\ \mathrm{cm}^{-3}$	$n_{\mathrm{H}} = 5000\ \mathrm{cm}^{-3}$
H	0.3310	0.3594
He	0.1000	0.1000
C	1.200(-4)	9.551(-5)
O	3.997(-4)	3.998(-4)
N	2.000(-4)	2.000(-4)
S	7.848(-8)	5.905(-8)
Fe	2.167(-9)	1.727(-9)
e^-	5.904(-4)	6.149(-4)
H_2	0.3345	0.3203
CH	1.121(-7)	9.438(-8)
C_2	1.301(-7)	1.018(-7)
CO	3.614(-7)	2.951(-7)
CN	5.151(-8)	5.107(-8)
CS	4.975(-9)	3.108(-9)
OH	3.096(-11)	1.131(-11)
O_2	2.062(-12)	3.990(-13)
NH	7.926(-12)	1.439(-12)
NO	9.760(-15)	3.374(-15)
N_2	3.048(-12)	7.518(-13)
SH	1.839(-17)	4.810(-18)
SO	1.136(-18)	1.768(-19)
H_2O	2.361(-13)	5.170(-14)
H_2S	1.172(-20)	2.762(-21)
HCO	5.439(-19)	6.165(-19)
HCN	1.061(-11)	8.930(-12)

Species X	Column density $N(\mathrm{X})/N_{\mathrm{H}}$	
	$n_{\mathrm{H}} = 1000\ \mathrm{cm}^{-3}$	$n_{\mathrm{H}} = 5000\ \mathrm{cm}^{-3}$
HNC	1.553(-12)	1.348(-12)
CH_2	1.258(-8)	1.101(-8)
C_2H	3.343(-9)	2.792(-9)
C_3	1.929(-12)	2.121(-14)
CO_2	2.643(-20)	7.378(-21)
OCS	7.113(-14)	9.392(-15)
NH_2	7.930(-13)	1.439(-13)
SO_2	4.176(-23)	3.055(-24)
CH_3	1.208(-11)	9.514(-12)
C_2H_2	4.869(-13)	3.016(-13)
C_3H	2.705(-12)	1.502(-12)
NH_3	2.761(-16)	5.106(-17)
CH_4	1.493(-14)	1.314(-14)
C_3H_2	2.073(-12)	1.101(-12)
H^+	9.092(-7)	7.225(-7)
H^-	5.729(-12)	1.469(-11)
He^+	5.125(-8)	1.504(-8)
C^+	5.792(-4)	6.039(-4)
O^+	2.472(-11)	1.039(-10)
N^+	1.226(-9)	3.666(-10)
S^+	9.917(-6)	9.938(-6)
Fe^+	2.978(-7)	2.983(-7)
H_2^+	1.206(-11)	2.311(-12)
HeH^+	1.988(-16)	2.489(-16)
CH^+	3.945(-11)	4.592(-11)
C_2^+	1.702(-11)	1.558(-11)
CO^+	1.540(-14)	9.222(-15)

Species X	Column density $N(\mathrm{X})/N_{\mathrm{H}}$	
	$n_{\mathrm{H}} = 1000$ cm^{-3}	$n_{\mathrm{H}} = 5000$ cm^{-3}
CN^+	6.419(-15)	4.558(-15)
CS^+	2.839(-12)	2.359(-12)
OH^+	1.071(-13)	8.216(-14)
O_2^+	8.825(-17)	1.066(-16)
NH^+	6.894(-15)	1.622(-15)
NO^+	1.804(-16)	6.758(-17)
N_2^+	2.431(-18)	6.433(-19)
SH^+	1.999(-17)	5.361(-18)
SO^+	4.509(-16)	1.732(-16)
H_3^+	2.012(-11)	4.056(-12)
H_2O^+	2.100(-14)	4.659(-15)
H_2S^+	3.179(-24)	8.813(-25)
HCO^+	2.945(-13)	3.073(-13)
HCN^+	1.272(-14)	1.281(-14)
HCS^+	4.959(-13)	4.397(-13)
HNO^+	1.041(-18)	2.356(-19)
HSO^+	2.904(-21)	4.878(-22)
CH_2^+	9.443(-11)	9.580(-11)
C_2H^+	7.246(-12)	6.927(-12)
C_3^+	1.747(-12)	1.665(-12)
C_2N^+	2.974(-14)	2.915(-14)
NH_2^+	1.026(-14)	2.156(-15)
N_2H^+	7.275(-19)	1.802(-19)
H_3O^+	1.957(-15)	4.302(-16)
H_3S^+	1.263(-23)	3.527(-24)
H_2CN^+	8.204(-15)	8.747(-15)
H_2NC^+	1.164(-19)	2.535(-20)

Species X	Column density $N(\mathrm{X})/N_{\mathrm{H}}$	
	$n_{\mathrm{H}} = 1000\ \mathrm{cm}^{-3}$	$n_{\mathrm{H}} = 5000\ \mathrm{cm}^{-3}$
HCO_2^+	2.441(-23)	8.066(-24)
$HOCS^+$	9.329(-24)	2.910(-25)
CH_3^+	2.987(-11)	3.203(-11)
$C_2H_2^+$	5.689(-12)	5.828(-12)
C_3H^+	2.902(-13)	2.978(-13)
NH_3^+	7.829(-16)	1.737(-16)
CH_4^+	1.418(-19)	1.960(-19)
$C_2H_3^+$	1.292(-17)	1.324(-17)
$C_3H_2^+$	1.279(-17)	7.975(-18)
NH_4^+	2.462(-19)	5.776(-20)
CH_5^+	2.048(-16)	2.214(-16)
$C_3H_3^+$	1.968(-15)	1.576(-15)
Para-H_2	0.3307	0.3052
Ortho-H_2	3.818(-3)	1.511(-2)
H_2 ($J = 0$)	0.3307	0.3052
H_2 ($J = 1$)	3.817(-3)	1.511(-2)
H_2 ($J = 2$)	3.806(-6)	3.995(-6)
H_2 ($J = 3$)	8.543(-7)	1.736(-6)
H_2 ($J = 4$)	9.497(-8)	1.628(-7)
H_2 ($J = 5$)	3.336(-8)	8.866(-8)
H_2 ($J = 6$)	4.344(-9)	9.753(-9)
H_2 ($J = 7$)	1.627(-9)	4.998(-9)
H_2 ($J = 8$)	1.817(-10)	6.271(-10)
H_2 ($J = 9$)	6.381(-11)	2.788(-10)
H_2 ($J = 10$)	5.037(-12)	2.682(-11)
CO ($J = 0$)	2.155(-7)	8.261(-8)
CO ($J = 1$)	1.345(-7)	1.593(-7)

Species X	Column density $N(\mathrm{X})/N_{\mathrm{H}}$	
	$n_{\mathrm{H}} = 1000$ cm^{-3}	$n_{\mathrm{H}} = 5000$ cm^{-3}
CO ($J = 2$)	1.095(-8)	4.716(-8)
CO ($J = 3$)	3.956(-10)	5.757(-9)
CO ($J = 4$)	5.035(-12)	2.930(-10)
CO ($J = 5$)	1.412(-13)	8.546(-12)
CO ($J = 6$)	5.332(-14)	3.912(-13)
CO ($J = 7$)	2.981(-14)	1.542(-13)
CO ($J = 8$)	1.763(-14)	9.100(-14)
CO ($J = 9$)	1.077(-14)	5.579(-14)
CO ($J = 10$)	6.703(-15)	3.476(-14)

Note: a (b) implies a$\times 10^{\mathrm{b}}$

The column densities in Table 8.1 are shown relative to the total hydrogen nuclei column density N_{H}. The edge of the nebula is assumed to have been reached when the column density of CO attains the value $N(\mathrm{CO}) = 3.8 \times 10^{15}$ cm^{-2} and this means in general that, for different values of hydrogen nuclei number density n_{H}, the modelled nebulae will exhibit different optical depths, linear depths and total hydrogen nuclei column densities as described below.

$n_{\mathrm{H}} = 1000$ cm^{-3}

Distance from star of inner edge of neutral shell:	1.835×10^{17} cm
Distance from star of outer edge of neutral shell:	1.065×10^{19} cm
Total visual extinction of neutral shell:	$A_V = 4.83$ mag
Total column density of hydrogen nuclei:	1.046×10^{22} cm^{-2}

$n_{\mathrm{H}} = 5000$ cm^{-3}

Distance from star of inner edge of neutral shell:	1.835×10^{17} cm
Distance from star of outer edge of neutral shell:	2.752×10^{18} cm
Total visual extinction of neutral shell:	$A_V = 5.92$ mag
Total column density of hydrogen nuclei:	1.284×10^{22} cm^{-2}

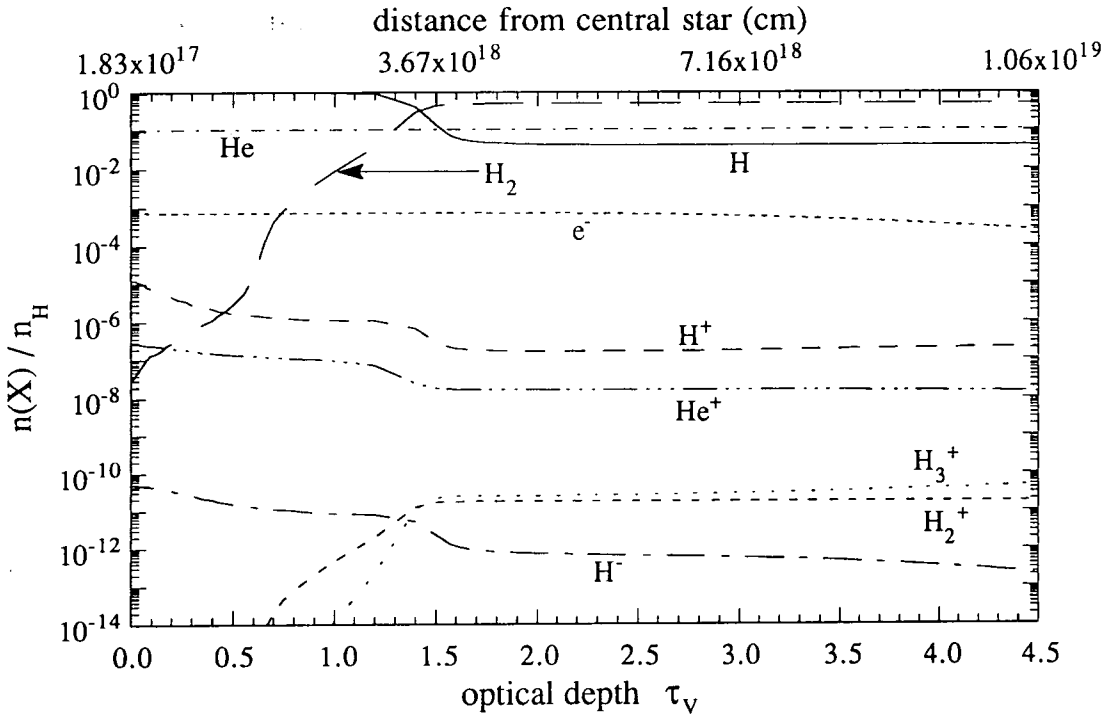

FIG. 8.7 - The abundances of the hydrogen/helium bearing species (and the electron abundance) through the nebula for a gas density of $n_{\rm H} = 1000$ cm^{-3}.

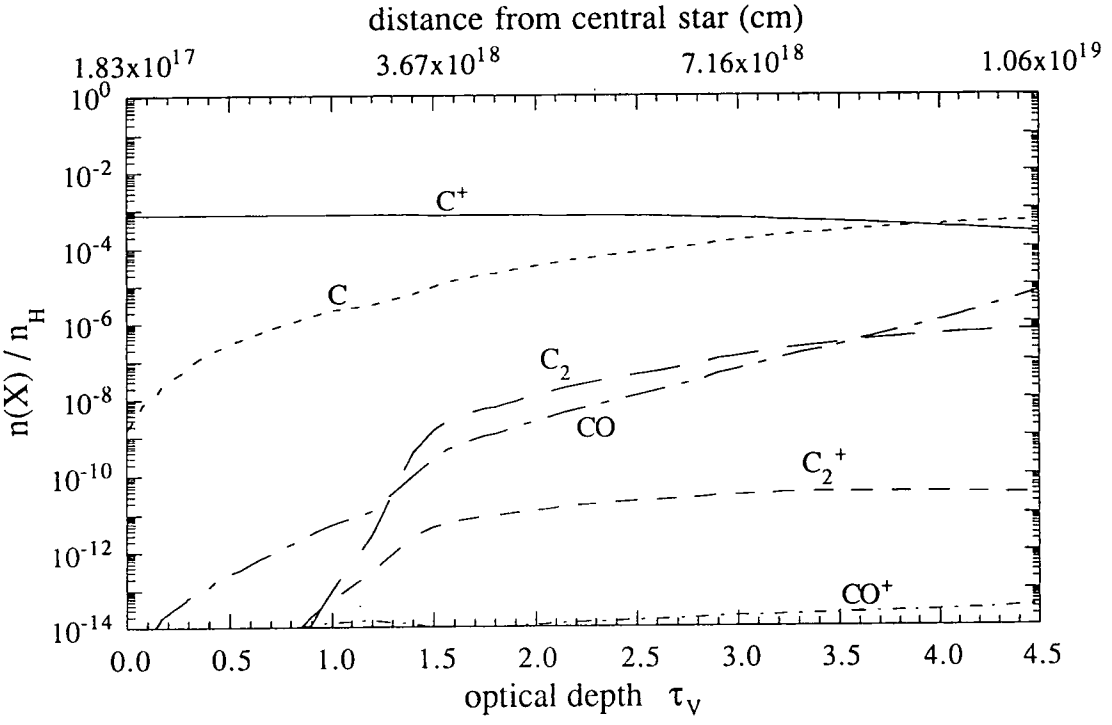

FIG. 8.8 - The abundances of the carbon bearing species through the nebula for a gas density of $n_{\rm H} = 1000$ cm^{-3}.

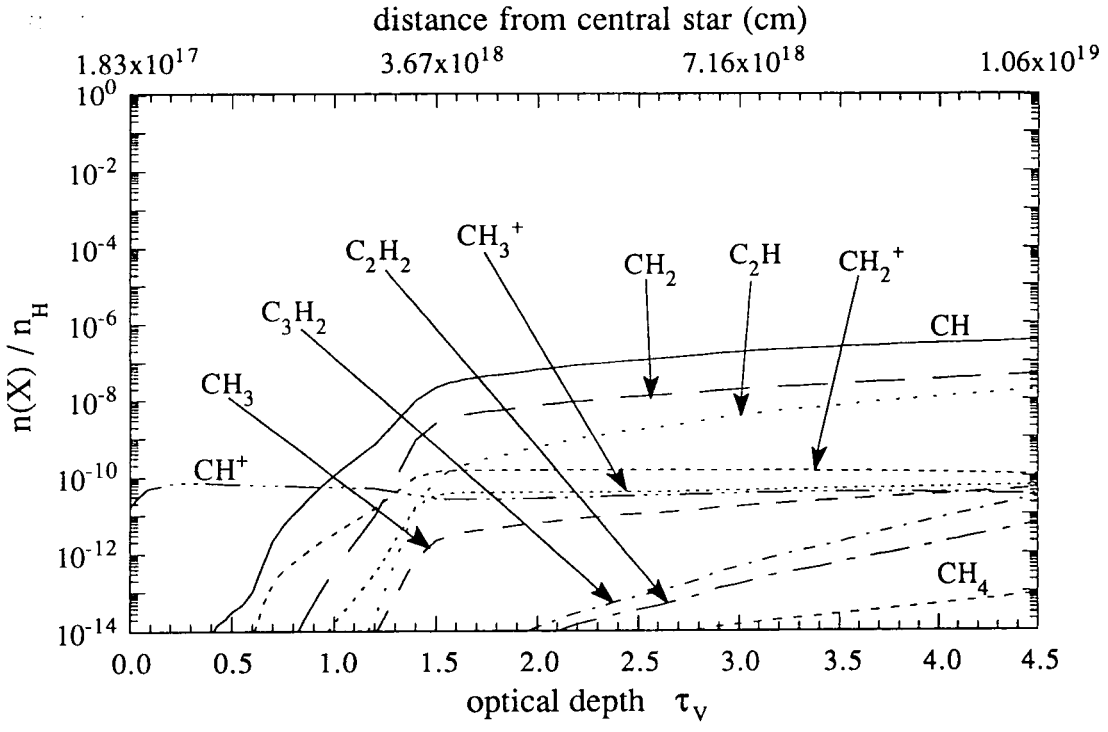

FIG. 8.9 - The abundances of the hydrocarbon species through the nebula for a gas density of $n_{\rm H} = 1000$ cm^{-3}.

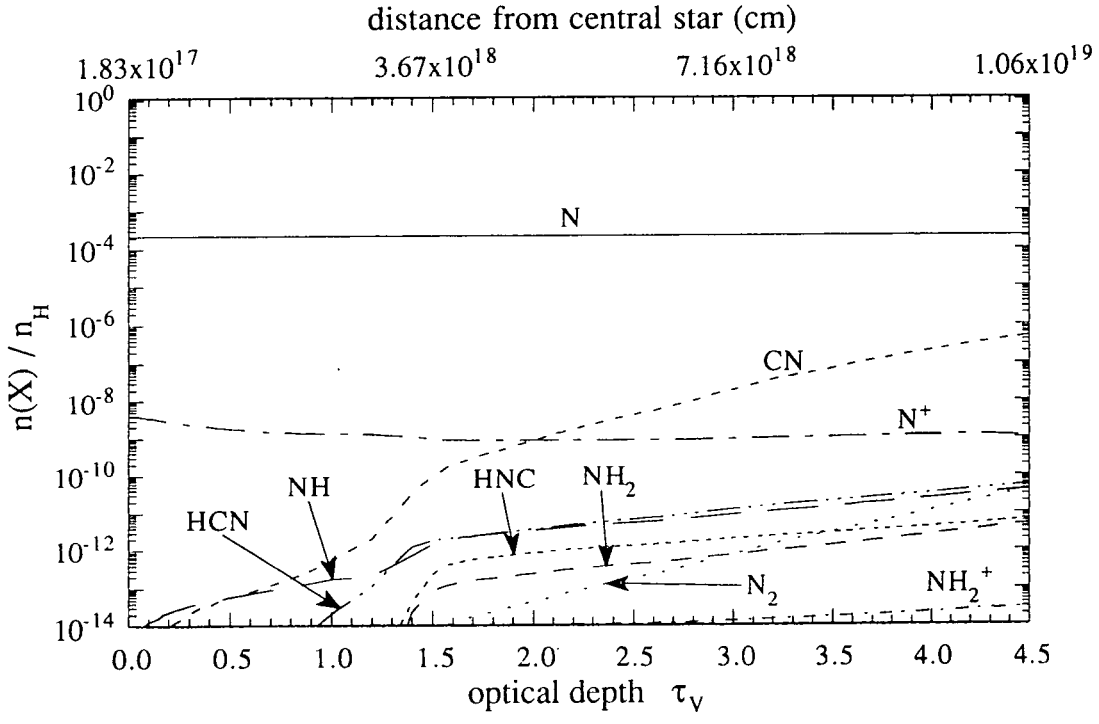

FIG. 8.10 - The abundances of the nitrogen bearing species through the nebula for a gas density of $n_{\rm H} = 1000$ cm^{-3}.

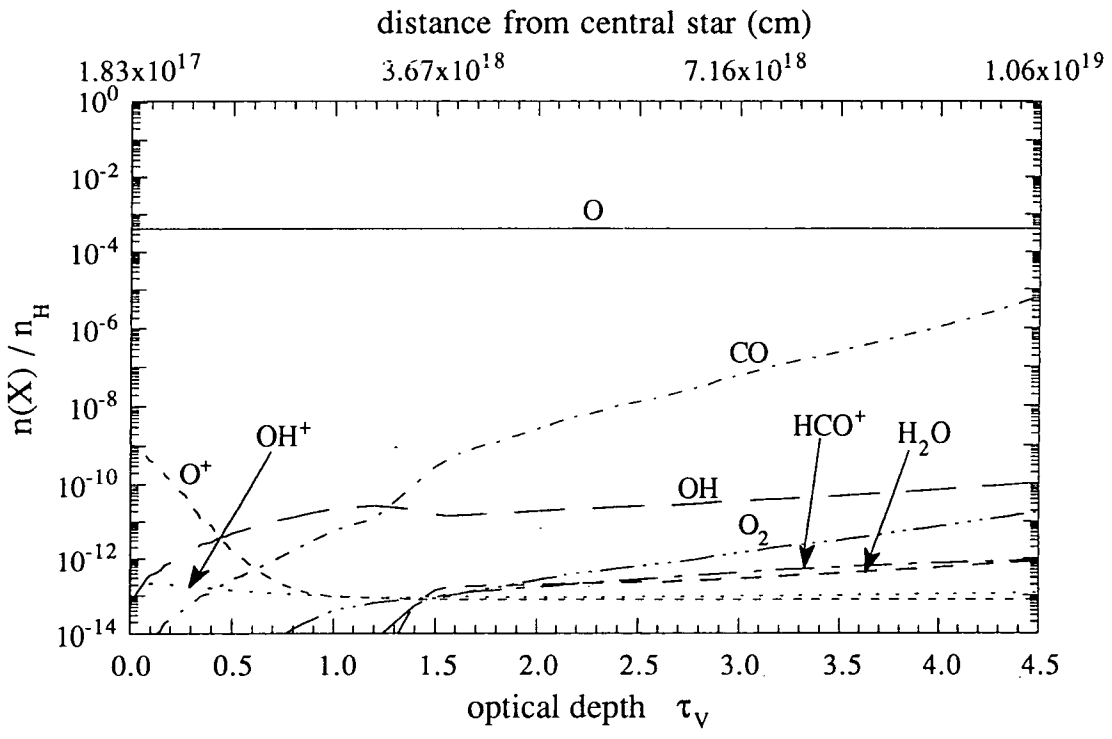

FIG. 8.11 - The abundances of the oxygen bearing species through the nebula for a gas density of $n_{\rm H} = 1000$ cm^{-3}.

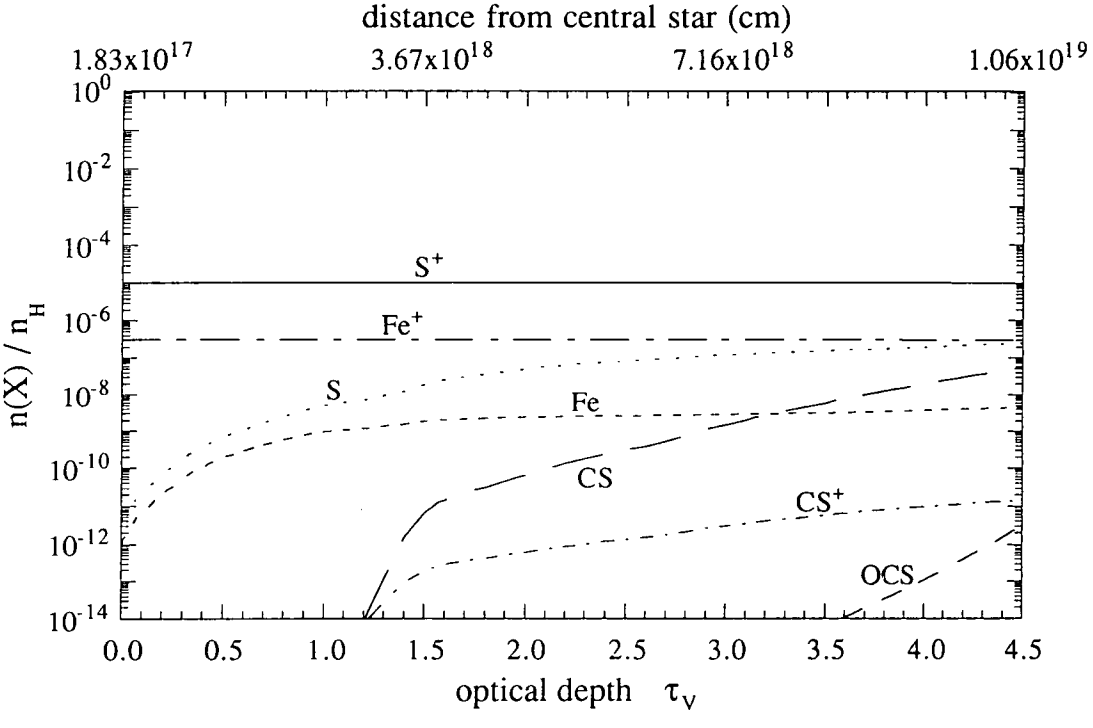

FIG. 8.12 - The abundances of the sulphur/iron bearing species through the nebula for a gas density of $n_{\rm H} = 1000$ cm^{-3}.

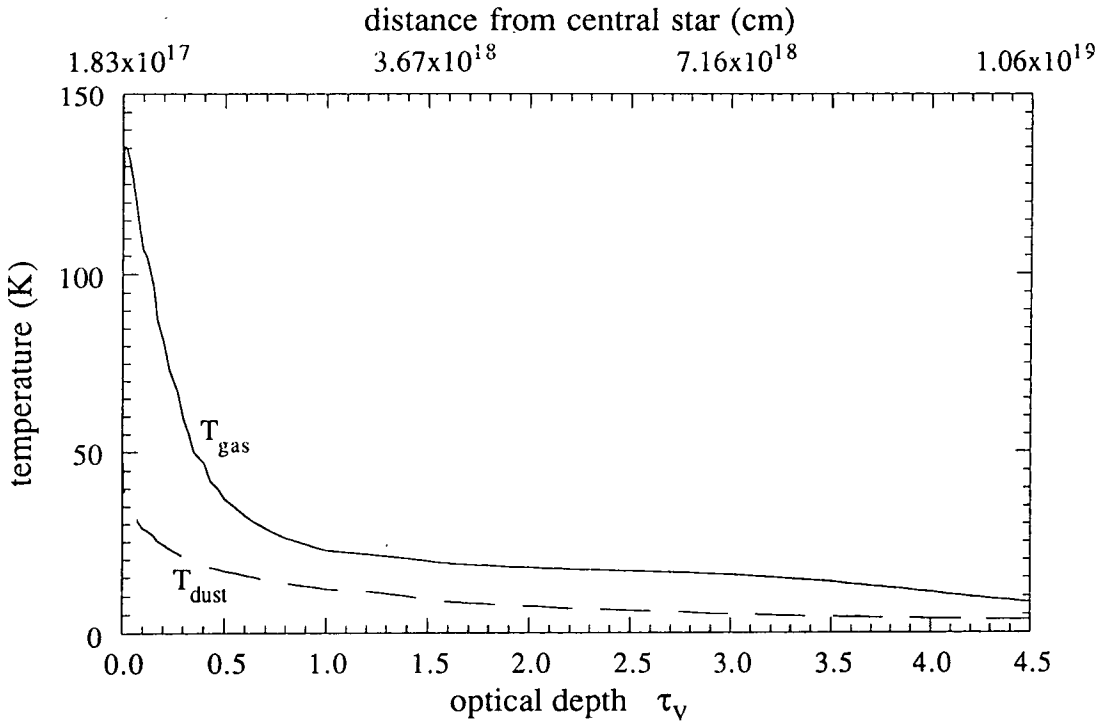

FIG. 8.13 - The gas and dust grain temperature profile through the nebula for a gas density of $n_{\rm H} = 1000$ cm^{-3}.

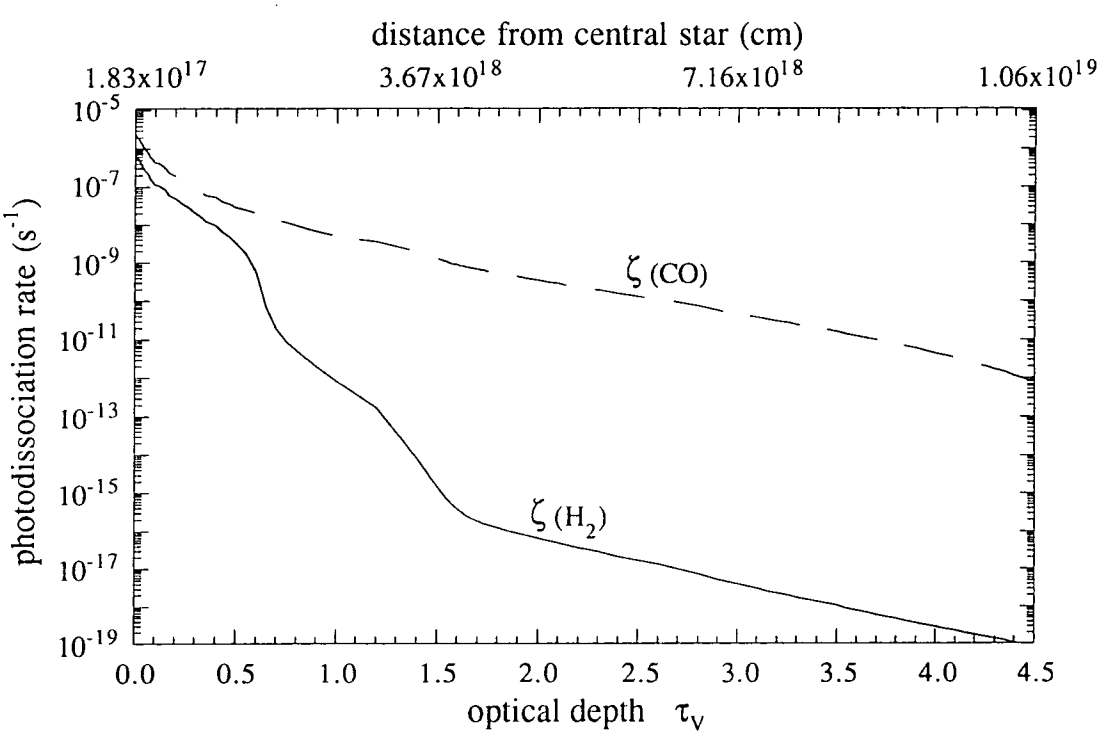

FIG. 8.14 - The computed H_2 and CO photodissociation rates through the nebula for a gas density of $n_{\rm H} = 1000$ cm^{-3}.

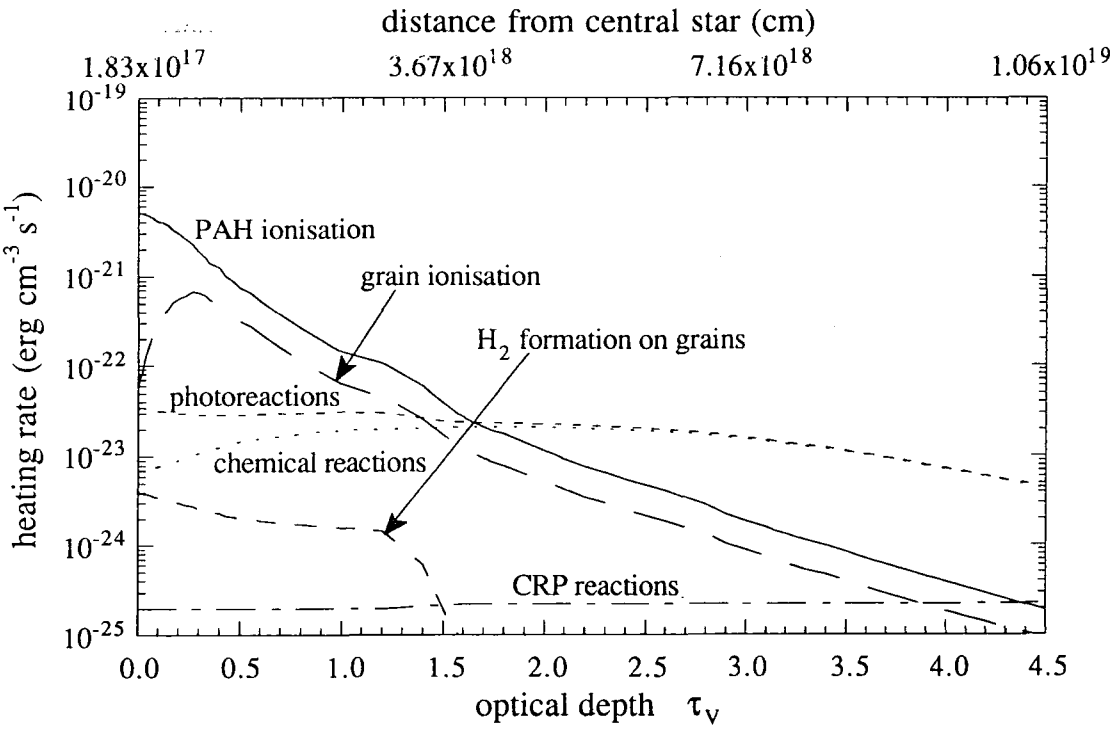

FIG. 8.15 - Contributions to the rate of heating of the gas for a gas density of $n_{\rm H} = 1000$ cm^{-3}.

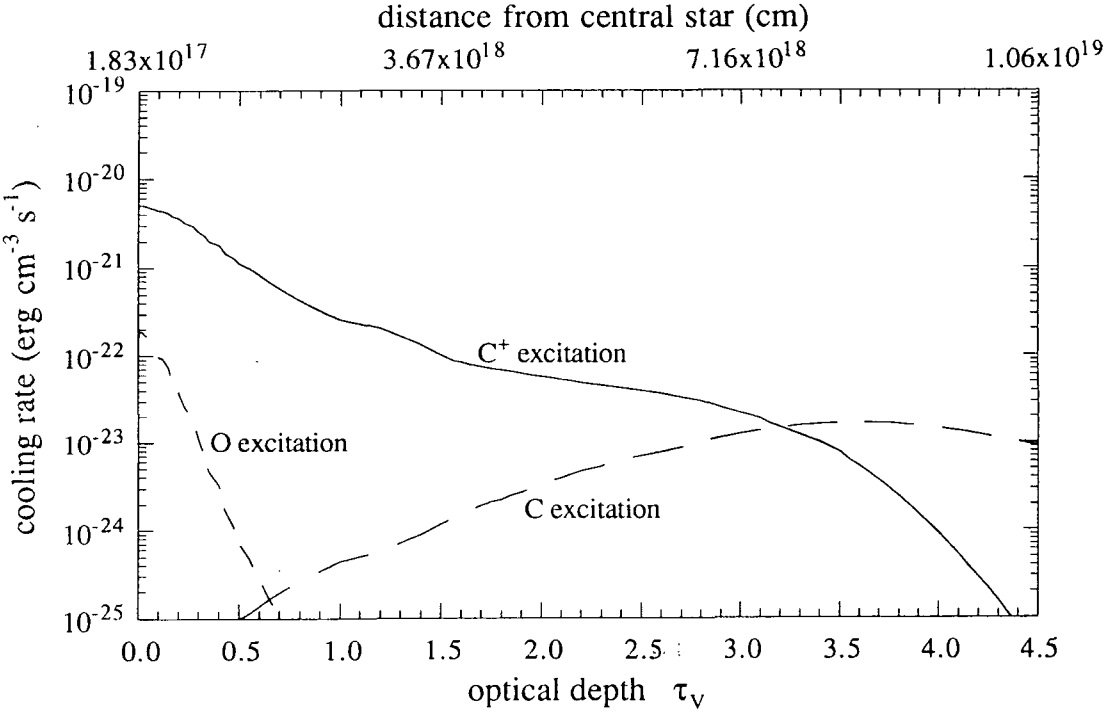

FIG. 8.16 - Contributions to the rate of cooling of the gas for a gas density of $n_{\rm H} = 1000$ cm^{-3}.

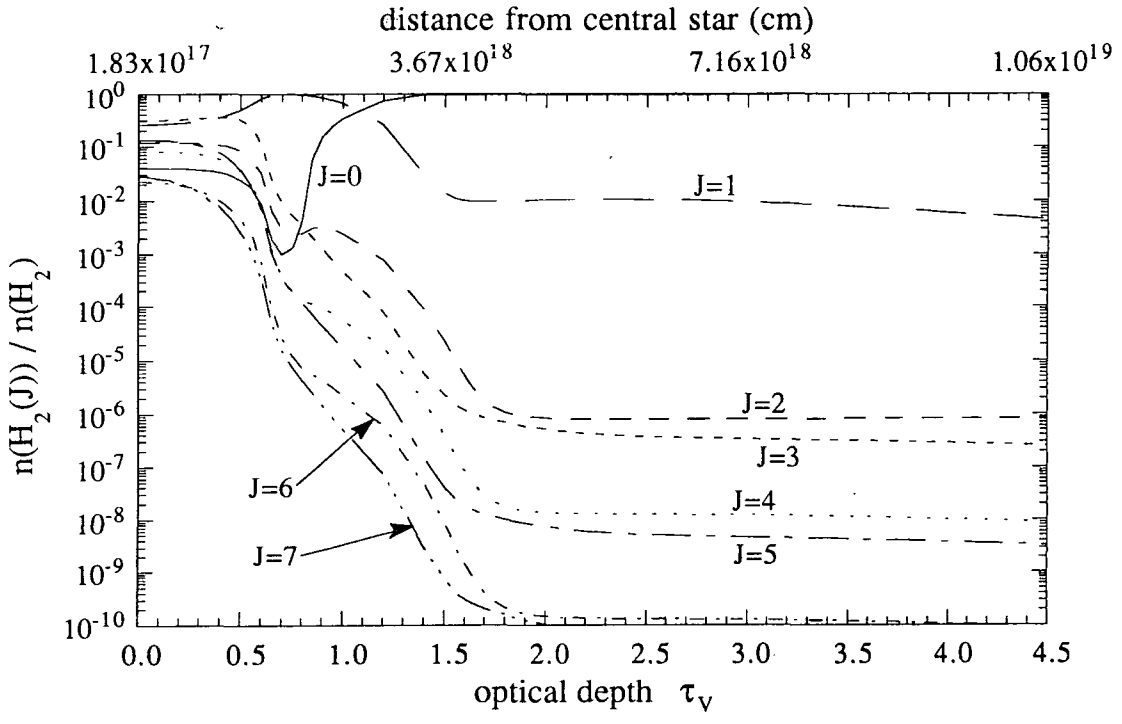

FIG. 8.17 - The relative populations of the rotational levels $0 \leq J \leq 7$ of H_2 for a gas density of $n_H = 1000$ cm^{-3}.

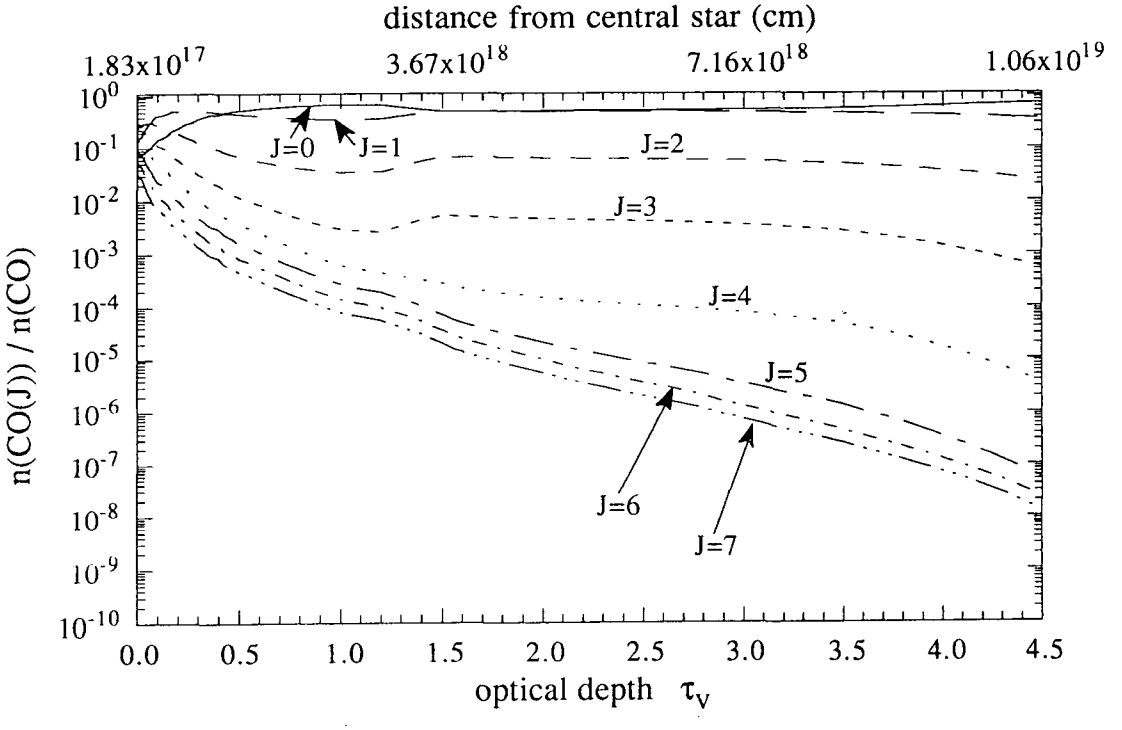

FIG. 8.18 - The relative populations of the rotational levels $0 \leq J \leq 7$ of CO for a gas density of $n_H = 1000$ cm^{-3}.

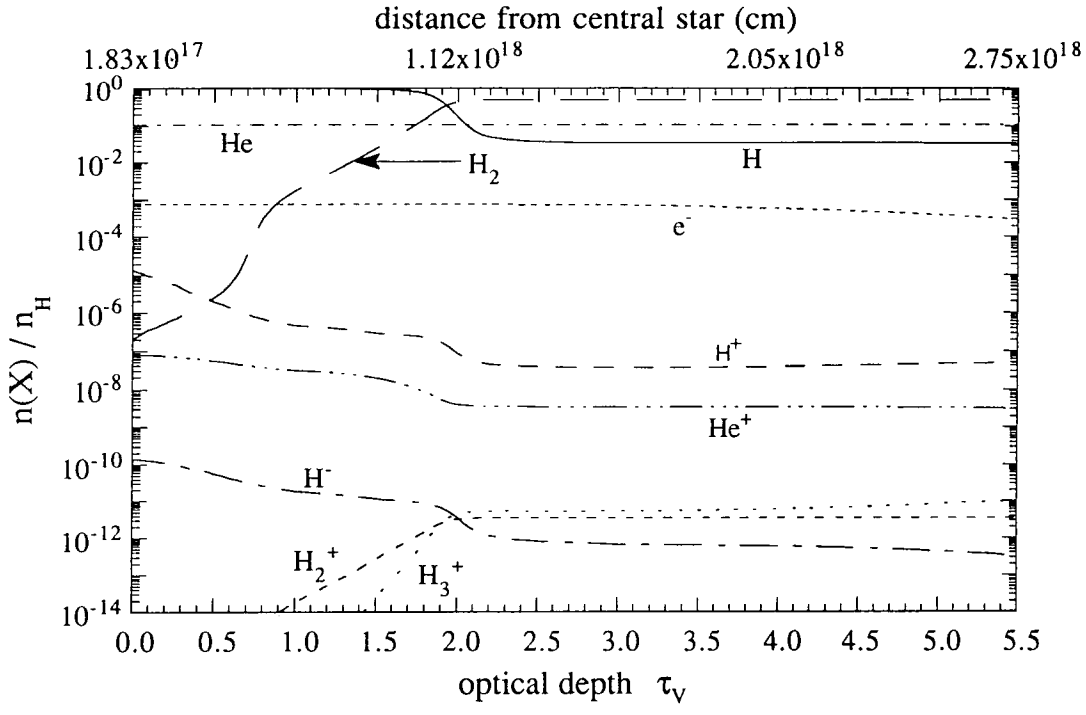

FIG. 8.19 - The abundances of the hydrogen/helium bearing species (and the electron abundance) through the nebula for a gas density of $n_{\rm H} = 5000$ cm^{-3}.

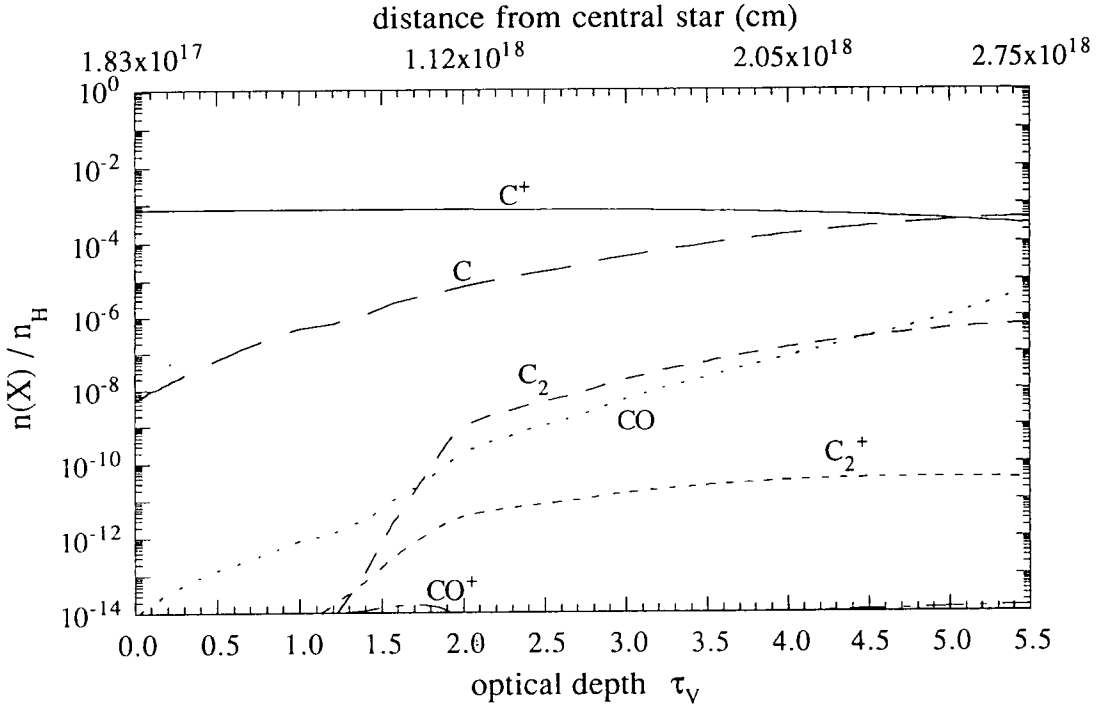

FIG. 8.20 - The abundances of the carbon bearing species through the nebula for a gas density of $n_{\rm H} = 5000$ cm^{-3}.

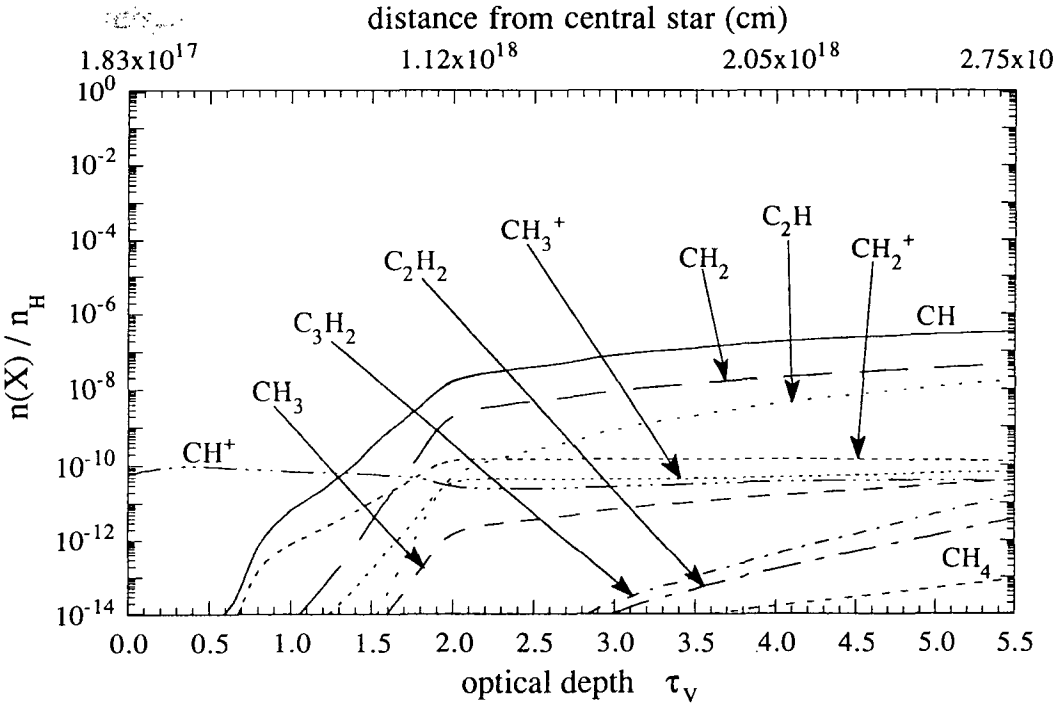

FIG. 8.21 - The abundances of the hydrocarbon species through the nebula for a gas density of $n_{\rm H} = 5000$ cm^{-3}.

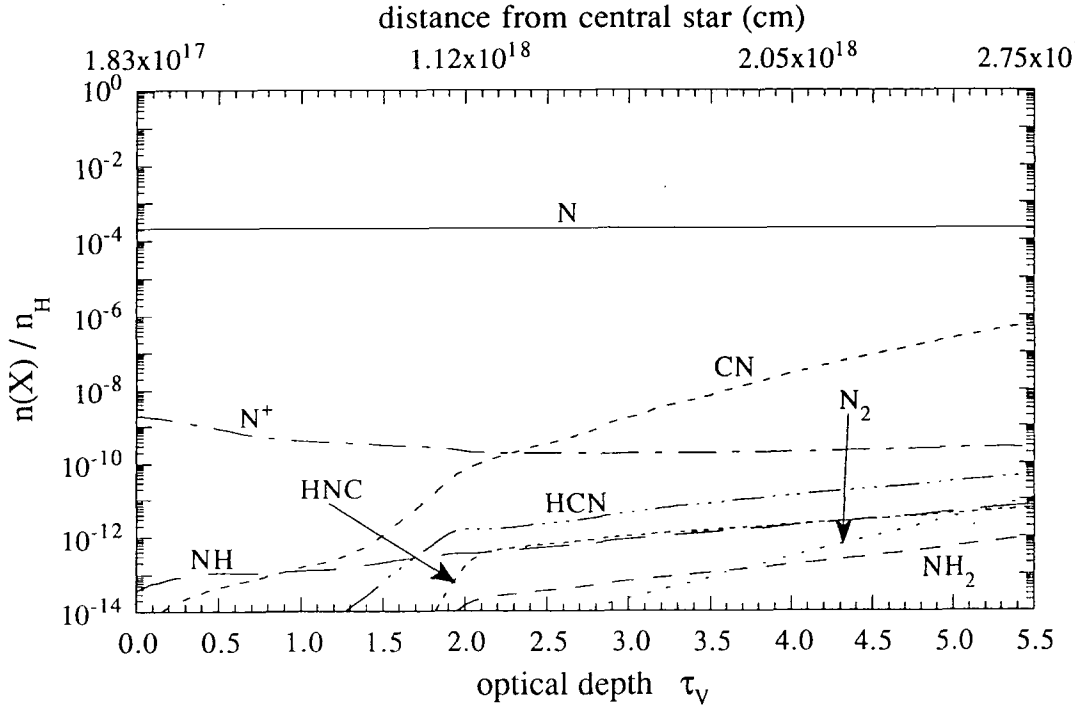

FIG. 8.22 - The abundances of the nitrogen bearing species through the nebula for a gas density of $n_{\rm H} = 5000$ cm^{-3}.

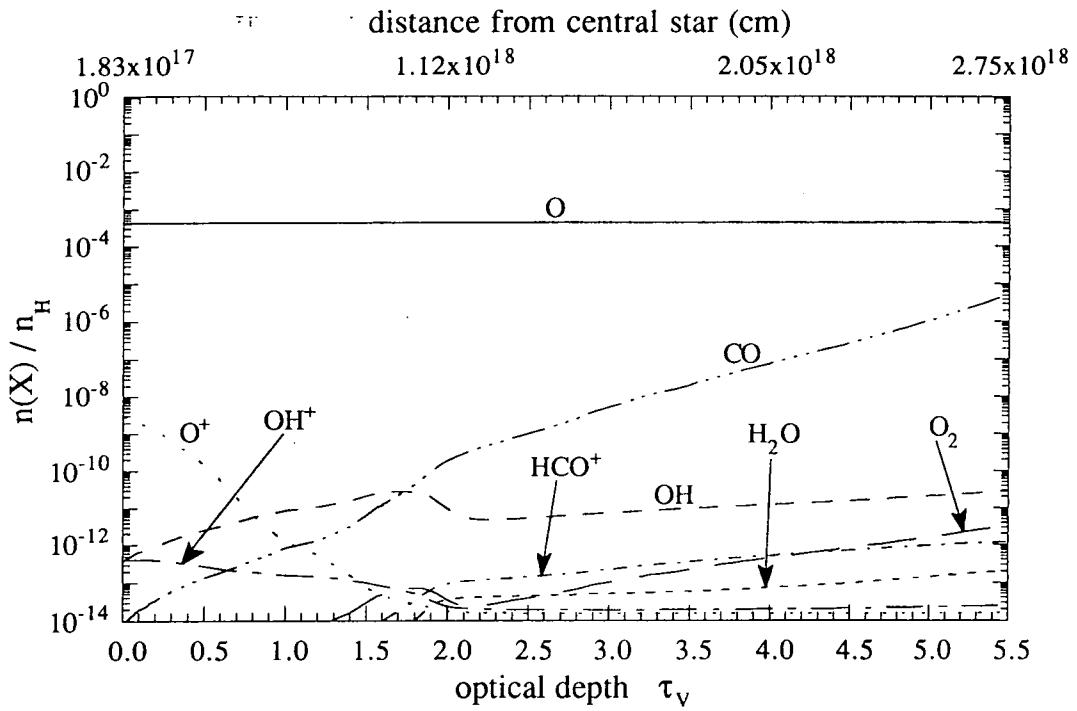

FIG. 8.23 - The abundances of the oxygen bearing species through the nebula for a gas density of $n_{\rm H} = 5000$ cm^{-3}.

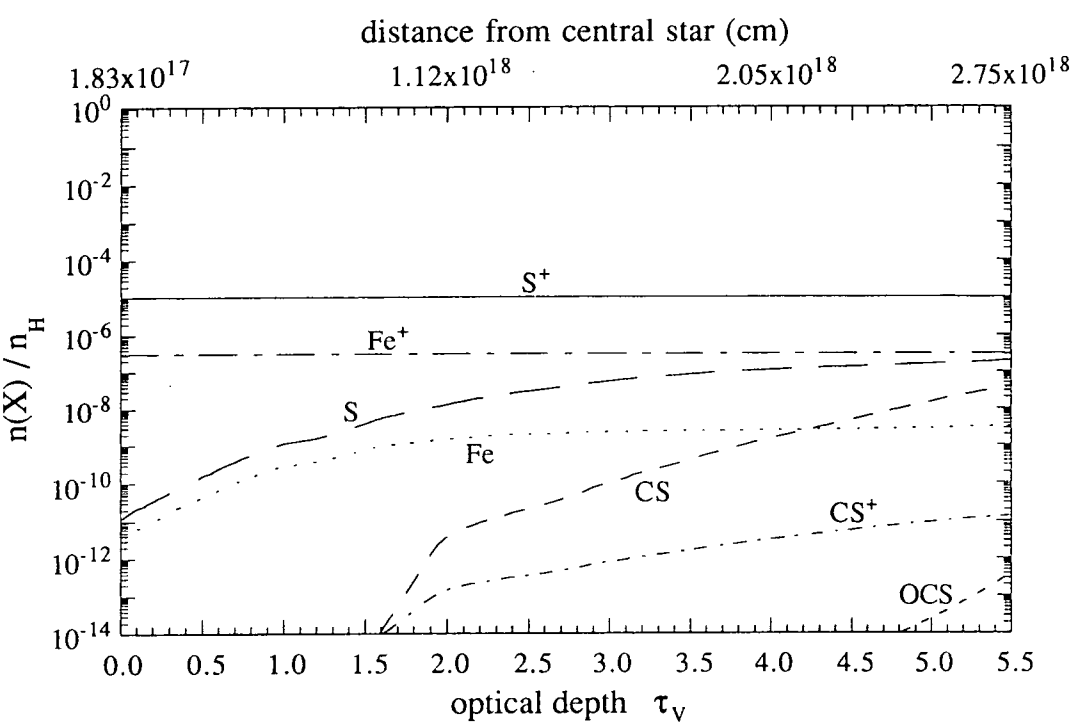

FIG. 8.24 - The abundances of the sulphur/iron bearing species through the nebula for a gas density of $n_{\rm H} = 5000$ cm^{-3}.

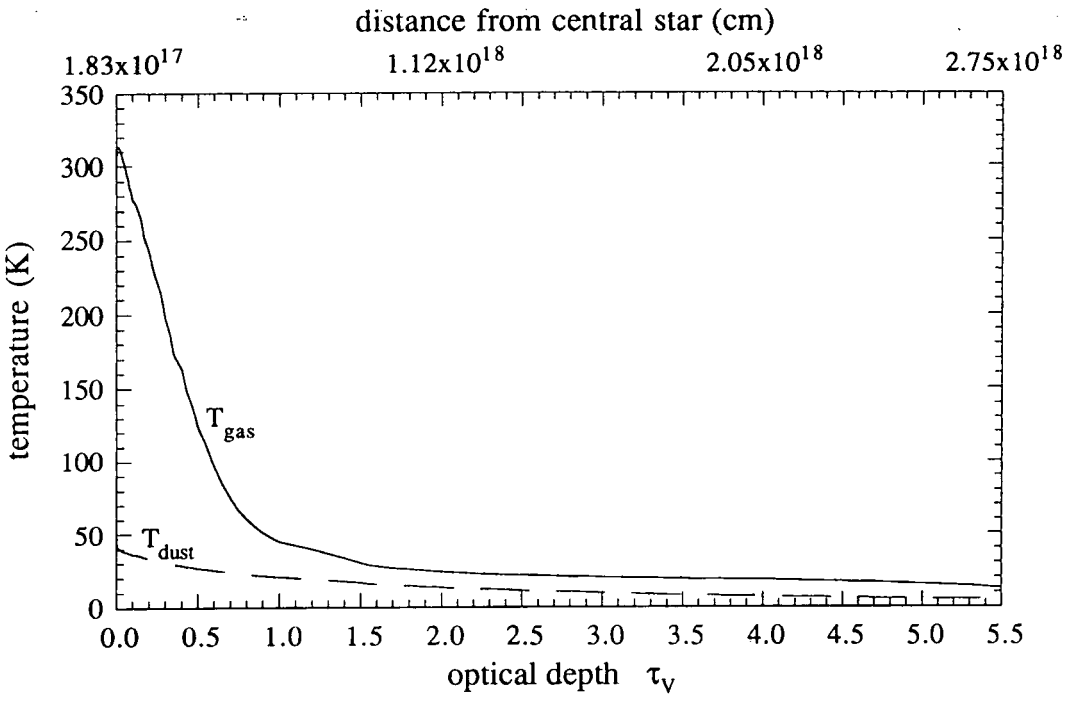

FIG. 8.25 - The gas and dust grain temperature profile through the nebula for a gas density of $n_{\rm H} = 5000$ cm^{-3}.

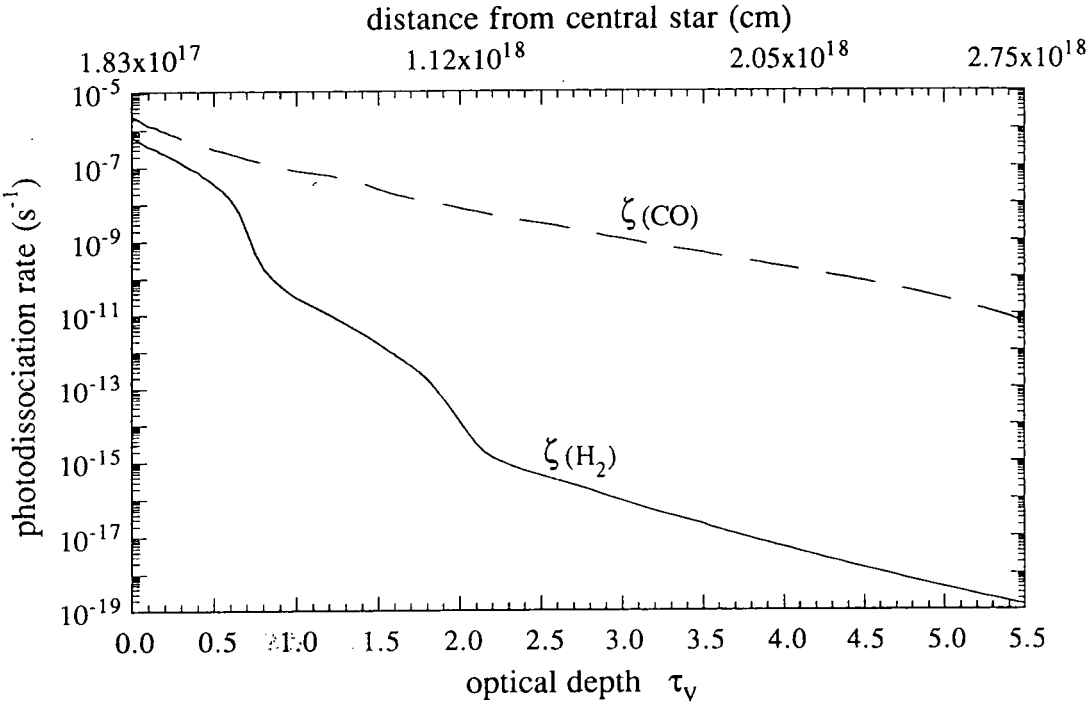

FIG. 8.26 - The computed H_2 and CO photodissociation rates through the nebula for a gas density of $n_{\rm H} = 5000$ cm^{-3}.

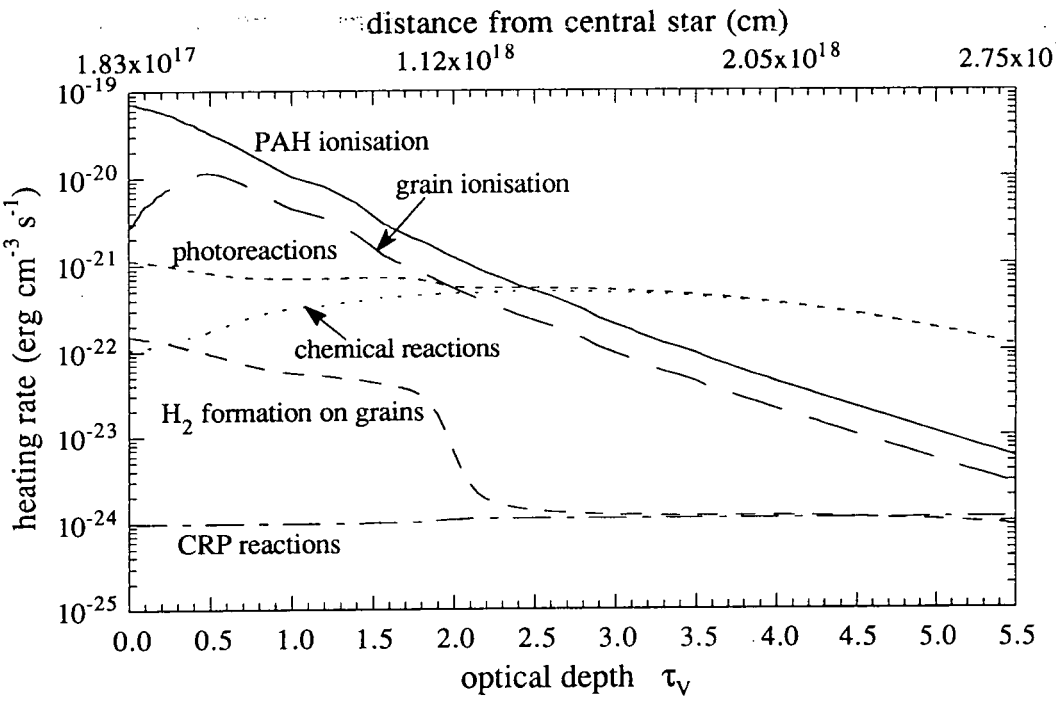

FIG. 8.27 - Contributions to the rate of heating of the gas for a gas density of $n_{\rm H} = 5000$ cm^{-3}.

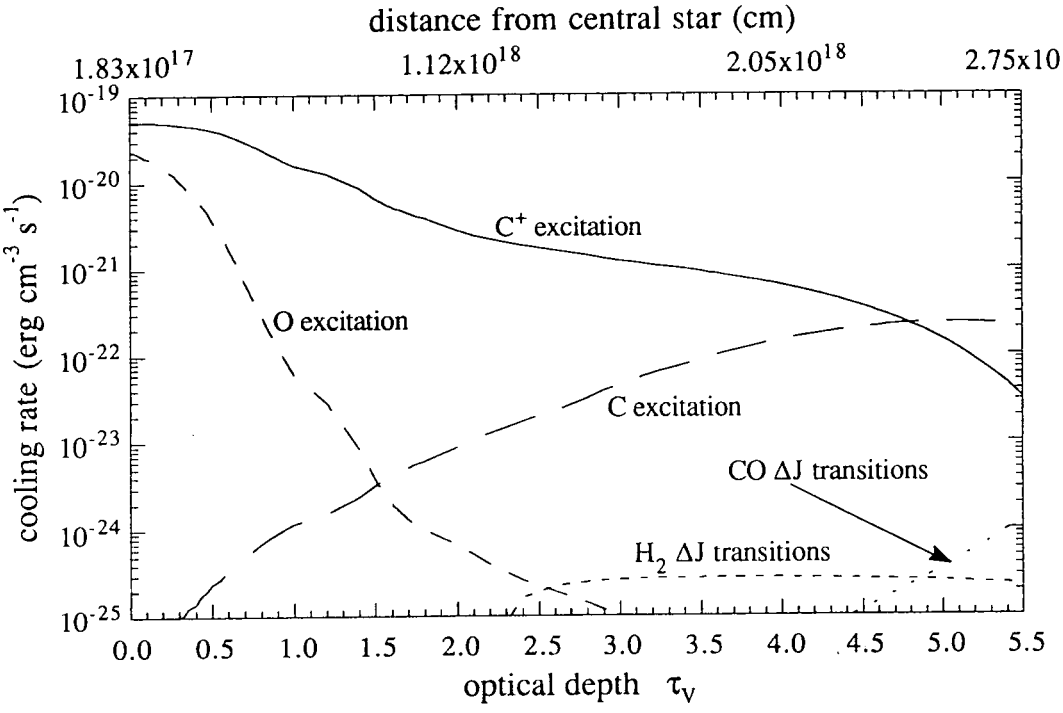

FIG. 8.28 - Contributions to the rate of cooling of the gas for a gas density of $n_{\rm H} = 5000$ cm^{-3}.

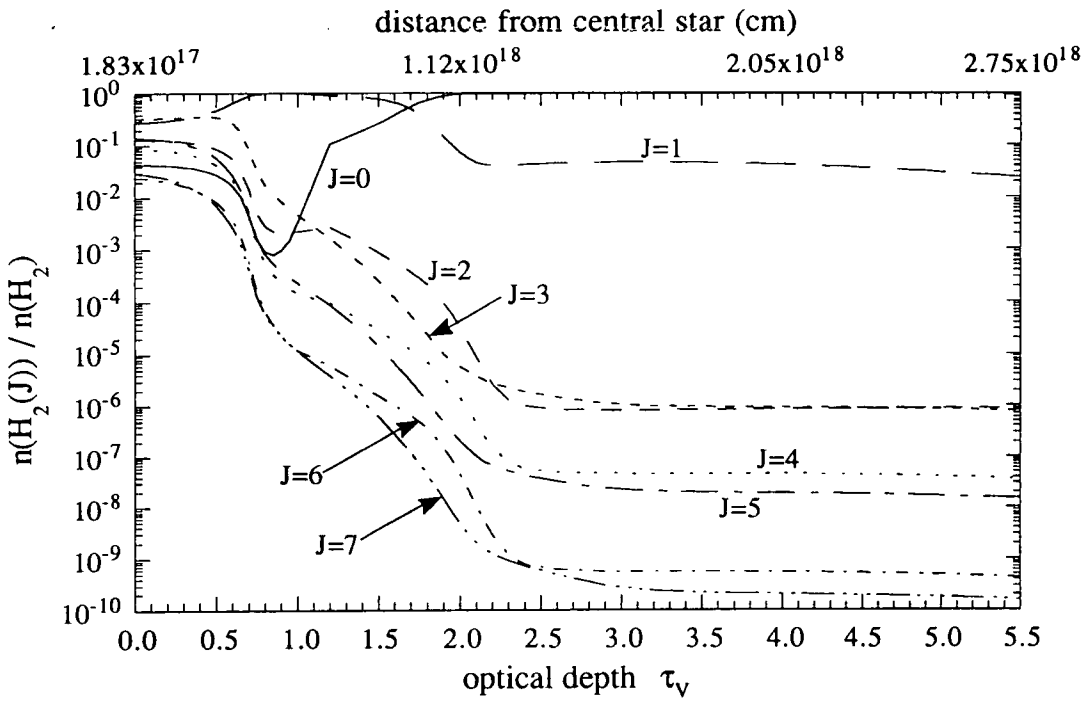

FIG. 8.29 - The relative populations of the rotational levels $0 \leq J \leq 7$ of H_2 for a gas density of $n_H = 5000$ cm^{-3}.

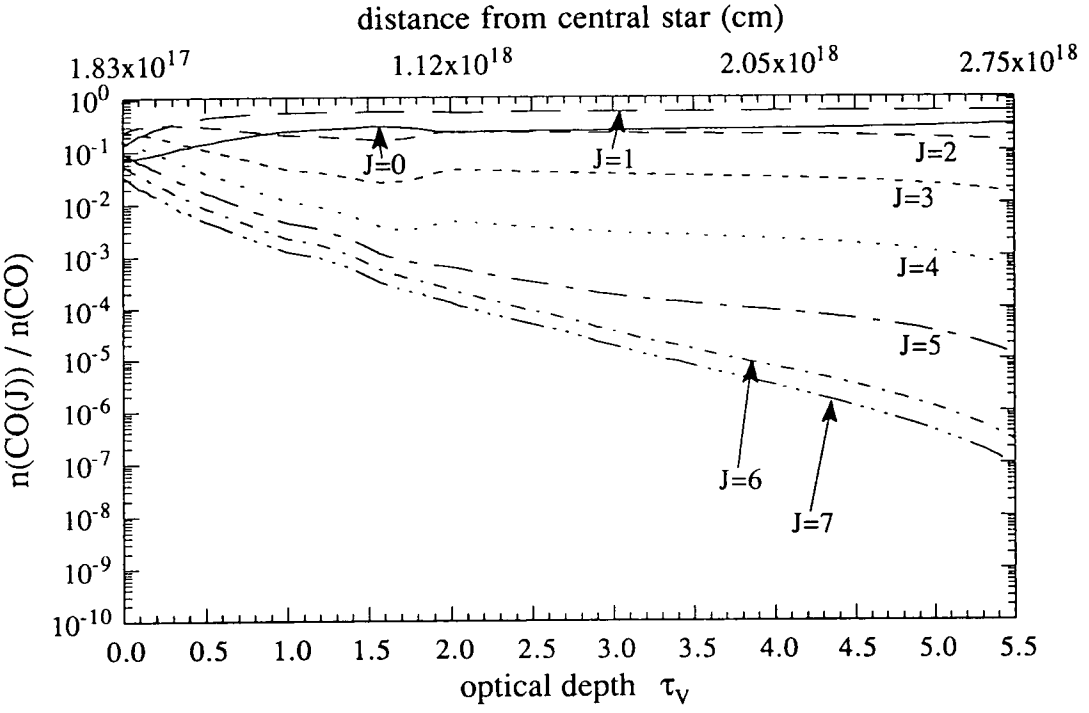

FIG. 8.30 - The relative populations of the rotational levels $0 \leq J \leq 7$ of CO for a gas density of $n_H = 5000$ cm^{-3}.

8.2 Comparison with molecular observations

The results of running the model have been compared with molecular observations of four planetary nebulae. Fig. 8.31 shows computed molecular column densities (relative to N(HCN)) derived from observations of NGC 6072. Fig. 8.32 shows relative column densities for the PN IC 4406. Both these sets of observations and calculations were performed by Cox *et al.* (1992). Fig. 8.33 shows molecular column densities relative to the the column density of CO in the PN NGC 7027 representing a combination of observations by Thronson and Bally (1986) and Cox *et al.* (1987). Fig. 8.34 shows column densities relative to HCN derived for the nebula NGC 2346 by Bachiller *et al.* (1989).

The results of the model are shown as functions of the assumed hydrogen nuclei number density $n_{\rm H}$ and it is clearly seen that the predicted column density ratios N(X)/N(HCN), or N(X)/N(CO), are very insensitive to the variation in $n_{\rm H}$. The only species which show appreciable deviation with $n_{\rm H}$ are the nitrogen-bearing species NH_3 and N_2H^+ where the ratios $N(NH_3)/N(CO)$ and $N(N_2H^+)/N(HCN)$ fall by almost an order of magnitude between $n_{\rm H} = 10^3$ cm^{-3} and $n_{\rm H} = 10^4$ cm^{-3} (Figs. 8.31/8.32 and 8.33 respectively). The observational data are represented on the graphs by the arrows on the right-hand vertical scale. Some of the data from Cox *et al.* (1992) are reported as upper limits, specifically [C_2H]/[HCN] and [N_2H^+]/[HCN] and all the data on NGC 7027 by Thronson and Bally (1986) and Cox *et al.* (1987) are reported as upper limits. The data on these nebulae are shown below.

NGC 6072

Species X	Relative column density x=[X]/[HCN]	$\log_{10} x + 12$	Reference
CO	1181	15.07	*a*
CN	12.9	13.11	*a*
HCO^+	0.64	11.81	*a*
HNC	0.22	11.34	*a*
C_2H	< 2.2	< 12.34	*a*
N_2H^+	< 0.11	< 11.04	*a*

IC 4406

Species X	Relative column density x=[X]/[HCN]	$\log_{10} x + 12$	Reference
CO	1600	15.20	*a*
CN	8.2	12.91	*a*
HCO^+	0.67	11.83	*a*
HNC	0.22	11.34	*a*
C_2H	< 2.9	< 12.46	*a*
N_2H^+	< 0.43	< 11.63	*a*

NGC 7027

Species X	Relative column density x=[X]/[CO]	$\log_{10} x + 12$	Reference
CN	$\leq 2 \times 10^{-4}$	≤ 8.301	*b*
CS	$\leq 3 \times 10^{-5}$	≤ 7.477	*b*
NH_3	$\leq 2 \times 10^{-5}$	≤ 7.301	*b*
C_2H	$\leq 7 \times 10^{-4}$	≤ 8.845	*b*
C_3H_2	$\leq 1 \times 10^{-5}$	≤ 7.000	*c*

NGC 2346

Species X	Relative column density x=[X]/[HCN]	$\log_{10} x + 12$	Reference
CO	350	14.54	*d*
HCO^+	0.7	11.85	*d*
HNC	1.0	12.00	*d*

References:

a - Cox *et al.* (1992)

b - Thronson and Bally (1986)

c - Cox *et al.* (1987)

d - Bachiller *et al.* (1989)

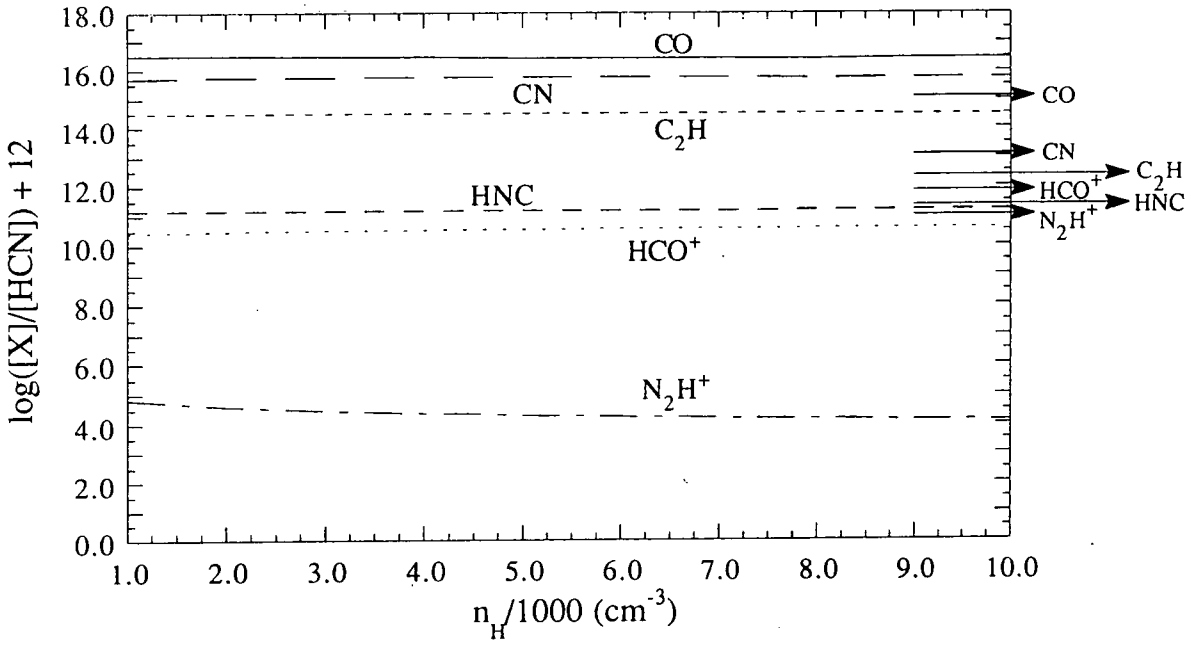

FIG. 8.31 - Model predictions of relative column densities compared with values derived from observation of NGC 6072 by Cox *et al.* (1992). Values derived for C_2H and N_2H^+ are upper limits.

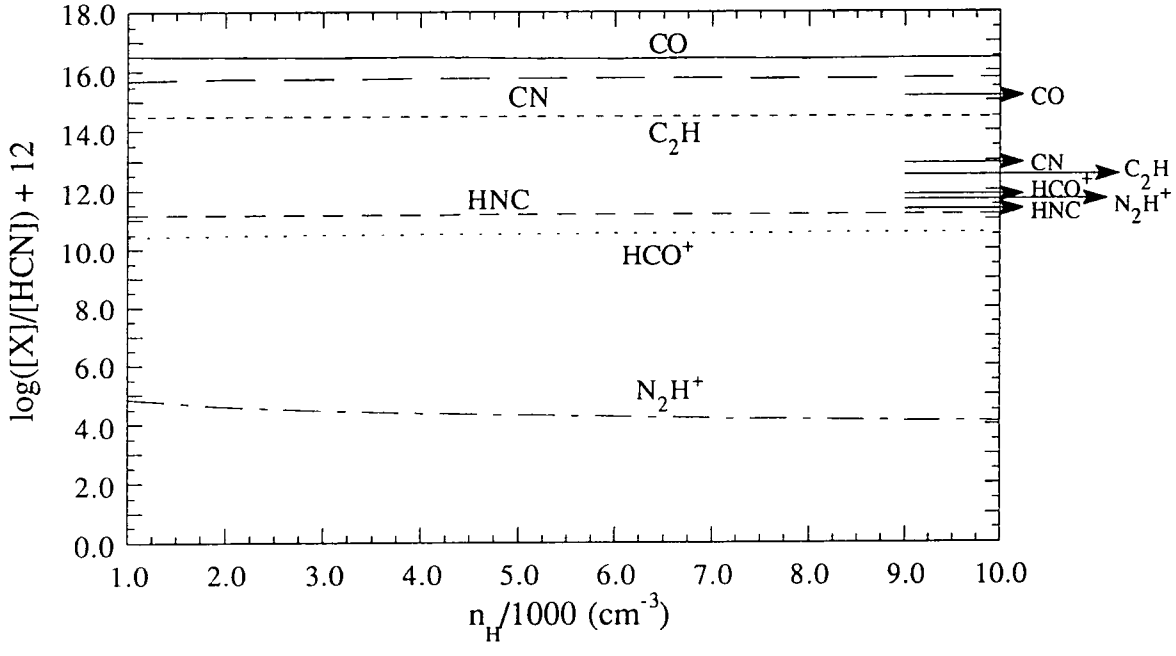

FIG. 8.32 - Model predictions of relative column densities compared with values derived from observation of IC 4406 by Cox *et al.* (1992). Values derived for C_2H and N_2H^+ are upper limits.

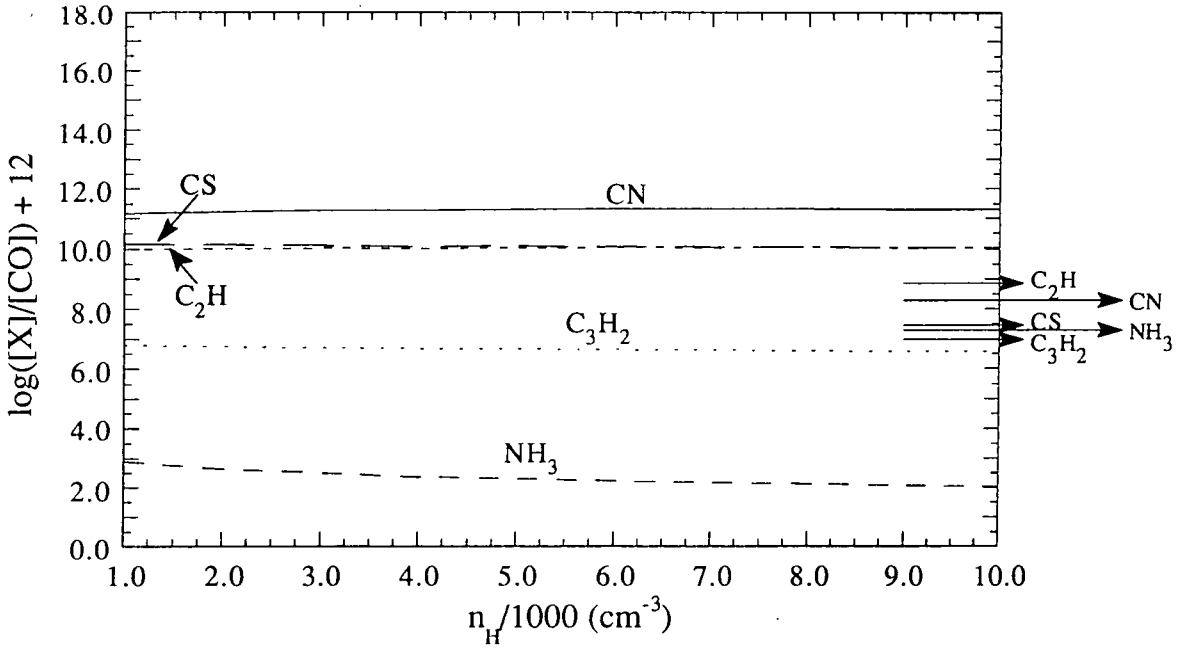

FIG. 8.33 - Model predictions of relative column densities compared with values derived from observation of NGC 7027 by Cox *et al.* (1987) and Thronson and Bally (1986). All the values derived from observation are upper limits.

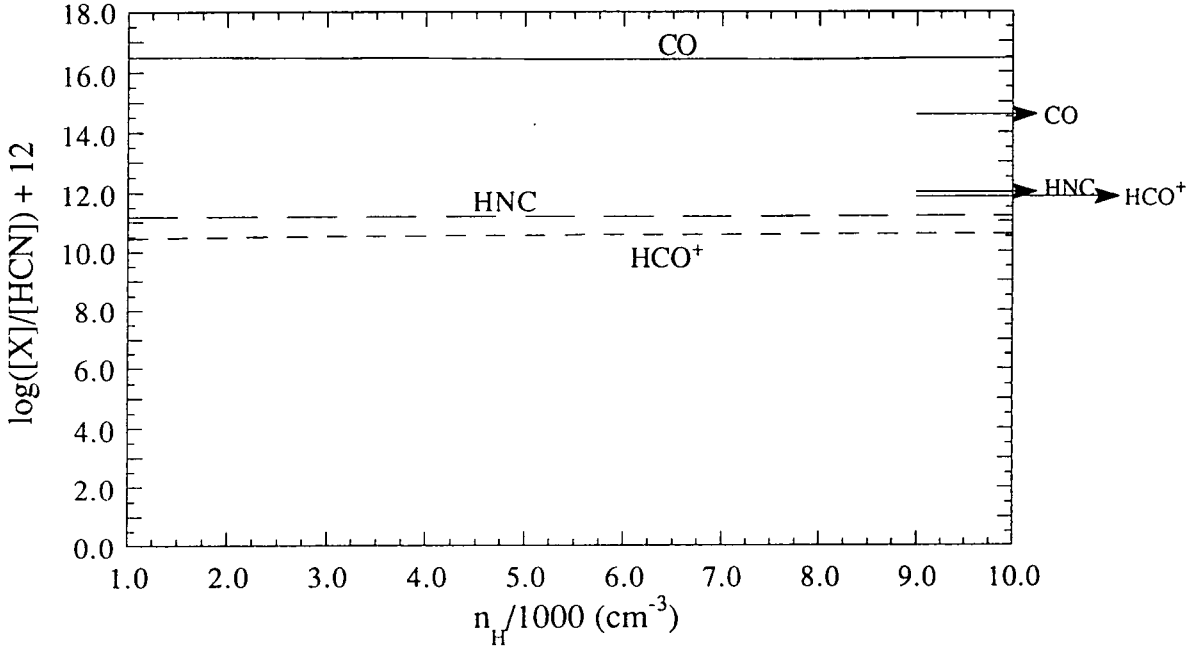

FIG. 8.34 - Model predictions of relative column densities compared with values derived from observation of NGC 2346 by Bachiller *et al.* (1989).

The model presented in this thesis is not based on a specific nebula, rather it is an attempt to model the chemistry and physics in what is hopefully a 'typical' carbon-rich planetary nebula. To compare the predictions of the model with observations of specific nebulae is, therefore, more of an attempt to see if the general nature of the model is correct and whether the assumptions made are valid rather than trying to reproduce observed molecular abundances as accurately as possible. If the elemental abundances in the model are similar to those in the observed nebulae then comparison of predicted and observed molecular abundances becomes at least meaningful. NGC 7027 is known to be carbon-rich with C/O$\approx$ 3 (Zuckerman and Aller 1986) but the C/O ratio for NGC 6072 and IC 4406 is uncertain. The molecular abundances in these nebulae are similar to NGC 6720 and NGC 7027 which are both carbon-rich and HCN emission was detected by Cox *et al.* from both nebulae which is usually thought to be an indicator of a carbon-rich environment (Deguchi *et al.* 1986). The CN lines are also very strong and CN has never been detected in oxygen-rich AGB circumstellar envelopes except TX Cam where the ratio of line intensities CN/HCN is about an order of magnitude (Olofsson *et al.* 1991). It is thus more likely that the molecular envelopes of these two nebulae are carbon-rich rather than oxygen-rich. Both are Type I nebulae with N/O ratios of 0.44 for NGC 6072 (Kaler *et al.* 1990) and 0.48 for IC 4406 (Perinotto 1991). The model assumes an N/O ratio of 0.5 (§3.1.1). The case for NGC 2346 seems to be less clear but, again, the detection of strong HCN emission lines would seem to indicate a carbon-rich environment.

The relative column densities of NH_3, N_2H^+ and C_3H_2 fall well below the upper limits imposed on these species by the observations. The predicted values of the $N(\mathrm{HNC})/N(\mathrm{HCN})$ ratio agree closely with the observational data on NGC 6072 and IC 4406, but fall short of the value derived for NGC 2346 by a factor of about seven (using the results for $n_{\mathrm{H}} = 1000$ cm^{-3}). All other predicted column densities exhibit very poor agreement with the observations. These are all carbon-bearing species and the trend in the figures is to predict far too much of the molecule relative to HCN (or CO). The exception to this rule is the molecule HCO^+. Observations of $N(\mathrm{HCO^+})/N(\mathrm{HCN})$ in the nebulae NGC 6072, IC 4406 and NGC 2346 show remarkable similarity. The predicted column density ratio falls short of the observational data by a factor of between 16 and 25, depending on the assumed value of n_{H}.

The principal mechanisms that could possibly affect the chemistry in the molecular region are as follows:

(1) UV flux from the central star

(2) Shocks impinging on inner part of molecular envelope, enabling endothermic

reactions to proceed

(3) Possible enhancement of photoionisation/dissociation through X-ray emission from central star

(4) Inhomogeneities in the gas structure (clumpiness) allowing shielding from photodissociation

(5) Influence of the interstellar radiation field

The effect of the UV flux is included in the model in a very detailed manner where radiative transfer in the lines of H, H_2 and CO are fully accounted for as well as continuum absorption by dust grains. Shock waves and soft X-ray ionisation and dissociation are not included in the model.

Recent observations suggest the general trend that the relative abundance of HCO^+ increases with the age of the nebula. Observations by Johansson *et al.* (1984) of the AGB star IRC+10°216 produced an upper limit for $[HCO^+]/[HCN]$ of 2×10^{-4} and for $[HCO^+]/[CO]$ an upper limit of 4×10^{-6}. It is thought that an AGB star is the precursor phase to a planetary nebula, the transition period lasting around 1000 years. The intermediate stellar phase is known as a proto-planetary nebula (PPN). Bujarrabal *et al.* (1988) made observations of the carbon-rich PPN CRL 618 and made a wealth of molecular identifications including HCO^+, CS, C_2H, HCN, HNC and C_3H_2. They deduced a value for $[HCO^+]/[HCN]$ of 0.4 and a surprisingly high value for $[HCO^+]/[CO]$ of 0.002. It is thus apparent that a considerably different chemistry operates in the circumstellar envelope of an AGB star than in the molecular shell of a planetary nebula. From the evidence cited a low HCO^+ abundance seems to be representative of the chemistry round an AGB star where the main molecular abundances are determined in the dense inner regions of the circumstellar envelope.

There are a number of possibilities to explain the discrepancies in the observed and predicted HCO^+ abundance. If a sufficiently large amount of H_2^+ exists in the molecular shell as well as neutral H_2 the reactive sequence

$$H_2^+ + H_2 \rightarrow H_3^+ + H$$

$$H_3^+ + CO \rightarrow HCO^+ + H_2$$

is very efficient and could possibly become more efficient than chemi-ionisation

$$CH + O \rightarrow HCO^+ + e^-$$

in producing the ion.

The difficulty is that the known cosmic ray ionisation rate of H_2 ($\sim 10^{-17}$ s^{-1}) is

far too small to produce the required amounts of H_2^+. A natural question to then ask is whether there is an alternative source of ionisation for molecular hydrogen. If the central star is of a sufficiently high temperature then a possible candidate is soft X-ray ionisation. The model presented in this thesis makes the simplifying assumption that all radiation shortward of the Lyman limit has been absorbed by atomic hydrogen in the ionised region and has been degraded in energy by subsequent fluorescence (§2.1.1) so that H_2 photoionisation cannot occur in the molecular shell. However, X-ray emission has been observed from eight PNe by Apparao and Tarafdar (1989) and the question then arises as to whether this radiation represents an important source of ionisation for H_2 and other species. Deguchi *et al.* (1990) detected strong emission in the HCO^+ $J = 1 \rightarrow 0$ line in the molecular envelope of NGC 7027. They tried to reproduce the observations by constructing a nebular model incorporating a central star of temperature 2.4×10^5 K and soft X-ray ionisation of H_2 assuming black body emission at X-ray energies. There are several objections to this hypothesis of X-ray ionisation. The central star temperature required to reproduce observed abundances of HCO^+ is in general far higher than 'typical' PN star temperatures and certainly cannot be invoked to explain HCO^+ abundances in more highly evolved PNe where the central star is on the cooling track.

The strongest argument against this idea is the fact that HCO^+ emission has been detected at comparable levels in PNe where the X-ray flux is deduced to differ widely due to the range in central star temperatures. Despite the consequent very large range in the H_2 ionisation rates the abundances of HCO^+ in the PNe studied are very similar (generally $[HCO^+]/[HCN] \sim 1$) which is incompatible with the theory of X-ray ionisation being the dominant route to formation of the molecule. Another possible explanation for the observed high abundance of HCO^+ is through rapid proton transfer reactions between CO and an ionised partner. The proton affinity of CO is 6.20 eV and there are a number of species with proton affinities less than this which could be possible contenders in such reactions as shown in Table 8.2 (from Duley and Williams 1984).

From a consideration of Figs. 8.10 and 8.11 it is apparent that only OH^+ and NH^+ have anywhere near the relative high abundance ($\sim 10^{-6}$ to 10^{-7}) necessary to form the required amounts of HCO^+. These species react with CO with a Langevin rate of $\sim 10^{-9}$ cm^3 s^{-1} (Prasad and Huntress 1980) but the model predicts abundances of these ions that are simply too small to account for sufficient production of HCO^+ to match observations. If this hypothesis is correct then there must be far more OH^+ and NH^+ in the nebulae being observed than is predicted by the model.

Table 8.2
Proton affinities of selected chemical species

Species	Proton affinity (eV)
CO	6.20
O	5.03
N	4.21
NH	6.12
CN	4.99
N_2	5.03

As far as the author is aware neither of these species has ever been observed in a planetary nebula environment presumably due to the fact no attempt has ever been made to detect specific emission lines of the ions. This state of affairs obviously leaves open the question of actual nebular abundances of the species. It is unlikely that a major component of the chemistry of OH^+ and NH^+ has been omitted in the chemical reaction network which effectively rules out the conjecture of proton transfer reactions dominating HCO^+ production.
The hypothesis of the presence of OH and OH^+ in PNe has received indirect evidence recently in the form of observation of ionised CO in NGC 7027 by Latter *et al.* (1993) based on mm and sub-mm rotational transitions in the molecule. With the assumption of no radiation in the neutral region capable of ionising the molecule, the detection of significant amounts of CO^+ in NGC 7027 suggests that OH is present in sufficient amounts to take part in ion-molecule reactions with C^+

$$C^+ + OH \rightarrow CO^+ + H$$

with a Langevin rate of 8×10^{-10} cm^3 s^{-1} (Croswell and Dalgarno 1985).
The most likely reason for the HCO^+ discrepancy is that shock waves have affected the chemistry of the observed nebulae. Shock waves passing through molecular gas are predicted to increase significantly the abundances of certain species, primarily through enabling previously suppressed endothermic reactions to proceed efficiently. In particular, models of diffuse molecular gas predict that the column densities of CH^+, CH and OH will exhibit increases of several orders of magnitude

when a shock wave passes through the material (Draine and Katz 1986).
The passage of a shock wave of sufficient velocity would enable the key endothermic reaction

$$C^+ + H_2 \rightarrow CH^+ + H - 0.39\,eV$$

to proceed efficiently.
In a post-shock environment where the kinetic temperature has been increased above $\sim$ 1000 K the reaction becomes important. At a temperature of 100 K the rate coefficient of the reaction is less than 10^{-30} cm^3 s^{-1} and is utterly negligible. At a temperature of 1000 K the rate coefficient is $\sim 10^{-12}$ cm^3 s^{-1} and is a very efficient production route to CH^+ because of the large abundances of C^+ and molecular hydrogen.
After the formation of CH^+ in this manner the primary route to HCO^+ is by the sequence:

$$CH^+ + H_2 \rightarrow CH_2^+ + H$$

then

$$CH_2^+ + O \rightarrow HCO^+ + H$$

or

$$CH_2^+ + H_2 \rightarrow CH_3^+ + H$$

$$CH_3^+ + O \rightarrow HCO^+ + H_2$$

which occur rapidly due to the large abundance of neutral oxygen (Fig. 8.11).
The fact that much more HCO^+ is detected in evolved planetary nebulae than in the precursor AGB phase strongly supports the theory of shock wave enhancement of the molecule. Current theory on the dynamical evolution of a PN incorporates the notion that at some point after the AGB phase matter streams out of the central star in a fast wind (one to four thousand km s^{-1}) and this forms a shock wave which impinges on the slower moving, outlying material to affect it dynamically and chemically. This theory would seem to tie in with models of shocked gas which predict an enhanced abundance of HCO^+ ions in the wake of a shock and the fact that an enhanced HCO^+ abundance is generally observed in evolved nebulae.
Whereas the invocation of shock waves is the most plausible explanation for the observed high abundance of HCO^+ it is difficult to marry this idea with the predictions this unshocked model makes with regard to other carbon-bearing species. The passage of a shock wave would have to reduce radically the predicted abundance ratios of the other molecules in question to bring the results in line with observations. It is impossible to predict with accuracy what effect a shock wave

would have on the results of the model without producing a complete shock model. It seems likely that incorporating a shock wave would increase the relative column density of CO through the reactions

$$CH^+ + O \rightarrow CO + H^+$$

$$C^+ + OH \rightarrow CO + H^+$$

and

$$CH_3^+ + O \rightarrow HCO^+ + H_2$$

followed by HCO^+ dissociative recombination.
The enhanced CH^+ abundance would also affect the abundance of CN through the ion-molecule reaction:

$$CH^+ + N \rightarrow CN + H^+$$

although the ion also effectively removes the radical through the reaction

$$CH^+ + CN \rightarrow C_2N^+ + H$$

There is other evidence to suggest that shock waves have affected the observed nebulae. The spatial and velocity distributions of the molecular gas in NGC 2346 and the fact the molecular cloud is highly disrupted suggests a strong interaction between the ionised and neutral envelopes. Vibrationally excited H_2 emission has been detected in the nebula (Zuckerman and Gatley 1988) and, when allowance is made for optical pumping of the molecule, this evidence strongly points to shock excitation of the gas. Vibrational excitation of H_2 and fragmentation of the gas cloud are predicted in the 'interacting winds' model of Kwok (1982).
Whereas the model predicts too little HCO^+, the probable reason being the omission of shock waves as outlined above, the column densities of the molecules CO, CN and C_2H relative to HCN are all much higher than observations. Since this trend is common to all the species a plausible explanation is that the modelled chemistry is producing too little HCN in relation to other species. The chemistry in the model is simplified in that formation of molecular species is assumed to occur entirely within the neutral envelope. The possibility exists however for molecules formed in the circumstellar envelope of the precursor AGB star to survive to the planetary nebula phase. This could occur through clumping of the gas which would enable greater effective shielding from photodissociation and would appear to be the most plausible explanation for the large [X]/[HCN] ratios predicted by the

Table 8.3
Molecular column densities relative to HCN in the PN NGC 6072 and the AGB star IRC+10°216

Species	[X]/[HCN]	
X	NGC 6072	IRC+10°216
CO	1181	50
CN	12.9	0.75
HCO^+	0.64	$\leq$0.0002
HNC	0.22	0.004
C_2H	<2.2	0.1

model.
Molecular observations of AGB stars reinforce this idea. Johansson *et al.* (1984) observed the AGB star IRC+10°216 and discovered that, in general, the molecular abundance ratios [X]/[HCN] were far lower than in PN neutral envelopes (by more than an order of magnitude) indicating a far greater relative abundance of HCN in the AGB circumstellar envelope as shown in Table 8.3. Observations of NGC 6072 by Cox *et al.* (1992) are shown for comparison.

There are two striking points evident from the data in the Table.

(i) The [X]/[HCN] ratio is substantially smaller in the AGB circumstellar gas than in the PN phase. The ratio is larger in the PN case by between one and two orders of magnitude (except for HCO^+, see below). Since the model predicts [X]/[HCN] ratios in the PN neutral region that are orders of magnitude too large this strongly suggests that there is some process occurring whereby the HCN in the AGB phase is being shielded from photodissociation and a large fraction is surviving to the PN phase. This does not negate the idea that formation of HCN occurs in the molecular region but it would seem unlikely that the abundance of CH_2^+ could be increased sufficiently to produce the required amounts of HCN via the reaction

$$CH_2^+ + N \rightarrow HCN^+ + H$$

followed by rapid charge exchange with H to form the neutral molecule.
The passage of a shock wave through the gas would tend to produce a greater abundance of CH_2^+ through CH^+/H_2 combination and hence produce an increased HCN production rate which ties in with the previous discussion on shock waves.

However it is difficult to see the production of CH_2^+ being increased sufficiently to account fully for the discrepancies between the predicted and observed [X]/[HCN] ratios.

The hypothesis that a substantial fraction of the neutral region exists in high density clumps capable of providing substantial shielding of molecules from photodissociation is supported by recent observations of neutral carbon in NGC 6720. Bachiller *et al.* (1994) observed the 609 μm ($^3P_1 \rightarrow ^3P_0$) fine structure line of CI in the planetary nebula. Comparison with CO observations of the nebula show that CI and CO have roughly similar spatial distributions with the ratio of the column densities $N(CI)/N(CO)$ ranging from 5 to 50 over the regions observed with a mean value of 10 (assuming a representative gas temperature of 100 K). Assuming that the molecular gas is in rough pressure equilibrium with the ionised gas these observations suggest that a large amount of the neutral material is compressed into clumps of density $\sim 10^5$ cm^{-3} immersed in the strong UV field of the central star.

(ii) The [HCO^+]/[HCN] ratio is much smaller in the case of the AGB circumstellar envelope, by more than three orders of magnitude and it is apparent that some physical/chemical process has occurred in the post-AGB object to increase dramatically the abundance of this molecular ion. As discussed above the most attractive explanation, based on the theoretical findings of Draine and Katz (1986), is that a shock wave has impinged on the interior of the molecular shell to increase the gas density and temperature in the wake of the shock and drive previously suppressed endothermic reactions. According to the models of Draine and Katz certain selected chemical species show marked increases in abundance in the wake of the shock, primarily CH^+, CH, OH and HCO^+.

The final point to address is the effect of the external interstellar radiation field on the nebular chemistry. Unlike shock waves and X-ray dissociation which are possible explanations for the observations, there is no question that the ISRF will have an effect on the nebular chemistry. The question is whether the effect is so substantial that omitting it in the model is a possible cause of the large discrepancies between prediction and observation.

The dissociating and ionising effect of the ISRF will have an important effect only in the very outermost section of the nebula. The intensity of the interstellar field in the UV is about four orders of magnitude weaker than the modelled spectrum from the central star incident on the neutral region and radiative transfer effects will quickly attenuate the incoming radiation. This spectrum of radiation will affect the chemistry in the nebula in a similar way to the central star spectrum, only

on a much reduced scale.

According to the theoretical work of van Dishoeck (1988) photoionisation and photodissociation rates of atoms and molecules typically have values of a few times 10^{-10} s^{-1} when exposed to the unattenuated interstellar radiation field (of e.g. Mathis *et al.* 1983). This then represents the photodissociation rate of a molecule at the very outermost edge of the nebula and will decrease with depth into the gas. Ion-molecule reactions between abundant species, occurring typically with a Langevin rate of $\sim 10^{-9}$ cm^3 s^{-1}, will thus tend to be more important than photoionisation and dissociation by the ISRF. For species where the chemistry is dominated by neutral exchange or other slow reactions exposure to the interstellar field will form a predominant part of the subsequent chemistry in the outermost region of the nebula.

Photodissociation by the ISRF would constitute the dominant destruction process for the two most important molecules, H_2 and CO. Near the outer edge of the nebula the ISRF would be much more intense than the outgoing central star spectrum. Fig. 8.4 shows the central star spectrum at an optical depth of $\tau_V = 2$ through the neutral region. It has already been attenuated by about two orders of magnitude from the intensity at $\tau_V = 0.5$ (Fig. 8.3) through dust absorption. The Mathis *et al.* (1983) ISRF has an intensity of approximately 5×10^{-17} erg cm^{-3} $Å^{-1}$ at 1000 Å, comparable with the envelope of the central star spectrum at $\tau_V = 2$. In the $n_H = 1000$ cm^{-3} model the outer edge of the cloud is situated at an optical depth of $\tau_V \approx 4.5$. At this optical depth it is obvious that the ISRF would be much stronger than the stellar field, although this extrapolation is not strictly valid since inclusion of the ISRF would cause the theoretical outer edge of the nebula to shift. However, inclusion of the ISRF would increase the optical depth of the outer edge because of the added effect of photodissociation of CO by the interstellar field and this would increase the dominance of the ISRF over the stellar field. It can thus be predicted with certainty that inclusion of the ISRF would decrease the abundance of these two molecules near the outer edge of the nebula, the effect being to return atomic hydrogen, carbon and oxygen into the gas.

The other molecules in the gas would similarly be affected by photodissociation by the ISRF. Photodissociation of CN is the dominant destruction route for the molecule throughout the nebula (§8.1) and inclusion of the ISRF would simply increase the rate of removal of the molecule. However, the results of van Dishoeck (1988) suggest that the photodissociation rate of CN in the unattenuated ISRF is several times smaller than the rate for HCN. Combining this with the fact that the CN photodissociation rate falls off more steeply with optical depth than HCN

means that inclusion of the ISRF is more likely to increase the final [CN]/[HCN] column density ratio, all other factors remaining static. The model in its present form predicts a [CN]/[HCN] ratio more than two orders of magnitude larger than observations of NGC 6072 and IC 4406 (Figs. 8.31 and 8.32 respectively). It is apparent that inclusion of the interstellar field would increase this discrepancy. The unattenuated photodissociation rate of HCN by the interstellar field is in fact so large (a value of 1.1×10^{-9} s^{-1} using the Mathis *et al.* ISRF is quoted by van Dishoeck with a possible factor of two uncertainty) that even molecules where the rate falls off less steeply than HCN are likely to exhibit an increased [X]/[HCN] ratio because the unattenuated rate is so much smaller. For example, in the case of C_2H, the unattenuated rate is more than three times smaller than the rate for HCN. Although the C_2H rate falls off less steeply it is still predicted to be smaller than the HCN rate after one magnitude of visual extinction and thus this crude analysis would suggest that the [C_2H]/[HCN] ratio would also increase thus exacerbating the already large discrepancy (Figs. 8.31 and 8.32).

8.3 Alternative models

The 'standard' model described in this thesis makes the assumption that the dust grains are composed of amorphous carbon with corresponding optical properties. This section examines results obtained by making the alternative assumption that the dust in the nebula is entirely composed of graphite, with considerably different UV absorption properties. The 'standard' model also does not take into account attenuation of the radiation field incident on the neutral region through absorption by dust in the ionised region. It is not possible to analyse this problem accurately as it has not been the purpose of this project to model the characteristics of the ionised region. Instead, to examine the general effects of utilising an initially attenuated field, the incident field described in §2.1 is simply reduced by an order of magnitude over the entire spectrum and the subsequent relative column densities are inspected for the two cases of amorphous carbon and graphitic dust in the neutral region.

8.3.1 Graphite grain model

The characteristics of 'standard' interstellar graphite grains were assumed. Values of τ_λ/τ_V (§7.2) for the case of graphite particles were derived from Mathis *et al.* (1983) and are reproduced in Table 8.4.

Table 8.4
Relative extinction for the case of graphite particles

Wavelength λ (Å)	τ_λ/τ_V	Wavelength λ (Å)	τ_λ/τ_V
910	4.10	2100	2.84
1000	3.40	2160	3.10
1300	1.84	2300	2.90
1430	1.48	2500	2.26
1800	1.73	3460	1.40
2000	2.42	4350	1.21

The characteristics of UV absorption by graphite - increasing τ_λ/τ_V with increasing frequency in the far ultraviolet and the 'peak' in absorption at around $\lambda = 2200$Å

are all evident from the data in the Table.

A comparison with Table 7.2 will quickly show that there is far greater relative extinction in the ultraviolet for the graphite case than for amorphous grains. Hence using the optical properties of graphite will mean that photoionisation and dissociation rates will decrease far more rapidly and will become negligible at a much smaller optical depth. Whereas carbon is in ionised form throughout almost the entire nebula with amorphous carbon grains (Fig. 8.8), the increased relative extinction in the UV afforded by graphite grain modelling means that the transition to neutral carbon will occur at a much lower optical depth with important consequences for the chemistry in the gas.

The values of τ_λ/τ_V reported by Mathis *et al.* are modelled mathematically as follows (where λ is in Å):

For 910 Å $< \lambda <$ 2160 Å:

$$\tau_\lambda/\tau_V = m_0 + m_1\lambda + m_2\lambda^2 + m_3\lambda^3 + m_4\lambda^4$$

where

$m_0 = 10.867$

$m_1 = -1.2465 \times 10^{-3}$

$m_2 = -1.4743 \times 10^{-5}$

$m_3 = 1.0441 \times 10^{-8}$

$m_4 = -1.9068 \times 10^{-12}$

For 2160 Å $\leq \lambda <$ 3500 Å:

$$\tau_\lambda/\tau_V = 5.935 - 1.3107 \times 10^{-3}\lambda$$

To relate linear distance through the nebula with optical depth the following standard interstellar parameters were assumed (see e.g. Spitzer 1978).

Relating amount of hydrogen to selective extinction (hence amount of dust):

$$\frac{N_{\rm H}}{E_{B-V}} = 5.8 \times 10^{21}\ {\rm cm}^{-2}\ {\rm mag}^{-1}$$

Ratio of total to selective extinction:

$$\frac{{\rm A}_V}{E_{B-V}} = 3.0$$

Since visual extinction and optical depth are related by the formula

$$\frac{A_V}{\tau_V} = 2.5 \log_{10} e$$

then, for standard interstellar grains, distance and optical depth are related by:

$$d\,(\mathrm{cm}) = \frac{2.099 \times 10^{21}}{n_{\mathrm{H}}\,(\mathrm{cm}^{-3})} \tau_V$$

Thus, for a constant hydrogen nuclei number density model (as here), linear distance is directly proportional to optical depth similar to the amorphous carbon grain model (§7.2).

For species with known (or estimated) photoionisation cross-section the different photoionisation rates will be automatically calculated correctly via the appropriate integral (equation (3.3)) since the attenuation of the radiation field $\Phi(\lambda)$ is calculated assuming optical properties of graphite. For species with unknown cross-section the photoionisation or dissociation rate is described by the formula (§3.2.1.1):

$$\zeta\,(\mathrm{s}^{-1}) = \gamma(r)\zeta_0 \exp(-\beta\tau_V)$$

The values of β appropriate for attenuation by amorphous carbon grains will not apply if the optical properties of the dust change radically, as they do when considering graphite. In general the values of β will be much higher for the case of graphite grains because dissociation and ionisation occur primarily through absorption in the ultraviolet and graphite grains produce a far higher relative extinction in the UV than the non-crystalline form. The values of β assumed for a graphite grain model were taken from van Dishoeck (1988) appropriate for optical properties of interstellar grains (computed adopting grain model 2 of Roberge *et al.* 1981). These values of β are invariably larger than the corresponding values for amorphous carbon by factors of about two to three.

Formation of molecular hydrogen is assumed to occur uniquely on the surface of dust grains (§3.2.2.1). If the physical properties of the dust change then it is inevitable that the crucial rate of formation of H_2 will also change. If the mean grain radius is still assumed to be $r_d = 100$ nm and that the sticking coefficient γ is unity then the two factors which will affect the rate are Υ, the ratio of dust mass to gas mass per unit volume, and ρ_d, the mass density of the grain material. For graphite $\rho_d = 2.3$ g cm^{-3} (compared to 1.8 g cm^{-3} for amorphous carbon).

Since interstellar graphite grains are assumed with the 'standard' interstellar relationship between $N_{\rm H}$ and E_{B-V} (see above) it would be inconsistent to utilise a value of Υ that differs from the canonical value for the ISM. As discussed in §7.1.1 this means that a value of $\Upsilon = 0.006$ is assumed for the graphite grain model. With these changed parameters the rate of formation of molecular hydrogen on dust grains becomes (§3.2.2.1):

$$\left(\frac{dn(\mathrm{H_2})}{dt}\right)_{\rm grain} = 3.31 \times 10^{-18} n_{\rm H} n(\mathrm{H}) T^{1/2} \ \mathrm{cm^{-3}\ s^{-1}}$$

For simplification the assumptions about the way the formation energy of H_2 (4.5 eV) is divided among the possible channels, and among the internal modes of the ejected molecule have not been changed (§4.1.1).

The results of running this graphite grain model of a PN neutral envelope with a constant hydrogen nuclei number density of $n_{\rm H} = 1000\ \mathrm{cm^{-3}}$ are shown below. As before, the outer edge of the nebula is assumed to have been reached when the column density of CO is approximately $3.8 \times 10^{15}\ \mathrm{cm^{-2}}$ (§8.1).

Table 8.5

Relative molecular column densities for a graphite grain model with $n_{\rm H} = 1000\ cm^{-3}$

Species X	x=[X]/[HCN]	$\log_{10} x + 12$	y=[X]/[CO]	$\log_{10} y + 12$
H	3.43 (10)	22.53	6.76 (5)	17.83
H_2	2.64 (10)	22.42	5.21 (5)	17.72
CO	5.07 (4)	16.70	1	12
CS	3.90 (3)	15.59	7.69 (-2)	10.89
CN	1.71 (3)	15.23	3.36 (-2)	10.53
C_2H	1.04 (2)	14.02	2.04 (-3)	9.310
C_3H_2	9.45 (-2)	10.98	1.86 (-6)	6.270
NH_3	9.00 (-5)	7.954	1.77 (-9)	3.249
HCN	1	12	1.97 (-5)	7.295
HNC	1.78 (-1)	11.25	3.51 (-6)	6.545
HCO^+	8.88 (-3)	9.948	1.75 (-7)	5.243
N_2H^+	9.29 (-8)	4.968	1.83 (-12)	0.2631

$n_H = 1000$ cm^{-3}

Distance from star of inner edge of neutral shell:	1.835×10^{17} cm
Distance from star of outer edge of neutral shell:	6.412×10^{18} cm
Total visual extinction of neutral shell:	$A_V = 2.28$ mag
Total column density of hydrogen nuclei:	6.229×10^{21} cm^{-2}

Comparing these results with the observed values in Figs. 8.31 to 8.34 the conclusion is quickly reached that using the physical and optical properties of graphite produces no better agreement than using amorphous carbon characteristics. For some relative column densities, e.g. [HCO^+]/[HCN] the disagreement is substantially worse. It is apparent that the large discrepancy between prediction and observation is not even partially resolved by adopting grain characteristics of crystalline carbon.

8.3.2 Amorphous carbon grains/initially attenuated field

The 'standard' model described in this thesis makes no attempt to take into account attenuation of the radiation field by dust in the ionised region, prior to impinging on the neutral envelope. The UV field energy density employed actually represents an upper limit to an actual spectrum that would exist at the ionised/neutral interface, given the central star parameters and chemical composition of the gas. To take this initial attenuation (crudely) into account the incident field is reduced by an order of magnitude over the entire spectrum to see if this produces an improvement in agreement with the observations.

The hydrogen nuclei number density was $n_H = 1000$ cm^{-3} and the run was terminated when the column density of CO reached 3.8×10^{15} cm^{-2}, as before. The grain characteristics used were those of amorphous carbon as in the 'standard' model. The results are shown in Table 8.6.

Comparing these results with Figs. 8.31 to 8.34 it is apparent that using an initially attenuated radiation spectrum produces a negligible change in the final relative molecular column densities.

$n_H = 1000$ cm^{-3}

Distance from star of inner edge of neutral shell:	1.835×10^{17} cm
Distance from star of outer edge of neutral shell:	7.079×10^{18} cm
Total visual extinction of neutral shell:	$A_V = 3.26$ mag
Total column density of hydrogen nuclei:	6.896×10^{21} cm^{-2}

Table 8.6

Relative molecular column densities for an amorphous carbon grain model and an attenuated incident radiation field with $n_H = 1000\ cm^{-3}$

Species X	x=[X]/[HCN]	$\log_{10} x + 12$	y=[X]/[CO]	$\log_{10} y + 12$
H	1.86 (10)	22.27	5.79 (5)	17.76
H_2	2.62 (10)	22.42	8.13 (5)	17.91
CO	3.22 (4)	16.51	1	12
CS	5.67 (2)	14.75	1.76 (-2)	10.25
CN	3.58 (3)	15.55	1.11 (-1)	11.05
C_2H	3.30 (2)	14.52	1.02 (-2)	10.01
C_3H_2	2.52 (-1)	11.40	7.83 (-6)	6.894
NH_3	2.77 (-5)	7.443	8.61 (-10)	2.935
HCN	1	12	3.10 (-5)	7.492
HNC	1.41 (-1)	11.15	4.38 (-6)	6.642
HCO^+	2.63 (-2)	10.42	8.15 (-7)	5.911
N_2H^+	5.97 (-8)	4.776	1.85 (-12)	0.2676

8.3.3 Graphite grains/initially attenuated field

In the same vein as the model described in §8.3.2 an incident field attenuated by one order of magnitude was employed using grain characteristics of graphite as in §8.3.1. A combination of these two factors means that the UV field, initially attenuated, will be rapidly weakened by the large relative extinction afforded by graphite grains in the ultraviolet so that at any given optical depth this particular model will exhibit the weakest radiation energy spectrum at a given wavelength. Hence photoionisation and dissociation will quickly become ineffective in the nebula and since the outer edge of the cloud is assumed to have been reached at a fixed column density of CO, this means the total optical depth of the neutral shell will be very small.

The hydrogen nuclei number density was $n_H = 1000\ cm^{-3}$ and the run was terminated when $N(CO)$ reached $3.8 \times 10^{15}\ cm^{-2}$. The results of the model are shown in Table 8.7.

$n_H = 1000\ cm^{-3}$

Distance from star of inner edge of neutral shell:	1.835×10^{17} cm
Distance from star of outer edge of neutral shell:	4.437×10^{18} cm
Total visual extinction of neutral shell:	$A_V = 1.63$ mag
Total column density of hydrogen nuclei:	$4.254 \times 10^{21}\ cm^{-2}$

Table 8.7

Relative molecular column densities for a graphite grain model and an attenuated incident radiation field with $n_H = 1000\ cm^{-3}$

Species X	x=[X]/[HCN]	$\log_{10} x + 12$	y=[X]/[CO]	$\log_{10} y + 12$
H	2.35 (10)	22.37	4.75 (5)	17.68
H_2	2.27 (10)	22.36	4.58 (5)	17.66
CO	4.94 (4)	16.69	1	12
CS	6.81 (3)	15.83	1.38 (-1)	11.14
CN	2.22 (3)	15.35	4.49 (-2)	10.65
C_2H	1.69 (2)	14.23	3.42 (-3)	9.534
C_3H_2	1.86 (-1)	11.27	3.77 (-6)	6.576
NH_3	6.23 (-5)	7.794	1.26 (-9)	3.100
HCN	1	12	2.02 (-5)	7.306
HNC	1.51 (-1)	11.18	3.05 (-6)	6.484
HCO^+	1.26 (-2)	10.10	2.55 (-7)	5.407
N_2H^+	6.68 (-8)	4.825	1.35 (-12)	0.1309

Comparing these results with Figs. 8.31 to 8.34 it can be seen that the [CN]/[HCN] and [C_2H]/[HCN] ratios have been marginally reduced towards the observational values of NGC 6072 and IC 4406, but nothing like the amount required to achieve even partial agreement. The [HCO^+]/[HCN] ratio has also been decreased and has thus moved further away from the ratio derived from observation of the two nebulae. Employing a graphite grain model with an initially attenuated radiation spectrum has not produced any notable improvement between model results and observation.

8.4 Conclusion

This thesis has described the theoretical basis for a computer model of the neutral region of planetary nebula. Rather than adopting the goal of attempting to model and reproduce accurately the molecular abundances in one particular nebula, the alternative approach of trying to model a 'typical' carbon-rich PN neutral envelope has been the underlying thought behind the project. The model inevitably rests on a certain amount of assumption, whenever possible the assumptions being wholly or partly justified by reference to observation or experiment. Because the model utilises results produced by a model of the ionised region of a planetary nebula (Stasińska, private communication) some parameters are constrained to certain values to avoid inconsistency and these include the central star temperature and the chemical composition of the gas. All other parameters are flexible and open to debate; the most likely values have been chosen based on existing evidence.

There are still many questions about PNe that remain unanswered and so a certain amount of speculation is involved in constructing such a model. The exact composition and optical properties of dust grains in the neutral region is by no means decided. In a carbon-rich environment the grains will presumably be carbon-rich but this could manifest itself as amorphous or crystalline in form. Much more likely is that there is a mixture of the two with other materials being present (e.g. silicates, ice) with a complex array of sizes and shapes. Nor are more exotic forms of carbonaceous dust ruled out. e.g. fullerenes (C_{60}). With such a fundamental issue being undecided the obvious procedure was to run the model employing both crystalline (graphite) and amorphous particle properties and analyse any differences in the predicted molecular abundances.

Observations of the PNe NGC 6072, IC 4406, NGC 7027 and NGC 2346 (Cox *et al.* 1992; Thronson and Bally 1986; Cox *et al.* 1987; Bachiller *et al.* 1989) have enabled relative molecular column densities in these nebulae to be estimated. Deducing column densities from observation of molecular line intensities is a procedure that itself requires certain assumptions to be made. It is in general not possible to determine both $T_{\rm gas}$ and $n(H_2)$ from a calculation of line intensity ratios (e.g. the rotational lines of CO), and thus one must be estimated to fix a value for second parameter. Bachiller *et al.* (1989) estimate a gas temperature of 100 K in the molecular envelope of NGC 2346 which, from their observations, fixes $n(H_2) = 1500$ cm^{-3}, the argument being that temperatures more than about 100 K in the neutral shell would seem unreasonable. Having to estimate nebular parameters in this manner means that there is considerable uncertainty in the calculated column densities. The uncertainties are reduced as much as possible by,

for example, quoting column densities relative to the column density of a molecule (e.g. HCN) because these are insensitive to the assumed model for the species of interest (Cox *et al.* 1992). It should be borne in mind however that values of relative column densities derived from observation also exhibit intrinsic uncertainty.
Relative molecular column densities predicted by this model of a carbon-rich neutral shell of a PN in general show very poor agreement with values derived from observations of the C-rich nebula NGC 7027 and the probably C-rich nebulae NGC 6072, IC 4406 and NGC 2346. Uncertainties in the column densities derived from observation cannot explain the large discrepancies that are seen to exist.
A 'standard' model of a nebula was described in the thesis with a central star temperature of 10^5 K, a He/H ratio of 0.1 and a C/O ratio of 1.75. Dust grains were assumed to be pure carbon and amorphous in nature with a mean size and dust/gas ratio derived from observations of PNe and the interstellar medium. A constant hydrogen nuclei number density was assumed but with the radiation field being diluted in a $1/r^2$ manner as well as being attenuated through line absorption by H, H_2 and CO and continuum absorption by the dust. The size of the nebula was determined by constraining the column density of CO to match the column density of CO derived from observation of the PN NGC 2346 (Bachiller *et al.* 1989).
Predicted column densities, relative to $N(\mathrm{HCN})$ or $N(\mathrm{CO})$, in general show very poor agreement with values derived from observation of the nebulae NGC 6072, IC 4406, NGC 7027 and NGC 2346 (Figs. 8.31 to 8.34 respectively). An exception is the predicted ratio $N(\mathrm{HNC})/N(\mathrm{HCN})$ which shows good agreement with observation and $N(\mathrm{N_2H^+})/N(\mathrm{HCN})$, $N(\mathrm{NH_3})/N(\mathrm{CO})$ and $N(\mathrm{C_3H_2})/N(\mathrm{CO})$ which fall below the upper limits imposed by observation. $N(\mathrm{HCO^+})/N(\mathrm{HCN})$ falls below the observed value consistently by a factor of a few and the trend with all other species is to predict values far in excess of observation. The discrepancy with $N(\mathrm{CO})/N(\mathrm{HCN})$ is always greater than an order of magnitude and other species exhibit a greater difference between prediction and observation. $N(\mathrm{CN})/N(\mathrm{HCN})$ exceeds observation of NGC 6072 and IC 4406 by more than two orders of magnitude and $N(\mathrm{C_2H})/N(\mathrm{HCN})$ exceeds the upper limit imposed on this ratio by observation of the two nebulae by about two orders of magnitude. A similar scenario is seen for the case of NGC 7027 where $N(\mathrm{CN})/N(\mathrm{CO})$, $N(\mathrm{CS})/N(\mathrm{CO})$ and $N(\mathrm{C_2H})/N(\mathrm{CO})$ all exceed the upper limits imposed by observation, by as much as three orders of magnitude in the case of CN.
To see if these large discrepancies are caused in part by assumptions in the model alternative physical conditions were imposed relating to the composition and attenuating effect of dust grains. Graphite grains produce a steep extinction curve

$E(\lambda, V)$ in the ultraviolet that rises with increasing frequency (Spitzer 1978) as opposed to the rather flat extinction curve of amorphous carbon derived from values of refractive index reported in the literature (Williams and Arakawa 1972; Duley 1984). A model was thus produced assuming pure carbon grains with a graphitic composition. Due to the much larger extinction in the UV such a model predicts photoionisation and dissociation rates that fall off much more rapidly with optical depth τ_V. The rate of production of molecular hydrogen is also affected since the molecule is believed to be formed uniquely on the surface of dust grains with a rate that depends on the density of the grains material as well as other dust related variables (§8.3).

An omission in the 'standard' model is attenuation of the outgoing stellar UV flux by dust grains in the ionised region of the nebula. To see if such initial attenuation of the radiation field would produce significant differences in predicted relative molecular abundances models were constructed where the energy density of the UV flux incident on the neutral region is reduced by an order of magnitude. The results of this, employing both amorphous and graphite dust grain models in the neutral region, were examined.

In all these alternative model scenarios the predicted relative column densities at best produce a very small improvement in agreement with observation for some species, usually offset by a deterioration in agreement with other species. It is obvious that even using radically different grain absorbing properties the models produce no better agreement with observation. The source of the large discrepancies lies at a much more fundamental level of the physics being modelled.

It could be argued that, even in planetary nebulae with similar chemical compositions, the inherently unpredictable nature of gas clumping coupled with differences in star temperature, possible shock wave structure and previous stellar history would mean that molecular abundances would differ by a large extent. If this were true then comparison of the results of this model with observation would be little more than meaningless. However, the evidence is that a very similar chemistry seems to operate in different PNe to produce very similar relative molecular column densities. Figs. 8.31, 8.32 and 8.34 show molecular column densities relative to N(HCN) in the PNe NGC 6072, IC 4406 and NGC 2346. Although there are obvious differences between the observations, e.g. N(HNC)/N(HCN) is a factor of a few higher in NGC 2346 than in the other two nebulae, the similarities in the derived molecular abundances are striking. This leads one to believe that very similar physics and chemistry operate in the different nebulae and that it is thus possible to construct a model to predict abundances in a 'typical' C-rich nebula.

The observations of large $N(HCO^+)/N$(HCN) ratios (relative to the model results)

would seem to necessitate the idea of shock waves affecting the nebular gas. According to the work of Draine and Katz (1986) the abundance of this molecular ion is greatly increased by the passage of a shock wave, the amount of increase obviously depending on the structure and speed of the shock. The shock wave causes a sharp increase in the gas temperature allowing the endothermic reaction

$$C^+ + H_2 \rightarrow CH^+ + H - 0.39\ eV$$

to proceed efficiently.

Due to the values of their ionisation potentials relative to H, carbon is primarily in ionised and oxygen primarily in neutral form so that after the above reaction HCO^+ can form rapidly via

$$CH^+ + H_2 \rightarrow CH_2^+ + H$$

followed by

$$CH_2^+ + O \rightarrow HCO^+ + H$$

or

$$CH_2^+ + H_2 \rightarrow CH_3^+ + H$$

$$CH_3^+ + O \rightarrow HCO^+ + H_2$$

occurring with Langevin rates of about 10^{-9} cm^3 s^{-1}.

Other species show a $N(X)/N(HCN)$ greatly in excess of observation and with too little carbon being locked up in CO (Fig. 8.33). The most attractive explanation for the disagreement is that a large amount of HCN, originally in the AGB phase of the star, has survived photodissociation during the transition to the evolved planetary nebula and the HCN observed is mostly a relic from the previous phase of stellar evolution. This implies a large extinction for the molecular gas brought about presumably by structural inhomogeneities in the expanding nebula. The model assumes no survival of molecular species from the AGB phase to the PN phase; this assumption appears to be wrong in the light of analysis of the results. This idea is supported by molecular observation of stars in the AGB phase. Observations by Johansson *et al.* (1984) of IRC+10°216 showed that there was much more HCN in the stellar envelope, relative to other species, than in the molecular envelopes of evolved PNe (§8.3). If molecular survival through the transition phase to PN is true then, even if very little reformation of HCN occurs in the planetary nebula compared to other species, observed $N(X)/N(HCN)$ ratios in PNe are more

explicable than trying to invoke sufficient production of the molecule from scratch through reactions involving, for example, CH_2^+ and N to form HCN^+ (equation (8.39)), followed by charge exchange with hydrogen.

It would seem to be a very interesting possible future project to build on the model described in this thesis and incorporate the physics and chemistry that this model seems to be lacking. Investigating the effect of substantial *initial* molecular abundances at the ionised/neutral interface and the effects of the passage of a shock wave through the gas are suggested by this work as the primary aspects to be followed up. There are also other aspects which, although seemingly of secondary importance, may prove to have influence on the results. Including the dissociating and ionising effect of the general interstellar radiation field on the exterior section of the nebula is a difficult problem to tackle as it would involve solution of the radiative transfer equation in two directions simultaneously. However, perhaps by using some sort of 'self-consistent' method, the difficulties in including this omission in the physics can presumably be overcome.

Including a more realistic gas density function $n_{\rm H}(r)$ is an obvious question to address in future enhancements to the model; the incorporation within this scenario of the effects of clumping of the gas also raises interesting possibilities. One can envisage a gas density function $n_{\rm H}(r) + \Delta n_{\rm H}$ where $\Delta n_{\rm H}$ is a perturbation to the function that depends on the local environment within the nebula.

This thesis has shown that an unshocked model of an initially fully atomic gas is insufficiently complex to account for observations of molecular column densities in carbon-rich planetary nebulae. Recommendations for future work have been outlined based on the findings of this project and hopefully these will be implemented by future researchers in the field.

Planetary nebulae remain enigmatic objects with many questions about their internal workings still lying unanswered. This project has hopefully achieved its goal of shedding a little more light on the answers and provides a basis for future PN modelling whereby, hopefully, all the answers about these curious objects may ultimately be illuminated.

Appendix A

Chemical species in the model

Species	Initial abundance (relative to H)	Specific enthalpy	
h	9.97 (-01)	51.63	
h2	1.00 (-12)	0.00	
he	1.00 (-01)	0.00	
c	1.00 (-12)	169.98	
ch	1.00 (-12)	141.60	
ch2	1.00 (-12)	93.90	
ch3	1.00 (-12)	34.80	
ch4	1.00 (-12)	-15.97	
o	4.00 (-04)	58.98	
o2	1.00 (-12)	0.00	
oH	1.00 (-12)	9.25	
h2o	1.00 (-12)	-57.10	
co	1.00 (-12)	-27.20	
co2	1.00 (-12)	-93.97	
c2	1.00 (-12)	198.20	
c3	1.00 (-12)	194.00	
c2h	1.00 (-12)	113.30	
c2h2	1.00 (-12)	54.32	
c3h	1.00 (-12)	126.00	***
c3h2	1.00 (-12)	26.00	***
n	2.00 (-04)	112.53	
nh	1.00 (-12)	85.40	
nh2	1.00 (-12)	45.90	
nh3	1.00 (-12)	-9.34	
cn	1.00 (-12)	103.20	
hco	1.00 (-12)	0.00	***
hcn	1.00 (-12)	32.39	
hnc	1.00 (-12)	48.00	
n2	1.00 (-12)	0.00	
no	1.00 (-12)	21.45	
s	1.00 (-12)	65.60	
sh	1.00 (-12)	32.60	

h2s	1.00 (-12)	-4.23	
cs	1.00 (-12)	63.00	
so	1.00 (-12)	1.20	
so2	1.00 (-12)	-70.30	
ocs	1.00 (-12)	-34.00	
fe	1.00 (-12)	98.70	
h+	3.00 (-03)	365.20	
h2+	1.00 (-12)	355.70	
h3+	1.00 (-12)	265.00	
he+	1.00 (-12)	567.00	
heh+	1.00 (-12)	500.00	***
c+	7.00 (-04)	429.70	
ch+	1.00 (-12)	387.00	
ch2+	1.00 (-12)	331.00	
ch3+	1.00 (-12)	262.00	
ch4+	1.00 (-12)	275.00	**
ch5+	1.00 (-12)	216.00	
o+	1.00 (-12)	373.00	
oh+	1.00 (-12)	309.00	
o2+	1.00 (-12)	278.40	
h2o+	1.00 (-12)	233.70	
h3o+	1.00 (-12)	143.00	
co+	1.00 (-12)	295.97	
hco+	1.00 (-12)	197.30	*
c2+	1.00 (-12)	476.00	
c2h+	1.00 (-12)	404.00	
c2h2+	1.00 (-12)	317.50	
c2h3+	1.00 (-12)	267.90	
c3+	1.00 (-12)	479.00	*
c3h+	1.00 (-12)	381.00	*
c3h2+	1.00 (-12)	281.00	**
c3h3+	1.00 (-12)	257.00	**
n+	1.00 (-12)	447.70	
nh+	1.00 (-12)	401.10	
nh2+	1.00 (-12)	302.70	
nh3+	1.00 (-12)	224.90	
nh4+	1.00 (-12)	151.00	*
cn+	1.00 (-12)	429.30	

c2n+	1.00 (-12)	387.00	**
hcn+	1.00 (-12)	346.00	
hco2+	1.00 (-12)	141.00	*
h2cn+	1.00 (-12)	226.00	*
h2nc+	1.00 (-12)	265.00	*
n2+	1.00 (-12)	359.30	
n2h+	1.00 (-12)	247.50	*
no+	1.00 (-12)	235.18	
hno+	1.00 (-12)	256.80	
s+	1.00 (-05)	304.00	
sh+	1.00 (-12)	271.80	
h2s+	1.00 (-12)	237.00	
h3s+	1.00 (-12)	190.00	
cs+	1.00 (-12)	324.00	
hcs+	1.00 (-12)	243.00	
so+	1.00 (-12)	239.20	
hso+	1.00 (-12)	0.00	***
hocs+	1.00 (-12)	181.00	
fe+	3.00 (-07)	280.24	
h-	1.00 (-12)	0.00	***

enthalpies of formation are in kcal/mol in standard state (298 K, 1 atm. pressure)

(*) measured at 300 K
(**) most stable isomer
(***) enthalpy unknown

Note: a (b) implies a $\times 10^{b}$

Appendix B

Chemical reaction set

reaction					gamma	alpha	beta
1. H2 formation on grains							
h	+h	=h2	-		2.44(-17)	0.50	
2. CRP interactions							
h	+crp	=h+	electr	-	4.60(-01)		
he	+crp	=he+	electr		5.00(-01)		
c	+crp	=c+	electr		1.80(+00)		
o	+crp	=o+	electr		2.80(+00)		
n	+crp	=n+	electr		2.10(+00)		
h2	+crp	=h+	h-		3.00(-04)		
h2	+crp	=h+	h	electr	2.20(-02)		
h2	+crp	=h	h		1.00(-01)		
h2	+crp	=h2+	electr		9.30(-01)		
ch	+crp	=c	h		1.46(+03)		
co	+crp	=co+	electr		3.00(+00)		
co	+crp	=c	o		1.82(+02)		
cn	+crp	=c	n		2.12(+04)		
c2	+crp	=c	c		4.74(+02)		
oh	+crp	=o	h		1.02(+03)		
o2	+crp	=o2+	electr		2.34(+02)		
o2	+crp	=o	o		1.50(+03)		
no	+crp	=n	o		9.64(+02)		
no	+crp	=no+	electr		9.88(+02)		
hcn	+crp	=cn	h		6.23(+03)		
hnc	+crp	=cn	h		6.23(+03)		
h2o	+crp	=oh	h		1.94(+03)		

```
h2s     +crp    =s       h2          1.03(+04)
h2s     +crp    =h2s+    electr      3.39(+03)
co2     +crp    =co      o           3.42(+03)
c2h     +crp    =c2      h           8.16(+03)
c3      +crp    =c2      c           2.24(+03)
ocs     +crp    =co      s           1.07(+04)
nh2     +crp    =nh      h           1.60(+02)
nh2     +crp    =nh2+    electr      1.30(+03)
so2     +crp    =so      o           1.77(+03)
c2h2    +crp    =c2h     h           1.03(+04)
c2h2    +crp    =c2h2+   electr      2.62(+03)
c3h     +crp    =c3      h           8.16(+03)
nh3     +crp    =nh2     h           2.63(+03)
nh3     +crp    =nh      h2          1.08(+03)
nh3     +crp    =nh3+    electr      1.15(+03)
ch4     +crp    =ch3     h           4.68(+03)
c3h2    +crp    =c3h     h           8.16(+03)
ch+     +crp    =c       h+          3.52(+02)
                    -
-------------------------------------------
3. ion-molecule reactions
-------------------------------------------
                    -
-------------------------------------------
3.i monatomic ions
-------------------------------------------
                    -
h+      +sh     =s+      h2          1.60(-09)  0.00     0.0
h+      +hco    =co+     h2          9.40(-10)  0.00     0.0
h+      +hco    =h2+     co          9.40(-10)  0.00     0.0
h+      +hcn    =h+      hnc         1.00(-09)  0.00  7850.0
h+      +hnc    =h+      hcn         1.00(-09)  0.00     0.0
h+      +ch2    =ch+     h2          1.40(-09)  0.00     0.0
h+      +co2    =hco+    o           4.20(-09)  0.00     0.0
h+      +c2h    =c2+     h2          1.50(-09)  0.00     0.0
h+      +ocs    =sh+     co          5.90(-09)  0.00     0.0
h+      +c2h2   =c2h+    h2          2.00(-09)  0.00     0.0
h+      +c3h    =c3+     h2          2.00(-09)  0.00     0.0
```

h+	+ch4	=ch3+	h2		2.28(-09)	0.00	0.0
h+	+c3h2	=c3h+	h2		2.00(-09)	0.00	0.0
he+	+h2	=h+	h	he	1.10(-13)	-.24	0.0
he+	+ch	=c+	h	he	1.10(-09)	0.00	0.0
he+	+co	=c+	o	he	1.50(-09)	0.00	0.0
he+	+cn	=c+	n	he	8.80(-10)	0.00	0.0
he+	+cn	=n+	c	he	8.80(-10)	0.00	0.0
he+	+cs	=c+	s	he	1.30(-09)	0.00	0.0
he+	+cs	=s+	c	he	1.30(-09)	0.00	0.0
he+	+c2	=c+	c	he	1.60(-09)	0.00	0.0
he+	+oh	=o+	h	he	5.50(-10)	0.00	0.0
he+	+o2	=o+	o	he	1.00(-09)	0.00	0.0
he+	+nh	=n+	h	he	1.10(-09)	0.00	0.0
he+	+no	=n+	o	he	1.38(-09)	0.00	0.0
he+	+no	=o+	n	he	2.24(-10)	0.00	0.0
he+	+n2	=n+	n	he	7.92(-10)	0.00	0.0
he+	+sh	=s+	h	he	1.70(-09)	0.00	0.0
he+	+so	=o+	s	he	8.30(-10)	0.00	0.0
he+	+so	=s+	o	he	8.30(-10)	0.00	0.0
he+	+hco	=co+	h	he	4.90(-10)	0.00	0.0
he+	+hco	=ch+	o	he	4.90(-10)	0.00	0.0
he+	+hco	=heh+	co		3.00(-10)	0.00	0.0
he+	+hcn	=cn+	h	he	1.46(-09)	0.00	0.0
he+	+hcn	=ch+	n	he	6.20(-10)	0.00	0.0
he+	+hcn	=c+	nh	he	7.75(-10)	0.00	0.0
he+	+hcn	=n+	ch	he	2.48(-10)	0.00	0.0
he+	+hnc	=cn+	h	he	1.55(-09)	0.00	0.0
he+	+hnc	=c+	nh	he	1.55(-09)	0.00	0.0
he+	+h2o	=oh+	h	he	2.30(-10)	-.94	0.0
he+	+h2o	=h+	oh	he	1.64(-10)	-.94	0.0
he+	+h2s	=s+	h2	he	3.60(-09)	0.00	0.0
he+	+h2s	=sh+	h	he	4.80(-10)	0.00	0.0
he+	+ch2	=c+	h2	he	7.50(-10)	0.00	0.0
he+	+ch2	=ch+	h	he	7.50(-10)	0.00	0.0
he+	+co2	=co+	o	he	7.70(-10)	0.00	0.0
he+	+co2	=o+	co	he	1.80(-10)	0.00	0.0
he+	+co2	=c+	o2	he	4.00(-11)	0.00	0.0
he+	+c2h	=c+	ch	he	5.10(-10)	0.00	0.0

he+	+c2h	=ch+	c	he		5.10(-10)	0.00	0.0
he+	+c2h	=c2+	h	he		5.10(-10)	0.00	0.0
he+	+ocs	=cs+	o	he		7.60(-10)	0.00	0.0
he+	+ocs	=s+	co	he		7.60(-10)	0.00	0.0
he+	+ocs	=co+	s	he		7.60(-10)	0.00	0.0
he+	+ocs	=o+	cs	he		7.60(-11)	0.00	0.0
he+	+nh2	=nh+	h	he		8.00(-10)	0.00	0.0
he+	+nh2	=n+	h2	he		8.00(-10)	0.00	0.0
he+	+so2	=s+	o2	he		8.60(-10)	0.00	0.0
he+	+so2	=so+	o	he		3.44(-09)	0.00	0.0
he+	+so2	=o2+	s	he		7.90(-10)	0.00	0.0
he+	+ch3	=ch+	h2	he		9.00(-10)	0.00	0.0
he+	+ch3	=ch2+	h	he		9.00(-10)	0.00	0.0
he+	+c2h2	=ch+	ch	he		7.70(-10)	0.00	0.0
he+	+c2h2	=c2+	h2	he		1.61(-09)	0.00	0.0
he+	+c2h2	=c2h+	h	he		8.75(-10)	0.00	0.0
he+	+c3h	=c3+	h	he		2.00(-09)	0.00	0.0
he+	+nh3	=nh2+	h	he		1.76(-09)	0.00	0.0
he+	+nh3	=nh+	h2	he		1.76(-10)	0.00	0.0
he+	+ch4	=h+	ch3	he		4.00(-10)	0.00	0.0
he+	+ch4	=ch+	h2	h	he	2.56(-10)	0.00	0.0
he+	+ch4	=ch2+	h2	he		8.48(-10)	0.00	0.0
he+	+ch4	=ch3+	h	he		8.00(-11)	0.00	0.0
he+	+c3h2	=c3h+	h	he		1.00(-09)	0.00	0.0
he+	+c3h2	=c3+	h2	he		1.00(-09)	0.00	0.0
c+	+h2	=ch+	h			1.50(-10)	0.00	5000.0
c+	+ch	=c2+	h			3.80(-10)	0.00	0.0
c+	+oh	=co+	h			8.00(-10)	0.00	0.0
c+	+oh	=h+	co			8.00(-10)	0.00	0.0
c+	+o2	=o+	co			5.15(-10)	0.00	0.0
c+	+o2	=co+	o			3.15(-10)	0.00	0.0
c+	+nh	=cn+	h			7.80(-10)	0.00	0.0
c+	+no	=n+	co			9.02(-10)	0.00	0.0
c+	+sh	=cs+	h			1.10(-09)	0.00	0.0
c+	+so	=s+	co			2.60(-10)	0.00	0.0
c+	+so	=cs+	o			2.60(-10)	0.00	0.0
c+	+so	=co+	s			2.60(-10)	0.00	0.0
c+	+hco	=ch+	co			4.80(-10)	0.00	0.0

c+	+hcn	=c2n+	h	3.40(-09)	0.00	0.0
c+	+hnc	=c2n+	h	3.40(-09)	0.00	0.0
c+	+h2o	=hco+	h	2.43(-09)	-.63	0.0
c+	+h2s	=hcs+	h	1.28(-09)	0.00	0.0
c+	+ch2	=c2h+	h	5.20(-10)	0.00	0.0
c+	+co2	=co+	co	1.10(-09)	0.00	0.0
c+	+c2h	=c3+	h	1.00(-09)	0.00	0.0
c+	+ocs	=cs+	co	1.60(-09)	0.00	0.0
c+	+ocs	=co+	cs	9.30(-10)	0.00	0.0
c+	+nh2	=hcn+	h	1.10(-09)	0.00	0.0
c+	+so2	=so+	co	2.30(-09)	0.00	0.0
c+	+ch3	=c2h2+	h	1.30(-09)	0.00	0.0
c+	+c2h2	=c3h+	h	2.20(-09)	0.00	0.0
c+	+nh3	=h2nc+	h	7.80(-10)	0.00	0.0
c+	+nh3	=h2cn+	h	7.80(-10)	0.00	0.0
c+	+nh3	=hcn+	h2	2.07(-10)	0.00	0.0
c+	+ch4	=c2h2+	h2	3.25(-10)	0.00	0.0
c+	+ch4	=c2h3+	h	9.75(-10)	0.00	0.0
o+	+h2	=oh+	h	1.20(-09)	0.00	0.0
o+	+ch	=co+	h	3.50(-10)	0.00	0.0
o+	+c2	=co+	c	4.80(-10)	0.00	0.0
o+	+oh	=o2+	h	3.60(-10)	0.00	0.0
o+	+nh	=no+	h	3.60(-10)	0.00	0.0
o+	+n2	=no+	n	1.20(-12)	0.00	0.0
o+	+hco	=oh+	co	4.30(-10)	0.00	0.0
o+	+c2h	=co+	ch	4.60(-10)	0.00	0.0
n+	+h2	=nh+	h	1.10(-14)	0.00	0.0
n+	+ch	=cn+	h	3.60(-10)	0.00	0.0
n+	+co	=no+	c	1.46(-10)	0.00	0.0
n+	+co	=c+	no	9.02(-10)	0.00	15400.0
n+	+oh	=no+	h	3.70(-10)	0.00	0.0
n+	+o2	=no+	o	2.37(-10)	0.00	0.0
n+	+o2	=o+	no	3.30(-11)	0.00	0.0
n+	+nh	=n2+	h	3.70(-10)	0.00	0.0
n+	+no	=n2+	o	7.95(-11)	0.00	0.0
n+	+hco	=nh+	co	4.50(-10)	0.00	0.0
s+	+h2	=sh+	h	2.20(-10)	0.00	9860.0
s+	+ch	=cs+	h	6.20(-10)	0.00	0.0

s+	+c2	=cs+	c		8.10(-10)	0.00	0.0
s+	+oh	=so+	h		6.10(-10)	0.00	0.0
s+	+oh	=sh+	o		2.90(-10)	0.00	8820.0
s+	+o2	=so+	o		2.30(-11)	0.00	0.0
s+	+hco	=sh+	co		3.60(-10)	0.00	0.0
s+	+ch2	=hcs+	h		1.00(-11)	0.00	0.0
s+	+nh3	=nh2+	sh		7.00(-11)	0.00	0.0

-

3.ii diatomic ions

-

h2+	+he	=heh+	h		3.00(-10)	0.00	6717.0
h2+	+c	=ch+	h		2.40(-09)	0.00	0.0
h2+	+o	=oh+	h		1.50(-09)	0.00	0.0
h2+	+n	=nh+	h		1.90(-09)	0.00	0.0
h2+	+h2	=h3+	h		2.10(-09)	0.00	0.0
h2+	+ch	=ch2+	h		7.10(-10)	0.00	0.0
h2+	+co	=hco+	h		2.80(-09)	0.00	0.0
h2+	+cn	=hcn+	h		1.20(-09)	0.00	0.0
h2+	+c2	=c2h+	h		1.10(-09)	0.00	0.0
h2+	+oh	=h2o+	h		7.60(-10)	0.00	0.0
h2+	+nh	=nh2+	h		7.60(-10)	0.00	0.0
h2+	+n2	=n2h+	h		2.00(-09)	0.00	0.0
h2+	+hco	=h3+	co		1.00(-09)	0.00	0.0
h2+	+h2o	=h3o+	h		3.40(-09)	0.00	0.0
h2+	+h2s	=sh+	h	h2	8.60(-10)	0.00	0.0
h2+	+h2s	=s+	h2	h2	7.70(-10)	0.00	0.0
h2+	+ch2	=ch3+	h		1.00(-09)	0.00	0.0
h2+	+c2h	=c2h2+	h		1.00(-09)	0.00	0.0
h2+	+c2h2	=c2h3+	h		4.80(-10)	0.00	0.0
h2+	+ch4	=ch5+	h		1.10(-10)	0.00	0.0
h2+	+ch4	=ch3+	h	h2	2.30(-09)	0.00	0.0
heh+	+h	=h2+	he		1.00(-10)	0.00	0.0
heh+	+h2	=h3+	he		1.80(-09)	0.00	0.0
ch+	+h	=c+	h2		1.50(-10)	0.00	0.0
ch+	+c	=c2+	h		1.20(-09)	0.00	0.0
ch+	+o	=co+	h		1.75(-10)	0.00	0.0

ch+	+n	=cn+	h		9.50(-11)	0.00	0.0
ch+	+n	=h+	cn		9.50(-11)	0.00	0.0
ch+	+s	=sh+	c		4.70(-10)	0.00	0.0
ch+	+s	=cs+	h		4.70(-10)	0.00	0.0
ch+	+h2	=ch2+	h		1.20(-09)	0.00	0.0
ch+	+ch	=c2+	h2		7.40(-10)	0.00	0.0
ch+	+cn	=c2n+	h		1.10(-09)	0.00	0.0
ch+	+c2	=c3+	h		1.00(-09)	0.00	0.0
ch+	+oh	=co+	h2		7.50(-10)	0.00	0.0
ch+	+o2	=hco+	o		4.80(-10)	0.00	0.0
ch+	+nh	=cn+	h2		7.60(-10)	0.00	0.0
ch+	+so	=oh+	cs		1.00(-09)	0.00	0.0
ch+	+so	=sh+	co		1.00(-09)	0.00	0.0
ch+	+hco	=ch2+	co		4.60(-10)	0.00	0.0
ch+	+hcn	=h2cn+	c		1.80(-09)	0.00	0.0
ch+	+hcn	=c2n+	h2		6.00(-10)	0.00	0.0
ch+	+h2o	=hco+	h2		1.45(-09)	0.00	0.0
ch+	+h2o	=h3o+	c		1.45(-09)	0.00	0.0
ch+	+h2s	=hcs+	h2		6.60(-10)	0.00	0.0
ch+	+ch2	=c2h+	h2		1.00(-09)	0.00	0.0
ch+	+c2h	=c3+	h2		9.80(-10)	0.00	0.0
ch+	+nh2	=hcn+	h2		1.10(-09)	0.00	0.0
ch+	+c2h2	=c3h2+	h		2.40(-09)	0.00	0.0
ch+	+nh3	=h2cn+	h2		1.84(-09)	0.00	0.0
ch+	+nh3	=nh4+	c		4.05(-10)	0.00	0.0
ch+	+ch4	=c2h2+	h2	h	1.60(-10)	0.00	0.0
ch+	+ch4	=c2h3+	h2		1.10(-10)	0.00	0.0
co+	+n	=no+	c		8.10(-11)	0.00	0.0
co+	+h2	=hco+	h		1.30(-09)	0.00	0.0
co+	+ch	=hco+	c		3.20(-10)	0.00	0.0
co+	+oh	=hco+	o		3.10(-10)	0.00	0.0
co+	+nh	=hco+	n		3.20(-10)	0.00	0.0
co+	+hcn	=hco+	cn		5.10(-10)	0.00	0.0
co+	+h2o	=hco+	oh		4.20(-10)	0.00	0.0
co+	+ch2	=hco+	ch		4.30(-10)	0.00	0.0
co+	+c2h	=hco+	c2		3.90(-10)	0.00	0.0
co+	+nh2	=hco+	nh		4.50(-10)	0.00	0.0
cn+	+h	=ch+	n		9.50(-11)	0.00	10200.0

cn+	+h2	=hcn+	h		1.00(-09)	0.00	0.0
cn+	+hco	=hcn+	co		3.70(-10)	0.00	0.0
cs+	+h2	=hcs+	h		4.80(-10)	0.00	0.0
c2+	+o	=c+	co		1.55(-10)	0.00	0.0
c2+	+o	=co+	c		1.55(-10)	0.00	0.0
c2+	+n	=c+	cn		8.30(-11)	0.00	0.0
c2+	+s	=cs+	c		5.80(-10)	0.00	0.0
c2+	+h2	=c2h+	h		1.40(-09)	0.00	0.0
c2+	+h2	=h+	c2h		1.50(-09)	0.00	1260.0
c2+	+ch	=c3+	h		3.20(-10)	0.00	0.0
c2+	+c2	=c3+	c		8.70(-10)	0.00	0.0
c2+	+o2	=co+	co		8.00(-10)	0.00	0.0
c2+	+nh	=c2n+	h		3.30(-10)	0.00	0.0
c2+	+nh	=c2h+	n		3.30(-10)	0.00	0.0
c2+	+hco	=c2h+	co		3.80(-10)	0.00	0.0
c2+	+hcn	=c2h+	cn		1.30(-09)	0.00	0.0
c2+	+hcn	=c3h+	n		1.30(-09)	0.00	0.0
c2+	+h2o	=c2h+	oh		4.40(-10)	0.00	0.0
c2+	+ch2	=c3h+	h		4.50(-10)	0.00	0.0
c2+	+ch4	=c2h+	ch3		2.38(-10)	0.00	0.0
c2+	+ch4	=c2h2+	ch2		1.82(-10)	0.00	0.0
c2+	+ch4	=ch3+	c2	h	1.96(-10)	0.00	0.0
c2+	+ch4	=c3h2+	h2		5.74(-10)	0.00	0.0
c2+	+ch4	=c3h3+	h		2.10(-10)	0.00	0.0
oh+	+h	=o+	h2		1.20(-09)	0.00	4060.0
oh+	+c	=ch+	o		1.20(-09)	0.00	0.0
oh+	+o	=o2+	h		7.10(-10)	0.00	0.0
oh+	+n	=no+	h		8.90(-10)	0.00	0.0
oh+	+s	=so+	h		4.30(-10)	0.00	0.0
oh+	+s	=sh+	o		4.30(-10)	0.00	0.0
oh+	+h2	=h2o+	h		1.01(-09)	0.00	0.0
oh+	+ch	=ch2+	o		3.50(-10)	0.00	0.0
oh+	+co	=hco+	o		1.00(-09)	0.00	0.0
oh+	+cn	=hcn+	o		1.00(-09)	0.00	0.0
oh+	+c2	=c2h+	o		4.80(-10)	0.00	0.0
oh+	+oh	=h2o+	o		7.00(-10)	0.00	0.0
oh+	+nh	=nh2+	o		3.60(-10)	0.00	0.0
oh+	+n2	=n2h+	o		9.50(-10)	0.00	0.0

oh+	+hco	=h2o+	co	2.80(-10)	0.00	0.0
oh+	+h2o	=h3o+	o	1.30(-09)	0.00	0.0
oh+	+ch2	=ch3+	o	4.80(-10)	0.00	0.0
oh+	+c2h	=c2h2+	o	4.50(-10)	0.00	0.0
oh+	+nh2	=nh3+	o	5.00(-10)	0.00	0.0
o2+	+c	=co+	o	5.20(-11)	0.00	0.0
o2+	+n	=no+	o	7.84(-11)	0.00	0.0
o2+	+s	=so+	o	5.40(-10)	0.00	0.0
o2+	+ch	=hco+	o	3.10(-10)	0.00	0.0
o2+	+c2	=co+	co	4.10(-10)	0.00	0.0
o2+	+nh	=hno+	o	3.20(-10)	0.00	0.0
nh+	+h	=n+	h2	6.52(-10)	0.00	0.0
nh+	+c	=ch+	n	1.60(-09)	0.00	0.0
nh+	+o	=oh+	n	1.00(-09)	0.00	0.0
nh+	+n	=n2+	h	1.30(-09)	0.00	0.0
nh+	+s	=sh+	n	6.90(-10)	0.00	0.0
nh+	+h2	=nh2+	h	1.27(-09)	0.00	0.0
nh+	+h2	=h3+	n	2.25(-10)	0.00	0.0
nh+	+ch	=ch2+	n	9.90(-10)	0.00	0.0
nh+	+co	=hco+	n	1.60(-09)	0.00	0.0
nh+	+cn	=hcn+	n	1.60(-09)	0.00	0.0
nh+	+c2	=hcn+	c	4.90(-10)	0.00	0.0
nh+	+c2	=c2h+	n	4.90(-10)	0.00	0.0
nh+	+oh	=h2o+	n	1.00(-09)	0.00	0.0
nh+	+nh	=nh2+	n	1.00(-09)	0.00	0.0
nh+	+n2	=n2h+	n	1.50(-09)	0.00	0.0
nh+	+h2o	=h3o+	n	1.40(-09)	0.00	0.0
nh+	+ch2	=ch3+	n	1.40(-09)	0.00	0.0
nh+	+c2h	=c2h2+	n	1.40(-09)	0.00	0.0
nh+	+nh2	=nh3+	n	1.50(-09)	0.00	0.0
n2+	+o	=no+	n	1.40(-10)	0.00	0.0
n2+	+h2	=n2h+	h	2.00(-09)	0.24	0.0
n2+	+hco	=n2h+	co	3.70(-10)	0.00	0.0
n2+	+h2o	=n2h+	oh	2.00(-09)	0.00	0.0
sh+	+h	=s+	h2	1.10(-10)	0.00	0.0
sh+	+c	=cs+	h	9.90(-10)	0.00	0.0
sh+	+o	=so+	h	2.90(-10)	0.00	0.0
sh+	+o	=s+	oh	2.90(-10)	0.00	0.0

sh+	+h2	=h2s+	h		1.90(-10)	0.00	8500.0
sh+	+ch	=ch2+	s		5.80(-10)	0.00	0.0
sh+	+oh	=h2s+	o		3.10(-10)	0.00	7500.0
sh+	+oh	=h2o+	s		4.30(-10)	0.00	9200.0
sh+	+hcn	=h2cn+	s		8.90(-10)	0.00	0.0
sh+	+h2o	=h3o+	s		6.30(-10)	0.00	0.0
sh+	+h2s	=h3s+	s		5.00(-10)	0.00	0.0
sh+	+nh3	=nh4+	s		9.75(-10)	0.00	0.0
so+	+h	=s+	oh		6.10(-10)	0.00	11385.0

-

3.iii triatomic ions

-

hco+	+h	=co+	h2		1.30(-09)	0.00	24500.0
hco+	+c	=ch+	co		1.10(-09)	0.00	0.0
hco+	+s	=sh+	co		3.30(-10)	0.00	0.0
hco+	+fe	=fe+	co	h	1.90(-09)	0.00	0.0
hco+	+ch	=ch2+	co		6.30(-10)	0.00	0.0
hco+	+cs	=hcs+	co		1.20(-09)	0.00	0.0
hco+	+c2	=c2h+	co		8.30(-10)	0.00	0.0
hco+	+oh	=hco2+	h		1.00(-09)	0.00	0.0
hco+	+oh	=h2o+	co		6.20(-10)	0.00	0.0
hco+	+o2	=hco2+	o		1.00(-09)	0.00	1450.0
hco+	+nh	=nh2+	co		6.40(-10)	0.00	0.0
hco+	+n2	=n2h+	co		8.80(-10)	0.00	11200.0
hco+	+sh	=h2s+	co		8.20(-10)	0.00	0.0
hco+	+so	=hso+	co		7.50(-10)	0.00	0.0
hco+	+hcn	=h2cn+	co		3.70(-09)	0.00	0.0
hco+	+hnc	=h2cn+	co		3.70(-09)	0.00	0.0
hco+	+h2o	=h3o+	co		2.50(-09)	0.00	0.0
hco+	+h2s	=h3s+	co		1.60(-09)	0.00	0.0
hco+	+ch2	=ch3+	co		8.60(-10)	0.00	0.0
hco+	+co2	=hco2+	co		1.00(-09)	0.00	5000.0
hco+	+c2h	=c2h2+	co		7.80(-10)	0.00	0.0
hco+	+ocs	=hocs+	co		1.10(-09)	0.00	0.0
hco+	+nh2	=nh3+	co		8.90(-10)	0.00	0.0
hco+	+ch3	=ch4+	co		1.40(-09)	0.00	9060.0

hco+	+c2h2	=c2h3+	co	1.36(-09)	0.00	0.0
hco+	+c3h	=c3h2+	co	1.40(-09)	0.00	0.0
hco+	+nh3	=nh4+	co	1.90(-09)	0.00	0.0
hco+	+ch4	=ch5+	co	9.90(-10)	0.00	4920.0
hco+	+c3h2	=c3h3+	co	1.40(-09)	0.00	0.0
hcn+	+h	=cn+	h2	1.00(-09)	0.00	15800.0
hcn+	+c	=ch+	cn	1.10(-09)	0.00	0.0
hcn+	+s	=sh+	cn	5.70(-10)	0.00	0.0
hcn+	+h2	=h2cn+	h	9.80(-10)	0.00	0.0
hcn+	+ch	=ch2+	cn	6.30(-10)	0.00	0.0
hcn+	+co	=hco+	cn	8.80(-10)	0.00	0.0
hcn+	+c2	=c2h+	cn	8.40(-10)	0.00	0.0
hcn+	+oh	=h2o+	cn	6.30(-10)	0.00	0.0
hcn+	+nh	=nh2+	cn	6.50(-10)	0.00	0.0
hcn+	+h2o	=h3o+	cn	8.50(-10)	0.00	0.0
hcn+	+hco	=h2cn+	co	3.70(-10)	0.00	0.0
hcn+	+hcn	=h2cn+	cn	1.00(-09)	0.00	0.0
hcn+	+ch2	=ch3+	cn	8.70(-10)	0.00	0.0
hcn+	+c2h	=c2h2+	cn	7.90(-10)	0.00	0.0
hcn+	+nh2	=nh3+	cn	9.00(-10)	0.00	0.0
hcn+	+nh3	=nh4+	cn	1.10(-09)	0.00	0.0
hcs+	+o	=hco+	s	1.00(-09)	0.00	0.0
hno+	+c	=ch+	no	1.00(-09)	0.00	0.0
hno+	+s	=sh+	no	1.10(-09)	0.00	0.0
hno+	+ch	=ch2+	no	6.20(-10)	0.00	0.0
hno+	+co	=hco+	no	1.00(-10)	0.00	0.0
hno+	+cn	=hcn+	no	8.70(-10)	0.00	0.0
hno+	+c2	=c2h+	no	8.20(-10)	0.00	0.0
hno+	+oh	=h2o+	no	6.20(-10)	0.00	0.0
hno+	+nh	=nh2+	no	6.30(-10)	0.00	0.0
hno+	+n2	=n2h+	no	8.10(-10)	0.00	0.0
hno+	+hcn	=h2cn+	no	9.90(-10)	0.00	0.0
hno+	+h2o	=h3o+	no	2.30(-09)	0.00	0.0
hno+	+ch2	=ch3+	no	8.60(-10)	0.00	0.0
hno+	+co2	=hco2+	no	1.00(-10)	0.00	0.0
hno+	+c2h	=c2h2+	no	7.70(-10)	0.00	0.0
hno+	+nh2	=nh3+	no	8.80(-10)	0.00	0.0
hno+	+nh3	=nh4+	no	1.10(-09)	0.00	0.0

h2o+	+c	=ch+	oh		1.10(-09)	0.00	0.0
h2o+	+o	=o2+	h2		7.00(-11)	0.00	0.0
h2o+	+n	=hno+	h		8.80(-11)	0.00	0.0
h2o+	+s	=hso+	h		4.30(-10)	0.00	0.0
h2o+	+s	=sh+	oh		4.30(-10)	0.00	0.0
h2o+	+h2	=h3o+	h		8.30(-10)	0.00	0.0
h2o+	+ch	=ch2+	oh		3.40(-10)	0.00	0.0
h2o+	+c2	=c2h+	oh		4.70(-10)	0.00	0.0
h2o+	+oh	=h3o+	o		6.90(-10)	0.00	0.0
h2o+	+nh	=h3o+	n		7.10(-10)	0.00	0.0
h2o+	+hco	=h3o+	co		2.80(-10)	0.00	0.0
h2o+	+hcn	=h2cn+	oh		1.10(-09)	0.00	0.0
h2o+	+h2o	=h3o+	oh		2.10(-09)	0.00	0.0
h2o+	+h2s	=h3s+	oh		7.00(-10)	0.00	0.0
h2o+	+h2s	=h3o+	sh		5.90(-10)	0.00	0.0
h2o+	+ch2	=ch3+	oh		4.70(-10)	0.00	0.0
h2o+	+c2h	=c2h2+	oh		4.40(-10)	0.00	0.0
h2o+	+nh2	=nh3+	oh		4.90(-10)	0.00	0.0
h2o+	+nh3	=nh4+	oh		9.00(-10)	0.00	0.0
h2o+	+ch4	=h3o+	ch3		1.30(-09)	0.00	0.0
h2s+	+h	=sh+	h2		2.00(-10)	0.00	0.0
h2s+	+c	=hcs+	h		1.00(-09)	0.00	0.0
h2s+	+o	=sh+	oh		3.10(-10)	0.00	0.0
h2s+	+o	=so+	h2		3.10(-10)	0.00	0.0
h2s+	+h2	=h3s+	h		1.40(-11)	0.00	2300.0
h2s+	+h2o	=h3o+	sh		8.10(-10)	0.00	0.0
h2s+	+h2s	=h3s+	sh		5.80(-10)	0.00	0.0
h2s+	+nh3	=nh4+	sh		1.36(-09)	0.00	0.0
h3+	+h	=h2+	h2		2.10(-09)	0.00	20000.0
h3+	+c	=ch+	h2		2.00(-09)	0.00	0.0
h3+	+o	=oh+	h2		8.00(-10)	0.00	0.0
h3+	+n	=nh2+	h		1.00(-09)	0.00	0.0
h3+	+s	=sh+	h2		2.60(-09)	0.00	0.0
h3+	+fe	=fe+	h2	h	4.90(-09)	0.00	0.0
h3+	+ch	=ch2+	h2		1.20(-09)	0.00	0.0
h3+	+co	=hco+	h2		1.70(-09)	0.00	0.0
h3+	+cn	=hcn+	h2		1.00(-09)	0.00	0.0
h3+	+cn	=h2cn+	h		1.00(-09)	0.00	0.0

h3+	+cs	=hcs+	h2	2.90(-09)	0.00	0.0
h3+	+c2	=c2h+	h2	1.80(-09)	0.00	0.0
h3+	+oh	=h2o+	h2	1.30(-09)	0.00	0.0
h3+	+nh	=nh2+	h2	1.30(-09)	0.00	0.0
h3+	+no	=hno+	h2	1.10(-09)	0.00	0.0
h3+	+n2	=n2h+	h2	1.30(-09)	0.00	0.0
h3+	+sh	=h2s+	h2	1.90(-09)	0.00	0.0
h3+	+so	=hso+	h2	1.90(-09)	0.00	0.0
h3+	+hcn	=h2cn+	h2	9.50(-09)	0.00	0.0
h3+	+hnc	=h2cn+	h2	9.50(-09)	0.00	0.0
h3+	+h2o	=h3o+	h2	4.30(-09)	0.00	0.0
h3+	+h2s	=h3s+	h2	3.70(-09)	0.00	0.0
h3+	+ch2	=ch3+	h2	1.70(-09)	0.00	0.0
h3+	+co2	=hco2+	h2	2.00(-09)	0.00	0.0
h3+	+c2h	=c2h2+	h2	1.70(-09)	0.00	0.0
h3+	+ocs	=hocs+	h2	1.90(-09)	0.00	0.0
h3+	+nh2	=nh3+	h2	1.80(-09)	0.00	0.0
h3+	+ch3	=ch4+	h2	2.10(-09)	0.00	0.0
h3+	+c2h2	=c2h3+	h2	2.90(-09)	0.00	0.0
h3+	+c3h	=c3h2+	h2	2.00(-09)	0.00	0.0
h3+	+nh3	=nh4+	h2	9.10(-09)	0.00	0.0
h3+	+ch4	=ch5+	h2	1.90(-09)	0.00	0.0
h3+	+c3h2	=c3h3+	h2	2.00(-09)	0.00	0.0
ch2+	+h	=ch+	h2	1.20(-09)	0.00	2700.0
ch2+	+c	=c2h+	h	1.20(-09)	0.00	0.0
ch2+	+o	=hco+	h	7.50(-10)	0.00	0.0
ch2+	+n	=hcn+	h	9.40(-10)	0.00	0.0
ch2+	+n	=cn+	h2	1.10(-10)	0.00	0.0
ch2+	+s	=hcs+	h	1.40(-09)	0.00	0.0
ch2+	+h2	=ch3+	h	7.00(-10)	0.00	0.0
ch2+	+ch	=c2h2+	h	7.20(-10)	0.00	0.0
ch2+	+c2	=c3h+	h	1.00(-09)	0.00	0.0
ch2+	+c2	=c2h+	ch	3.20(-10)	0.00	8000.0
ch2+	+o2	=hco+	oh	9.10(-10)	0.00	0.0
ch2+	+nh	=h2cn+	h	7.50(-10)	0.00	0.0
ch2+	+ch2	=c2h3+	h	1.00(-09)	0.00	0.0
ch2+	+c2h	=c3h2+	h	9.50(-10)	0.00	0.0
ch2+	+c2h2	=c3h3+	h	2.50(-09)	0.00	0.0

ch2+	+nh3	=nh4+	ch	2.53(-09)	0.00	0.0
c2h+	+h	=c2+	h2	1.40(-09)	0.00	10240.0
c2h+	+c	=c3+	h	1.10(-09)	0.00	0.0
c2h+	+o	=ch+	co	1.10(-10)	0.00	0.0
c2h+	+o	=hco+	c	1.10(-10)	0.00	0.0
c2h+	+o	=co+	ch	1.10(-10)	0.00	0.0
c2h+	+n	=c2n+	h	8.30(-10)	0.00	0.0
c2h+	+n	=ch+	cn	9.00(-11)	0.00	0.0
c2h+	+h2	=c2h2+	h	1.70(-09)	0.00	0.0
c2h+	+ch	=c3h+	h	3.20(-10)	0.00	0.0
c2h+	+ch	=ch2+	c2	3.20(-10)	0.00	0.0
c2h+	+hco	=c2h2+	co	7.60(-10)	0.00	0.0
c2h+	+hcn	=h2cn+	c2	2.70(-09)	0.00	0.0
c2h+	+ch2	=ch3+	c2	4.40(-10)	0.00	0.0
c2h+	+ch2	=c3h2+	h	4.40(-10)	0.00	0.0
c2h+	+nh2	=nh3+	c2	4.60(-10)	0.00	0.0
c2h+	+nh3	=nh4+	c2	5.50(-10)	0.00	0.0
c2h+	+ch4	=c2h2+	ch3	5.50(-10)	0.00	0.0
c2h+	+ch4	=c3h3+	h2	5.50(-10)	0.00	0.0
c2n+	+h	=c+	hcn	3.40(-09)	0.00	200.0
c2n+	+h2	=ch+	hcn	7.00(-10)	0.00	5230.0
c2n+	+h2	=c2h2+	n	1.30(-10)	0.00	10000.0
c2n+	+nh3	=n2h+	c2h2	1.90(-10)	0.00	0.0
c2n+	+nh3	=h2cn+	hcn	1.70(-09)	0.00	0.0
c3+	+h	=c+	c2h	1.00(-09)	0.00	6200.0
c3+	+h2	=c3h+	h	3.00(-10)	0.00	0.0
nh2+	+h	=nh+	h2	1.27(-09)	0.00	24000.0
nh2+	+c	=ch+	nh	1.20(-09)	0.00	0.0
nh2+	+o	=hno+	h	7.20(-11)	0.00	0.0
nh2+	+n	=n2h+	h	9.10(-11)	0.00	0.0
nh2+	+s	=sh+	nh	4.40(-10)	0.00	0.0
nh2+	+h2	=nh3+	h	2.70(-10)	0.00	0.0
nh2+	+ch	=ch2+	nh	3.50(-10)	0.00	0.0
nh2+	+co	=hco+	nh	6.40(-10)	0.00	6100.0
nh2+	+cn	=h2cn+	n	1.00(-10)	0.00	0.0
nh2+	+c2	=c2h+	nh	9.70(-10)	0.00	0.0
nh2+	+oh	=h2o+	nh	7.10(-10)	0.00	0.0
nh2+	+o2	=no+	h2o	1.00(-10)	0.00	0.0

nh2+	+nh	=nh3+	n	7.30(-10)	0.00	0.0
nh2+	+hcn	=h2cn+	nh	1.20(-09)	0.00	0.0
nh2+	+h2o	=nh3+	oh	1.00(-10)	0.00	0.0
nh2+	+h2o	=h3o+	nh	1.60(-09)	0.00	0.0
nh2+	+h2o	=nh4+	o	3.00(-11)	0.00	0.0
nh2+	+h2s	=h3s+	nh	2.40(-10)	0.00	0.0
nh2+	+ch2	=ch3+	nh	4.90(-10)	0.00	0.0
nh2+	+c2h	=c2h2+	nh	9.10(-10)	0.00	0.0
nh2+	+nh2	=nh3+	nh	1.00(-09)	0.00	0.0
nh2+	+nh3	=nh4+	nh	1.00(-09)	0.00	0.0
n2h+	+h	=n2+	h2	2.10(-09)	0.00	30300.0
n2h+	+c	=ch+	n2	1.10(-09)	0.00	0.0
n2h+	+o	=oh+	n2	1.40(-10)	0.00	3400.0
n2h+	+s	=sh+	n2	1.10(-09)	0.00	0.0
n2h+	+h2	=h3+	n2	1.80(-09)	0.00	8300.0
n2h+	+ch	=ch2+	n2	6.30(-10)	0.00	0.0
n2h+	+co	=hco+	n2	8.80(-10)	0.00	0.0
n2h+	+c2	=c2h+	n2	8.30(-10)	0.00	0.0
n2h+	+oh	=h2o+	n2	6.20(-10)	0.00	0.0
n2h+	+nh	=nh2+	n2	6.40(-10)	0.00	0.0
n2h+	+no	=hno+	n2	3.40(-10)	0.00	0.0
n2h+	+hcn	=h2cn+	n2	1.00(-09)	0.00	0.0
n2h+	+h2o	=h3o+	n2	2.60(-09)	0.00	0.0
n2h+	+ch2	=ch3+	n2	8.60(-10)	0.00	0.0
n2h+	+co2	=hco2+	n2	1.40(-09)	0.00	0.0
n2h+	+c2h	=c2h2+	n2	7.80(-10)	0.00	0.0
n2h+	+nh2	=nh3+	n2	8.90(-10)	0.00	0.0
n2h+	+nh3	=nh4+	n2	2.30(-09)	0.00	0.0
n2h+	+ch4	=ch5+	n2	9.00(-10)	0.00	0.0

-

3.iv four-atom ions

-

hco2+	+h	=hco+	oh	1.00(-09)	0.00	7500.0
hco2+	+c	=ch+	co2	1.00(-09)	0.00	0.0
hco2+	+o	=hco+	o2	1.00(-09)	0.00	0.0
hco2+	+co	=hco+	co2	1.00(-09)	0.00	0.0

hco2+	+no	=hno+	co2		1.00(-10)	0.00	0.0
hco2+	+n2	=n2h+	co2		1.40(-09)	0.00	6400.0
hco2+	+h2o	=h3o+	co2		7.80(-10)	0.00	0.0
hco2+	+ch4	=ch5+	co2		7.80(-10)	0.00	0.0
h2cn+	+h	=hcn+	h2		9.80(-10)	0.00	34400.0
h2cn+	+ch	=ch2+	hcn		6.30(-10)	0.00	0.0
h2cn+	+h2o	=h3o+	hcn		4.50(-09)	0.00	2460.0
h2cn+	+h2o	=h3o+	hnc		4.50(-09)	0.00	10300.0
h2cn+	+ch2	=ch3+	hcn		8.70(-10)	0.00	0.0
h2cn+	+nh2	=nh3+	hcn		8.90(-10)	0.00	0.0
h2cn+	+nh3	=nh4+	hcn		2.20(-09)	0.00	0.0
h3o+	+h	=h2o+	h2		6.10(-10)	0.00	20500.0
h3o+	+c	=hco+	h2		1.00(-11)	0.00	0.0
h3o+	+s	=sh+	h2o		3.20(-10)	0.00	4930.0
h3o+	+fe	=fe+	h2o	h	3.10(-09)	0.00	0.0
h3o+	+ch	=ch2+	h2o		6.80(-10)	0.00	0.0
h3o+	+cn	=h2cn+	oh		4.50(-09)	0.00	0.0
h3o+	+c2	=c2h+	h2o		9.20(-10)	0.00	0.0
h3o+	+hcn	=h2cn+	h2o		4.50(-09)	0.00	0.0
h3o+	+hnc	=h2cn+	h2o		4.50(-09)	0.00	0.0
h3o+	+h2s	=h3s+	h2o		1.90(-09)	0.00	0.0
h3o+	+ch2	=ch3+	h2o		9.40(-10)	0.00	0.0
h3o+	+c2h	=c2h2+	h2o		2.20(-10)	0.00	4100.0
h3o+	+nh2	=nh3+	h2o		9.70(-10)	0.00	0.0
h3o+	+c2h2	=c2h3+	h2o		1.00(-09)	0.00	7330.0
h3o+	+c3h	=c3h2+	h2o		2.00(-09)	0.00	0.0
h3o+	+nh3	=nh4+	h2o		2.20(-09)	0.00	0.0
h3o+	+c3h2	=c3h3+	h2o		3.00(-09)	0.00	0.0
h3s+	+h	=h2s+	h2		6.00(-11)	0.00	0.0
h3s+	+hcn	=h2cn+	h2s		1.90(-09)	0.00	0.0
h3s+	+nh3	=nh4+	h2s		1.90(-09)	0.00	0.0
ch3+	+h	=ch2+	h2		7.00(-10)	0.00	10560.0
ch3+	+c	=c2h+	h2		1.20(-09)	0.00	0.0
ch3+	+o	=hco+	h2		3.10(-10)	0.00	0.0
ch3+	+o	=h3+	co		1.30(-11)	0.00	0.0
ch3+	+n	=hcn+	h2		6.70(-11)	0.00	0.0
ch3+	+n	=h2cn+	h		6.70(-11)	0.00	0.0
ch3+	+s	=hcs+	h2		1.40(-09)	0.00	0.0

ch3+	+h2	=ch4+	h	2.00(-10)	0.00	32500.0
ch3+	+ch	=c2h2+	h2	7.10(-10)	0.00	0.0
ch3+	+c2	=c3h+	h2	9.90(-10)	0.00	0.0
ch3+	+o2	=hco+	h2o	4.30(-11)	0.00	0.0
ch3+	+nh	=h2cn+	h2	7.40(-10)	0.00	0.0
ch3+	+so	=hocs+	h2	9.50(-10)	0.00	0.0
ch3+	+hco	=ch4+	co	4.40(-10)	0.00	0.0
ch3+	+h2o	=h3o+	ch2	1.00(-09)	0.00	13300.0
ch3+	+ch2	=c2h3+	h2	9.90(-10)	0.00	0.0
ch3+	+c2h	=c3h2+	h2	5.00(-10)	0.00	0.0
ch3+	+c2h	=c3h3+	h	5.00(-10)	0.00	0.0
ch3+	+c2h2	=c3h3+	h2	1.20(-09)	0.00	0.0
ch3+	+nh3	=nh4+	ch2	1.60(-09)	0.00	0.0
c2h2+	+h	=c2h+	h2	1.70(-09)	0.00	17500.0
c2h2+	+c	=c3h+	h	1.10(-09)	0.00	0.0
c2h2+	+n	=ch+	hcn	2.50(-11)	0.00	0.0
c2h2+	+n	=ch+	hnc	2.50(-11)	0.00	2600.0
c2h2+	+n	=c2n+	h2	2.25(-10)	0.00	0.0
c2h2+	+h2	=c2h3+	h	5.00(-10)	0.00	800.0
c2h2+	+ch	=c3h2+	h	6.40(-10)	0.00	0.0
c2h2+	+c2	=c2h+	c2h	8.50(-10)	0.00	800.0
c2h2+	+hco	=c2h3+	co	3.70(-10)	0.00	0.0
c2h2+	+hcn	=h2cn+	c2h	3.00(-11)	0.00	0.0
c2h2+	+h2o	=h3o+	c2h	2.20(-10)	0.00	0.0
c2h2+	+h2s	=c2h3+	sh	4.60(-11)	0.00	0.0
c2h2+	+h2s	=h3s+	c2h	4.60(-11)	0.00	0.0
c2h2+	+ch2	=c3h3+	h	8.80(-10)	0.00	0.0
c2h2+	+nh2	=nh3+	c2h	4.50(-10)	0.00	0.0
c2h2+	+nh3	=nh4+	c2h	9.61(-10)	0.00	0.0
c3h+	+h	=c3+	h2	3.00(-10)	0.00	23300.0
c3h+	+h2	=c3h2+	h	1.00(-09)	0.00	500.0
c3h+	+h2o	=hco+	c2h2	2.48(-10)	0.00	0.0
c3h+	+h2o	=c2h3+	co	2.02(-10)	0.00	0.0
c3h+	+nh3	=h2cn+	c2h2	8.00(-10)	0.00	0.0
c3h+	+ch4	=c2h3+	c2h2	2.25(-10)	0.00	0.0
c3h+	+ch4	=c3h3+	ch2	2.25(-10)	0.00	0.0
nh3+	+h	=nh2+	h2	2.25(-10)	0.00	12800.0
nh3+	+c	=ch2+	nh	1.00(-11)	0.00	0.0

nh3+	+o	=hno+	h2		1.00(-11)	0.00	0.0
nh3+	+h2	=nh4+	h		2.40(-12)	0.00	0.0
nh3+	+ch	=nh4+	c		6.90(-10)	0.00	0.0
nh3+	+c2	=c2h2+	nh		1.00(-11)	0.00	0.0
nh3+	+oh	=nh4+	o		7.00(-10)	0.00	0.0
nh3+	+nh	=nh4+	n		7.10(-10)	0.00	0.0
nh3+	+hco	=nh4+	co		4.20(-10)	0.00	0.0
nh3+	+h2o	=nh4+	oh		2.50(-10)	0.00	0.0
nh3+	+h2s	=nh4+	sh		6.00(-10)	0.00	0.0
nh3+	+h2s	=h3s+	nh2		1.10(-10)	0.00	0.0
nh3+	+ch2	=ch3+	nh2		9.60(-10)	0.00	0.0
nh3+	+nh2	=nh4+	nh		1.00(-11)	0.00	0.0
nh3+	+nh3	=nh4+	nh2		2.30(-09)	0.00	0.0

-

3.v five-atom ions

-

ch4+	+h	=ch3+	h2		2.00(-10)	0.00	0.0
ch4+	+h2	=ch5+	h		4.00(-11)	0.00	0.0
ch4+	+co	=hco+	ch3		1.40(-09)	0.00	0.0
ch4+	+hcn	=h2cn+	ch3		3.30(-09)	0.00	0.0
ch4+	+h2o	=h3o+	ch3		2.50(-09)	0.00	0.0
ch4+	+h2s	=ch5+	sh		9.00(-11)	0.00	0.0
ch4+	+h2s	=h3s+	ch3		7.20(-10)	0.00	0.0
ch4+	+c2h2	=c2h3+	ch3		1.24(-09)	0.00	0.0
ch4+	+c2h2	=c3h3+	h2	h	1.51(-10)	0.00	0.0
ch4+	+nh3	=nh4+	ch3		1.49(-09)	0.00	0.0
ch4+	+nh3	=ch5+	nh2		6.32(-11)	0.00	0.0
ch4+	+ch4	=ch5+	ch3		1.50(-09)	0.00	0.0
c2h3+	+h	=c2h2+	h2		1.90(-10)	0.00	0.0
c2h3+	+hcn	=h2cn+	c2h2		1.60(-09)	0.00	0.0
c2h3+	+h2o	=h3o+	c2h2		1.11(-09)	0.00	0.0
c2h3+	+h2s	=h3s+	c2h2		8.40(-10)	0.00	0.0
c2h3+	+nh3	=nh4+	c2h2		2.48(-09)	0.00	0.0
c3h2+	+h	=c3h+	h2		1.00(-09)	0.00	24300.0
c3h2+	+h2	=c3h3+	h		1.00(-10)	0.00	2000.0
nh4+	+h	=nh3+	h2		1.00(-09)	0.00	11000.0

nh4+	+c	=h2cn+	h2	1.00(-11)	0.00	0.0
nh4+	+oh	=nh3+	h2o	2.50(-10)	0.00	3400.0
nh4+	+n2	=n2h+	nh3	2.30(-09)	0.00	44000.0

-

3.vi six-atom ions

-

ch5+	+h	=ch4+	h2	4.00(-11)	0.00	2200.0
ch5+	+c	=ch+	ch4	1.20(-09)	0.00	0.0
ch5+	+o	=h3o+	ch2	2.16(-10)	0.00	0.0
ch5+	+s	=sh+	ch4	1.30(-09)	0.00	0.0
ch5+	+ch	=ch2+	ch4	6.90(-10)	0.00	0.0
ch5+	+co	=hco+	ch4	9.90(-10)	0.00	0.0
ch5+	+c2	=c2h+	ch4	9.50(-10)	0.00	0.0
ch5+	+oh	=h2o+	ch4	7.00(-10)	0.00	0.0
ch5+	+nh	=nh2+	ch4	7.10(-10)	0.00	0.0
ch5+	+hcn	=c2h3+	nh3	1.00(-09)	0.00	5120.0
ch5+	+hcn	=h2cn+	ch4	1.20(-09)	0.00	0.0
ch5+	+hnc	=c2h3+	nh3	1.00(-09)	0.00	0.0
ch5+	+h2o	=h3o+	ch4	3.70(-09)	0.00	0.0
ch5+	+ch2	=ch3+	ch4	9.60(-10)	0.00	0.0
ch5+	+c2h	=c2h2+	ch4	9.00(-10)	0.00	0.0
ch5+	+nh2	=nh3+	ch4	9.90(-10)	0.00	0.0
ch5+	+c2h2	=c2h3+	ch4	1.56(-09)	0.00	0.0
ch5+	+nh3	=nh4+	ch4	2.30(-09)	0.00	0.0
c3h3+	+h	=c3h2+	h2	1.00(-10)	0.00	0.0

-

---

4. charge transfer reactions

-

4.i monatomic ions

-

h+	+o	=o+	h	7.00(-10)	0.00	232.0
h+	+s	=s+	h	1.30(-09)	0.00	0.0

h+	+fe	=fe+	h		7.40(-09)	0.00	0.0
h+	+h2	=h2+	h		1.00(-10)	0.00	21200.0
h+	+ch	=ch+	h		1.90(-09)	0.00	0.0
h+	+cn	=cn+	h		2.10(-09)	0.00	6150.0
h+	+cs	=cs+	h		4.90(-09)	0.00	0.0
h+	+c2	=c2+	h		3.10(-09)	0.00	0.0
h+	+oh	=oh+	h		2.10(-09)	0.00	0.0
h+	+o2	=o2+	h		1.17(-09)	0.00	0.0
h+	+nh	=nh+	h		2.10(-09)	0.00	0.0
h+	+no	=no+	h		1.90(-09)	0.00	0.0
h+	+sh	=sh+	h		1.60(-09)	0.00	0.0
h+	+so	=so+	h		3.20(-09)	0.00	0.0
h+	+hco	=hco+	h		9.40(-10)	0.00	0.0
h+	+hcn	=hcn+	h		1.10(-08)	0.00	12.0
h+	+h2o	=h2o+	h		8.20(-09)	0.00	0.0
h+	+h2s	=h2s+	h		7.60(-09)	0.00	0.0
h+	+ch2	=ch2+	h		1.40(-09)	0.00	0.0
h+	+c2h	=c2h+	h		1.50(-09)	0.00	0.0
h+	+c3	=c3+	h		4.00(-09)	0.00	0.0
h+	+nh2	=nh2+	h		2.90(-09)	0.00	0.0
h+	+ch3	=ch3+	h		3.40(-09)	0.00	0.0
h+	+c2h2	=c2h2+	h		2.00(-09)	0.00	0.0
h+	+c3h	=c3h+	h		2.00(-09)	0.00	0.0
h+	+nh3	=nh3+	h		5.20(-09)	0.00	0.0
h+	+ch4	=ch4+	h		1.52(-09)	0.00	0.0
h+	+c3h2	=c3h2+	h		2.00(-09)	0.00	0.0
he+	+h	=h+	he	photon	1.90(-15)	0.00	0.0
he+	+oh	=oh+	he		5.50(-10)	0.00	0.0
he+	+n2	=n2+	he		4.08(-10)	0.00	0.0
he+	+h2o	=h2o+	he		4.86(-11)	-.94	0.0
he+	+h2s	=h2s+	he		3.10(-10)	0.00	0.0
he+	+c2h2	=c2h2+	he		2.45(-10)	0.00	0.0
he+	+nh3	=nh3+	he		2.64(-10)	0.00	0.0
he+	+ch4	=ch4+	he		1.60(-11)	0.00	0.0
c+	+s	=s+	c		1.50(-09)	0.00	0.0
c+	+fe	=fe+	c		2.60(-09)	0.00	0.0
c+	+ch	=ch+	c		3.80(-10)	0.00	0.0
c+	+cs	=cs+	c		1.60(-09)	0.00	700.0

c+	+c2	=c2+	c	1.10(-10)	0.00	9120.0
c+	+no	=no+	c	3.40(-09)	0.00	0.0
c+	+so	=so+	c	2.60(-10)	0.00	0.0
c+	+hco	=hco+	c	4.80(-10)	0.00	0.0
c+	+h2s	=h2s+	c	4.25(-10)	0.00	0.0
c+	+ch2	=ch2+	c	5.20(-10)	0.00	0.0
c+	+nh3	=nh3+	c	5.29(-10)	0.00	0.0
o+	+h	=h+	o	6.00(-10)	0.00	0.0
o+	+fe	=fe+	o	2.90(-09)	0.00	0.0
o+	+ch	=ch+	o	3.50(-10)	0.00	0.0
o+	+c2	=c2+	o	4.80(-10)	0.00	0.0
o+	+oh	=oh+	o	3.60(-10)	0.00	0.0
o+	+o2	=o2+	o	3.00(-12)	0.00	0.0
o+	+nh	=nh+	o	3.60(-10)	0.00	0.0
o+	+no	=no+	o	1.00(-12)	0.00	0.0
o+	+hco	=hco+	o	4.30(-10)	0.00	0.0
o+	+h2o	=h2o+	o	2.30(-09)	0.00	0.0
o+	+h2s	=h2s+	o	1.80(-09)	0.00	0.0
o+	+ch2	=ch2+	o	9.70(-10)	0.00	0.0
o+	+c2h	=c2h+	o	4.60(-10)	0.00	0.0
o+	+nh2	=nh2+	o	1.00(-09)	0.00	0.0
n+	+ch	=ch+	n	3.60(-10)	0.00	0.0
n+	+co	=co+	n	8.25(-10)	0.00	0.0
n+	+cn	=cn+	n	1.10(-09)	0.00	0.0
n+	+c2	=c2+	n	1.00(-09)	0.00	0.0
n+	+oh	=oh+	n	3.70(-10)	0.00	0.0
n+	+o2	=o2+	n	2.81(-10)	0.00	0.0
n+	+nh	=nh+	n	3.70(-10)	0.00	0.0
n+	+no	=no+	n	4.51(-10)	0.00	0.0
n+	+hco	=hco+	n	4.50(-10)	0.00	0.0
n+	+hcn	=hcn+	n	1.20(-09)	0.00	0.0
n+	+h2o	=h2o+	n	2.60(-09)	0.00	0.0
n+	+ch2	=ch2+	n	1.00(-09)	0.00	0.0
n+	+c2h	=c2h+	n	9.50(-10)	0.00	0.0
n+	+nh2	=nh2+	n	1.00(-09)	0.00	0.0
s+	+fe	=fe+	s	1.80(-10)	0.00	0.0
s+	+no	=no+	s	3.20(-10)	0.00	0.0
s+	+sh	=sh+	s	9.70(-10)	0.00	350.0

```
s+      +hco     =hco+     s                  3.60(-10)  0.00      0.0
s+      +nh3     =nh3+     s                  1.60(-09)  0.00      0.0
                      -
-------------------------------------------
4.ii diatomic ions
-------------------------------------------
                      -
h2+     +h       =h+       h2                 6.40(-10)  0.00      0.0
h2+     +ch      =ch+      h2                 7.10(-10)  0.00      0.0
h2+     +co      =co+      h2                 6.00(-10)  0.00      0.0
h2+     +cn      =cn+      h2                 1.20(-09)  0.00      0.0
h2+     +c2      =c2+      h2                 1.10(-09)  0.00      0.0
h2+     +oh      =oh+      h2                 7.60(-10)  0.00      0.0
h2+     +o2      =o2+      h2                 8.00(-10)  0.00      0.0
h2+     +nh      =nh+      h2                 7.60(-10)  0.00      0.0
h2+     +no      =no+      h2                 1.10(-09)  0.00      0.0
h2+     +hco     =hco+     h2                 1.00(-09)  0.00      0.0
h2+     +hcn     =hcn+     h2                 2.70(-09)  0.00      0.0
h2+     +h2o     =h2o+     h2                 3.90(-09)  0.00      0.0
h2+     +h2s     =h2s+     h2                 2.70(-09)  0.00      0.0
h2+     +ch2     =ch2+     h2                 1.00(-09)  0.00      0.0
h2+     +c2h     =c2h+     h2                 1.00(-09)  0.00      0.0
h2+     +nh2     =nh2+     h2                 2.10(-09)  0.00      0.0
h2+     +ch3     =ch3+     h2                 1.00(-09)  0.00      0.0
h2+     +c2h2    =c2h2+    h2                 4.80(-09)  0.00      0.0
h2+     +nh3     =nh3+     h2                 5.70(-09)  0.00      0.0
h2+     +ch4     =ch4+     h2                 1.40(-09)  0.00      0.0
ch+     +s       =s+       ch                 4.70(-10)  0.00      0.0
ch+     +fe      =fe+      ch                 2.60(-10)  0.00      0.0
ch+     +no      =no+      ch                 1.00(-09)  0.00      0.0
ch+     +hco     =hco+     ch                 4.60(-10)  0.00      0.0
ch+     +nh3     =nh3+     ch                 4.59(-10)  0.00      0.0
co+     +h       =h+       co                 7.50(-10)  0.00      0.0
co+     +c       =c+       co                 1.10(-10)  0.00      0.0
co+     +o       =o+       co                 1.40(-10)  0.00      0.0
co+     +s       =s+       co                 1.10(-09)  0.00      0.0
co+     +ch      =ch+      co                 3.20(-10)  0.00      0.0
co+     +c2      =c2+      co                 8.40(-10)  0.00      0.0
```

co+	+oh	=oh+	co	3.10(-10)	0.00	0.0
co+	+o2	=o2+	co	7.60(-10)	0.00	0.0
co+	+nh	=nh+	co	3.20(-10)	0.00	0.0
co+	+no	=no+	co	3.30(-10)	0.00	0.0
co+	+hco	=hco+	co	7.40(-10)	0.00	0.0
co+	+hcn	=hcn+	co	5.10(-10)	0.00	0.0
co+	+h2o	=h2o+	co	4.20(-10)	0.00	0.0
co+	+ch2	=ch2+	co	4.30(-10)	0.00	0.0
co+	+c2h	=c2h+	co	3.90(-10)	0.00	0.0
co+	+nh2	=nh2+	co	4.50(-10)	0.00	0.0
cn+	+h	=h+	cn	1.90(-10)	0.00	0.0
cn+	+c	=c+	cn	1.10(-10)	0.00	0.0
cn+	+o	=o+	cn	6.50(-11)	0.00	0.0
cn+	+s	=s+	cn	1.10(-09)	0.00	0.0
cn+	+ch	=ch+	cn	6.40(-10)	0.00	0.0
cn+	+co	=co+	cn	8.90(-10)	0.00	0.0
cn+	+c2	=c2+	cn	8.50(-10)	0.00	0.0
cn+	+oh	=oh+	cn	6.40(-10)	0.00	0.0
cn+	+o2	=o2+	cn	7.80(-10)	0.00	0.0
cn+	+nh	=nh+	cn	6.50(-10)	0.00	0.0
cn+	+no	=no+	cn	8.10(-10)	0.00	0.0
cn+	+hco	=hco+	cn	3.70(-10)	0.00	0.0
cn+	+hcn	=hcn+	cn	1.00(-09)	0.00	0.0
cn+	+h2o	=h2o+	cn	8.60(-10)	0.00	0.0
cn+	+ch2	=ch2+	cn	8.80(-10)	0.00	0.0
cn+	+c2h	=c2h+	cn	8.00(-10)	0.00	0.0
cn+	+nh2	=nh2+	cn	9.10(-10)	0.00	0.0
cs+	+fe	=fe+	cs	1.70(-10)	0.00	0.0
c2+	+c	=c+	c2	1.10(-10)	0.00	0.0
c2+	+s	=s+	c2	5.80(-10)	0.00	0.0
c2+	+ch	=ch+	c2	3.20(-10)	0.00	0.0
c2+	+oh	=oh+	c2	6.50(-10)	0.00	0.0
c2+	+no	=no+	c2	8.30(-10)	0.00	0.0
c2+	+hco	=hco+	c2	3.80(-10)	0.00	0.0
c2+	+ch2	=ch2+	c2	4.50(-10)	0.00	0.0
c2+	+nh2	=nh2+	c2	4.60(-10)	0.00	0.0
oh+	+s	=s+	oh	4.30(-10)	0.00	0.0
oh+	+ch	=ch+	oh	3.50(-10)	0.00	0.0

oh+	+c2	=c2+	oh	4.80(-10)	0.00	0.0
oh+	+o2	=o2+	oh	2.00(-10)	0.00	0.0
oh+	+nh	=nh+	oh	3.60(-10)	0.00	0.0
oh+	+no	=no+	oh	4.60(-10)	0.00	0.0
oh+	+hco	=hco+	oh	2.80(-10)	0.00	0.0
oh+	+h2o	=h2o+	oh	1.50(-09)	0.00	0.0
oh+	+ch2	=ch2+	oh	4.80(-10)	0.00	0.0
oh+	+c2h	=c2h+	oh	4.50(-10)	0.00	0.0
oh+	+nh2	=nh2+	oh	5.00(-10)	0.00	0.0
oh+	+nh3	=nh3+	oh	1.20(-09)	0.00	0.0
o2+	+c	=c+	o2	5.20(-11)	0.00	0.0
o2+	+s	=s+	o2	5.40(-10)	0.00	0.0
o2+	+fe	=fe+	o2	1.10(-09)	0.00	0.0
o2+	+ch	=ch+	o2	3.10(-10)	0.00	0.0
o2+	+c2	=c2+	o2	4.10(-10)	0.00	0.0
o2+	+no	=no+	o2	4.40(-10)	0.00	0.0
o2+	+hco	=hco+	o2	3.60(-10)	0.00	0.0
o2+	+h2s	=h2s+	o2	1.40(-09)	0.00	0.0
o2+	+ch2	=ch2+	o2	4.30(-10)	0.00	0.0
o2+	+nh2	=nh2+	o2	8.70(-10)	0.00	0.0
o2+	+nh3	=nh3+	o2	2.00(-09)	0.00	0.0
nh+	+s	=s+	nh	6.90(-10)	0.00	0.0
no+	+fe	=fe+	no	1.00(-09)	0.00	0.0
n2+	+h	=h+	n2	1.90(-10)	0.00	0.0
n2+	+c	=c+	n2	1.10(-10)	0.00	0.0
n2+	+n	=n+	n2	1.00(-11)	0.00	0.0
n2+	+s	=s+	n2	1.10(-09)	0.00	0.0
n2+	+fe	=fe+	n2	4.30(-10)	0.00	0.0
n2+	+ch	=ch+	n2	6.30(-10)	0.00	0.0
n2+	+co	=co+	n2	7.00(-11)	0.00	0.0
n2+	+cn	=cn+	n2	1.00(-10)	0.00	0.0
n2+	+c2	=c2+	n2	8.40(-10)	0.00	0.0
n2+	+oh	=oh+	n2	6.30(-10)	0.00	0.0
n2+	+o2	=o2+	n2	5.00(-11)	0.00	0.0
n2+	+nh	=nh+	n2	6.50(-10)	0.00	0.0
n2+	+no	=no+	n2	3.30(-10)	0.00	0.0
n2+	+hco	=hco+	n2	3.70(-10)	0.00	0.0
n2+	+hcn	=hcn+	n2	1.00(-09)	0.00	0.0

```
n2+     +h2o     =h2o+     n2                2.20(-09)  0.00      0.0
n2+     +ch2     =ch2+     n2                8.70(-10)  0.00      0.0
n2+     +c2h     =c2h+     n2                7.90(-10)  0.00      0.0
n2+     +nh2     =nh2+     n2                8.90(-10)  0.00      0.0
sh+     +s       =s+       sh                9.70(-10)  0.00      0.0
sh+     +fe      =fe+      sh                1.60(-09)  0.00      0.0
sh+     +no      =no+      sh                3.30(-10)  0.00      0.0
sh+     +h2s     =h2s+     sh                5.00(-10)  0.00   1000.0
sh+     +nh3     =nh3+     sh                5.25(-10)  0.00      0.0
so+     +fe      =fe+      so                1.60(-09)  0.00      0.0
so+     +nh3     =nh3+     so                1.30(-09)  0.00      0.0
                    -
-----------------------------------------
4.iii triatomic ions
-----------------------------------------
                    -
hcn+    +h       =h+       hcn               1.10(-08)  0.00      0.0
hcn+    +o       =o+       hcn               6.50(-11)  0.00      0.0
hcn+    +s       =s+       hcn               5.70(-10)  0.00      0.0
hcn+    +o2      =o2+      hcn               7.70(-10)  0.00      0.0
hcn+    +no      =no+      hcn               8.10(-10)  0.00      0.0
hco+    +fe      =fe+      hco               1.90(-09)  0.00      0.0
h2o+    +h       =h+       h2o               8.20(-09)  0.00  11460.0
h2o+    +s       =s+       h2o               4.30(-10)  0.00      0.0
h2o+    +fe      =fe+      h2o               1.50(-09)  0.00      0.0
h2o+    +ch      =ch+      h2o               3.40(-10)  0.00      0.0
h2o+    +c2      =c2+      h2o               4.70(-10)  0.00      0.0
h2o+    +o2      =o2+      h2o               2.00(-10)  0.00      0.0
h2o+    +no      =no+      h2o               9.10(-10)  0.00      0.0
h2o+    +hco     =hco+     h2o               2.80(-10)  0.00      0.0
h2o+    +h2s     =h2s+     h2o               8.90(-10)  0.00      0.0
h2o+    +ch2     =ch2+     h2o               4.70(-10)  0.00      0.0
h2o+    +c2h     =c2h+     h2o               4.40(-10)  0.00      0.0
h2o+    +nh2     =nh2+     h2o               4.90(-10)  0.00      0.0
h2o+    +nh3     =nh3+     h2o               2.20(-09)  0.00      0.0
h2s+    +hco     =hco+     h2s               7.00(-10)  0.00      0.0
h2s+    +s       =s+       h2s               1.10(-09)  0.00      0.0
h2s+    +fe      =fe+      h2s               1.80(-09)  0.00      0.0
```

```
h2s+    +no     =no+    h2s          3.70(-10)  0.00      0.0
h2s+    +sh     =sh+    h2s          5.00(-10)  0.00      0.0
h2s+    +nh3    =nh3+   h2s          3.40(-10)  0.00      0.0
ch2+    +no     =no+    ch2          9.80(-10)  0.00      0.0
c2h+    +h      =h+     c2h          1.50(-09)  0.00  11500.0
c2h+    +s      =s+     c2h          1.20(-09)  0.00      0.0
nh2+    +s      =s+     nh2          4.40(-10)  0.00      0.0
nh2+    +ch     =ch+    nh2          3.50(-10)  0.00      0.0
nh2+    +no     =no+    nh2          9.40(-10)  0.00      0.0
nh2+    +hco    =hco+   nh2          4.30(-10)  0.00      0.0
nh2+    +h2s    =h2s+   nh2          3.40(-10)  0.00      0.0
nh2+    +ch2    =ch2+   nh2          4.90(-10)  0.00      0.0
nh2+    +nh3    =nh3+   nh2          1.50(-09)  0.00      0.0
                -
-------------------------------------------
4.iv four-atom ions
-------------------------------------------
                -
ch3+    +fe     =fe+    ch3          2.40(-09)  0.00      0.0
ch3+    +no     =no+    ch3          9.40(-10)  0.00      0.0
ch3+    +hco    =hco+   ch3          4.40(-10)  0.00      0.0
c2h2+   +fe     =fe+    c2h2         2.00(-09)  0.00      0.0
c2h2+   +no     =no+    c2h2         8.10(-10)  0.00      0.0
c2h2+   +hco    =hco+   c2h2         5.00(-10)  0.00      0.0
c2h2+   +h2s    =h2s+   c2h2         2.20(-09)  0.00      0.0
c2h2+   +nh3    =nh3+   c2h2         2.14(-09)  0.00      0.0
c3h+    +nh3    =nh3+   c3h          8.00(-10)  0.00      0.0
nh3+    +fe     =fe+    nh3          2.30(-09)  0.00      0.0
nh3+    +no     =no+    nh3          9.20(-10)  0.00      0.0
nh3+    +hco    =hco+   nh3          4.20(-10)  0.00      0.0
                -
-------------------------------------------
4.v five-atom ions
-------------------------------------------
                -
ch4+    +h2s    =h2s+   ch4          5.90(-10)  0.00      0.0
ch4+    +c2h2   =c2h2+  ch4          1.13(-09)  0.00      0.0
ch4+    +nh3    =nh3+   ch4          1.58(-09)  0.00      0.0
```

```
-
-------------------------------------------
5. neutral exchange reactions
-------------------------------------------
-
```

h	+h2	=h	h	h	4.67(-07)	-1.00	55000.0
h	+ch	=c	h2		1.73(-11)	0.50	2200.0
h	+ch	=c	h	h	6.00(-09)	0.00	40200.0
h	+co	=c	oh		1.10(-10)	0.50	77700.0
h	+c2	=c	ch		4.67(-10)	0.50	30450.0
h	+oh	=o	h2		4.20(-12)	1.00	3500.0
h	+oh	=o	h	h	6.00(-09)	0.00	50900.0
h	+o2	=oh	o		1.63(-09)	-.90	8750.0
h	+o2	=o	o	h	6.00(-09)	0.00	52300.0
h	+nh	=n	h2		8.66(-10)	0.50	2400.0
h	+no	=nh	o		1.44(-10)	0.50	38200.0
h	+no	=oh	n		7.27(-11)	0.50	24460.0
h	+sh	=s	h2		2.50(-11)	0.00	0.0
h	+so	=oh	s		5.90(-10)	-.31	11100.0
h	+so	=sh	o		1.73(-11)	0.50	19930.0
h	+hco	=co	h2		3.00(-10)	0.00	0.0
h	+hnc	=hcn	h		1.00(-10)	0.50	200.0
h	+h2o	=oh	h2		5.24(-12)	1.90	9265.0
h	+h2o	=oh	h	h	5.80(-09)	0.00	52900.0
h	+h2s	=sh	h2		1.29(-11)	0.00	860.0
h	+ch2	=ch	h2		2.28(-11)	0.67	12850.0
h	+ocs	=sh	co		1.70(-11)	0.00	2000.0
h	+nh2	=nh	h2		5.25(-12)	0.79	2200.0
h	+so2	=so	oh		9.25(-09)	-.74	14700.0
h	+ch3	=ch2	h2		5.18(-11)	0.17	5600.0
h	+nh3	=nh2	h2		6.32(-11)	0.17	5700.0
h	+ch4	=ch3	h2		3.00(-10)	0.00	6560.0
c	+h2	=ch	h		1.16(-09)	0.50	14100.0
c	+ch	=c2	h		1.73(-11)	0.50	0.0
c	+co	=c2	o		2.94(-11)	0.50	58025.0
c	+cn	=c2	n		7.27(-12)	0.50	19300.0
c	+oh	=co	h		1.10(-10)	0.50	0.0
c	+oh	=ch	o		2.25(-11)	0.50	14800.0

c	+o2	=co	o		3.30(-11)	0.50	0.0
c	+nh	=cn	h		1.10(-10)	0.50	0.0
c	+nh	=ch	n		1.73(-11)	0.50	4000.0
c	+no	=cn	o		1.10(-10)	0.50	0.0
c	+no	=co	n		1.73(-11)	0.50	4000.0
c	+n2	=cn	n		3.81(-11)	0.50	22750.0
c	+sh	=cs	h		2.00(-11)	0.00	0.0
c	+sh	=ch	s		1.20(-11)	0.58	5880.0
c	+so	=co	s		7.20(-11)	0.00	0.0
c	+so	=cs	o		1.70(-10)	0.00	0.0
c	+hco	=ch	co		1.00(-11)	0.00	0.0
c	+nh2	=hnc	h		2.00(-11)	0.50	0.0
o	+h2	=oh	h		1.55(-13)	2.80	2980.0
o	+ch	=co	h		9.50(-11)	0.50	0.0
o	+ch	=oh	c		1.73(-11)	0.50	4000.0
o	+cn	=co	n		1.80(-11)	0.50	50.0
o	+cn	=no	c		3.81(-11)	0.50	14545.0
o	+cs	=co	s		2.70(-10)	0.00	760.0
o	+cs	=so	c		4.68(-11)	0.50	28940.0
o	+c2	=co	c		5.00(-11)	0.50	0.0
o	+oh	=o2	h		3.10(-11)	-.36	0.0
o	+nh	=oh	n		2.90(-11)	0.50	0.0
o	+nh	=no	h		1.73(-11)	0.50	0.0
o	+no	=o2	n		7.50(-13)	1.00	16000.0
o	+sh	=so	h		1.60(-10)	0.00	100.0
o	+sh	=oh	s		1.70(-11)	0.67	950.0
o	+so	=s	o2		6.60(-13)	0.00	2760.0
o	+hco	=oh	co		1.59(-10)	1.00	0.0
o	+hcn	=oh	cn		8.70(-12)	0.00	4100.0
o	+hnc	=co	nh		2.00(-10)	0.50	200.0
o	+h2o	=oh	oh		1.10(-11)	0.00	9240.0
o	+h2s	=sh	oh		1.40(-11)	0.00	1920.0
o	+ch2	=co	h	h	2.00(-11)	0.50	0.0
o	+ch2	=ch	oh		1.79(-11)	0.70	13100.0
o	+ch2	=hco	h		1.44(-11)	0.50	2000.0
o	+c2h	=co	ch		1.00(-10)	0.00	250.0
o	+c3	=co	c2		5.00(-11)	0.50	0.0
o	+ocs	=so	co		2.60(-11)	0.00	2250.0

o	+nh2	=nh	oh		3.50(-12)	0.50	0.0
o	+so2	=so	o2		9.27(-11)	-.46	9140.0
o	+ch3	=co	h2	h	1.80(-10)	0.50	0.0
o	+c3h	=c2h	co		5.00(-11)	0.50	0.0
o	+c2h2	=c2h	oh		5.30(-09)	0.00	8520.0
o	+c2h2	=ch2	co		8.70(-11)	0.00	1800.0
o	+nh3	=nh2	oh		2.50(-12)	0.00	3020.0
o	+ch4	=ch3	oh		3.50(-11)	0.00	4550.0
o	+c3h2	=c2h2	co		5.00(-11)	0.50	0.0
n	+h2	=nh	h		8.66(-10)	0.50	14600.0
n	+ch	=cn	h		2.10(-11)	0.00	0.0
n	+cn	=n2	c		7.30(-10)	0.00	4500.0
n	+c2	=cn	c		5.00(-11)	0.50	0.0
n	+oh	=no	h		5.30(-11)	0.00	50.0
n	+o2	=no	o		3.30(-12)	1.00	3150.0
n	+nh	=n2	h		5.00(-11)	0.50	0.0
n	+no	=n2	o		3.40(-11)	0.00	50.0
n	+so	=no	s		1.73(-11)	0.50	750.0
n	+hco	=hcn	o		1.70(-10)	0.00	0.0
n	+ch2	=hcn	h		2.00(-11)	0.50	0.0
n	+ch3	=hcn	h2		2.00(-11)	0.50	0.0
n	+ch3	=hcn	h	h	8.60(-11)	0.50	0.0
s	+h2	=sh	h		1.04(-10)	.132	9620.0
s	+ch	=cs	h		1.10(-12)	0.00	0.0
s	+ch	=sh	c		1.73(-11)	0.50	4000.0
s	+cn	=cs	n		1.73(-11)	0.50	0.0
s	+c2	=cs	c		1.73(-11)	0.50	0.0
s	+oh	=so	h		1.00(-10)	0.50	100.0
s	+oh	=sh	o		3.81(-11)	0.50	0.0
s	+o2	=so	o		4.04(-12)	0.00	265.0
s	+nh	=sh	n		1.73(-11)	0.50	4000.0
s	+no	=so	n		1.14(-11)	0.50	17260.0
h2	+h2	=h	h	h2	1.00(-08)	0.00	84100.0
h2	+ch	=ch2	h		2.38(-10)	0.00	1760.0
h2	+ch	=c	h	h2	6.00(-09)	0.00	40200.0
h2	+cn	=hcn	h		3.53(-13)	3.31	756.0
h2	+c2	=c2h	h		1.60(-10)	0.00	1419.0
h2	+oh	=h2o	h		9.54(-13)	2.00	1490.0

h2	+oh	=o	h	h2	6.00(-09)	0.00	50900.0
h2	+o2	=oh	oh		4.20(-12)	0.00	9300.0
h2	+o2	=o	o	h2	6.00(-09)	0.00	52300.0
h2	+nh	=nh2	h		5.25(-12)	0.79	6700.0
h2	+sh	=h2s	h		6.41(-12)	.087	8050.0
h2	+h2o	=oh	h	h2	5.80(-09)	0.00	52900.0
h2	+ch2	=ch3	h		5.18(-11)	0.17	6400.0
h2	+ch3	=ch4	h		3.00(-10)	0.00	5460.0
h2	+c2h	=c2h2	h		1.14(-11)	0.00	950.0
h2	+nh2	=nh3	h		6.22(-11)	0.50	6300.0
ch	+oh	=hco	h		1.44(-11)	0.50	5000.0
ch	+o2	=hco	o		1.44(-11)	0.50	3000.0
ch	+no	=hco	n		2.70(-11)	0.00	5000.0
ch	+n2	=hcn	n		1.70(-13)	0.00	9560.0
ch	+hco	=ch2	co		2.87(-12)	0.70	500.0
ch	+ch4	=ch2	ch3		2.28(-11)	0.70	3000.0
co	+oh	=co2	h		4.40(-13)	-1.15	390.0
co	+sh	=ocs	h		5.95(-14)	1.12	8330.0
cn	+oh	=hcn	o		5.30(-12)	0.00	1500.0
cn	+o2	=co	no		5.30(-13)	0.00	0.0
cn	+nh	=hcn	n		2.94(-12)	0.50	1000.0
cn	+no	=n2	co		5.30(-13)	0.00	0.0
cn	+hco	=hcn	co		5.72(-12)	0.50	0.0
cn	+ch2	=ch	hcn		5.30(-12)	0.00	2500.0
cn	+ch3	=hcn	ch2		9.21(-12)	0.70	1500.0
cn	+ch4	=hcn	ch3		2.87(-11)	0.70	2500.0
cs	+oh	=ocs	h		1.55(-13)	1.12	800.0
oh	+cs	=ocs	h		9.39(-14)	1.12	800.0
oh	+oh	=h2o	o		1.00(-11)	0.00	550.0
oh	+nh	=h2o	n		1.44(-11)	0.50	1000.0
oh	+so	=so2	h		5.40(-11)	0.00	0.0
oh	+hco	=h2o	co		1.59(-11)	1.00	0.0
oh	+hcn	=h2o	cn		1.00(-10)	0.60	2500.0
oh	+hnc	=h2o	cn		2.00(-10)	0.50	200.0
oh	+h2s	=sh	h2o		6.30(-12)	0.00	80.0
oh	+ch2	=ch3	o		1.44(-11)	0.50	3000.0
oh	+ch2	=h2o	ch		1.44(-11)	0.50	3000.0
oh	+nh2	=nh	h2o		1.00(-13)	0.00	0.0

```
oh      +nh2    =nh3     o                    1.00(-13)  0.00      0.0
oh      +ch3    =h2o     ch2                  5.42(-11)  0.70   1000.0
oh      +c2h2   =h2o     c2h                  1.30(-11)  0.00   2335.0
oh      +nh3    =nh2     h2o                  2.30(-12)  0.00    800.0
oh      +ch4    =h2o     ch3                  2.40(-12)  0.00   1710.0
o2      +hnc    =co2     nh                   2.00(-11)  0.50   2000.0
o2      +so     =so2     o                    1.40(-12)  0.00   2820.0
o2      +ch2    =hco     oh                   1.70(-10)  0.00   1800.0
o2      +c2h    =hco     co                   1.70(-11)  0.00   3500.0
nh      +nh     =h2      n2                   1.70(-11)  0.00      0.0
nh      +no     =n2      o       h            4.70(-11)  0.50      0.0
no      +no     =n2      o2                   2.20(-10)  0.00  38060.0
no      +nh2    =n2      h2o                  1.60(-10)  0.00      0.0
sh      +sh     =h2s     s                    1.30(-11)  0.50      0.0
hco     +ch2    =ch3     co                   2.87(-12)  0.70    500.0
hco     +ch3    =ch4     co                   9.18(-12)  0.50      0.0
h2o     +ch3    =ch4     oh                   1.20(-11)  0.00  12900.0
ch2     +ch2    =ch      ch3                  1.44(-11)  0.50   3000.0
ch2     +ch4    =ch3     ch3                  1.19(-10)  0.70  10000.0
ch3     +nh3    =nh2     ch4                  1.70(-13)  0.00   5100.0
                    -
-------------------------------------------
6. chemi-ionisation
-------------------------------------------
                    -
ch      +o      =hco+    electr               2.00(-11)  0.44      0.0
                    -
-------------------------------------------
7. radiative recombinations
-------------------------------------------
                    -
h+      +electr =h       photon               3.61(-12)  -.75      0.0
he+     +electr =he      photon               4.50(-12)  -.67      0.0
c+      +electr =c       photon               4.40(-12)  -.61      0.0
o+      +electr =o       photon               3.40(-12)  -.63      0.0
n+      +electr =n       photon               3.80(-12)  -.62      0.0
s+      +electr =s       photon               3.90(-12)  -.63      0.0
fe+     +electr =fe      photon               3.70(-12)  -.65      0.0
```

```
h2s+   +electr =h2s     photon              1.10(-10)  -.70     0.0
ch3+   +electr =ch3     photon              1.10(-10)  -.70     0.0
                    -
-------------------------------------------
8. molecular recombinations
-------------------------------------------
                    -
h2+    +electr =h       h                   2.42(-09)  -.50     0.0
heh+   +electr =h       he                  2.00(-07)  -.50     0.0
ch+    +electr =c       h                   2.89(-07)  -.50     0.0
co+    +electr =c       o                   1.80(-07)  -.50     0.0
cn+    +electr =c       n                   1.80(-07)  -.50     0.0
cs+    +electr =c       s                   2.00(-07)  -.50     0.0
c2+    +electr =c       c                   2.00(-07)  -.50     0.0
oh+    +electr =o       h                   7.50(-08)  -.50     0.0
o2+    +electr =o       o                   1.95(-07)  -.70     0.0
nh+    +electr =n       h                   2.00(-07)  -.50     0.0
no+    +electr =n       o                   4.30(-07)  -.37     0.0
n2+    +electr =n       n                   1.80(-07)  -.39     0.0
sh+    +electr =s       h                   2.00(-07)  -.50     0.0
so+    +electr =s       o                   2.00(-07)  -.50     0.0
hco+   +electr =co      h                   2.40(-07)  -.69     0.0
hcn+   +electr =cn      h                   1.50(-07)  -.50     0.0
hcn+   +electr =ch      n                   1.50(-07)  -.50     0.0
hcs+   +electr =cs      h                   7.00(-07)  -.50     0.0
hno+   +electr =no      h                   3.00(-07)  -.50     0.0
hso+   +electr =so      h                   2.00(-07)  -.50     0.0
h2o+   +electr =oh      h                   3.15(-07)  -.50     0.0
h2o+   +electr =o       h2                  2.00(-07)  -.50     0.0
h2s+   +electr =sh      h                   1.50(-07)  -.50     0.0
h2s+   +electr =s       h       h           1.50(-07)  -.50     0.0
h3+    +electr =h2      h                   1.50(-07)  -.50     0.0
h3+    +electr =h       h       h           1.10(-07)  -.50     0.0
ch2+   +electr =ch      h                   2.50(-07)  -.50     0.0
ch2+   +electr =c       h2                  2.50(-07)  -.50     0.0
c2h+   +electr =c2      h                   2.70(-07)  -.50     0.0
c2h+   +electr =ch      c                   2.70(-07)  -.50     0.0
c2n+   +electr =c2      n                   1.00(-07)  -.50     0.0
```

c2n+	+electr =cn	c		2.00(-07)	-.50	0.0
c3+	+electr =c2	c		3.00(-07)	-.50	0.0
nh2+	+electr =n	h	h	1.50(-07)	-.50	0.0
nh2+	+electr =nh	h		1.50(-07)	-.50	0.0
n2h+	+electr =n2	h		1.70(-07)	-1.0	0.0
hco2+	+electr =co2	h		2.24(-07)	-.50	0.0
hco2+	+electr =co	oh		1.16(-07)	-.50	0.0
hocs+	+electr =oh	cs		2.00(-07)	-.50	0.0
hocs+	+electr =ocs	h		2.00(-07)	-.50	0.0
h2cn+	+electr =hnc	h		1.75(-07)	-.50	0.0
h2cn+	+electr =hcn	h		1.75(-07)	-.50	0.0
h2nc+	+electr =hnc	h		1.75(-07)	-.50	0.0
h2nc+	+electr =nh2	c		1.75(-07)	-.50	0.0
h3o+	+electr =oh	h2		8.45(-07)	-.50	0.0
h3o+	+electr =oh	h	h	6.50(-07)	-.50	0.0
h3o+	+electr =h2o	h		4.55(-07)	-.50	0.0
h3s+	+electr =h2s	h		3.00(-07)	-.50	0.0
h3s+	+electr =sh	h2		1.00(-07)	-.50	0.0
ch3+	+electr =ch2	h		1.50(-07)	-.50	0.0
ch3+	+electr =ch	h2		1.50(-07)	-.50	0.0
ch3+	+electr =ch	h	h	1.50(-07)	-.50	0.0
c2h2+	+electr =c2h	h		1.50(-07)	-.50	0.0
c2h2+	+electr =ch	ch		1.50(-07)	-.50	0.0
c2h2+	+electr =c2	h	h	2.00(-07)	-.50	0.0
c3h+	+electr =c2	ch		2.25(-07)	-.50	0.0
c3h+	+electr =c2h	c		2.25(-07)	-.50	0.0
nh3+	+electr =nh2	h		3.00(-07)	-.50	0.0
nh3+	+electr =nh	h	h	5.00(-07)	-.50	0.0
ch4+	+electr =ch2	h2		3.70(-07)	-.50	0.0
ch4+	+electr =ch2	h	h	3.00(-07)	-.50	0.0
ch4+	+electr =ch3	h		3.70(-07)	-.50	0.0
c2h3+	+electr =ch2	ch		1.35(-07)	-.50	0.0
c2h3+	+electr =c2h	h2		1.35(-07)	-.50	0.0
c2h3+	+electr =c2h2	h		3.00(-08)	-.50	0.0
c3h2+	+electr =c2h2	c		3.00(-07)	-.50	0.0
c3h2+	+electr =c2	ch2		3.00(-07)	-.50	0.0
c3h2+	+electr =c3h	h		1.50(-07)	-.50	0.0
c3h2+	+electr =c2h	ch		1.50(-07)	-.50	0.0

```
nh4+   +electr =nh2     h2              7.60(-07)  -.50     0.0
nh4+   +electr =nh2     h       h       3.00(-07)  -.50     0.0
nh4+   +electr =nh3     h               7.60(-07)  -.50     0.0
ch5+   +electr =ch      h2      h2      8.75(-08)  -.30     0.0
ch5+   +electr =ch2     h2      h       8.75(-08)  -.30     0.0
ch5+   +electr =ch3     h2              8.75(-08)  -.30     0.0
ch5+   +electr =ch4     h               8.75(-08)  -.30     0.0
c3h3+  +electr =c3h2    h               1.50(-07)  -.50     0.0
c3h3+  +electr =c2h2    ch              1.50(-07)  -.50     0.0
                        -
-----------------------------------------
9. radiative association
-----------------------------------------
                        -
c      +h      =ch      photon          1.00(-17)  0.00     0.0
c      +c      =c2      photon          1.00(-17)  0.00     0.0
c      +n      =cn      photon          1.00(-17)  0.00     0.0
o      +h      =oh      photon          5.00(-19)  0.00     0.0
o      +o      =o2      photon          4.90(-20)  1.58     0.0
co     +s      =ocs     photon          1.60(-17) -3.20     0.0
so     +o      =so2     photon          3.20(-16) -1.60     0.0
h+     +h      =h2+     photon          2.00(-20)  1.00     0.0
h+     +he     =heh+    photon          1.00(-18)  0.00     0.0
c+     +h      =ch+     photon          7.00(-17)  0.00     0.0
c+     +h2     =ch2+    photon          4.00(-16)  -.20     0.0
sh+    +h2     =h3s+    photon          1.00(-15)  0.00     0.0
ch3+   +h2     =ch5+    photon          6.00(-15)  0.00     0.0
c3h+   +h2     =c3h3+   photon          3.00(-13)  -1.0     0.0
                        -
-----------------------------------------
10. radiative attachment
-----------------------------------------
                        -
h      +electr =h-      photon          3.00(-16)  1.00     0.0
                        -
-----------------------------------------
11. associative detachment
-----------------------------------------
```

```
                    -
h-      +h      =h2     electr          1.30(-09)  0.00     0.0
h-      +c      =ch     electr          1.00(-09)  0.00     0.0
h-      +o      =oh     electr          1.00(-09)  0.00     0.0
h-      +n      =nh     electr          1.00(-09)  0.00     0.0
h-      +ch     =ch2    electr          1.00(-10)  0.00     0.0
h-      +co     =hco    electr          5.00(-11)  0.00     0.0
h-      +cn     =hcn    electr          1.00(-10)  0.00     0.0
h-      +c2     =c2h    electr          1.00(-09)  0.00     0.0
h-      +oh     =h2o    electr          1.00(-10)  0.00     0.0
h-      +nh     =nh2    electr          1.00(-10)  0.00     0.0
h-      +ch2    =ch3    electr          1.00(-09)  0.00     0.0
h-      +c2h    =c2h2   electr          1.00(-09)  0.00     0.0
h-      +nh2    =nh3    electr          1.00(-09)  0.00     0.0
h-      +ch3    =ch4    electr          1.00(-09)  0.00     0.0
                    -
-------------------------------------------
12. mutual neutralisation
-------------------------------------------
                    -
h-      +h+     =h      h               2.30(-07)  -.50     0.0
h-      +he+    =h      he              2.30(-07)  -.50     0.0
h-      +c+     =h      c               2.30(-07)  -.50     0.0
h-      +o+     =h      o               2.30(-07)  -.50     0.0
h-      +n+     =h      n               2.30(-07)  -.50     0.0
h-      +s+     =h      s               2.30(-07)  -.50     0.0
h-      +fe+    =h      fe              2.30(-07)  -.50     0.0
h-      +h2+    =h      h2              2.30(-07)  -.50     0.0
h-      +ch+    =h      ch              2.30(-07)  -.50     0.0
h-      +co+    =h      co              2.30(-07)  -.50     0.0
h-      +oh+    =h      oh              2.30(-07)  -.50     0.0
                    -
-------------------------------------------
13. dissociative neutralisation
-------------------------------------------
                    -
h-      +hco+   =co     h2              2.30(-07)  -.50     0.0
h-      +h3+    =h2     h2              2.30(-07)  -.50     0.0
```

```
h-      +h3o+   =oh      h2      h          2.30(-07)  -.50     0.0
h-      +h3o+   =h2o     h2                 2.30(-07)  -.50     0.0
h-      +nh4+   =nh3     h2                 2.30(-07)  -.50     0.0
                    -
-----------------------------------------
14. photo-events
-----------------------------------------
                    -
-----------------------------------------
14.i with cross-section data
-----------------------------------------
                    -
h-      +photon =h       electr             -1.0       0.00     0.0
c       +photon =c+      electr             -1.0       0.00     0.0
c2      +photon =c2+     electr             -1.0       0.00     0.0
h2o     +photon =h2o+    electr             -1.0       0.00     0.0
s       +photon =s+      electr             -1.0       0.00     0.0
fe      +photon =fe+     electr             -1.0       0.00     0.0
nh3     +photon =nh3+    electr             -1.0       0.00     0.0
ch      +photon =ch+     electr             -1.0       0.00     0.0
ch2     +photon =ch2+    electr             -1.0       0.00     0.0
ch3     +photon =ch3+    electr             -1.0       0.00     0.0
ch4     +photon =ch4+    electr             -1.0       0.00     0.0
c2h     +photon =c2h+    electr             -1.0       0.00     0.0
c2h2    +photon =c2h2+   electr             -1.0       0.00     0.0
oh      +photon =oh+     electr             -1.0       0.00     0.0
o2      +photon =o2+     electr             -1.0       0.00     0.0
nh      +photon =nh+     electr             -1.0       0.00     0.0
nh2     +photon =nh2+    electr             -1.0       0.00     0.0
no      +photon =no+     electr             -1.0       0.00     0.0
sh      +photon =sh+     electr             -1.0       0.00     0.0
cs      +photon =cs+     electr             -1.0       0.00     0.0
so      +photon =so+     electr             -1.0       0.00     0.0
                    -
-----------------------------------------
14.ii without cross-section data
-----------------------------------------
                    -
```

ch	+photon	=c	h		6.60(-10)	0.00	0.82
cn	+photon	=c	n		2.50(-10)	0.00	1.05
cs	+photon	=c	s		6.30(-10)	0.00	0.71
c2	+photon	=c	c		1.70(-10)	0.00	0.75
oh	+photon	=o	h		2.90(-10)	0.00	0.77
o2	+photon	=o	o		5.30(-10)	0.00	0.66
nh	+photon	=n	h		3.30(-10)	0.00	0.68
no	+photon	=n	o		3.30(-10)	0.00	0.72
n2	+photon	=n	n		2.10(-10)	0.00	1.20
sh	+photon	=s	h		6.50(-10)	0.00	0.67
so	+photon	=s	o		2.40(-09)	0.00	0.74
hco	+photon	=h	co		1.00(-09)	0.00	0.50
hcn	+photon	=cn	h		1.10(-09)	0.00	0.79
hnc	+photon	=cn	h		1.10(-09)	0.00	0.79
h2o	+photon	=oh	h		5.50(-10)	0.00	0.76
ocs	+photon	=s	co		2.40(-09)	0.00	0.75
ch2	+photon	=ch	h		4.90(-10)	0.00	0.79
c2h	+photon	=c2	h		3.40(-10)	0.00	0.67
nh2	+photon	=nh	h		5.00(-10)	0.00	0.83
ch3	+photon	=ch2	h		3.20(-10)	0.00	0.67
ch3	+photon	=ch	h2		3.20(-10)	0.00	0.67
c2h2	+photon	=c2h	h		2.10(-09)	0.00	0.71
c3h	+photon	=c2	ch		1.00(-09)	0.00	0.70
c3h	+photon	=c3h+	electr		1.00(-10)	0.00	1.00
nh3	+photon	=nh2	h		7.80(-10)	0.00	0.74
nh3	+photon	=nh	h2		7.80(-10)	0.00	0.74
ch4	+photon	=ch	h	h2	8.10(-10)	0.00	0.76
ch4	+photon	=ch2	h2		8.10(-10)	0.00	0.76
ch4	+photon	=ch3	h		8.10(-10)	0.00	0.76
c3h2	+photon	=c3h	h		1.20(-09)	0.00	0.67
c3h2	+photon	=c3h2+	electr		1.00(-10)	0.00	1.00
h2+	+photon	=h+	h		3.80(-10)	0.00	0.72
heh+	+photon	=he	h+		1.00(-12)	0.00	0.70
ch+	+photon	=h+	c		2.50(-10)	0.00	0.94
ch+	+photon	=c+	h		2.00(-12)	0.00	0.94
co+	+photon	=c+	o		3.00(-11)	0.00	1.00
c2+	+photon	=c+	c		1.00(-11)	0.00	0.70
oh+	+photon	=o+	h		8.50(-12)	0.00	1.05

```
hco+    +photon =co+     h                3.00(-10)  0.00    1.00
h2o+    +photon =oh+     h                3.00(-10)  0.00    0.76
h2o+    +photon =o+      h2               1.00(-10)  0.00    0.76
h2o+    +photon =oh      h+               1.00(-10)  0.00    0.76
h2o+    +photon =o       h2+              1.00(-10)  0.00    0.76
h3+     +photon =h2+     h                5.00(-13)  0.00    0.90
h3+     +photon =h+      h2               5.00(-13)  0.00    0.70
ch2+    +photon =ch+     h                1.70(-09)  0.00    0.76
h3o+    +photon =h2o+    h                1.50(-11)  0.00    0.76
h3o+    +photon =oh+     h2               5.00(-11)  0.00    0.76
h3o+    +photon =oh      h2+              5.00(-11)  0.00    0.76
h3o+    +photon =h2o     h+               5.00(-11)  0.00    0.76
ch3+    +photon =ch2+    h                1.00(-09)  0.00    0.76
ch3+    +photon =ch+     h2               1.00(-09)  0.00    0.76
ch4+    +photon =ch3+    h                1.00(-09)  0.00    0.76
ch4+    +photon =ch2+    h2               1.00(-09)  0.00    0.76
ch5+    +photon =ch4+    h                1.00(-09)  0.00    0.76
ch5+    +photon =ch3+    h2               1.00(-09)  0.00    0.76
                         -
-----------------------------------------
14.iii calculated in program
-----------------------------------------
                         -
h2      +photon =h       h                0.00       0.00    0.0
co      +photon =c       o                0.00       0.00    0.0
                         -
```

Note: a(b) implies $a \times 10^b$

Primary sources for rate coefficient data

H_2 formation on grains:	Hollenbach *et al.* (1971)
Cosmic ray reactions:	Gredel *et al.* (1989) Prasad and Huntress (1980)
Ion-molecule reactions:	UMIST rate file (Flower, private communication) Prasad and Huntress (1980)
Charge transfer reactions:	UMIST rate file (Flower, private communication)

	Prasad and Huntress (1980)
Neutral exchange reactions:	UMIST rate file (Flower, private communication) Leen and Groff (1988) Prasad and Huntress (1980)
Recombination reactions:	Millar *et al.* (1988) Prasad and Huntress (1980)
Radiative association:	Prasad and Huntress (1980)
Negative ion reactions:	Prasad and Huntress (1980)
Photodissociation reactions:	van Dishoeck (1988)

γ values derived from Mathis *et al.* (1983) interstellar radiation field

β values derived from Roberge *et al.* (1981) dust grain model (3)

Sources for photoionisation cross-section data

H^- (photodetachment)	Doughty *et al.* (1966)
C	Hofmann *et al.* (1983)
S	Chapman and Henry (1971)
Fe	Lombardi *et al.* (1978)
C_2	Padial *et al.* (1985)
H_2O	Haddad and Samson (1986)
NH_3	Samson *et al.* (1987)

All other photoionisation reactions (with known threshold wavelength) are assumed to exhibit a constant photoionisation cross-section of $\sigma = 10^{-17}$ cm^2 between the Lyman limit of hydrogen and the threshold wavelength.

Appendix C

FORTRAN program GRAIN to compute the absorption, scattering and extinction efficiency factors for a spherical body using Mie scattering theory

```
      program grain
      implicit double precision(a-h, o-z)
      double complex m, a, b, alpha, beta, xa, xb
      double complex bessel(0:1, -100:100)
      common / bess / bessel
c     Program to calculate the extinction, scattering and
c     absorption efficiency factors of an absorbing and
c     scattering sphere with complex refractive index at
c     different wavelengths according to Mie theory
      pi = 3.1415926535d0
      iscrn = 6
      print *
      print *,'Program to calculate efficiency factors for'
      print *,'extinction, scattering and absorption'
      print *,'of a spherical grain which absorbs and scatters'
      print *,'radiation with a complex refractive index according'
      print *,'to Mie theory'
      print *
      print *,'Enter radius of grain (nm)'
      read *, rad
c     Convert radius to Angstrom
      rad = rad * 10.0d0
   10 print *
      print *,'Enter wavelength of radiation in vacuo (Angstrom)'
      print *,'Enter zero to terminate program'
      read *, xlam0
      if (xlam0 .gt. 0.0d0) then
         print *,'For the grain material:'
         print *,'Enter REAL part of refractive index'
         read *, gr
         print *,'Enter IMAGINARY part of refractive index'
         read *, gi
```

```
      m = dcmplx(gr, gi)
      q = 2.0d0 * pi * rad / xlam0
      alpha = dcmplx(q, 0.0d0)
      beta  = m * q
c     Perform calculation
      print *,'Wait .....'
c     Calculate spherical Bessel functions up to large negative
c     and positive orders for the two complex arguments
c     alpha and beta
      call miller(0, alpha, nm)
      nmax = nm
      call miller(1, beta, nm)
      if (nm .lt. nmax) nmax = nm
      xtinc = 0.0d0
      scatt = 0.0d0
      do 20 n = 1, nmax
         xa = a(n, alpha, beta, m)
         xb = b(n, alpha, beta, m)
         xt = dble(2*n + 1) * (2.0d0 -  dreal(xa + xb))
         xtinc = xtinc + xt
         xt = dble(2*n + 1) * (cdabs(xa - (1.0d0, 0.0d0))**2
     .         + cdabs(xb - (1.0d0, 0.0d0))**2)
         scatt = scatt + xt
20    continue
      xtinc = xtinc / q**2
      scatt = scatt / (2.0d0 * q**2)
      absor = xtinc - scatt
      if (xtinc .lt. 1.0d-10) xtinc = 0.0d0
      if (scatt .lt. 1.0d-10) scatt = 0.0d0
      if (absor .lt. 1.0d-10) absor = 0.0d0
      albedo = scatt / xtinc
      print *
      write (iscrn, 1000) q
      write (iscrn, 1001) xtinc
      write (iscrn, 1002) scatt
      write (iscrn, 1003) absor
      if (xtinc .ne. 0.0d0) then
         write (iscrn, 1004) albedo
```

```
         else
            write (iscrn, 1005)
         end if
         goto 10
      end if
 1000 format(1x, 'q (2 pi / lambda0) = ',1pd10.3)
 1001 format(1x, 'Extinction efficiency factor Q(e) = ',1pd10.3)
 1002 format(1x, 'Scattering efficiency factor Q(s) = ',1pd10.3)
 1003 format(1x, 'Absorption efficiency factor Q(a) = ',1pd10.3)
 1004 format(1x, 'Albedo of grain   Q(s)/Q(e)       = ',1pd10.3)
 1005 format(1x, 'Albedo of grain   Q(s)/Q(e)       =  infinity')
      stop
      end


      subroutine miller(j, z1, nmax)
c     Routine to compute the spherical Bessel function for the
c     complex argument z1 - Miller's method is used to compute
c     large positive orders of the functions and the recurrence
c     relation is used, starting from J(-1/2), to compute large
c     negative orders of the function (see Abramowitz and Stegun
c     for a summary of Millers method to compute the Bessel
c     function)
      implicit double precision(a-z)
      double complex z1, test, b0, p
      double complex bessel(0:1, -100:100)
      integer j, i, k, nmax
      common / bess / bessel
      data bessel / 402*(0.0d0,0.0d0) /
      pi = 3.1415926535d0
      e = dexp(1.0d0)
c     Use the asymptotic form for the Bessel function to determine
c     the largest value of positive order to use
      i = 0
   10 di = dble(i) + 0.5d0
      test = (e * z1 / (2.0d0 * di))**di /
     .    dsqrt(2.0d0 * pi * di)
      if (cdabs(test) .lt. 1.0d-20) goto 20
```

```
      i = i + 1
      goto 10
   20 if (i .gt. 98) i = 98
      nmax = i - 10
      bessel(j, i) = (1.0d0, 1.0d0)
      bessel(j, i+1) = (0.0d0, 0.0d0)
      do 30 k = i-1, 0, -1
         bessel(j, k) = dble(2*k + 3) * bessel(j, k+1) / z1 -
     .      bessel(j, k+2)
   30 continue
      b0 = cdsqrt(2.0d0 / (pi * z1)) * cdsin(z1)
      p = b0 / bessel(j, 0)
      do 40 k = 0, i
         bessel(j, k) = bessel(j, k) * p
   40 continue
c     Calculate spherical Bessel functions of negative order
      bessel(j, -1) = cdsqrt(2.0d0 / (pi * z1)) * cdcos(z1)
      do 50 k = -2, -i, -1
         bessel(j, k) = dble(2*k + 3) * bessel(j, k+1) / z1 -
     .      bessel(j, k+2)
   50 continue
      return
      end


      double complex function a(n, alpha, beta, m)
c     Calculate the a(n) coefficient
      implicit double precision(a-z)
      double complex a, alpha, beta, m, x, y
      double complex psi, zeta, theta
      double complex dpsi, dzeta, dtheta, dnb, pnb
      integer n
      dnb = dpsi(n, 1, beta)
      pnb = m * psi(n, 1, beta)
      x = dtheta(n, 0, alpha) * pnb - dnb * theta(n, 0, alpha)
      y = dzeta(n, 0, alpha) * pnb - dnb * zeta(n, 0, alpha)
      a = dble((-1)**n) * x / y
      return
```

```
      end


      double complex function b(n, alpha, beta, m)
c     Calculate the b(n) coefficient
      implicit double precision(a-z)
      double complex b, alpha, beta, m, x, y
      double complex psi, zeta, theta
      double complex dpsi, dzeta, dtheta, dnb, pnb
      integer n
      dnb = m * dpsi(n, 1, beta)
      pnb = psi(n, 1, beta)
      x = dtheta(n, 0, alpha) * pnb - dnb * theta(n, 0, alpha)
      y = dzeta(n, 0, alpha) * pnb - dnb * zeta(n, 0, alpha)
      b = dble((-1)**n) * x / y
      return
      end


      double complex function psi(n, j, z1)
c     Calculate the value of psi(z1)
      implicit double precision(a-z)
      double complex psi, z1, bessel(0:1, -100:100)
      integer n, j
      common / bess / bessel
      pi = 3.1415926535d0
      psi = cdsqrt(pi * z1 / 2.0d0) * bessel(j, n)
      return
      end


      double complex function zeta(n, j, z1)
c     Calculate the value of zeta(z1)
      implicit double precision(a-z)
      double complex zeta, psi, z1, bessel(0:1, -100:100)
      integer n, j
      common / bess / bessel
```

```
      pi = 3.1415926535d0
      zeta = psi(n, j, z1)
      zeta = zeta + (0.0d0, 1.0d0) * dble((-1)**(n+1)) *
     .    cdsqrt(pi * z1 / 2.0d0) * bessel(j, -(n+1))
      zeta = zeta * (0.0d0, 1.0d0) * dble((-1)**n)
      return
      end


      double complex function theta(n, j, z1)
c     Calculate the value of theta(z1)
      implicit double precision(a-z)
      double complex theta, psi, z1, bessel(0:1, -100:100)
      integer n, j
      common / bess / bessel
      pi = 3.1415926535d0
      theta = psi(n, j, z1)
      theta = theta + (0.0d0, 1.0d0) * dble((-1)**n) *
     .    cdsqrt(pi * z1 / 2.0d0) * bessel(j, -(n+1))
      theta = theta * (0.0d0, -1.0d0)
      return
      end


      double complex function dpsi(n, j, z1)
c     Calculate the value of psi'(z1)
      implicit double precision(a-z)
      double complex dpsi, z1, sqz, bessel(0:1, -100:100)
      integer n, j
      common / bess / bessel
      pi = 3.1415926535d0
      sqz = cdsqrt(z1)
      dpsi = bessel(j, n)/sqz + bessel(j, n-1)*sqz -
     .    bessel(j, n+1)*sqz
      dpsi = dpsi * 0.5d0 * dsqrt(pi / 2.0d0)
      return
      end
```

```
      double complex function dzeta(n, j, z1)
c     Calculate the value of zeta'(z1)
      implicit double precision(a-z)
      double complex dzeta, z1, dpsi, bessel(0:1, -100:100)
      integer n, j
      common / bess / bessel
      pi = 3.1415926535d0
      dzeta = bessel(j, -(n+2)) - bessel(j, -n) +
     .    bessel(j, -(n+1))/z1
      dzeta = dzeta * 0.5d0 * cdsqrt(pi * z1 / 2.0d0)
      dzeta = dzeta + (0.0d0, 1.0d0) * dble((-1)**n) *
     .    dpsi(n, j, z1)
      return
      end


      double complex function dtheta(n, j, z1)
c     Calculate the value of theta'(z1)
      implicit double precision(a-z)
      double complex dtheta, z1, dpsi, bessel(0:1, -100:100)
      integer n, j
      common / bess / bessel
      pi = 3.1415926535d0
      dtheta = bessel(j, -(n+2)) - bessel(j, -n) +
     .    bessel(j, -(n+1))/z1
      dtheta = dtheta * 0.5d0 * dble((-1)**n) *
     .    cdsqrt(pi * z1 / 2.0d0)
      dtheta = dtheta - (0.0d0, 1.0d0) * dpsi(n, j, z1)
      return
      end
```

Appendix D

Parameters of the spectral lines included in the incident radiation field

Kinetic temperature for Doppler velocities: 10^4 K
Bulk turbulent velocity in ionised region: 8 km s^{-1}
Hβ energy flux at ionised/neutral interface: 0.5880 erg cm^{-2} s^{-1}

Line intensity is expressed relative to the Hβ line

Species	Central Wavelength λ_0 (Å)	Thermal Doppler velocity V_{thermal} (km s^{-1})	Relative Intensity x	FWHM $\Delta\lambda_D$ ($\times 10^{-2}$Å)
H I	1216	12.8	20.50	10.20
C I	2967	3.72	5.654×10^{-4}	14.54
C I	1561	3.72	2.537×10^{-4}	7.652
C II	1335	3.72	4.482×10^{-2}	6.544
C II	1037	3.72	1.217×10^{-3}	5.083
C III	977	3.72	5.548×10^{-2}	4.789
C IV	1549	3.72	1.723	7.593
N I	1135	3.45	1.497×10^{-5}	5.494
N II	1085	3.45	3.986×10^{-3}	5.252
N III	992	3.45	4.828×10^{-3}	4.802
N V	1240	3.45	4.122×10^{-3}	6.002
O I	1356	3.22	3.145×10^{-3}	6.497
O I	1304	3.22	3.254×10^{-4}	6.248
O VI	1034	3.22	2.239×10^{-6}	4.954
Mg I	2852	2.63	6.926×10^{-5}	13.34
Mg II	2798	2.63	1.867×10^{-2}	13.09
Si II	2334	2.43	1.855×10^{-2}	10.84
Si II	1195	2.43	7.288×10^{-6}	5.551

Species	Central Wavelength λ_0 (Å)	Thermal Doppler velocity V_{thermal} (km s^{-1})	Relative Intensity x	FWHM $\Delta\lambda_D$ ($\times 10^{-2}$Å)
Si II	1308	2.43	1.240×10^{-5}	6.076
Si II	1814	2.43	5.061×10^{-4}	8.427
Si II	1263	2.43	5.295×10^{-5}	5.867
Si II	1531	2.43	7.060×10^{-5}	7.112
Si III	1892	2.43	6.533×10^{-3}	8.789
Si III	1207	2.43	2.602×10^{-4}	5.607
Si IV	1397	2.43	1.135×10^{-3}	6.490
S I	1429	2.78	5.958×10^{-7}	6.724
S II	1256	2.78	6.435×10^{-4}	5.910
S III	1199	2.78	4.132×10^{-4}	5.642
S III	1014	2.78	3.689×10^{-4}	4.771
S III	1729	2.78	7.787×10^{-3}	8.136
S IV	1400	2.78	4.993×10^{-3}	6.588
S V	1194	2.78	6.521×10^{-4}	5.618
Ar V	1160	2.04	2.071×10^{-5}	5.321
Ar VI	1000	2.04	3.768×10^{-6}	4.587
C II	2326	3.72	7.648×10^{-1}	11.40
N II	2141	3.45	6.504×10^{-2}	10.36
O III	1663	3.22	1.640×10^{-1}	7.968
O V	1215	3.22	1.153×10^{-3}	5.822
Fe VII	1491	1.73	2.179×10^{-8}	6.780
Mg V	2417	2.63	4.180×10^{-8}	11.31
Mg V	1316	2.63	3.880×10^{-8}	6.157
Mg VI	1207	2.63	5.400×10^{-11}	5.647
Ar V	2691	2.04	6.640×10^{-4}	12.34

Species	Central Wavelength λ_0 (Å)	Thermal Doppler velocity V_{thermal} (km s^{-1})	Relative Intensity x	FWHM $\Delta\lambda_D$ ($\times 10^{-2}$Å)
Mg V	2780	2.63	1.600×10^{-5}	13.01
Mg VI	1847	2.63	2.530×10^{-9}	8.642
Ne V	2973	2.87	7.340×10^{-6}	14.04
O I	2972	3.22	9.930×10^{-5}	14.24
O III	2321	3.22	2.730×10^{-2}	11.12
Ne III	1815	2.87	5.470×10^{-3}	8.571
Ne V	1575	2.87	2.050×10^{-5}	7.437
C III	1910	3.72	3.350×10^{-8}	9.363
C III	1909	3.72	1.940	9.358
C III	1907	3.72	2.270	9.348
N III	1754	3.45	2.090×10^{-2}	8.490
N III	1752	3.45	6.760×10^{-2}	8.481
N III	1750	3.45	1.110×10^{-1}	8.471
N III	1744	3.45	2.290×10^{-1}	8.442
N IV	1488	3.45	6.430×10^{-10}	7.203
N IV	1486	3.45	3.520×10^{-2}	7.193
N IV	1483	3.45	4.720×10^{-2}	7.179
O II	2471	3.22	8.710×10^{-2}	11.84
O II	2471	3.22	2.240×10^{-2}	11.84
O IV	1407	3.22	1.780×10^{-3}	6.741
O IV	1405	3.22	5.780×10^{-3}	6.732
O IV	1401	3.22	8.390×10^{-3}	6.713
O IV	1394	3.22	1.850×10^{-2}	6.679
Ne IV	2425	2.87	3.270×10^{-2}	11.45
Ne IV	2423	2.87	4.620×10^{-2}	11.44

Species	Central Wavelength λ_0 (Å)	Thermal Doppler velocity V_{thermal} (km s^{-1})	Relative Intensity x	FWHM $\Delta\lambda_D$ ($\times 10^{-2}$Å)
Ne IV	1602	2.87	1.050×10^{-3}	7.565
Ne IV	1602	2.87	2.620×10^{-3}	7.565
Ar IV	2869	2.04	3.890×10^{-3}	13.16
Ar IV	2854	2.04	9.320×10^{-3}	13.09
Fe II	2600	1.73	2.320×10^{-3}	11.82
Fe III	1122	1.73	1.430×10^{-5}	5.102
Fe VI	1944	1.73	3.420×10^{-7}	8.840
C I	1646	3.72	5.306×10^{-4}	8.068
C II	1335	3.72	1.979×10^{-3}	6.544
C II	1335	3.72	2.716×10^{-1}	6.544
C II	2326	3.72	5.805×10^{-2}	11.40
C III	1909	3.72	4.518×10^{-2}	9.358
C III	1909	3.72	9.157×10^{-2}	9.358
C III	2297	3.72	3.952×10^{-2}	11.26
N III	1744	3.45	1.456×10^{-2}	8.442
N IV	1483	3.45	5.523×10^{-4}	7.179
N IV	1483	3.45	8.714×10^{-4}	7.179
N IV	1719	3.45	2.580×10^{-4}	8.321
O IV	1342	3.22	2.141×10^{-4}	6.430
O IV	1394	3.22	8.948×10^{-4}	6.679

Appendix E

Parameters for Lyman transitions $n = 1 \rightarrow n'$ for atomic hydrogen

n'	Oscillator strength $f_{n=1,n'}$	Wavelength λ (Å)	1/lifetime Γ (s^{-1})
2	4.162×10^{-1}	1215.670	6.265×10^{8}
3	7.910×10^{-2}	1025.722	1.897×10^{8}
4	2.899×10^{-2}	972.5370	8.126×10^{7}
5	1.394×10^{-2}	949.7430	4.203×10^{7}
6	7.799×10^{-3}	937.8030	2.450×10^{7}
7	4.814×10^{-3}	930.7480	1.549×10^{7}
8	3.183×10^{-3}	926.2260	1.041×10^{7}
9	2.216×10^{-3}	923.1500	7.335×10^{6}
10	1.605×10^{-3}	920.9630	5.359×10^{6}
11	1.201×10^{-3}	919.3510	4.034×10^{6}
12	9.214×10^{-4}	918.1290	3.162×10^{6}
13	7.227×10^{-4}	917.1810	2.450×10^{6}
14	5.774×10^{-4}	916.4290	1.964×10^{6}
15	4.686×10^{-4}	915.8240	1.598×10^{6}
16	3.856×10^{-4}	915.3290	1.318×10^{6}
17	3.211×10^{-4}	914.9190	1.099×10^{6}
18	2.702×10^{-4}	914.5760	9.264×10^{5}
19	2.296×10^{-4}	914.2860	7.881×10^{5}
20	1.967×10^{-4}	914.0390	6.760×10^{5}
21	1.698×10^{-4}	913.8260	5.853×10^{5}
22	1.476×10^{-4}	913.6410	5.091×10^{5}
23	1.291×10^{-4}	913.4800	4.455×10^{5}

n'	Oscillator strength $f_{n=1,n'}$	Wavelength λ (Å)	1/lifetime Γ (s^{-1})
24	1.136×10^{-4}	913.3390	3.921×10^{5}
25	1.005×10^{-4}	913.2150	3.466×10^{5}
26	8.928×10^{-5}	913.1040	3.084×10^{5}
27	7.970×10^{-5}	913.0060	2.754×10^{5}
28	7.144×10^{-5}	912.9180	2.469×10^{5}
29	6.429×10^{-5}	912.8390	2.223×10^{5}
30	5.806×10^{-5}	912.7680	2.008×10^{5}
31	5.261×10^{-5}	912.7030	1.820×10^{5}
32	4.782×10^{-5}	912.6450	1.654×10^{5}
33	4.360×10^{-5}	912.5920	1.508×10^{5}
34	3.986×10^{-5}	912.5430	1.379×10^{5}
35	3.653×10^{-5}	912.4980	1.264×10^{5}
36	3.357×10^{-5}	912.4580	1.162×10^{5}
37	3.092×10^{-5}	912.4200	1.070×10^{5}
38	2.854×10^{-5}	912.3850	9.879×10^{4}
39	2.640×10^{-5}	912.3530	9.138×10^{4}
40	2.446×10^{-5}	912.3240	8.470×10^{4}
41	2.270×10^{-5}	912.2960	7.865×10^{4}
42	2.111×10^{-5}	912.2710	7.316×10^{4}
43	1.968×10^{-5}	912.2470	6.818×10^{4}
44	1.836×10^{-5}	912.2250	6.363×10^{4}
45	1.716×10^{-5}	912.2040	5.949×10^{4}
46	1.607×10^{-5}	912.1850	5.569×10^{4}
47	1.506×10^{-5}	912.1660	5.221×10^{4}
48	1.414×10^{-5}	912.1490	4.901×10^{4}
49	1.329×10^{-5}	912.1330	4.607×10^{4}
50	1.251×10^{-5}	912.1180	4.337×10^{4}

Appendix F

Application of the condition of stationarity to two and three level atomic multiplets

In equilibrium, the relative populations of the excited fine structure states of thermally important species are governed by the condition of stationarity:

Number of transitions into level i per unit time	=	Number of transitions out of level i per unit time

The outcome of applying this criterion to two and three level multiplets is shown below.

(1) Two level multiplet

Let C_{ij} represent the coefficient for collisional excitation from level i to level j (where $i < j$), C_{ji} be the coefficient for collisional de-excitation from level j to level i and A_{ji} be the Einstein coefficient for spontaneous decay from level j to level i (see Chapter 6).
For a two level multiplet let the ground level be denoted by 1 with a number density of n_1 and the upper level be denoted by 2 with a number density of n_2. Application of the condition of stationarity to the ground level yields:

$$n_1 C_{12} = n_2(C_{21} + A_{21}) \tag{F.1}$$

Hence

$$\frac{n_1}{n_2} = \frac{C_{21} + A_{21}}{C_{12}} \tag{F.2}$$

The fraction of the atoms in the excited fine structure level 2 is given by:

$$f_2^{(2)} = \frac{n_2}{n_1 + n_2}$$

Hence

$$\frac{1}{f_2^{(2)}} = 1 + \frac{n_1}{n_2} = \frac{C_{12} + C_{21} + A_{21}}{C_{12}}$$

Thus:

$$f_2^{(2)} = \frac{C_{12}}{C_{12} + C_{21} + A_{21}} \tag{F.3}$$

(2) Three level multiplet

For a three level multiplet the algebra is considerably more involved. Let the ground level be denoted by 1 with a number density of n_1 and the upper levels be denoted by 2, 3 with number densities of n_2 and n_3 respectively. Applying the condition of stationarity to the three different levels gives:

$$n_1(C_{12} + C_{13}) = n_2(A_{21} + C_{21}) + n_3(A_{31} + C_{31}) \tag{F.4}$$

$$n_2(A_{21} + C_{21} + C_{23}) = n_1 C_{12} + n_3(A_{32} + C_{32}) \tag{F.5}$$

$$n_3(A_{31} + A_{32} + C_{31} + C_{32}) = n_1 C_{13} + n_2 C_{23} \tag{F.6}$$

Getting an expression for n_1 from equation (F.4) and substituting this into equation (F.5) gives, after some algebraic manipulation:

$$\frac{n_2}{n_3} = \frac{C_{12}(A_{31} + C_{31}) + (A_{32} + C_{32})(C_{12} + C_{13})}{C_{13}(A_{21} + C_{21}) + C_{23}(C_{12} + C_{13})} \tag{F.7}$$

Getting an expression for n_3 from equation (F.6) and substituting into equation (F.5) yields:

$$\frac{n_1}{n_2} = \frac{(A_{21} + C_{21})(A_{31} + A_{32} + C_{31} + C_{32}) + C_{23}(A_{32} + C_{31})}{C_{12}(A_{31} + A_{32} + C_{31} + C_{32}) + C_{13}(A_{32} + C_{32})} \tag{F.8}$$

From equation (F.5) an expression for n_2 may be computed which, when substituted into equation (F.4) gives:

$$\frac{n_1}{n_3} = \frac{(A_{32} + C_{32})(A_{21} + C_{21}) + (A_{31} + C_{31})(A_{21} + C_{21} + C_{23})}{C_{12}C_{23} + C_{13}(A_{21} + C_{21} + C_{23})} \tag{F.9}$$

The fraction of atoms in the excited level 2 is given by:

$$f_2^{(3)} = \frac{n_2}{n_1 + n_2 + n_3}$$

Hence

$$\frac{1}{f_2^{(3)}} = 1 + \frac{n_1}{n_2} + \frac{n_3}{n_2}$$

Using equations (F.7) and (F.8) this gives after much algebra:

$$f_2^{(3)} = \frac{(C_{12} + C_{13})(A_{32} + C_{32}) + C_{12}(A_{31} + C_{31})}{\alpha + \beta + \gamma} \tag{F.10}$$

where

$$\alpha = (C_{32} + A_{32})(C_{12} + C_{13} + A_{21} + C_{21})$$

$$\beta = C_{12}(A_{31} + C_{31} + C_{23})$$

$$\gamma = (C_{23} + C_{21} + A_{21})(C_{31} + A_{31} + C_{13})$$

The fraction of atoms in the excited level 3 is given by:

$$f_3^{(3)} = \frac{n_3}{n_1 + n_2 + n_3}$$

So that

$$\frac{1}{f_3^{(3)}} = 1 + \frac{n_1}{n_3} + \frac{n_2}{n_3}$$

Using equations (F.7) and (F.9) this then gives:

$$f_3^{(3)} = \frac{C_{13}(A_{21} + C_{21}) + C_{23}(C_{12} + C_{13})}{\alpha + \beta + \gamma} \tag{F.11}$$

where α, β and γ are defined as above.

Appendix G

Solution to the integrals $\int_0^\alpha x^3/(e^x-1)\,dx$ and $\int_0^\alpha x^4/(e^x-1)\,dx$

(1) Solution to

$$\mathrm{I} = \int_0^\alpha \frac{x^3}{e^x - 1}\,dx \tag{G.1}$$

Dividing through by e^x gives:

$$\mathrm{I} = \int_0^\alpha \frac{x^3 e^{-x}}{1 - e^{-x}}\,dx \tag{G.2}$$

Expand the denominator as a Taylor series about $x = 0$:

$$\frac{1}{1 - e^{-x}} = 1 + e^{-x} + e^{-2x} + e^{-3x} + \ldots = \sum_{n=0}^{\infty} e^{-nx} \tag{G.3}$$

Hence:

$$\mathrm{I} = \int_0^\alpha x^3 e^{-x} \sum_{n=0}^{\infty} e^{-nx}\,dx \tag{G.4}$$

Incorporating the exponential into the summation gives:

$$\mathrm{I} = \int_0^\alpha x^3 \sum_{n=1}^{\infty} e^{-nx}\,dx \tag{G.5}$$

Interchanging the order of summation and integration:

$$\mathrm{I} = \sum_{n=1}^{\infty} \int_0^\alpha x^3 e^{-nx}\,dx \tag{G.6}$$

Hence we need to solve the integral

$$\mathrm{J} = \int_0^\alpha x^3 e^{-nx}\,dx \tag{G.7}$$

This integral can easily be solved by employing integration by parts three times. The result is:

$$\mathrm{J} = \frac{6}{n^4} - \frac{e^{-n\alpha}}{n}\left(\frac{6}{n^3} + \frac{6\alpha}{n^2} + \frac{3\alpha^2}{n} + \alpha^3\right) \tag{G.8}$$

Hence:

$$\mathrm{I} = 6\sum_{n=1}^{\infty} \frac{1}{n^4} - \sum_{n=1}^{\infty} \frac{e^{-n\alpha}}{n}\left(\frac{6}{n^3} + \frac{6\alpha}{n^2} + \frac{3\alpha^2}{n} + \alpha^3\right) \tag{G.9}$$

The value of the first sum is

$$\sum_{n=1}^{\infty} \frac{1}{n^4} = \zeta(4) = \frac{\pi^4}{90} \tag{G.10}$$

Where $\zeta(k)$ is the Riemann zeta function defined as $\zeta(k) = \sum_{n=1}^{\infty} 1/n^k$.
Hence the final result is:

$$\mathrm{I} = \int_0^{\alpha} \frac{x^3}{e^x - 1}\, dx = \frac{\pi^4}{15} - \sum_{n=1}^{\infty} \frac{e^{-n\alpha}}{n}\left(\frac{6}{n^3} + \frac{6\alpha}{n^2} + \frac{3\alpha^2}{n} + \alpha^3\right) \tag{G.11}$$

(2) Solution to

$$\mathrm{I} = \int_0^{\alpha} \frac{x^4}{e^x - 1}\, dx \tag{G.12}$$

Exactly the same steps are performed as in equations (G.2) to (G.6) to give:

$$\mathrm{I} = \sum_{n=1}^{\infty} \int_0^{\alpha} x^4 e^{-nx}\, dx \tag{G.13}$$

The integral to solve is thus:

$$\mathrm{J} = \int_0^{\alpha} x^4 e^{-nx}\, dx \tag{G.14}$$

This is solved by applying integration by parts four times to give:

$$\mathrm{J} = \frac{24}{n^5} - \frac{e^{-n\alpha}}{n}\left(\frac{24}{n^4} + \frac{24\alpha}{n^3} + \frac{12\alpha^2}{n^2} + \frac{4\alpha^3}{n} + \alpha^4\right) \tag{G.15}$$

The final result is thus:

$$\mathrm{I} = \int_0^{\alpha} \frac{x^4}{e^x - 1}\, dx = 24\zeta(5) - \sum_{n=1}^{\infty} \frac{e^{-n\alpha}}{n}\left(\frac{24}{n^4} + \frac{24\alpha}{n^3} + \frac{12\alpha^2}{n^2} + \frac{4\alpha^3}{n} + \alpha^4\right) \tag{G.16}$$

The numerical value of $\zeta(5)$ is approximately 1.03693.

References

Abgrall H.,Le Bourlot J.,Pineau des Forêts G.,Roueff E.,Flower D.R.,Heck L. 1992, *A.&A.* 253,525

Abgrall H.,Roueff E. 1989, *A.&A. Suppl.* 79,313

Abramowitz M.,Stegun I.A 1965, in *Handbook of Mathematical Functions*, (New York: Dover)

Adamson A.W. 1986, in *A Textbook of Physical Chemistry (Third edition)*, (London: Academic Press)

Allamandola L.J. 1984, in *Galactic and Extragalactic Infrared Spectroscopy*, eds. M. Kessler, J. Phillips (Dordrecht: Reidel)

Allamandola L.J.,Norman C.A. 1978, *A.&A.* 66,129

Allamandola L.J.,Tielens A.G.G.M.,Barker J.R. 1987, in *Interstellar Processes*, eds. D.J. Hollenbach, H.A. Thronson (Dordrecht: Reidel)

Allamandola L.J.,Tielens A.G.G.M.,Barker J.R. 1985, *Ap. J.* 290,L25

Allamandola L.J.,Tielens A.G.G.M.,Barker J.R. 1989, *Ap. J. Suppl.* 71,733

Aller L.H.,Czyzak S.J. 1983, *Ap. J. Suppl.* 51,211

Aller L.H.,Ross J.E.,O'Mara B.J.,Keyes C.D. 1981, *M.N.R.A.S.* 197,95

Anicich V.G.,Huntress W.T. 1986, *Ap. J. Suppl.* 62,553

Apparao K.M.V.,Tarafdar S.P. 1989, *Ap. J.* 344,826

Arthurs A.M.,Dalgarno A. 1960, *Proc. Roy. Soc. London* A256,540

Bachiller R.,Huggins P.J.,Cox P.,Forveille T. 1994, *A.&A.* 281,L93

Bachiller R.,Planesas P.,Martin-Pintado J.,Bujarrabal V.,Tafalla M. 1989, *A.&A.* 210,366

Bakes E.L.O.,Tielens A.G.G.M. 1994, *Ap. J.* 427,822

Barlow M.J. 1983, in *Planetary Nebulae (IAU Symposium 103)*, ed. D.R. Flower (Dordrecht: Reidel)

Barlow M.J.,Silk J. 1977, *Ap. J.* 215,800

Bates D.R.,Herbst E. 1988, in *Rate Coefficients in Astrochemistry*, eds. T.J. Millar, D.A. Williams (Dordrecht: Kluwer)

Berrington K.A. 1988, *J. Phys. B* 21,1083

Bieging J.H.,Nguyen-Q-Rieu 1988, *Ap. J.* 329,L107

Black J.H. 1978,*Ap. J.* 222,125

Black J.H.,Dalgarno A. 1976, *Ap. J.* 203,132

Black J.H.,Dalgarno A. 1977, *Ap. J. Suppl.* 34,405

Bode M.F. 1988, in *Dust in the Universe*, eds. M.E. Bailey, D.A. Williams (Cambridge: Cambridge University Press)

Bohlin R.C.,Marionni P.A.,Stecher T.P. 1975, *Ap. J.* 202,415

Bohlin R.C.,Savage B.D.,Drake J.F. 1978, *Ap. J.* 224,132

Böhringer H.,Arnold F. 1986, *J. Chem. Phys.* 84,1459

Borghesi A.,Bussoletti E.,Colangeli L.,Minafra A.,Rubini F. 1983, *Infrared Physics* 23,321

Bouchet P.,Lequeux J.,Maurice E.,Prevot L.,Prevot-Burnichon M.L. 1985, *A.&A.* 149,330

Breit G.,Teller E. 1940, *Ap. J.* 91,215

Bujarrabal V.,Gomez-Gonzalez J.,Bachiller R.,Martin-Pintado J. 1988, *A.&A.* 204,242

Burke J.R.,Hollenbach D.J. 1983, *Ap. J.* 265,223

Burton M.G.,Hollenbach D.J.,Tielens A.G.G.M. 1990, *Ap. J.* 365,620

Bussoletti E.,Colangeli L.,Borghesi A.,Orofino V. 1987, *A.&A. Suppl.* 70,257

Cernicharo J.,Guélin M.,Martin-Pintado J.,Peñalver J.,Mauersberger R. 1989, *A.&A.* 222,L1

Cesarsky C.J.,Völk H.J. 1978, *A.&A.* 70,367

Chapman R.D.,Henry R.J.W. 1972, *Ap. J.* 168,169

Cohen M.,Allamandola L.J.,Tielens A.G.G.M.,Bregman J.,Simpson J.P., Witteborn F.C.,Wooden D.,Rank D. 1986, *Ap. J.* 302,737

Cohen M.,Barlow M.J. 1974, *Ap. J.* 193,401

Cohen M.,Harrington J.P.,Hess R. 1984, *Ap. J.* 283,687

Cohen N.,Westburg K.R. 1983, *J. Phys. Chem. Ref. Data* 12,531

Cox P.,Gusten R.,Henkel C. 1987, *A.&A.* 181,L19

Cox P.,Huggins P.J.,Bachiller R.,Forveille T. 1991, *A.&A.* 250,533

Cox P.,Omont A.,Huggins P.J.,Bachiller R.,Forveille T. 1992, *A.&A.* 266,420

Cravens T.E.,Dalgarno A. 1978, *Ap. J.* 219,750

Croswell K.,Dalgarno A. 1985, *Ap. J.* 289,618

Dalgarno A.,Black J.H.,Weisheit J.C. 1973, *Astrophys. Letters* 14,77

Dalgarno A.,Herzberg G.,Stephens T.L. 1970, *Ap. J.* 162,49

Danby G.,Flower D.R.,Monteiro T.S. 1987, *M.N.R.A.S.* 226,739

Deguchi S.,Claussen M.J.,Goldsmith P.F. 1980, *Ap. J.* 303,810

Deguchi S.,Izumiura H.,Kaifu N.,Mao X.,Nguyen-Q-Rieu,Ukita N. 1990, *Ap. J.* 351,522

Deguchi S.,Izumiura H.,Nguyen-Q-Rieu,Shibata K.M.,Ukita N.,Yamamura I. 1992, *Ap. J.* 392,597

de Freitas Pacheco J.A.,Maciel W.J.,Costa R.D.D. 1992, *A.&A.* 261,579

de Jong T. 1972, *A.&A.* 20,263

de Jong T. 1977, *A.&A.* 55,137

de Jong T. 1980, *Highlights Astr.* 5,301

Désert F.-X.,Boulanger F.,Puget J.L. 1990, *A.&A.* 237,215

d'Hendecourt L.,Leger A. 1987, *A.&A.* 180,L9

Doughty N.A.,Fraser P.A.,McEachran R.P. 1966, *M.N.R.A.S.* 132,255

Draine B.T. 1978, *Ap. J. Suppl.* 36,595

Draine B.T.,Katz N. 1986, *Ap. J.* 310,392

Drayson S.R. 1976, *J. Quant. Spectrosc. Radiat. Transfer* 16,611

Duley W.W.,Williams D.A. 1981, *M.N.R.A.S.* 196,269

Duley W.W.,Williams D.A. 1984, in *Interstellar Chemistry*, (London: Academic Press)

Duley W.W.,Williams D.A. 1986, *M.N.R.A.S.* 223,177

Dwek E.,Sellgren K.,Soifer B.T.,Werner M.W. 1980, *Ap. J.* 238,140

Eidelsberg M.,Benayoun J.J.,Viala Y.,Rostas F. 1991, *A.&A. Suppl.* 90,231

Eidelsberg M.,Rostas F. 1990, *A.&A.* 235,472

Elitzur M.,Watson W.D. 1978a, *Ap. J.* 222,L141

Elitzur M.,Watson W.D. 1978b, *A.&A.* 70,443

Federman S.R.,Glassgold A.E.,Kwan J. 1979, *Ap. J.* 227,466

Feuerbacher B.,Fitton B. 1972, *J. Appl. Phys.* 43,1563

Feuerbacher B.,Willis R.F.,Fitton B. 1973, *Ap. J.* 181,101

Flower D.R. 1989, *J. Phys. B* 22,2319

Flower D.R. 1990, in *Molecular Collisions in the Interstellar Medium*, (Cambridge: Cambridge University Press)

Flower D.R.,Launay J.M. 1977, *J. Phys. B* 10,3673

Flower D.R.,Launay J.M. 1985, *M.N.R.A.S.* 214,271

Forrest W.J.,McCarthy J.F.,Houck J.R. 1980, *Ap. J.* 240,L37

Forveille T.,Huggins P.J. 1991, *A.&A.* 248,599

Gallegos E.J. 1968, *J. Phys. Chem.* 72,3452

Gammie C.F.,Knapp G.R.,Young K.,Phillips T.G.,Falgarone E. 1989, *Ap. J.* 345,L87

Gerlich D. 1990, *J. Chem. Phys.* 92,2377

Gillett F.C.,Forrest W.J.,Merrill K.M. 1973, *Ap. J.* 183,87

Gillett F.C.,Low F.J.,Stein W.A. 1967, *Ap. J.* 149,L97

Gondhalekar P.M.,Phillips A.P.,Wilson R. 1980, *A.&A.* 85,272

Gradshteyn I.S.,Ryzhik I.M. 1980, in *Tables of Integrals, Series and Products*, (San Diego: Academic Press)

Gredel R.,Lepp S.,Dalgarno A.,Herbst E. 1989, *Ap. J.* 347,289

Green S.,Hutson J.M. 1986, MOLSCAT computer code (Collaborative Computational Project No. 6, UK Science and Engineering Research Council)

Green S.,Thaddeus P. 1976, *Ap. J.* 205,766

Gussie G.T.,Taylor A.R.,Dewdney P.E.,Roger R.S. 1994, *M.N.R.A.S.* in press

Habing H.J. 1968, *Bull. Astr. Inst. Netherlands* 19,421

Haddad G.N.,Samson J.A.R. 1986, *J. Chem. Phys.* 84,6623

Harrington J.P.,Seaton M.J.,Adams S.,Lutz J.H. 1982, *M.N.R.A.S.* 199,517

Hayes M.A.,Nussbaumer H. 1984, *A.&A.* 134,193

Herbst E.,Adams N.G.,Smith D. 1984, *Ap. J.* 285,618

Herbst E.,Klemperer W. 1973, *Ap. J.* 185,505

Hicks T.R.,Phillips J.P.,Reay N.K. 1976, *M.N.R.A.S.* 176,409

Hoare M.G. 1990, *M.N.R.A.S.* 244,193

Hoare M.G.,Roche P.F.,Clegg R.E.S. 1992, *M.N.R.A.S.* 258,257

Hofmann H.,Saha H.P.,Treffitz E. 1983, *A.&A.* 126,415

Hollenbach D.J.,Shull J.M. 1977, *Ap. J.* 216,419

Hollenbach D.J.,Takahashi T.,Tielens A.G.G.M. 1991, *Ap. J.* 377,192

Hollenbach D.J.,Werner M.W.,Salpeter E.E. 1971, *Ap. J.* 163,165

Howe D.A.,Millar T.J.,Williams D.A. 1992, *M.N.R.A.S.* 255,217

Huggins P.J. 1993, in *Planetary Nebulae (IAU Symposium 155)*, eds. R. Weinberger, A. Acker (Dordrecht: Reidel)

Huggins P.J.,Glassgold A.E.,Morris M. 1984, *Ap. J.* 279,284

Huggins P.J.,Healy A.P. 1989, *Ap. J.* 346,201

Hummer D.G.,Kunasz P.B. 1980, *Ap. J.* 236,609

Jaquet R.,Staemmler V.,Smith R.D.,Flower D.R. 1992, *J. Phys. B* 25,285

Johansson L.E.B.,Andersson C.,Elldér J.,Friberg P.,Hjalmarson Å., Höglund B., Irvine W.M.,Olofsson H.,Rydbeck G. 1984, *A.&A.* 130,227

Johnson C.T.,Burke P.G.,Kingston A.E. 1987, *J. Phys. B* 20,2553

Kaler J.B.,Shaw R.A.,Kwitter K.B. 1990, *Ap. J.* 359,392

Karpas Z.,Anicich V.G.,Huntress W.T. 1979, *J. Chem. Phys.* 70,2877

Knapp G.R. 1985, *Ap. J.* 293,273

Koike C.,Hasegawa H.,Manabe A. 1980, *Astrophys. Sp. Sci.* 67,495

Krishna Swamy K.S.,O'Dell C.R. 1968, *Ap. J.* 151,L61

Kwan J. 1977, *Ap. J.* 216,713

Kwok S. 1982, *Ap. J.* 258,280

Lang K.R. 1986, in *Astrophysical Formulae*, (New York: Springer-Verlag)

Latter W.B. 1991, *Ap. J.* 377,187

Latter W.B.,Walker C.K.,Maloney P.R. 1993, *Ap. J.* 419,L97

Launay J.M. 1977, *J. Phys. B* 10,3665

Launay J.M.,Roueff E. 1977a, *J. Phys. B* 10,879

Launay J.M.,Roueff E. 1977b, *A.&A.* 56,289

Lavendy H.,Robbe J.M.,Gandara G. 1987, *J. Phys. B* 20,3067

Le Bourlot J.,Pineau des Forêts G.,Roueff E.,Flower D.R. 1993, *A.&A.* 267,233

Leen T.M.,Graff M.M. 1988, *Ap. J.* 325,411

Leger A.,Puget J.L. 1984, *A.&A.* 137,L5

Leger A.,d'Hendecourt L.,Defourneau D. 1989, *A.&A.* 216,148

Letzelter C.,Eidelsberg M.,Rostas F.,Breton J.,Thieblemont B. 1987, *Chem. Phys.* 114,273

Levine R.D.,Bernstein R.B. 1974, in *Molecular Reaction Dynamics*, (New York: Oxford University Press)

Levine R.D.,Bernstein R.B.,Kahana P.,Procaccia I.,Upchurch E.T. 1976, *J. Chem. Phys.* 64,796

Likkel L.,Forveille T.,Omont A.,Morris M. 1988, *A.&A.* 198,L1

Lombardi G.G.,Smith P.L.,Parkinson W.H. 1978, *Phys. Rev. A* 18,2131

Mandl F. 1978, in *Statistical Physics*, (New York: Wiley)

Mandy M.E.,Martin P.G. 1993, *Ap. J. Suppl.* 86,199

Marchand A. 1987, in *Polycyclic Aromatic Hydrocarbons and Astrophysics*, eds. A. Leger, L.B. d'Hendecourt, N. Boccara (Dordrecht: Reidel)

Marionni P.A.,Harrington J.P. 1981, in *The Universe at Ultraviolet Wavelengths*, ed. R. Chapman (NASA CP 2171)

Marquette J.B.,Rebrion C.,Rowe B.R. 1989, *A.&A.* 213,L29

Martin C.,Hurwitz M.,Bowyer S. 1990, *Ap. J.* 354,220

Martin W. 1987, *A.&A.* 182,290

Mathis J.S. 1986, in *Interrelationships Among Circumstellar, Interstellar and Interplanetary Dust*, eds. J. Nuth, R. Stencel (NASA CP 2403)

Mathis J.S.,Mezger P.S.,Panagia N. 1983, *A.&A.* 128,212

Mathis J.S.,Rumpl W.,Nordsieck K.H. 1977, *Ap. J.* 217,425

McCarthy J.F.,Forrest W.J.,Houck J.R. 1978, *Ap. J.* 224,109

McDaniel E.W. 1989, in *Atomic Collisions*, (New York: Wiley)

Menzel D.H.,Pekeris C.L. 1935, *M.N.R.A.S.* 96,77

Merrill K.M.,Soifer B.T.,Russell R.W. 1975, *Ap. J.* 200,L37

Mezger P.G.,Mathis J.S.,Panagia N. 1982, *A.&A.* 105,372

Mie G. 1908, *Ann. Physik* 25,377

Mies F.H. 1973, *Phys. Rev. A* 7,942

Millar T.J.,de Frees D.J.,McLean A.D., Herbst E. 1988, *A.&A.* 194, 250

Miller J.H.,Mallard W.G.,Smyth K.C. 1984, *J. Phys. Chem.* 88,4963

Monteiro T.S.,Flower D.R. 1987, *M.N.R.A.S.* 228,101

Moorhead J.M.,Lowe R.P.,Maillard J.-P.,Wehlau W.H.,Bernath P.F. 1988, *Ap. J.* 326,899

Moseley H. 1980, *Ap. J.* 238,892

Moseley S.H.,Silverberg R.F. 1986, in *Interrelationships Among Circumstellar, Interstellar and Interplanetary Dust*, eds. J. Nuth, R. Stencel (NASA CP 2403)

Moskovitz M. 1991, *Ann. Rev. Phys. Chem.* 42,465

Mufson S.L.,Lyon J.,Marionni P. 1975, *Ap. J.* 201,L85

Nee J.B.,Lee L.C. 1985, *Ap. J.* 291,202

Nussbaumer H.,Rusca C. 1979, *A.&A.* 72,129

Olofsson H.,Johansson L.,Nguyen-Q-Rieu,Sopka R.J.,Zuckerman B. 1982, *B.A.A.S.* 14,895

Olofsson H.,Lindqvist M.,Nyman L.-Å.,Winnberg A.,Nguyen-Q-Rieu 1991, *A.& A.* 245,611

Omont A. 1986, *A.&A.* 164,159

Osterbrock D.E. 1974a, in *Astrophysics of Gaseous Nebulae*, (San Francisco: W.H.Freeman and Co.)

Osterbrock D.E. 1974b, *P.A.S.P.* 86,609

Padial N.T.,Collins L.A.,Schneider B.I. 1985, *Ap. J.* 298,369

Panagia N.,Ranieri M. 1973, *Mem. Soc. Roy. Sci. Liege*, Series 6, V, 275

Perinotto M. 1991, *Ap. J. Suppl.* 76,687

Philipp H.R. 1977, *Phys. Rev.* 16,2896

Pineau des Forêts G.,Flower D.R.,Hartquist T.W.,Dalgarno A. 1986, *M.N.R.A.S.* 220,801

Pottasch S.R.,Wesselius P.R.,van Duinen R.J. 1979, *A.&A.* 74,L15

Prasad S.S.,Huntress W.T. 1980, *Ap. J. Suppl.* 43,1

Press W.H.,Teukolsky S.A.,Vetterling W.T.,Flannery B.P. 1992, *Numerical Recipes in FORTRAN (Second edition)*, (Cambridge: Cambridge University Press)

Procaccia I.,Levine R.D. 1976, *J. Chem. Phys.* 64,808

Puget J.L.,Leger A.,Boulanger F. 1985, *A.&A.* 142,L19

Roberge W.G.,Dalgarno A.,Flannery B.P. 1981, *Ap. J.* 243,817

Rouan D.,Leger A.,Omont A.,Giard M. 1992, *A.&A.* 253,498

Russell R.W.,Soifer B.T.,Willner S.P. 1977, *Ap. J.* 217,L149

Samson J.A.R.,Haddad G.N.,Kilcoyne L.D. 1987, *J. Chem. Phys.* 87,6416

Savage B.D. 1975, *Ap. J.* 199,92

Schadee A. 1967, *J. Quant. Spectrosc. Radiat. Transfer* 7,169

Schofield K. 1967, *Planetary and Space Science* 15,643

Schröder K.,Staemmler V.,Smith M.D.,Flower D.R.,Jaquet R. 1991, *J. Phys. B* 24,2487

Scott N.S.,Taylor K.T. 1982, *Comput. Phys. Commun.* 25,347

Seaton M.J. 1983, in *Planetary Nebulae (IAU Symposium 103)*, ed. D.R. Flower (Dordrecht: Reidel)

Sellgren K. 1984, *Ap. J.* 277,623

Sellgren K.,Allamandola L.J.,Bregman J.D.,Werner M.W.,Wooden D.H. 1985, *Ap. J.* 299,416

Shepherd M.C., Cohen R.J.,Gaylard M.J.,West M.E. 1990, *Nature* 344,522

Shibata K.M.,Deguchi S.,Hirano N.,Kameya O.,Tamura S. 1993, *Ap. J.* 415,708

Shields G.A. 1978, *Ap. J.* 219,565

Smith F.T. 1961, *J. Chem. Phys.* 34,793

Smith I.W.M. 1988, in *Rate Coefficients in Astrochemistry*, eds. T.J. Millar, D.A. Williams (Dordrecht: Kluwer)

Spitzer L. 1968, in *Diffuse Matter in Space*, (New York: Wiley)

Spitzer L. 1978, in *Physical processes in the Interstellar Medium*, (New York: Wiley)

Spitzer L.,Greenstein J.L. 1951, *Ap. J.* 114,407

Staemmler V.,Flower D.R. 1991, *J. Phys. B* 24,2343

Staemmler V.,Jaquet R. 1985, *Chem. Phys.* 92,141

Stein S.E. 1978, *J. Phys. Chem.* 82,566

Stein S.E.,Brown R.L. 1987, in *Molecular Structure and Energetics vol.2*, eds. J.F. Leibman, A. Greenberg (New York: VCH Publishers Inc.)

Stein S.E.,Fahr A. 1985, *J. Phys. Chem.* 89,3714

Stephens T.L.,Dalgarno A. 1972, *J. Quant. Spectrosc. Radiat. Transfer* 12,569

Taylor A.R.,Gussie G.T.,Pottasch S.R. 1990, *Ap. J.* 351,515

Telesco C.M.,Harper D.A. 1977, *Ap. J.* 211,475

Terenin A.,Villessov F. 1964, *Adv. Photochem.* 2,385

Terzian Y.,Saunders D. 1972, *Ap. J.* 77,350

Thronson H.A.,Bally J. 1986, *Ap. J.* 300,749

Thronson H.A.,Mozurkewich D. 1983, *Ap. J.* 271,611

Tielens A.G.G.M.,Allamandola L.J. 1987, in *Interstellar Processes*, eds. D.J. Hollenbach, H.A. Thronson (Dordrecht: Reidel)

Tielens A.G.G.M.,Hollenbach D.J. 1985, *Ap. J.* 291,722

Torres-Peimbert S.,Pena M. 1981, *Rev. Mex. Astr. Astrof.* 6,301

Treffers R.R.,Fink U.,Larson H.P.,Gautier T.N. 1976, *Ap. J.* 209,793

Turner J.,Kirby-Docken K.,Dalgarno A. 1977, *Ap. J. Suppl.* 35,281

van Dishoeck E.F. 1988, in *Rate Coefficients in Astrochemistry*, eds. T.J. Millar, D.A. Williams (Dordrecht: Kluwer)

van Dishoeck E.F.,Black J.H. 1986, *Ap. J. Suppl.* 62,109

Verstraete L.,Leger A.,d'Hendecourt L.,Dutuit O.,Defourneau D. 1990, *A.&A.* 237,436

Viala Y.P. 1986, *A.&A. Suppl.* 64,391

Viala Y.P.,Roueff E.,Abgrall H. 1988, *A.&A.* 190,215

Whitcomb S.E.,Gatley I.,Hildebrand R.H.,Keene J.,Sellgren K.,Werner M.W. 1981, *Ap. J.* 246,416

Wickramasinghe N.C. 1973, in *Light Scattering Functions for Small Particles*, (London: Adam Hilger)

Wiese W.L.,Smith M.W.,Glennon B.M. 1966, in *Atomic Transition Probabilities (H to Ne)*, (NSRDS-NBS 4)

Willner S.P. 1984, in *Galactic and Extragalactic Infrared Spectroscopy*, eds. M. Kessler, J. Phillips (Dordrecht: Reidel)

Yamamoto S.,Saito S.,Kawaguchi K.,Kaifu N.,Suzuki H.,Ohishi M. 1987, *Ap. J.* 317,L119

Zuckerman B.,Aller L.H. 1986, *Ap. J.* 301,772

Zuckerman B.,Gatley I. 1988, *Ap. J.* 324,501